
Mind the *Sim-to-Real* Gap & Think Like a Scientist*

Harsh Parikh[†]
 Amazon SCOT, Seattle, USA
 Yale University, New Haven, USA

Gabriel Levin-Konigsberg
 Amazon SCOT, Seattle, USA

Dominique Perrault-Joncas
 Amazon SCOT, Seattle, USA

Alexander Volfovsky[‡]
 Amazon SCOT, Seattle, USA
 Duke University, Durham, USA

Abstract

Suppose a planner has a pre-trained simulator of a sequential decision problem and the option to run real experiments in the field. The simulator is cheap to query but inherits confounding and drift from its calibration data. Experimentation is unbiased but consumes one real unit per trial. We study when, and how, the planner should supplement the simulator with experiments. We give three results. First, an extended simulation lemma decomposes the simulator’s value error into a calibration–deployment shift that randomization can identify and a parametric residual that no further interaction can reduce. Second, the value gap between the simulator-optimal policy and the optimum splits into a local component, on states the deployed policy already visits, and a reachability component, on states it does not. The reachability component stays bounded away from zero at any horizon under purely passive learning. Third, we propose Fisher-SEP, a simulation-aided experimental policy (SEP) that minimizes the posterior predictive variance of a target policy’s value, with reward-only and transition-only specializations. Two case studies illustrate the regimes. In a vending-machine supply chain, front-loaded experimentation overtakes posterior updating once the horizon is long enough to amortize the pilot. In an HIV mobile-testing example with a corridor that separates a well-surveilled region from a poorly-surveilled one, only designed exploration reaches the poorly-surveilled region.

1 Introduction

A mobile HIV-testing program plans where to send vans each week. The team has a pre-trained *simulator* of neighborhood prevalence — a probabilistic forecast model that, for each zone and each weekly testing choice, predicts the expected number of new cases found, fit to two years of clinic data [Gonsalves et al., 2018, Warren et al., 2025] — and a fixed weekly budget of vans. The simulator ranks zones by expected new-case yield, so the cheap option is to deploy the resulting route as is. The other option is to divert a fraction of vans to zones the simulator ranks low. Diverting costs immediate outreach in well-served areas, but it is the only way to learn whether a low-ranked zone is genuinely low-prevalence or has merely never been tested. This is the question we study.

*The first half of the title borrows the London Underground announcement *Mind the Gap*, which the paper takes as a metaphor for the local-and-reachability decomposition of the value gap (Proposition 1). The second half borrows the children’s song *Think Like a Scientist* by GoNoodle, and points at the prescription: use the simulator to choose where to experiment, rather than to choose a policy to deploy.

[†]Corresponding author: harsh.parikh@yale.edu

[‡]Corresponding author: alexander.volfovsky@duke.edu

This question is more general than HIV testing. A planner with a pre-trained simulator of any real-world system has to decide whether, when, and how to supplement it with real-world data. The simulator is built from history, and that history was collected under actions chosen in presence of a *hidden state*: a feature of the world that affects rewards and transitions but is not directly observed. Because the historical operator’s actions and the hidden state may be correlated, the simulator’s calibration data confounds the action’s effect with the effect of the hidden state. This is what causal inference calls *confounding* [Pearl, 2009, Bareinboim and Pearl, 2016]: the conditional mean reward in the calibration data combines the causal effect of the action and the effect of the hidden state given the operator’s choice. (Concretely: if the historical operator only sent vans to a zone when prevalence was high, then high prevalence and “send a van” are both elevated in the data, and the simulator cannot tell whether the high yield came from the zone or from the operator’s choice.)

A second problem persists even after deployment. Large regions of the state-action space may never appear in any trajectory the planner generates. The causal-inference name for this is a *positivity violation*: a state-action pair with zero probability under the deployed policy produces no evidence, so no amount of further online data speaks to it [Parikh et al., 2024a, 2025b]. Confounding and positivity violations are two faces of the same picture. The simulator is a *Markov decision process* (MDP) on the observed state — a model whose next state and reward are Markov functions of the current state and action. The world is a partially observable MDP (POMDP), which generalizes an MDP by letting the relevant state have both an observed and a hidden component [Zhang and Bareinboim, 2016, Namkoong et al., 2020]. (Throughout, *simulator* means a pre-trained dynamics model treated as an MDP, and *experimentation* means a deliberately randomized real-world study.)

These observations motivate two questions. *Given a pre-trained simulator, when should a planner run real-world experiments?* And, *how is the simulator best used*: as a tool to learn a deployable policy or as a tool to choose experiments?

Offline reinforcement learning (RL) and confounded MDPs supply tools for learning from logged data and diagnosing latent confounders [Levine et al., 2020, Wang et al., 2021, Zhang and Bareinboim, 2016, Kallus and Zhou, 2018], but treat the historical dataset as the only signal and do not jointly optimize its use against future field experiments. Bayes-adaptive MDPs (where the unknown MDP parameters are treated as hidden state and updated by Bayes’ rule from observed rewards and transitions) and posterior sampling formalize how a posterior should adapt during deployment [Duff, 2002, Guez et al., 2012, Osband et al., 2013, Russo et al., 2018], but update over the same parametric family the simulator already uses and assume positivity rather than diagnose when it fails. Sim-to-real and hybrid RL combine simulated and real interaction, including simulator-directed Fisher-information-based exploration [Tobin et al., 2017, Wagenmaker and Jamieson, 2024, Ball et al., 2023, Song et al., 2023, Memmel et al., 2024], but typically deploy the simulator as a warm start. Causal transportability characterizes when effects identified in one population transfer to another [Bareinboim and Pearl, 2016, Parikh et al., 2025a, Lanners et al., 2025], but stops short of saying which experiments to run when transport fails. Multi-fidelity Bayesian optimization treats the simulator as a cheap surrogate for a black-box objective [Poloczek et al., 2017, Kandasamy et al., 2017], but does not separate states the deployed policy visits from those it does not. Our framework addresses a question that is logically prior to all of these: for a given simulator and finite planning horizon, which portion of the value gap is closable by passive online updating, and which portion requires deliberate experimentation? See Appendix H for a detailed comparison.

Contributions. We work in a finite-latent decision-theoretic framework where the simulator is an MDP on the observed state and the world is a POMDP. We name the planner’s three options: trust the simulator and deploy (the *simulator-optimal policy*, SOP), take the simulator as a Bayesian prior and update passively (the *adaptive SOP*, A-SOP), or use the simulator’s structure to choose experiments (a *simulation-aided experimental policy*, SEP). The simulator’s error decomposes into a component on states the deployed policy visits (its visitation support) and a component on states it does not, and these two components do not respond to online data in the same way. (i) *Gap decomposition*. The value gap between the deployed policy and the optimal one decomposes into a *local* part, on the deployed policy’s visitation support, and a *reachability* part, on states outside it (Proposition 1, Theorem 6). Posterior-mean-optimal online updating asymptotically closes the local part but provably leaves the reachability part open. (ii) *Fisher-SEP*. We propose Fisher-SEP, a Fisher-information-directed instance of SEP that minimizes the posterior predictive variance (PVV) of the value of a chosen target policy (Definition 5), with two specializations for transition-known and reward-known regimes. (iii) *Case studies and diagnostic*. A vending-machine supply chain

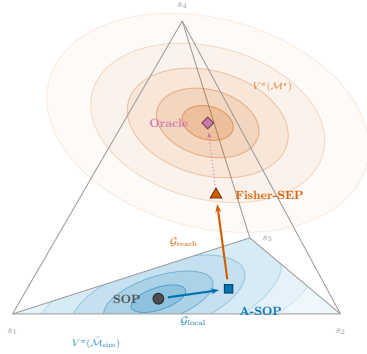


Figure 1: Gap decomposition on the visitation simplex for a four-state example. Blue contours: value under the simulator’s model, confined to a face of the simplex. Orange contours: value under the true environment, peaking at the corner the simulator ignores. Policies that either trust the simulator (●) or update online without experimenting (■) remain on the simulator’s face and close only the local gap; an experimental policy (▲) reaches the ignored corner and closes the reachability gap.

instantiates the local regime. An HIV mobile-testing campaign instantiates the reachability regime. A per-pair diagnostic, the Exploration Priority Index (EPI), gives a per-pair score for how much pilot effort an (s, a) pair deserves (Remark 5).

Organization. Section 2 fixes the world, the simulator, and the policy classes. Section 3 states the gap decomposition. Section 4 defines Fisher-SEP. Section 5 reports the case studies. Section 6 closes. Figure 1 illustrates the decomposition on a four-state example.

2 Setup

A population of n units, indexed by $i \in \{1, \dots, n\}$, evolves over discrete time $t \in \{0, \dots, T\}$ with discount factor $\gamma \in [0, 1)$ — a weight that downweights rewards received far in the future, so the infinite-sum value is finite; the *effective horizon* $T_{\text{eff}} := 1/(1 - \gamma)$ summarizes how far the policy plans ahead. Each unit has an *observed state* $S_{i,t} \in \mathbb{S}$ and a *hidden state* $H_{i,t} \in \mathbb{H}$, with \mathbb{S} and \mathbb{H} finite. The planner chooses an action $A_{i,t} \in \mathbb{A}$ from a finite set, observes a reward $R_{i,t} \sim \rho(\cdot | S_{i,t}, A_{i,t}, H_{i,t}) \in [0, R_{\text{max}}]$, and the state transitions as $(S_{i,t+1}, H_{i,t+1}) \sim \wp(\cdot | S_{i,t}, A_{i,t}, H_{i,t})$. Write $\bar{r}(s, a, h) := \mathbb{E}[R | s, a, h]$ for the expected reward at the truth and $\wp_S(\cdot | s, a, h)$ for the next-observed-state kernel.

Because H is hidden, the planner sees only the marginal process over (S, A, R) , and that marginal is not Markov on S alone: past S, A trajectories carry information about the current H . The hidden state plays two roles. First, it carries *confounding*: in the calibration data on which the simulator was trained, the historical operator’s actions depended on H , so $A \not\perp H | S$ (read: A is *not* conditionally independent of H given S) in that data. Second, it carries *drift*: the conditional of H given S moved between calibration and deployment. Throughout, $\mathbb{P}_t(H | S)$ denotes the deployment-time conditional, and $\mathbb{P}_{\text{calib}}(H | S, A)$ denotes the calibration-time conditional. In causal-inference language, the simulator is calibrated to the observational $\mathbb{E}[R | S, A]$, while the planner cares about the interventional $\mathbb{E}[R | S, \text{do}(A)]$. The two coincide only when $A \perp H | S$ in the calibration data.

Three layers of approximation. The simulator is an MDP on S . The world is a POMDP on (S, H) . To compare the two, we need an MDP on S alone; we construct one by averaging the hidden state out at every step, which loses information (the true world has memory in H that this construction discards) but the loss is bounded and decays geometrically when latent dynamics are contracting (Remark 1). The gap between simulator and world factors through two such intermediate Markov objects on S , each obtained by averaging H out against a different conditional. Let \mathcal{M}^* denote the truth. The *deployment-time Markov projection* $\mathcal{M}_{\text{obs}}^* = (\rho_{\text{obs}}^*, \wp_{\text{obs}}^*)$ averages H out at every step under the deployment-time conditional $\mathbb{P}_t(H | S)$, treating H as if it were drawn fresh from this conditional independent of the past (S, A) trajectory; the true POMDP marginal over (S, A, R) is not Markov on S alone (since the past trajectory carries information about the current H), so this projection is itself an approximation, with cost ϵ^{hist} analyzed in Remark 1. The *calibration kernel* $\mathcal{M}_{\text{calib}} = (\bar{\rho}_{\text{calib}}, \bar{\wp}_{\text{calib}})$ averages H out under the calibration-time conditional $\mathbb{P}_{\text{calib}}(H | S, A)$; this is the limit of the simulator’s training procedure under infinite calibration data and a perfectly specified parametric family. The simulator $\hat{\mathcal{M}}_{\text{sim}} = (\hat{\rho}_{\text{sim}}, \hat{\wp}_{\text{sim}})$ deviates from $\bar{\mathcal{M}}_{\text{calib}}$ by finite-sample noise and parametric misspecification.

The four objects sit on a chain

$$\mathcal{M}^* \xrightarrow{\epsilon^{\text{hist}}} \mathcal{M}_{\text{obs}}^* \xrightarrow{\epsilon^h} \bar{\mathcal{M}}_{\text{calib}} \xrightarrow{\epsilon^m} \hat{\mathcal{M}}_{\text{sim}}, \quad (1)$$

with intermediate kernels

$$\begin{aligned} \rho_{\text{obs}}^*(s, a) &:= \mathbb{E}_{H \sim \mathbb{P}_t(\cdot | s)}[\bar{r}(s, a, H)], & \wp_{\text{obs}}^*(\cdot | s, a) &:= \mathbb{E}_{H \sim \mathbb{P}_t(\cdot | s)}[\wp_S(\cdot | s, a, H)], \\ \bar{\rho}_{\text{calib}}(s, a) &:= \mathbb{E}_{H \sim \mathbb{P}_{\text{calib}}(\cdot | s, a)}[\bar{r}(s, a, H)], & \bar{\wp}_{\text{calib}}(\cdot | s, a) &:= \mathbb{E}_{H \sim \mathbb{P}_{\text{calib}}(\cdot | s, a)}[\wp_S(\cdot | s, a, H)]. \end{aligned} \quad (2)$$

$$(3)$$

The three arrows correspond to three distinct sources of error.

- ϵ^{hist} (*Markov-projection error*): the cost of replacing the history-dependent $\mathbb{P}(H_t | \mathcal{H}_t)$ with the time- t Markov conditional $\mathbb{P}_t(H | S_t)$. Reduced by latent-dynamics contraction (Remark 1). Not reduced by any deployment-time intervention.
- ϵ^h (*calibration–deployment regime shift*): the cost of replacing $\mathbb{P}_t(H | S)$ with $\mathbb{P}_{\text{calib}}(H | S, A)$. This is the *drift* term named earlier — the gap between the deployment and calibration conditionals on H . Reduced by a randomized S -measurable pilot, which severs the calibration regime’s $H \rightarrow A$ edge (Lemma 2, Section 4). Not reduced by passive interaction.
- ϵ^m (*functional misspecification*): the cost of replacing $\bar{\mathcal{M}}_{\text{calib}}$ with the simulator’s actual finite-sample, possibly mis-specified output. Irreducible by any further interaction with the real world.

Randomization can pay down ϵ^h , cannot reach ϵ^m , and we set ϵ^{hist} aside on contraction grounds (Remark 1). By the triangle inequality, $|\hat{\rho}_{\text{sim}}(s, a) - \rho_{\text{obs}}^*(s, a)| \leq \epsilon_r^h(s, a) + \epsilon_r^m(s, a)$, with the analogous inequality for transitions; the per-component definitions of $\epsilon_r^h, \epsilon_r^m, \epsilon_p^h, \epsilon_p^m$ appear in Lemma 1.

Remark 1 (What ϵ^{hist} is, in one sentence). ϵ^{hist} is the price of treating the POMDP marginal over (S, A, R) as Markov on S alone: the (s, a) -sup distance between the exact history-dependent POMDP marginal and $\mathcal{M}_{\text{obs}}^*$. When the latent dynamics have a forgetting property — small differences in past hidden states wash out over time, formalized as a contracting Jacobian (spectral radius $\rho(L) < 1$ on the one-step spread operator) — ϵ^{hist} decays geometrically in horizon, $\epsilon^{\text{hist}} \leq \rho(L)^T \cdot \|H_0 - H_\infty\|_\infty$, where H_∞ is the latent-state fixed point. The analysis throughout this paper treats ϵ^{hist} as negligible relative to the calibration error ϵ^h and the misspecification residual ϵ^m on the right of (1). Non-contracting dynamics are returned to in Section 6.

The hidden-state distribution is taken to be stationary within an episode but may differ between episodes (e.g., calibration vs. deployment).

Assumptions. Four assumptions support the analysis. Three are housekeeping (tabular state, observability, conjugacy); the substantive one is Assumption 3 (calibration distribution), which is where the confounding bias enters.

Assumption 1 (Bounded rewards, finite tabular state). $\mathbb{S}, \mathbb{A}, \mathbb{H}$ are finite. $R_{i,t} \in [0, R_{\max}]$ almost surely. $\gamma \in [0, 1)$.

Assumption 2 (Observable-state policies). The planner’s policy at time t depends only on the observed history $\{S_{j,s}, A_{j,s}, R_{j,s}\}_{j, s \leq t}$. In particular, it does not condition on H .

Assumption 3 (Calibration distribution). The simulator was trained from trajectories collected under a behavior policy $\pi^{\text{beh}}(a | s, h)$ with $A \not\perp H | S$. This induces a calibration conditional $\mathbb{P}_{\text{calib}}(H | S, A)$ that differs from the deployment conditional $\mathbb{P}_t(H | S)$, so the simulator implicitly learns $\mathbb{E}[R | S, A]$ rather than $\mathbb{E}[R | S, \text{do}(A)]$ and inherits a confounding bias

$$\beta_{\text{conf}}(s, a) = \sum_h \bar{r}(s, a, h) [\mathbb{P}_{\text{calib}}(h | s, a) - \mathbb{P}_t(h | s)]$$

that does not shrink with more observational data of the same kind.

Assumption 4 (Conjugate independent priors). The planner’s prior on the parameters of $\mathcal{M}_{\text{obs}}^*$ factorises across (s, a) : a Gaussian prior on the reward parameter $\theta_{s,a}$ with variance $\sigma_{s,a}^{(0)2}$, and a Dirichlet prior on the transition $\wp_{\text{obs}}^*(\cdot | s, a)$ with total concentration $\alpha_{s,a}^{(0)} = \sum_{s'} \alpha_{s,a,s'}^{(0)}$.

Assumptions 1 and 2 are standard tabular and observability constraints. The function-approximation extension is left to future work (Section 6). Assumption 3 is the substantive one: it makes simulator

error *structural*, in the sense that no amount of further observational data of the same kind shrinks $\beta_{\text{conf}}(s, a)$. Assumption 4 gives closed-form posteriors and the block-diagonal Fisher form used in Section 4. The hierarchical extension is in Appendix C.18.

Value function and Bayes objective. For a policy π and an MDP $\mathcal{M} = (\rho, \wp)$ on \mathbb{S} , write

$$V^\pi(\mathcal{M}) := \mathbb{E}^{\pi, \mathcal{M}} \left[\sum_{t=0}^T \gamma^t \sum_i R_{i,t} \right]$$

for the discounted population value of running π on \mathcal{M} . We measure policy quality by the Bayes risk of $V^\pi(\mathcal{M}^*)$ over the prior \mathcal{P} of Assumption 4:

$$W(\pi) := \mathbb{E}_{\mathcal{M}^* \sim \mathcal{P}} [V^\pi(\mathcal{M}^*)] = \mathbb{E}_{\mathcal{M}^* \sim \mathcal{P}} \left[\mathbb{E}^{\pi, \mathcal{M}^*} \left[\sum_{t=0}^T \gamma^t \sum_i R_{i,t} \right] \right]. \quad (4)$$

The inner expectation is over the policy’s interaction with a single drawn world. The outer expectation averages over draws of the unknown world from the prior, which gives a single objective comparable across A-SOP and SEP. This is the standard Bayes-adaptive objective. Under Assumption 4 it reduces to the closed-form posterior recursion of posterior-sampling-style analyses [Osband et al., 2013, Russo et al., 2018].

Policy classes. Let \mathcal{F}_t denote the observed-history filtration, the sigma-algebra generated by $\{(S_{j,s}, A_{j,s}, R_{j,s}) : j \leq n, s \leq t\}$, and let b_t denote the conjugate posterior over \mathcal{M}^* started from the prior in Assumption 4 and updated from \mathcal{F}_t . Let $d_\pi(s) := (1 - \gamma) \sum_{t=0}^\infty \gamma^t \mathbb{P}_\pi(S_t = s)$ denote the discounted state-visitation distribution under π .

- Definition 1** (Policy classes). (i) Non-adaptive (Π_{na}): $\pi_t(\cdot \mid s)$ depends only on the current observed state and is fixed before any data is collected.
(ii) Passive-learning (Π_{passive}): stochastic policies $\pi_t(\cdot \mid S_t, b_t)$ measurable with respect to the observed state and the current Bayesian posterior b_t , with b_t updated from \mathcal{F}_t via the conjugate rules of Assumption 4.⁴
(iii) Adaptive (Π_{adapt}): the full class of history-dependent policies $\pi_t(\cdot \mid \mathcal{F}_t)$, including those that deliberately deviate from the posterior optimum to gather information.

The three classes correspond to three uses of observed data. The non-adaptive class ignores it. The passive class uses it to update beliefs but not to direct exploration. The adaptive class can use it for both. Whether to run a real-world experiment is the question of whether to leave Π_{passive} for Π_{adapt} , and at what cost. We define one named policy in each class.

Definition 2 (Simulator-optimal policy, SOP). $\pi_{\text{sim}}^* := \arg \max_{\pi \in \Pi_{\text{na}}} V^\pi(\hat{\mathcal{M}}_{\text{sim}})$. The SOP is trained on the simulator and deployed without updates from real-world data.

Definition 3 (Adaptive simulator-optimal policy, A-SOP). $\pi_{\text{sim}}^a := \arg \max_{\pi \in \Pi_{\text{passive}}} W(\pi)$, restricted to the posterior-mean-optimal subclass: at each t , the A-SOP plays the action a that maximizes the expected return under the posterior-mean MDP, $\pi_t(s) = \arg \max_a \mathbb{E}_{\mathcal{M} \sim b_t} [Q^{\mathcal{M}}(s, a)]$, where $Q^{\mathcal{M}}(s, a)$ is the state-action value under \mathcal{M} . The A-SOP takes the simulator as a Bayesian prior and updates from observed data without ever deliberately deviating from the posterior-mean-optimal action. Thompson sampling is the posterior-sampling instance of Π_{passive} . Neither deliberately deviates from the posterior; they differ in whether they sample from it or collapse to its mean.

Definition 4 (Simulation-aided experimental policy, SEP). A SEP is a policy in Π_{adapt} specified by a triple $(\mathcal{D}, \pi^{\text{explore}}, \pi^{\text{exploit}})$: a design criterion \mathcal{D} that scores exploration policies using $\hat{\mathcal{M}}_{\text{sim}}$, an explorer π^{explore} that optimizes \mathcal{D} , and an exploiter π_t^{exploit} that is posterior-mean-optimal under b_t . A SEP allocates a fraction of decisions to π^{explore} and the rest to π_t^{exploit} , choosing the fraction and the explorer’s distribution by minimizing \mathcal{D} . Section 4 fills in a concrete \mathcal{D} .

The SOP’s visitation distribution does not adapt. The A-SOP’s visitation distribution stays close to the SOP’s, since the A-SOP’s exploit action is posterior-mean-optimal and the posterior is anchored at the simulator. The SEP’s visitation distribution can move outside the SOP’s support by spending pilot budget on the explorer.

⁴Non-adaptive policies are the constant-belief subclass of passive-learning policies, so $\Pi_{\text{na}} \subseteq \Pi_{\text{passive}}$ holds by definition. The strict inclusion $\Pi_{\text{na}} \subsetneq \Pi_{\text{passive}}$ is witnessed by any policy with non-degenerate belief updates.

3 Value gap decomposition

A simulator's value error has two distinct components. The calibration data may have been collected under one regime while deployment lives in another, producing a regime shift that randomization can identify. Alternatively, the simulator's parametric family may not include the true kernel, producing a misspecification residual that no further interaction can remove. The two components look the same in aggregate but respond differently to a pilot. This section gives three results that separate them. Lemma 1 extends the simulation lemma to expose the calibration–deployment shift and the parametric residual as separate terms. Proposition 1 decomposes the value gap into a local part (on visited states) and a reachability part (on unvisited states). The reachability part is non-vacuous: a combination-lock construction in Appendix E exhibits an MDP on which it stays $\Omega(R_{\max})$ at any horizon. Proofs are in Appendix A.

3.1 Simulation lemma

The classical simulation lemma [Kearns and Singh, 2002] bounds the value loss when a planner deploys under the wrong MDP: if the model has per-pair reward error $\epsilon_r(s, a)$ (absolute difference in mean reward) and per-pair transition error $\epsilon_p(s, a)$ (total-variation distance in next-state distribution), then for any policy π , the values under model and truth differ by a weighted sum scaling linearly in the effective horizon $T_{\text{eff}} = 1/(1 - \gamma)$ for reward and quadratically ($\gamma R_{\max} T_{\text{eff}}^2$) for transitions. The classical bound treats ϵ_r and ϵ_p as monolithic. Lemma 1 splits each into a calibration–deployment piece ϵ^h , generated by the gap between $\mathbb{P}_{\text{calib}}(H | S, A)$ and $\mathbb{P}_t(H | S)$ (Section 2), and a misspecification residual ϵ^m that contains the remaining error.

Lemma 1 (Simulation lemma, structural decomposition). *Under Assumptions 1–3, let ρ_{obs}^* , \wp_{obs}^* , $\bar{\rho}_{\text{calib}}$, $\bar{\wp}_{\text{calib}}$ be the kernels defined in Section 2. Define*

$$\epsilon_r(s, a) := |\hat{\rho}_{\text{sim}}(s, a) - \rho_{\text{obs}}^*(s, a)|, \quad \epsilon_p(s, a) := \|\hat{\wp}_{\text{sim}}(\cdot | s, a) - \wp_{\text{obs}}^*(\cdot | s, a)\|_1.$$

By the triangle inequality through $\bar{\rho}_{\text{calib}}$ (resp. $\bar{\wp}_{\text{calib}}$), each splits as $\epsilon_r(s, a) \leq \epsilon_r^h(s, a) + \epsilon_r^m(s, a)$ and $\epsilon_p(s, a) \leq \epsilon_p^h(s, a) + \epsilon_p^m(s, a)$, where the calibration–deployment pieces are

$$\epsilon_r^h(s, a) := |\rho_{\text{obs}}^*(s, a) - \bar{\rho}_{\text{calib}}(s, a)|, \quad \epsilon_p^h(s, a) := \|\wp_{\text{obs}}^*(\cdot | s, a) - \bar{\wp}_{\text{calib}}(\cdot | s, a)\|_1,$$

and the misspecification residuals are

$$\epsilon_r^m(s, a) := |\hat{\rho}_{\text{sim}}(s, a) - \bar{\rho}_{\text{calib}}(s, a)|, \quad \epsilon_p^m(s, a) := \|\hat{\wp}_{\text{sim}}(\cdot | s, a) - \bar{\wp}_{\text{calib}}(\cdot | s, a)\|_1.$$

Writing $\epsilon_r := \max_{s,a} \epsilon_r(s, a)$ and $\epsilon_p := \max_{s,a} \epsilon_p(s, a)$, for any policy π depending on observed states only,

$$|V^\pi(\mathcal{M}_{\text{obs}}^*) - V^\pi(\hat{\mathcal{M}}_{\text{sim}})| \leq \frac{2}{1 - \gamma} (\epsilon_r^h + \epsilon_r^m) + \frac{2\gamma R_{\max}}{(1 - \gamma)^2} (\epsilon_p^h + \epsilon_p^m). \quad (5)$$

The decision to experiment depends on the ratio ϵ^h/ϵ^m , not on the absolute size of the simulator's error. When ϵ^m dominates, no pilot of any length reduces the value error. When ϵ^h dominates, randomization is informative. A randomized S -measurable pilot identifies ϵ^h at any pair it covers, since randomizing actions independently of H severs the calibration regime's $H \rightarrow A$ edge and recovers $\mathcal{M}_{\text{obs}}^*$ rather than $\mathcal{M}_{\text{calib}}$. The misspecification residual ϵ^m persists at every pair, since it lies in the simulator's parametric family rather than in the data.

Corollary 1 (Post-pilot finite-sample form). *Let $\mathcal{I} \subseteq \mathbb{S} \times \mathbb{A}$ be the pilot-covered pairs with $n_{s,a}$ samples at $(s, a) \in \mathcal{I}$ gathered under an S -measurable randomized pilot. Then there exist absolute constants $c_r, c_p > 0$ such that, for any policy π depending on observed states only, with probability at least $1 - \delta$,*

$$\begin{aligned} |V^\pi(\mathcal{M}_{\text{obs}}^*) - V^\pi(\hat{\mathcal{M}}_{\text{sim}})| &\leq \frac{2}{1 - \gamma} \left[\max_{(s,a) \in \mathcal{I}} c_r \sqrt{\frac{\log(1/\delta)}{n_{s,a}}} + \max_{(s,a) \notin \mathcal{I}} \epsilon_r^h(s, a) + \epsilon_r^m \right] \\ &\quad + \frac{2\gamma R_{\max}}{(1 - \gamma)^2} \left[\max_{(s,a) \in \mathcal{I}} c_p \sqrt{\frac{|\mathbb{S}| \log(1/\delta)}{n_{s,a}}} + \max_{(s,a) \notin \mathcal{I}} \epsilon_p^h(s, a) + \epsilon_p^m \right]. \end{aligned}$$

The corollary is the planner-facing form. At pilot-covered pairs, the calibration–deployment sup norm is replaced by a Hoeffding-style $O(1/\sqrt{n_{s,a}})$ rate for rewards and a Weissman-style $O(\sqrt{|\mathcal{S}|}/n_{s,a})$ rate [Weissman et al., 2003] for transitions. At uncovered pairs the original sup-norm bound is retained, and ϵ^m persists everywhere. The proof is Azuma–Hoeffding at each covered pair combined with (5); see Appendix A. The constants in (5) are those of Kearns and Singh [2002]. Lobel and Parr [2024] give a tighter constant in policy-dependent settings, which does not affect the per-pair Fisher-SEP ranking in Section 4 because that ranking is invariant to a common multiplicative factor.

Remark 2 (Horizon asymmetry). *With $T_{\text{eff}} = 1/(1 - \gamma)$ (the effective horizon, Section 2), the bound in (5) says the reward contribution is $O(T_{\text{eff}}\epsilon_r)$ and the transition contribution is $O(T_{\text{eff}}^2 R_{\text{max}}\epsilon_p)$. Their ratio $T_{\text{eff}}R_{\text{max}}\epsilon_p/\epsilon_r$ is a worst-case-over-MDPs diagnostic, not a point estimate of which error dominates on the specific deployment.*

The decomposition has two implications. Before any pilot is run, the structural split bounds the value gain achievable from experimentation. When ϵ^m dominates, the bound is small and a pilot is not warranted on value-of-experimentation grounds. The simulator’s stated prior parameters $\sigma^{(0)}$ and $\alpha^{(0)}$ in Assumption 4 bound the planner’s posterior uncertainty, but they do not estimate ϵ_r or ϵ_p themselves. After a short pilot, the residual ratio $\hat{\epsilon}_p/\hat{\epsilon}_r$ at covered pairs is estimable from post-pilot residuals (Appendix B). This ratio determines whether the local or reachability regime applies.

3.2 Local and reachability gaps

The three policy classes from Section 2 carry the next result: Π_{na} (the SOP), Π_{passive} (the A-SOP), Π_{adapt} (any SEP). We call $\text{supp}(d_\pi)$ the *visitation support* of π , the set of states π visits with positive discounted probability — the formal name for what the introduction’s contributions block called the set of states the deployed policy visits. The proposition says two things: $W(\cdot)$ is monotone across the three classes, and the design gap \mathcal{G} — the value attainable by introducing experimental design, relative to the SOP — splits cleanly by visitation support.

Proposition 1 (Dominance chain and gap decomposition). *Under Assumptions 1–4,*

$$\sup_{\pi \in \Pi_{\text{na}}} W(\pi) \leq \sup_{\pi \in \Pi_{\text{passive}}} W(\pi) \leq \sup_{\pi \in \Pi_{\text{adapt}}} W(\pi).$$

Let $\Pi_{\text{SEP}} \subset \Pi_{\text{adapt}}$ be the SEP class of Definition 4. Write $W_{\text{na}}^ = W(\pi_{\text{sim}}^*)$ and $W_{\text{SEP}}^* = \sup_{\pi \in \Pi_{\text{SEP}}} W$, and let $\Pi_{\text{SEP}}^{\text{loc}} := \{\pi \in \Pi_{\text{SEP}} : \text{supp}(d_\pi) \subseteq \text{supp}(d_{\pi_{\text{sim}}^*})\}$ be the SEPs whose visitation support is contained in the SOP’s. The design gap $\mathcal{G} := W_{\text{SEP}}^* - W_{\text{na}}^* \geq 0$ decomposes as $\mathcal{G} = \mathcal{G}_{\text{local}} + \mathcal{G}_{\text{reach}}$, with*

$$\mathcal{G}_{\text{local}} := \sup_{\pi \in \Pi_{\text{SEP}}^{\text{loc}}} W(\pi) - W_{\text{na}}^* \geq 0, \quad \mathcal{G}_{\text{reach}} := \mathcal{G} - \mathcal{G}_{\text{local}} \geq 0. \quad (6)$$

$\mathcal{G}_{\text{local}}$ is the value attainable by an explorer whose visitation support coincides with the SOP’s, by choosing different actions at states the SOP already visits. The A-SOP closes this term asymptotically: at visited states, online data shrinks the posterior, and once the posterior places the optimal action on the correct alternative the A-SOP matches it. $\mathcal{G}_{\text{reach}}$ is the value attainable only by visiting states outside the SOP’s visitation support. It is invisible to passive learning, since evidence at an unvisited (s, a) is generated only by an action with zero probability under the posterior-mean-optimal policy.

The decomposition mirrors the within- versus out-of-positivity distinction in causal inference. The local gap is the *within-positivity* case: the deployed policy already produces evidence at every relevant (s, a) , so the inference problem is one of waiting for enough samples. The reachability gap is the *out-of-positivity* case: the relevant (s, a) pairs lie outside the deployed policy’s support and produce *no* evidence under it, so no amount of waiting helps. Recall that *positivity* requires every action to have nonzero probability under the data-generating mechanism at every covariate value [Pearl, 2009]; the analog here is that every state has positive discounted visitation under the deployed policy. Any policy that closes the reachability gap must deliberately visit states outside the deployed policy’s visitation support [Parikh et al., 2024a, 2025b]. The simulator’s prior provides the extrapolation outside the SOP’s support, and Section 4 uses that prior to choose where the extrapolation is informative enough to act on. The inequalities in (6) are weak in general; the reachability-separation construction in Appendix E (Theorem 6) shows that on a concrete MDP the reachability part is bounded away from zero, summarized below.

Remark 3 (Which gap dominates). *Under the horizon asymmetry of Remark 2, $\mathcal{G}_{\text{local}}$ is driven mostly by reward errors (a wrong action at a visited state costs one period of suboptimal payoff), and $\mathcal{G}_{\text{reach}}$ is driven mostly by transition errors (a wrong belief about where an action leads redirects the trajectory).*

The reachability term $\mathcal{G}_{\text{reach}}$ is non-vacuous. Appendix E (Theorem 6) constructs a deterministic combination-lock MDP — a chain in which the simulator gets every transition right except at the terminal state, where it underestimates the reward by a multiplicative factor $\eta < 1$ — on which $\mathcal{G}_{\text{reach}} \geq (1 - \eta)R_{\text{max}}$ for any $T_{\text{eff}} \geq k$, with k the chain length. The bound is independent of horizon: when the simulator’s miscalibration is concentrated on states the deployed policy never reaches, the gap is not closed by additional online interaction at any horizon. A directed explorer that allocates $\Omega(k)$ exploratory steps to the terminal state recovers the gap up to $o(1)$. A class-level extension to stochastic transitions is conjectured (Conjecture 2, Appendix E.7); it is established for posterior-mean-optimal policies, bounded-temperature softmax, polynomial-shrinkage upper-confidence-bound (UCB) policies, and Thompson sampling under Assumption 4, with the unconditional case open.

Section 4 turns to the design question: which experimental policy minimizes posterior uncertainty about the target policy’s value, given a fixed pilot budget?

4 Fisher-information design

Section 3 shows that the reachability gap closes only when the simulator is used to choose where to experiment. This section specifies a Bayesian design criterion \mathcal{D} for the SEP class of Definition 4: a posterior predictive variance of a target policy’s value. We name the SEP that minimizes this criterion *Fisher-SEP* (Definition 5), and identify two natural specializations.

4.1 Posterior predictive value variance

The criterion to minimize is the posterior variance of a chosen target policy’s value, rather than the variance of every parameter. Designs that target overall parameter variance, such as A-optimal design (which minimizes the trace of the inverse Fisher of all parameters and so weights every parameter equally) [Chaloner and Verdinelli, 1995, Pukelsheim, 2006], allocate pilot budget to parameters whose perturbations do not change the deployed value. Regret-minimization explorers such as ϵ -greedy (which explores by random action) treat all unknowns as exchangeable and do not distinguish local from reachability errors. We propose a target-policy-aware criterion: weight each parameter by how much it would change the deployed policy’s value if perturbed. Parameters that do not affect a target policy’s value contribute nothing to the target-policy posterior variance, so allocating pilot effort to them is wasteful. The value gradient $\nabla_{\theta} V^{\pi^{\text{tgt}}}$ summarizes which parameters affect the value of the target policy π^{tgt} , and its squared entries give the rate at which a parameter error at (s', a') propagates into a value error.

We use the label *posterior predictive value variance* (PVV) because the quantity measures prediction error on $V^{\pi^{\text{tgt}}}$. Strictly, it is the posterior variance of the target-policy value functional, not a predictive variance over observables. Recall that the *delta method* approximates the posterior variance of a smooth functional $V(\theta)$ as $(\nabla_{\theta} V)^{\top} \text{Cov}(\theta) \nabla_{\theta} V$, valid when the posterior on θ is approximately Gaussian; under that approximation, the posterior variance of $V^{\pi^{\text{tgt}}}$ and a predictive variance over observables agree (Theorem 3, Appendix A).

Definition 5 (Posterior predictive value variance, PVV; Fisher-SEP). *The criterion operates with a target policy π^{tgt} (held fixed) and an explorer policy π (the argmin variable). The parameter vector at (s', a') stacks the reward parameter $r_{s', a'} := \rho_{\text{obs}}^*(s', a')$, the interventional mean reward under $\mathcal{M}_{\text{obs}}^*$ identified by a randomized S-measurable pilot (Lemma 2), and the transition vector $p_{s', a'} := \varphi_{\text{obs}}^*(\cdot | s', a') \in \Delta(\mathbb{S})$, as $\theta_{s', a'} := (r_{s', a'}, p_{s', a'})$. Under Assumption 4, the prior covariance is block-diagonal,*

$$\Sigma_{\theta}(s', a') := \text{blkdiag}\left((\sigma_{s', a'}^{(0)})^2, \Sigma_p(s', a')\right), \quad (7)$$

with reward block $(\sigma_{s', a'}^{(0)})^2$ from Assumption 4 and transition block $\Sigma_p(s', a') = (\alpha_{s', a'}^{(0)})^{-1}(\text{diag}(p_0) - p_0 p_0^{\top})$, the Dirichlet prior covariance on the simplex tangent at the prior

mean $p_0 := \alpha_{s',a'}^{(0)}/\alpha_{s',a'}^{(0)}$. Recall that the Fisher information of an observation likelihood quantifies how much each observation tells us about a parameter; concretely, it is the expected outer product of the score $\partial \log p(R, S' | s', a', \theta)/\partial \theta$. Larger Fisher information means more information per observation, so the posterior contracts faster. We write $\mathcal{I}_\theta^{\text{int}}(s', a')$ for the per-observation interventional Fisher information, the Fisher of the interventional likelihood $\mathbb{P}(\cdot | s', \text{do}(a'))$ identified from a randomized S -measurable pilot (Lemma 2), as opposed to the observed-data Fisher under the behavior policy, which is biased under $A \not\perp H | S$ (Assumption 3; Appendix A.8 makes the distinction precise). It is also block-diagonal,

$$\mathcal{I}_\theta^{\text{int}}(s', a') := \text{blkdiag}(\tau_{s',a'}^{\text{int}}, \mathcal{I}_p^{\text{int}}(s', a')), \quad (8)$$

with reward block $\tau_{s',a'}^{\text{int}} := \text{Var}(R | s', \text{do}(a'))^{-1}$ the inverse interventional reward variance and transition block $\mathcal{I}_p^{\text{int}}(s', a') = \text{diag}(p_{s',a'})^{-1}$ projected onto the simplex tangent at $p_{s',a'}$. The expected pilot count at (s', a') is $n_{s',a'}(\pi) := T \cdot d_\pi(s') \cdot \pi(a' | s')$. The PVV criterion is

$$\text{PVV}(\pi; \pi^{\text{tgt}}) := \sum_s d_{\pi^{\text{tgt}}}(s) \sum_{(s', a')} \nabla_\theta V^{\pi^{\text{tgt}}}(s)^\top [\Sigma_\theta(s', a')^{-1} + n_{s',a'}(\pi) \mathcal{I}_\theta^{\text{int}}(s', a')]^{-1} \nabla_\theta V^{\pi^{\text{tgt}}}(s). \quad (9)$$

The joint gradient $\nabla_\theta V^{\pi^{\text{tgt}}}(s) = (\partial V^{\pi^{\text{tgt}}}(s)/\partial r_{s',a'}, \nabla_{p(\cdot|s',a')} V^{\pi^{\text{tgt}}}(s))$ stacks a scalar reward sensitivity and a $|\mathbb{S}|$ -vector transition sensitivity. Both are supplied by the Bellman resolvent $(I - \gamma P^{\pi^{\text{tgt}}})^{-1}$, where $P^{\pi^{\text{tgt}}}$ is the $|\mathbb{S}| \times |\mathbb{S}|$ transition matrix induced on \mathbb{S} by the target policy π^{tgt} — entries $P^{\pi^{\text{tgt}}}(s' | s) = \sum_a \pi^{\text{tgt}}(a | s) \wp_{\text{obs}}^*(s' | s, a)$ — and the resolvent's (s, s') entry is the expected discounted number of visits to s' when π^{tgt} starts from s (by the geometric series $(I - \gamma P^{\pi^{\text{tgt}}})^{-1} = \sum_{k=0}^{\infty} \gamma^k (P^{\pi^{\text{tgt}}})^k$, valid because $\gamma < 1$). Fisher-SEP is the SEP whose design criterion is PVV: $\mathcal{D} := \text{PVV}(\cdot; \pi^{\text{tgt}})$, with $\pi^* = \arg \min_\pi \text{PVV}(\pi; \pi^{\text{tgt}})$ over stochastic explorers.

The expression in (9) is a delta-method posterior variance for $V^{\pi^{\text{tgt}}}$. The outer sum, weighted by $d_{\pi^{\text{tgt}}}(s)$, is over states the target visits. The inner sum is over candidate pilot pairs (s', a') . At each pair the contribution is a quadratic form in the value gradient, weighted by the inverse posterior precision $\Sigma_\theta^{-1} + n \mathcal{I}_\theta^{\text{int}}$. Pairs whose value-gradient contribution is small contribute little to the criterion. Pairs with large contribution dominate. The block-diagonal structure separates the contribution into reward and transition pieces.

Note that π enters PVV only through the pilot counts $n_{s',a'}(\pi)$ inside the block inverse. The value gradient and the target visitation are properties of π^{tgt} alone and are fixed once the target policy is chosen. PVV is convex in $n(\pi)$, since the inverse of an increasing positive-definite matrix is matrix-decreasing, so the minimization is well-posed and admits a closed-form first-order optimum on the simplex of explorer visitation distributions (Appendix B).

Block-diagonality of $\mathcal{I}_\theta^{\text{int}}$ comes from the MDP factorization $\mathbb{P}(R, S' | s, a, h) = \rho(R | s, a, h) \wp_S(S' | s, a, h)$: under intervention, reward and next-state are conditionally independent given (s, a, h) , and S -measurability of the pilot preserves the independence after marginalizing over h . The corresponding observed-data Fisher under the behavior policy does not block-diagonalize, since marginalizing over H couples the two likelihoods. This is the consequence of $A \not\perp H | S$ (Assumption 3). Identification therefore requires a randomized S -measurable pilot.

Corollary 2 (Fisher-SEP-R, reward-dominates special case). *When the transition block of $\Sigma_\theta(s', a')$ is pre-pinned at every (s', a') on the target's support (either because transitions are known given action, or because the target's value is insensitive to transition perturbations at those pairs beyond what the reward gradient already captures), the transition-block contribution to (9) vanishes and the block inverse decomposes. The joint PVV reduces to*

$$\text{PVV}_r(\pi; \pi^{\text{tgt}}) = \sum_s d_{\pi^{\text{tgt}}}(s) \sum_{(s', a')} \frac{\left(\partial V^{\pi^{\text{tgt}}}(s)/\partial r_{s',a'}\right)^2}{(\sigma_{s',a'}^{(0)})^{-2} + n_{s',a'}(\pi) \tau_{s',a'}^{\text{int}}}, \quad (10)$$

the sum of prior and pilot-observation precisions, inverted per (s', a') .

Corollary 3 (Fisher-SEP-T, transition-dominates special case). *When the reward block of $\Sigma_\theta(s', a')$ is pre-pinned by an exact observation model, or the reward-gradient block is dominated by the*

transition-gradient block at the horizon scale T_{eff} , the reward-block contribution to (9) vanishes. The joint PVV reduces to

$$\text{PVV}_p(\pi; \pi^{\text{tgt}}) = \sum_s d_{\pi^{\text{tgt}}}(s) \sum_{(s', a')} \nabla_{p(\cdot|s', a')} V^{\pi^{\text{tgt}}}(s)^\top \left[\Sigma_p(s', a')^{-1} + n_{s', a'}(\pi) \mathcal{I}_p^{\text{int}}(s', a') \right]^{-1} \nabla_{p(\cdot|s', a')} V^{\pi^{\text{tgt}}}(s), \quad (11)$$

with Bellman-resolvent gradient (an $|\mathbb{S}|$ -vector indexed by the destination s'')

$$\left[\nabla_{p(\cdot|s', a')} V^{\pi^{\text{tgt}}}(s) \right]_{s''} = \gamma \left[(I - \gamma P^{\pi^{\text{tgt}}})^{-1} \right]_{s, s'} \cdot \pi^{\text{tgt}}(a' | s') \cdot V^{\pi^{\text{tgt}}}(s'').$$

The two specializations correspond to the two case-study regimes. Fisher-SEP-R applies when transitions are well-calibrated (e.g., physics-pinned dynamics) and reward parameters carry the residual error. Fisher-SEP-T applies when transitions encode geography or accessibility and reward parameters are pinned by an exact observation model. The *navigation-restricted* variant of Fisher-SEP-T constrains the explorer to actions whose target-policy transitions are reachable in the environment graph; this is the variant used in the HIV case study (Section 5.2) and analyzed formally in Appendix D.13 (Conjecture 1 bounds the navigation-restricted PVV gap to the unrestricted minimizer by an overlap constant; Theorem 5 establishes the bound on a regular subclass).

Remark 4 (Explore under ignorance). *For any (s', a') with $n_{s', a'}(\pi) = 0$ and $\nabla_\theta V^{\pi^{\text{tgt}}}(s) \neq 0$ for some s in the target's support, the contribution to $\text{PVV}(\pi; \pi^{\text{tgt}})$ is*

$$\sum_s d_{\pi^{\text{tgt}}}(s) \cdot \nabla_\theta V^{\pi^{\text{tgt}}}(s)^\top \Sigma_\theta(s', a') \nabla_\theta V^{\pi^{\text{tgt}}}(s), \quad (12)$$

which is positive and finite whenever the prior covariance $\Sigma_\theta(s', a')$ has positive mass. Any π' with $n_{s', a'}(\pi') > 0$ strictly reduces it.

Fisher-SEP therefore allocates pilot budget to pairs that are target-relevant but explorer-unvisited, even when the simulator's prior is tight on mean (small Σ_θ) but weak in observation precision (small $\tau_{s', a'}^{\text{int}}$). This is the difference between Fisher-SEP and a regret-minimization explorer: Fisher-SEP can prioritize an (s', a') at which the simulator's prior is narrow, provided the target's value gradient at that pair is large. Pilot budget is allocated where small parameter errors propagate into large value errors, not where the prior variance is widest.

4.2 Identification and exploration priority

Computing PVV requires the per-pair observation precision $\tau_{s, a}^{\text{int}}$, the inverse interventional reward variance. The empirical reward variance under the historical behavior policy is biased under $A \not\perp H | S$ (Assumption 3). A randomized S -measurable pilot identifies the interventional precision instead.

Lemma 2 (Identification from S -measurable randomized policies). *Under Assumption 2, if $\pi^{\text{exp}}(a | s, h) = \pi^{\text{exp}}(a | s)$ for all h , then reward samples at (s, a) under π^{exp} are marginally identically distributed as $R \sim \mathbb{P}(\cdot | s, \text{do}(a))$, independent across units (within a unit, samples may be auto-correlated through $H_{i, t}$). The empirical reward variance consistently estimates $(\tau_{s, a}^{\text{int}})^{-1}$.*

The recipe is short. A fraction of decisions is allocated to a randomized S -measurable explorer $\pi^{\text{exp}}(a | s)$. The empirical reward variance at each (s, a) pair is consistent for $1/\tau_{s, a}^{\text{int}}$. Note that this identification depends on π^{exp} being S -measurable: if the explorer conditioned on H , the empirical variance would estimate $\text{Var}_{\pi^{\text{beh}}}(R | s, a)$ instead, with bias bounded by a propensity-odds sensitivity constant (the worst-case ratio of historical-behavior to randomized propensity at (s, a) ; Appendix A).

Remark 5 (EPI as a per- (s, a) readout). *A per- (s, a) version of PVV's contribution in the data-starved limit gives an Exploration Priority Index, useful as a diagnostic. In reward-variance units so the ranking is invariant to reward rescaling,*

$$\text{EPI}(s, a) = d_{\pi_{\text{sim}}^*}(s) \cdot \left[\frac{(\sigma_{s, a}^{(0)})^2 + \hat{\beta}_{\text{conf}}(s, a)^2}{R_{\text{max}}^2} + \frac{\gamma(|\mathbb{S}| - 1)}{(1 - \gamma)\alpha_{s, a}^{(0)}} \right].$$

Both terms are dimensionless. $\hat{\beta}_{\text{conf}}(s, a)$ is estimated post-pilot as $|\hat{\rho}_{\text{sim}}(s, a) - \hat{\rho}_{\text{pilot}}(s, a)|$ at covered pairs, with a conservative upper bound elsewhere (Appendix B). PVV remains the primary prescription. The EPI is a per- (s, a) readout, useful for diagnosis and debugging the prescription, not for replacing it.

The two terms separate the sources of uncertainty PVV reduces. The first combines the prior reward variance with the squared estimated confounding bias. The second is a transition-uncertainty term scaling as the effective horizon T_{eff} and the simplex tangent dimension. The factor $d_{\tau_{\text{sim}}^*}(s)$ weights by SOP visitation, so unvisited states contribute zero and high-traffic states are ranked higher.

5 Case studies

Two case studies anchor the local and reachability regimes. A vending-machine supply chain instantiates the local regime: every machine is reachable, the simulator’s error is a miscalibration at visited states, and the question is whether a deliberate pilot pays for itself before the horizon ends. An HIV mobile-testing program instantiates the reachability regime: a corridor cell separates a well-calibrated region from a region the simulator never sampled, and the question is whether a planner anchored to the simulator ever crosses the corridor. Both are constructed mechanism illustrations, not calibrated deployments. The vending data-generating process (DGP) draws seasonality from Singh [2022] but is otherwise synthetic. The HIV DGP draws SIS dynamics from Gonsalves et al. [2018], Warren et al. [2025] on a stylized 5×8 grid.

Comparators are as follows. The *oracle* acts optimally given the hidden state H and serves as the upper benchmark. *SOP* and *A-SOP* are defined in Section 2. *Thompson sampling* (Posterior Sampling for Reinforcement Learning, PSRL, Osband et al. [2013], Russo et al. [2018]) samples one MDP from the posterior at each step and acts greedily. *Fisher-SEP-R* and *Fisher-SEP-T* are the reward-only and transition-only specializations of Fisher-SEP (Section 4, Corollaries 2 and 3); the HIV case study uses the navigation-restricted variant of Fisher-SEP-T introduced after Corollary 3. *UCRL2* [Jaksch et al., 2010] and *UCBVI* [Azar et al., 2017] are optimism-based regret-minimization baselines run on a coarser 2×2 state representation, included as a representation-handicapped reference rather than a representation-matched comparison (Appendix C.16). Values are reported as means over 30 *common-seed trials* (paired evaluation on the same environment realization), with \pm marking the half-width of the marginal 95% confidence interval (CI). Headline separations use the paired Wilcoxon signed-rank test on per-seed differences, and values are reported in *percentage points* (pp) of the oracle’s value.

5.1 Vending-machine supply chain

An operator runs five vending machines, each stocking three product categories across three customer segments. The historical operator observed a latent demand multiplier $H_{i,t}$ at each machine and conditioned stocking on it, yielding $A \not\perp H \mid S$ (Assumption 3). The simulator captures only 39–47% of true demand at two of the five machines, with the under-calibration concentrated on a high-demand segment that historically had concentrated stocking. Observations are censored: the planner sees $\min(\text{demand}, \text{stock})$, so stock-outs at under-calibrated machines suppress observations of true demand at exactly those machines. The simulator’s error is on the reward side and at visited states. Policies are evaluated at $T \in \{100, 200, 400, 800, 1600\}$ days. The full DGP is in Appendix 3.2.

Table 1 reports value as a percentage of oracle cash. The SOP degrades from 89.0% at $T = 100$ to 37.7% at $T = 1600$, consistent with Lemma 1. A-SOP and Thompson sampling close the local gap by updating off the SOP’s path. Both reach about 70% at $T = 1600$ and are statistically indistinguishable in paired tests. Fisher-SEP-R incurs a short-horizon cost from front-loaded randomization (76.6% at $T = 100$), reaches parity at $T = 800$, and at $T = 1600$ leads A-SOP by +4.83 pp ($p = 0.005$) and Thompson by +3.92 pp ($p = 0.008$).

After a five-day randomized pilot (the first five days of Fisher-SEP-R’s exploration phase, in which the explorer mixes uniformly over actions to identify $\tau_{s,a}^{\text{int}}$ at covered pairs by Lemma 2), the residual ratio $\hat{\epsilon}_p/\hat{\epsilon}_r$ at the under-calibrated machines is approximately 2 to 3 (Appendix B.5). Combining this with the post-pilot Corollary 1 places the predicted Fisher-SEP-R crossover at $T \approx 400\text{--}600$, consistent with the observed crossover between $T = 400$ and $T = 800$. This is an in-sample descriptive consistency check, not a held-out validation. The pattern matches Remark 3: at short horizons the reward-error term $T_{\text{eff}}\epsilon_r$ dominates and A-SOP closes it on the SOP’s path; at long horizons the transition-error term $T_{\text{eff}}^2 R_{\text{max}}\epsilon_p$ dominates and Fisher-SEP-R’s front-loaded pilot is amortized over enough exploitation steps to repay the cost.

Table 1: Vending supply chain, % of oracle cash (mean \pm 95% CI half-width, 30 common-seed trials). Bold: best non-oracle policy per horizon. DGP in Appendix 3.2.

Policy	$T=100$	$T=200$	$T=400$	$T=800$	$T=1600$
Oracle	100.0 \pm 1.2	100.0 \pm 1.8	100.0 \pm 2.5	100.0 \pm 4.1	100.0 \pm 3.7
SOP	89.0 \pm 0.9	78.8 \pm 1.2	66.8 \pm 1.6	48.6 \pm 2.1	37.7 \pm 1.9
A-SOP	89.0 \pm 0.9	82.2 \pm 1.3	75.6 \pm 2.0	66.8 \pm 3.3	70.7 \pm 4.1
Thompson (PSRL)	88.5 \pm 1.3	82.6 \pm 1.8	76.6 \pm 2.8	68.6 \pm 2.7	71.2 \pm 3.4
Fisher-SEP-R	76.6 \pm 1.7	73.2 \pm 2.5	68.5 \pm 3.7	68.8 \pm 4.8	75.3 \pm 6.5
UCRL2	88.7 \pm 1.1	77.5 \pm 1.4	63.0 \pm 2.2	62.5 \pm 5.6	70.3 \pm 7.1
UCBVI	84.0 \pm 1.3	75.1 \pm 2.1	64.0 \pm 2.8	65.2 \pm 5.3	73.1 \pm 6.5

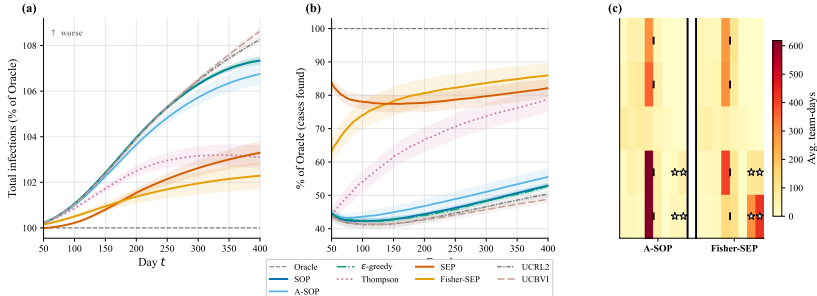


Figure 2: HIV mobile-testing program (30 common-seed trials, ± 2 standard error (SE) bands). **(a)** Total active infections as % of oracle (higher is worse): SOP and A-SOP let the outbreak grow; navigation-restricted Fisher-SEP-T contains it within 30 days. **(b)** Cumulative cases found: Fisher-SEP-T reaches 85.2% at $T = 400$; A-SOP plateaus near 58%; Thompson partly closes the gap via posterior-sample exploration but trails Fisher-SEP-T. **(c)** Visitation heatmaps: A-SOP stays in Region A; Fisher-SEP-T crosses the corridor within days.

5.2 HIV mobile-testing program

A mobile testing program operates over a 5×8 grid with eight testing teams per day. A wall with a single corridor cell splits the grid into two regions. Region A is well-surveilled. Region B is peri-urban (an under-surveilled region) and requires a three-day community-engagement warmup before testing yields can be realized [Gonsalves et al., 2018, Warren et al., 2025]. Disease dynamics follow an SIS (Susceptible-Infected-Susceptible) compartmental model. The hidden state $H_{i,t}$ is each cell’s true active-infection prevalence. Region B contains a previously-unsampled cluster (a “hidden cluster” in the sense that the simulator’s training data never reached it) with true prevalence 30%. The simulator, calibrated from clinic-based surveillance that never sampled Region B, estimates Region-B prevalence at 2%. The simulator’s error is concentrated outside the SOP’s visitation support, the $\mathcal{G}_{\text{reach}}$ regime of Proposition 1. Policies are evaluated at $T \in \{50, 100, 200, 300, 400\}$ days. The full DGP, including a magnitude ablation that sweeps the Region-B underestimate from $5 \times$ to $30 \times$, is in Appendix D.

Figure 2 shows infection containment (panel a), cumulative cases found (panel b), and per-zone visitation heatmaps (panel c). Active infections grow under SOP and A-SOP, neither of which crosses the corridor in time. Navigation-restricted Fisher-SEP-T contains the outbreak within 30 days. Cumulative cases plateau for A-SOP at 58.1% of oracle at $T = 400$, with corridor-crossing rate below 5% over a 400-day deployment. Thompson reaches 76.9% as occasional high posterior draws push some teams across. Fisher-SEP-T reaches 85.2%. Panel (c) shows the visitation heatmaps. A-SOP’s visitation is concentrated in Region A. Fisher-SEP-T’s visitation crosses the corridor within days.

The headline separations at $T = 400$ are: Fisher-SEP-T – A-SOP, +27.1 pp ($p < 10^{-3}$); Fisher-SEP-T – Thompson, +8.3 pp ($p = 0.003$); Fisher-SEP-T – optimism baselines, +34.8 pp on the coarser 2×2 representation. UCRL2 and UCBVI cross the corridor in 80–87% of trials but plateau, since they do not prioritize *which* corridor crossings carry the most target-relevant information. They

treat all unvisited cells equally. We leave a *navigation-matched* Thompson variant — Thompson sampling restricted to the same navigation graph that Fisher-SEP-T’s navigation-restricted explorer uses — to future work.

Remark 4 explains the mechanism. Although the simulator’s prior at Region-B cells is concentrated (it predicts 2% prevalence with high confidence), the target’s value gradient at those cells is non-trivial: SIS dynamics couple the two regions through the Bellman resolvent, so errors in the Region-B prevalence estimate propagate to Region-A’s near-term infection-load forecast. Fisher-SEP-T responds to this gradient through the explore-under-ignorance contribution (12) of Remark 4. A-SOP, anchored at the posterior mean, does not. Thompson partially closes the gap because occasional high posterior draws send some teams through the corridor. The residual 8.3 pp gap to navigation-restricted Fisher-SEP-T reflects the cost of using the simulator as a sampling distribution rather than to choose where to experiment.

The same reasoning applies more broadly. When a simulator’s miscalibration is concentrated at unreachable states, the gap is not closed by additional online interaction at any horizon: the unreachable states never produce evidence, so there is no asymptotic rate to wait out. Even when the simulator is $15\times$ off on Region-B prevalence, Fisher-SEP-T finds the cluster, since the Bellman resolvent in the value gradient depends on the simulator’s connectivity pattern rather than on its parameter values.

6 Discussion

The local-reachability decomposition is the central observation of this paper. The simulator’s value gap, relative to the deployment-time projection, splits into a local part on states that the deployed policy already visits and a reachability part on states it does not. The two parts respond differently to additional data. Passive online updating closes the local part, since the deployed policy continues to generate evidence at visited states. Closing the reachability part requires deliberate exploration, since the evidence required to identify the relevant parameters is generated only by actions that lie outside the support of the deployed policy. Fisher-SEP allocates a real-world pilot to minimize the posterior predictive variance of a target policy’s value, using the simulator as a Bayesian prior over how parameter errors propagate.

The decomposition mirrors the within-positivity versus out-of-positivity distinction in causal inference (Section 3). The local gap is a within-positivity inference problem: the deployed policy already produces evidence at every relevant (s, a) . The reachability gap is an out-of-positivity one: the relevant (s, a) pairs lie outside the deployed policy’s support and produce no evidence under it. Online updating treats the latter as a slow version of the former, but Theorem 6 (with Conjecture 2 on a regular subclass) shows that the difference is structural rather than asymptotic. The reachability gap is bounded away from zero on the combination-lock construction at any horizon, and the off-fork visitation probability under any passive learner decays geometrically in chain length on the regular subclass studied in Appendix E.7. The implication for causal inference is that no amount of additional observational data identifies a state-action pair outside the deployed policy’s support [Parikh et al., 2024a, 2025b].

Two consequences follow. The horizon trade-off (Remark 3, Table 1) — whether the horizon is long enough for passive learning to amortize a pilot — applies only to the local component. On the reachability side, horizon is not the right axis. When the gap is dominated by reachability, increasing T does not amortize the pilot against passive learning, because passive learning never reaches the relevant states. The right diagnostic is not the magnitude of the simulator’s error but where that error sits relative to the deployed policy’s visitation. The residual ratio $\hat{\epsilon}_p/\hat{\epsilon}_r$ at covered pairs (Appendix B.5) addresses the local side. The Exploration Priority Index (Remark 5) is the per-pair readout for the reachability side.

Fisher-SEP is not an algorithm for producing a more accurate simulator. It changes how the simulator is used. The sim-to-real literature trains policies inside a simulator and deploys them outside [Tobin et al., 2017, Wagenmaker and Jamieson, 2024, Memmel et al., 2024]. Fisher-SEP uses the same simulator as a Bayesian prior on how parameter errors propagate to target value, then allocates real-world evidence accordingly. The key technical object is the Bellman resolvent $(I - \gamma P^{\pi^{\text{tgt}}})^{-1}$ in the gradient of Definition 5: it summarizes which states reach which others under the target policy, and PVV weights the simulator’s prior covariance at (s', a') by that propagation factor.

This is why Fisher-SEP performs well even when the simulator’s parameter values are far from accurate at unvisited states. In the HIV case study the simulator is $15\times$ off on Region-B prevalence, and Fisher-SEP-T still finds the cluster, since the resolvent gradient depends on the simulator’s connectivity rather than on its parameter values. The framework’s requirement on the simulator is therefore weaker than the sim-to-real literature’s: the simulator need not be accurate, but its connectivity pattern on the target’s visitation must be approximately correct.

Thompson sampling closes part of the reachability gap because occasional high posterior draws send teams across the corridor in the HIV case study. Empirically this gives a $+18.8$ pp lift over A-SOP at $T = 400$ (Thompson reaches 76.9% of oracle, A-SOP plateaus at 58.1%). Thompson is not a representation-matched competitor for Fisher-SEP, however. It samples target and explorer from the same posterior, does not respect a navigation restriction, and pays full posterior-sample variance for every parameter, including those whose perturbations do not change the target’s value. Fisher-SEP-T leads Thompson by $+8.3$ pp at $T = 400$ (85.2% of oracle), which reflects the cost of using the simulator as a sampling distribution rather than to choose where to experiment. Appendix E.7, Remark 26 shows that Thompson sampling satisfies the asymptotic $o(1)$ claim of Conjecture 2 on a regular subclass, with rate governed by p^* . We leave a navigation-matched Thompson variant to future work.

Limitations and future work

The framework is tabular with finite latent state. Lemma 1 extends conceptually to function approximation by replacing the sup-norm with appropriate function-space norms, but the closed-form posterior in Assumption 4 does not. A Gaussian-process or Bayesian-neural-network treatment of the parameter posterior is the natural successor. The technical challenge is computing $\nabla_{\theta} V^{\pi^{\text{tgt}}}$ when θ is infinite-dimensional.

A natural further question is which minimal assumptions on the simulator preserve Fisher-SEP’s usefulness, and how to diagnose their failure online. The post-pilot residual diagnostic (Appendix B.5) is a starting point. A more general representation-mismatch test that detects misspecification before the pilot is run, perhaps via residual structure on the calibration data, is open.

The independent prior across (s, a) pairs in Assumption 4 is conservative. Under a hierarchical prior (e.g., a Gaussian-process kernel encoding spatial proximity), part of the reachability gap is transportable into the deployed policy’s visitation support by passive learning, with the closable fraction governed by the kernel’s effective rank. Appendix C.18 (Proposition 9) bounds this closable fraction; quantifying it in finite samples is open.

Conjecture 2 establishes the geometric reachability-gap rate on a regular subclass of passive policies (posterior-mean-optimal, bounded-temperature softmax, polynomial-shrinkage upper-confidence-bound (UCB) policies). The unconditional version remains open. A counterexample with $p^* \rightarrow 1$ would identify the regularity conditions under which posterior sampling fails to escape a reachability gap.

The analysis treats ϵ^{hist} as negligible, justified by latent-state contraction (Remark 1). Non-contracting dynamics, slowly mixing latent states, would inflate ϵ^{hist} and require a belief-state-policy generalization that we do not pursue here.

Ethical considerations

The phrase “hidden cluster” in Section 5.2 is a statistical label, not a clinical one: it names a region the simulator’s training data never reached, not a population characteristic. We use it to map cleanly to the formal $\mathcal{G}_{\text{reach}}$ object. Real outreach programs work *with* under-surveilled communities, and the framework’s language should be read with that translation in mind.

Fisher-SEP’s concentration of exploration in under-surveilled regions is statistically efficient under a value-centric objective, but it can shift short-term testing access away from already-served communities. Any operational use should include domain-specific ethical review, community-level consent and engagement, and quantitative equity constraints on the exploration allocation, designed jointly by methodologists, clinicians, and community representatives. Examples include capping the per-community fraction of exploration capacity, or requiring equal-or-better cumulative testing rates across communities, even at a cost to the value-maximizing allocation. The residual-ratio diagnostic

and the Fisher-SEP prescription provide decision support. They do not replace allocation decisions, and the framework characterizes the trade-off without resolving it.

Summary

Passive online updating closes the local component of the simulator’s value gap. Deliberate exploration is required to close the reachability component. Which component dominates is determined by the ratio ϵ^h/ϵ^m at visited states (Lemma 1) and by the deployed policy’s visitation support relative to the simulator’s miscalibration (Proposition 1, Theorem 6). Fisher-SEP gives a Bayesian design criterion for the second case. The simulator’s contribution is its connectivity pattern on the target policy’s visitation, not its point accuracy on parameter values.

References

- Adaptive Platform Trials Coalition. Adaptive platform trials: Definition, design, conduct and reporting considerations. *Nature Reviews Drug Discovery*, 18(10):797–807, 2019.
- A. E. Ades, Guobing Lu, and Karl Claxton. Expected value of sample information calculations in medical decision modeling. *Medical Decision Making*, 24(2):207–227, 2004.
- Alekh Agarwal, Daniel Hsu, Satyen Kale, John Langford, Lihong Li, and Robert Schapire. Taming the monster: A fast and simple algorithm for contextual bandits. In *International Conference on Machine Learning (ICML)*, pages 1638–1646. PMLR, 2014.
- Shipra Agrawal and Navin Goyal. Analysis of Thompson sampling for the multi-armed bandit problem. In *Conference on Learning Theory (COLT)*, pages 39.1–39.26. JMLR, 2012.
- Ilge Akkaya, Marcin Andrychowicz, Maciek Chociej, Mateusz Litwin, Bob McGrew, Arthur Petron, Alex Paino, Matthias Plappert, Glenn Powell, Raphael Ribas, et al. Solving rubik’s cube with a robot hand. *arXiv preprint arXiv:1910.07113*, 2019.
- Adam Allevato, Elaine Schaertl Short, Mitch Pryor, and Andrea Thomaz. Tunenet: One-shot residual tuning for system identification and sim-to-real robot task transfer. In *Conference on Robot Learning (CoRL)*, pages 445–455. PMLR, 2020.
- John Asmuth, Lihong Li, Michael L. Littman, Ali Nouri, and David Wingate. A Bayesian sampling approach to exploration in reinforcement learning (BOSS). In *Conference on Uncertainty in Artificial Intelligence (UAI)*, 2009.
- Jean-Yves Audibert and Sébastien Bubeck. Best arm identification in multi-armed bandits. In *Conference on Learning Theory (COLT)*, pages 41–53, 2010.
- Peter Auer, Nicolò Cesa-Bianchi, and Paul Fischer. Finite-time analysis of the multiarmed bandit problem. *Machine Learning*, 47(2):235–256, 2002.
- Mohammad Gheshlaghi Azar, Ian Osband, and Rémi Munos. Minimax regret bounds for reinforcement learning. In *International Conference on Machine Learning (ICML)*, pages 263–272. PMLR, 2017.
- Philip J. Ball, Laura Smith, Ilya Kostrikov, and Sergey Levine. Efficient online reinforcement learning with offline data. *International Conference on Machine Learning (ICML)*, 2023.
- Elias Bareinboim and Judea Pearl. Causal inference and the data-fusion problem. *Proceedings of the National Academy of Sciences*, 113(27):7345–7352, 2016.
- Ann D. Barker, Carrie C. Sigman, Gary J. Kelloff, Nola M. Hylton, Donald A. Berry, and Laura J. Esserman. I-SPY 2: An adaptive breast cancer trial design in the setting of neoadjuvant chemotherapy. *Clinical Pharmacology & Therapeutics*, 86(1):97–100, 2009.
- Andrew Bennett and Nathan Kallus. Proximal reinforcement learning: Efficient off-policy evaluation in partially observed Markov decision processes. *Operations Research*, 2024. doi: 10.1287/opre.2021.0781. Online publication 2023; print 2024. arXiv:2110.15332.

- Felix Berkenkamp, Matteo Turchetta, Angela Schoellig, and Andreas Krause. Safe model-based reinforcement learning with stability guarantees. In *Advances in Neural Information Processing Systems (NeurIPS)*, volume 30, pages 908–918, 2017.
- Ron Berman, Leonid Pekelis, Aisling Scott, and Christophe Van den Bulte. False discovery in A/B testing. *Management Science*, 68(9):6762–6782, 2022.
- Donald A. Berry. Bayesian clinical trials. *Nature Reviews Drug Discovery*, 5(1):27–36, 2006.
- Donald A. Berry. Adaptive clinical trials in oncology. *Nature Reviews Clinical Oncology*, 9(4):199–207, 2012. Cite key retained for backward compatibility (year is 2012).
- Scott M. Berry, Jason T. Connor, and Roger J. Lewis. The platform trial: An efficient strategy for evaluating multiple treatments. *JAMA*, 313(16):1619–1620, 2015.
- Tom Blau, Edwin V. Bonilla, Iadine Chades, and Amir Dezfouli. Optimizing sequential experimental design with deep reinforcement learning. In *International Conference on Machine Learning (ICML)*, pages 2107–2128. PMLR, 2022.
- Ronen I. Brafman and Moshe Tennenholtz. R-max: A general polynomial time algorithm for near-optimal reinforcement learning. *Journal of Machine Learning Research*, 3:213–231, 2002.
- Alan Brennan, Samer Kharroubi, Anthony O’Hagan, and Jim Chilcott. Calculating partial expected value of perfect information via Monte Carlo sampling algorithms. *Medical Decision Making*, 27(4):448–470, 2007.
- Andrew Briggs, Karl Claxton, and Mark Sculpher. *Decision Modelling for Health Economic Evaluation*. Oxford University Press, Oxford, 2006.
- Kathryn Chaloner and Isabella Verdinelli. Bayesian experimental design: A review. *Statistical Science*, 10(3):273–304, 1995.
- Yevgen Chebotar, Ankur Handa, Viktor Makoviychuk, Miles Macklin, Jan Issac, Nathan Ratliff, and Dieter Fox. Closing the sim-to-real loop: Adapting simulation randomization with real world experience. In *International Conference on Robotics and Automation (ICRA)*, pages 8973–8979. IEEE, 2019.
- Chun-Hung Chen, Jianwu Lin, Enver Yücesan, and Stephen E. Chick. Simulation budget allocation for further enhancing the efficiency of ordinal optimization. *Discrete Event Dynamic Systems*, 10(3):251–270, 2000.
- Fengdi Chen, Mohammad Ghavamzadeh, Yinlam Chow, and Alan Malek. Multi-fidelity hybrid reinforcement learning via information gain maximization. In *arXiv preprint arXiv:2509.14848*, 2025.
- Stephen E. Chick and Koichiro Inoue. New two-stage and sequential procedures for selecting the best simulated system. *Operations Research*, 49(5):732–743, 2001.
- Stephen E. Chick, Jürgen Branke, and Christian Schmidt. Sequential sampling to myopically maximize the expected value of information. *INFORMS Journal on Computing*, 22(1):71–80, 2010.
- Karl Claxton. The irrelevance of inference: A decision-making approach to the stochastic evaluation of health care technologies. *Journal of Health Economics*, 18(3):341–364, 1999.
- Karl Claxton, Mark Sculpher, and Michael Drummond. A rational framework for decision making by the National Institute for Clinical Excellence (NICE). *The Lancet*, 360(9334):711–715, 2002.
- Issa J. Dahabreh, Sarah E. Robertson, Eric J. Tchetgen Tchetgen, Elizabeth A. Stuart, and Miguel A. Hernán. Generalizing causal inferences from randomized trials: Counterfactual and graphical identification. *Biometrics*, 2019.
- Morris H. DeGroot. *Optimal Statistical Decisions*. McGraw-Hill, New York, 1970.

- Irina Degtiar and Sherri Rose. A review of generalizability and transportability. *Annual Review of Statistics and Its Application*, 10:501–524, 2023.
- Avinash K. Dixit and Robert S. Pindyck. *Investment Under Uncertainty*. Princeton University Press, Princeton, NJ, 1994.
- Michael O’Gordon Duff. *Optimal Learning: Computational Procedures for Bayes-Adaptive Markov Decision Processes*. PhD thesis, University of Massachusetts Amherst, 2002.
- Arnaud Fickinger. Statistical guarantees for offline domain randomization. *arXiv preprint arXiv:2506.10133*, 2025.
- Adam Foster, Desi R. Ivanova, Ilyas Malik, and Tom Rainforth. Deep adaptive design: Amortizing sequential bayesian experimental design. In *International Conference on Machine Learning (ICML)*, pages 3384–3395. PMLR, 2021.
- Dylan J. Foster and Alexander Rakhlin. Beyond UCB: Optimal and efficient contextual bandits with regression oracles. In *International Conference on Machine Learning (ICML)*, pages 3199–3210. PMLR, 2020.
- Dylan J. Foster, Alekh Agarwal, Miroslav Dudík, Haipeng Luo, and Robert E. Schapire. Practical contextual bandits with regression oracles. In *International Conference on Machine Learning (ICML)*, pages 1539–1548. PMLR, 2018.
- Peter I. Frazier, Warren B. Powell, and Savas Dayanik. A knowledge-gradient policy for sequential information collection. *SIAM Journal on Control and Optimization*, 47(5):2410–2439, 2008.
- Peter I. Frazier, Warren B. Powell, and Savas Dayanik. The knowledge-gradient policy for correlated normal beliefs. *INFORMS Journal on Computing*, 21(4):599–613, 2009.
- Justin Fu, Mohammad Norouzi, Ofir Nachum, George Tucker, Ziyu Wang, Alexander Novikov, Mengjiao Yang, Michael R. Zhang, Yutian Chen, Aviral Kumar, Cosmin Paduraru, Sergey Levine, and Tom Le Paine. Benchmarks for reinforcement learning with biased offline data and imperfect simulators. In *arXiv preprint arXiv:2407.00806*, 2024.
- Scott Fujimoto, David Meger, and Doina Precup. Off-policy deep reinforcement learning without exploration. In *International Conference on Machine Learning (ICML)*, pages 2052–2062. PMLR, 2019.
- John Gittins, Kevin Glazebrook, and Richard Weber. *Multi-Armed Bandit Allocation Indices*. John Wiley & Sons, Chichester, 2nd edition, 2011.
- John C. Gittins. Bandit processes and dynamic allocation indices. *Journal of the Royal Statistical Society: Series B (Methodological)*, 41(2):148–164, 1979.
- Gregg S. Gonsalves, Forrest W. Crawford, Paul D. Cleary, Edward H. Kaplan, and A. David Paltiel. An adaptive approach to locating mobile HIV testing services. *Medical Decision Making*, 38(2): 262–272, 2018.
- Arthur Guez, David Silver, and Peter Dayan. Efficient Bayes-adaptive reinforcement learning using sample-based search. In *Advances in Neural Information Processing Systems (NeurIPS)*, volume 25, pages 1025–1033, 2012.
- Vitor Hadad, David A. Hirshberg, Ruohan Zhan, Stefan Wager, and Susan Athey. Confidence intervals for policy evaluation in adaptive experiments. *Proceedings of the National Academy of Sciences*, 118(15):e2014602118, 2021.
- Danijar Hafner, Jurgis Pasukonis, Jimmy Ba, and Timothy Lillicrap. Mastering diverse domains through world models. *arXiv preprint arXiv:2301.04104*, 2023.
- Nicklas Hansen, Hao Su, and Xiaolong Wang. Temporal difference learning for model predictive control. In *International Conference on Machine Learning (ICML)*. PMLR, 2022.
- Nicklas Hansen, Xiaolong Wang, and Hao Su. TD-MPC2: Scalable, robust world models for continuous control. In *International Conference on Learning Representations (ICLR)*, 2024.

- Elad Hazan, Sham M. Kakade, Karan Singh, and Abby Van Soest. Provably efficient maximum entropy exploration. In *International Conference on Machine Learning (ICML)*, 2019.
- Anna Heath, Natalia Kunst, Christopher Jackson, Mark Strong, Fernando Alarid-Escudero, Jeremy D. Goldhaber-Fiebert, Gianluca Baio, Nicolas A. Menzies, and Hawre Jalal. Calculating the expected value of sample information in practice: Considerations from 3 case studies. *Medical Decision Making*, 40(3):314–326, 2020.
- L. Jeff Hong, Zhiyuan Huang, and Henry Lam. Review on ranking and selection: A new perspective. *Frontiers of Engineering Management*, 8(3):321–343, 2021.
- Ronald A. Howard. Information value theory. *IEEE Transactions on Systems Science and Cybernetics*, 2(1):22–26, 1966.
- Steven R. Howard, Aaditya Ramdas, Jon McAuliffe, and Jasjeet Sekhon. Time-uniform, nonparametric, nonasymptotic confidence sequences. *The Annals of Statistics*, 49(2):1055–1080, 2021.
- Feifang Hu and William F. Rosenberger. *The Theory of Response-Adaptive Randomization in Clinical Trials*. John Wiley & Sons, Hoboken, NJ, 2006.
- Melody Y. Huang and Harsh Parikh. Towards generalizing inferences from trials to target populations. *arXiv preprint arXiv:2402.17042*, 2024.
- Desi R. Ivanova, Adam Foster, Steven Kleinegesse, Michael U. Gutmann, and Tom Rainforth. Implicit deep adaptive design: Policy-based experimental design without likelihoods. In *Advances in Neural Information Processing Systems (NeurIPS)*, volume 34, pages 25785–25798, 2021.
- Thomas Jaksch, Ronald Ortner, and Peter Auer. Near-optimal regret bounds for reinforcement learning. *Journal of Machine Learning Research*, 11:1563–1600, 2010.
- Hawre Jalal and Fernando Alarid-Escudero. A gaussian approximation approach for value of information analysis. *Medical Decision Making*, 38(2):174–188, 2018.
- Michael Janner, Justin Fu, Marvin Zhang, and Sergey Levine. When to trust your model: Model-based policy optimization. In *Advances in Neural Information Processing Systems (NeurIPS)*, volume 32, pages 12519–12530, 2019.
- Christopher Jennison and Bruce W. Turnbull. *Group Sequential Methods with Applications to Clinical Trials*. Chapman and Hall/CRC, Boca Raton, FL, 1999.
- Chi Jin, Zeyuan Allen-Zhu, Sébastien Bubeck, and Michael I. Jordan. Is Q-learning provably efficient? In *Advances in Neural Information Processing Systems (NeurIPS)*, volume 31, pages 4863–4873, 2018.
- Chi Jin, Akshay Krishnamurthy, Max Simchowitz, and Tiancheng Yu. Reward-free exploration for reinforcement learning. In *International Conference on Machine Learning (ICML)*, 2020.
- Ramesh Johari, Pete Koomen, Leonid Pekelis, and David Walsh. Always valid inference: Continuous monitoring of A/B tests. *Operations Research*, 70(3):1806–1821, 2022.
- Sham Kakade and John Langford. Approximately optimal approximate reinforcement learning. In *International Conference on Machine Learning (ICML)*, pages 267–274, 2002.
- Nathan Kallus and Angela Zhou. Confounding-robust policy improvement. In *Advances in Neural Information Processing Systems (NeurIPS)*, volume 31, 2018.
- Nathan Kallus, Aahlad Manas Puli, and Uri Shalit. Removing hidden confounding by experimental grounding. In *Advances in Neural Information Processing Systems (NeurIPS)*, volume 31, 2018.
- Kirthevasan Kandasamy, Gautam Dasarathy, Junier B. Oliva, Jeff Schneider, and Barnabás Póczos. Gaussian process bandit optimisation with multi-fidelity evaluations. In *Advances in Neural Information Processing Systems (NeurIPS)*, volume 29, pages 992–1000, 2016.

- Kirthevasan Kandasamy, Gautam Dasarathy, Jeff Schneider, and Barnabás Póczos. Multi-fidelity bayesian optimisation with continuous approximations. In *International Conference on Machine Learning (ICML)*, pages 1799–1808. PMLR, 2017.
- Kirthevasan Kandasamy, Gautam Dasarathy, Barnabás Póczos, and Jeff Schneider. Multi-fidelity gaussian process bandit optimisation. *Journal of Artificial Intelligence Research*, 66:151–196, 2019.
- Maximilian Kasy and Anja Sautmann. Adaptive treatment assignment in experiments for policy choice. *Econometrica*, 89(1):113–132, 2021.
- Masahiro Kato, Kyohei Okumura, Takuya Ishihara, and Toru Kitagawa. Adaptive experimental design for policy learning. In *International Conference on Machine Learning (ICML)*, 2024. arXiv:2401.03756. Cite key retained for backward compatibility.
- Emilie Kaufmann, Olivier Cappé, and Aurélien Garivier. On the complexity of best-arm identification in multi-armed bandit models. *Journal of Machine Learning Research*, 17(1):1–42, 2016.
- Emilie Kaufmann, Pierre Ménard, Omar Darwiche Domingues, Anders Jonsson, Edouard Leurent, and Michal Valko. Adaptive reward-free exploration. In *Algorithmic Learning Theory (ALT)*, 2021.
- Michael Kearns and Satinder Singh. Near-optimal reinforcement learning in polynomial time. *Machine Learning*, 49(2–3):209–232, 2002.
- Rahul Kidambi, Aravind Rajeswaran, Praneeth Netrapalli, and Thorsten Joachims. MOREL: Model-based offline reinforcement learning. In *Advances in Neural Information Processing Systems (NeurIPS)*, volume 33, pages 21810–21823, 2020.
- Seong-Hee Kim and Barry L. Nelson. Selecting the best system. In *Simulation*, volume 13 of *Handbooks in Operations Research and Management Science*, pages 501–534. Elsevier, 2006.
- Ron Kohavi, Roger Longbotham, Dan Sommerfield, and Randal M. Henne. Controlled experiments on the web: Survey and practical guide. *Data Mining and Knowledge Discovery*, 18(1):140–181, 2009.
- Ron Kohavi, Diane Tang, and Ya Xu. *Trustworthy Online Controlled Experiments: A Practical Guide to A/B Testing*. Cambridge University Press, Cambridge, 2020.
- Ilya Kostrikov, Ashvin Nair, and Sergey Levine. Offline reinforcement learning with implicit q-learning. In *International Conference on Learning Representations (ICLR)*, 2022.
- Aviral Kumar, Aurick Zhou, George Tucker, and Sergey Levine. Conservative q-learning for offline reinforcement learning. In *Advances in Neural Information Processing Systems (NeurIPS)*, volume 33, pages 1179–1191, 2020.
- Tze Leung Lai and Herbert Robbins. Asymptotically efficient adaptive allocation rules. *Advances in Applied Mathematics*, 6(1):4–22, 1985.
- Sascha Lange, Thomas Gabel, and Martin Riedmiller. Batch reinforcement learning. In *Reinforcement Learning: State-of-the-Art*, pages 45–73. Springer, 2012.
- Quinn Lanners, Cynthia Rudin, Alexander Volfovsky, and Harsh Parikh. Data fusion for partial identification of causal effects. *arXiv preprint arXiv:2505.24296*, 2025.
- Eric Hans Lee, Valerio Perrone, Cedric Archambeau, and Matthias Seeger. Cost-aware bayesian optimization. *arXiv preprint arXiv:2003.10870*, 2020.
- Sergey Levine, Aviral Kumar, George Tucker, and Justin Fu. Offline reinforcement learning: Tutorial, review, and perspectives on open problems. In *arXiv preprint arXiv:2005.01643*, 2020.
- Lihong Li, Wei Chu, John Langford, and Robert E. Schapire. A contextual-bandit approach to personalized news article recommendation. In *International Conference on World Wide Web (WWW)*, pages 661–670. ACM, 2010.

- Sam Lobel and Ronald Parr. The bellman operator is a contraction mapping in ℓ_p norms (and so is the simulation lemma): An optimal tightness bound for the simulation lemma. *Reinforcement Learning Journal*, 2:785–797, 2024. Reinforcement Learning Conference (RLC) 2024; arXiv:2406.16249.
- Xiuyuan Lu, Benjamin Van Roy, Vikranth Dwaracherla, Morteza Ibrahimi, Ian Osband, and Zheng Wen. Reinforcement learning, bit by bit. *Foundations and Trends in Machine Learning*, 2023.
- Filip Matějka and Alisdair McKay. Rational inattention to discrete choices: A new foundation for the multinomial logit model. *American Economic Review*, 105(1):272–298, 2015.
- Tatsuya Matsushima, Hiroki Furuta, Yutaka Matsuo, Ofir Nachum, and Shixiang Gu. Deployment-efficient reinforcement learning via model-based offline optimization. In *International Conference on Learning Representations (ICLR)*, 2021.
- Robert McDonald and Daniel Siegel. The value of waiting to invest. *Quarterly Journal of Economics*, 101(4):707–727, 1986.
- Rachael Meager. Understanding the average impact of microcredit expansions: A Bayesian hierarchical analysis of seven randomized experiments. *American Economic Journal: Applied Economics*, 11(1):57–91, 2019.
- Bhairav Mehta, Manfred Diaz, Florian Golber, Christopher Sim, Peter Englert, and Dieter Fox. Active domain randomization. In *Conference on Robot Learning (CoRL)*, pages 1162–1176. PMLR, 2020.
- Marius Memmel, Andrew Wagenmaker, Chuning Zhang, Mingyu Yin, Dieter Fox, and Abhishek Gupta. ASID: Active exploration for system identification in robotic manipulation. In *International Conference on Learning Representations (ICLR)*, 2024.
- Aditya Modi, Nan Jiang, Ambuj Tewari, and Satinder Singh. Sample complexity of reinforcement learning using linearly combined model ensembles. In *Artificial Intelligence and Statistics (AISTATS)*, 2020.
- Stephen Morris and Philipp Strack. The Wald problem and the relation of sequential sampling and ex-ante information costs. *SSRN Working Paper*, 2019.
- Fabio Muratore, Fabio Ramos, Greg Turk, Wenhao Yu, Michael Gienger, and Jan Peters. Robot learning from randomized simulations: A review. *Frontiers in Robotics and AI*, 9:799893, 2022.
- Hongseok Namkoong, Ramtin Keramati, Steve Yadlowsky, and Emma Brunskill. Off-policy policy evaluation for sequential decisions under unobserved confounding. In *Advances in Neural Information Processing Systems (NeurIPS)*, volume 33, 2020.
- Xinkun Nie, Xiaoying Tian, Jonathan Taylor, and James Zou. Why adaptively collected data have negative bias and how to correct for it. In *International Conference on Artificial Intelligence and Statistics (AISTATS)*, pages 1261–1269. PMLR, 2018.
- Haoyi Niu, Yiwen Qiu, Ming Li, Guyue Zhou, Jianming HU, and Xianyuan Zhan. When to trust your simulator: Dynamics-aware hybrid offline-and-online reinforcement learning. *Advances in Neural Information Processing Systems (NeurIPS)*, 35:36599–36612, 2022.
- Haoyi Niu, Tianying Ji, Bingqi Liu, Haocheng Zhao, Xiangyu Zhu, Jianying Zheng, Pengfei Huang, Guyue Zhou, Jianming Hu, and Xianyuan Zhan. H2O+: An improved framework for hybrid offline-and-online RL with dynamics gaps. In *arXiv preprint arXiv:2309.12716*, 2023. Cite key retained for backward compatibility.
- Peter C. O’Brien and Thomas R. Fleming. A multiple testing procedure for clinical trials. *Biometrics*, 35(3):549–556, 1979.
- Ian Osband, Daniel Russo, and Benjamin Van Roy. (more) efficient reinforcement learning via posterior sampling. In *Advances in Neural Information Processing Systems (NeurIPS)*, volume 26, pages 3003–3011, 2013.

- Harsh Parikh, Rachael Ross, Elizabeth Stuart, and Kara Rudolph. Who are we missing? a principled approach to characterizing the underrepresented population. *arXiv preprint arXiv:2401.14512*, 2024a.
- Harsh Parikh, Rachael Ross, Elizabeth A. Stuart, and Kara E. Rudolph. Who are we missing? A principled approach to characterizing the underrepresented population. *arXiv preprint arXiv:2401.14512*, 2024b.
- Harsh Parikh, Marco Morucci, Vittorio Orlandi, Sudeepa Roy, Cynthia Rudin, and Alexander Volfovsky. A double machine learning approach to combining experimental and observational data. *Observational Studies*, 2025a. arXiv preprint arXiv:2307.01449.
- Harsh Parikh, Rachael Ross, Eric Kern, Kara Rudolph, and José R. Zubizarreta. Regularizing extrapolation in causal inference. *arXiv preprint arXiv:2509.17180*, 2025b.
- Judea Pearl. *Causality: Models, Reasoning, and Inference*. Cambridge University Press, Cambridge, 2nd edition, 2009.
- Judea Pearl and Elias Bareinboim. Transportability of causal and statistical relations: A formal approach. In *Proceedings of the AAAI Conference on Artificial Intelligence*, volume 25, pages 247–254, 2011.
- Benjamin Peherstorfer, Karen Willcox, and Max Gunzburger. Survey of multifidelity methods in uncertainty propagation, inference, and optimization. *SIAM Review*, 60(3):550–591, 2018.
- Xue Bin Peng, Marcin Andrychowicz, Wojciech Zaremba, and Pieter Abbeel. Sim-to-real transfer of robotic control with dynamics randomization. In *IEEE International Conference on Robotics and Automation (ICRA)*, pages 3803–3810. IEEE, 2018.
- Robert S. Pindyck. Investments of uncertain cost. *Journal of Financial Economics*, 34(1):53–76, 1993.
- Stuart J. Pocock. Group sequential methods in the design and analysis of clinical trials. *Biometrika*, 64(2):191–199, 1977.
- Matthias Poloczek, Jialei Wang, and Peter I. Frazier. Multi-information source optimization. In *Advances in Neural Information Processing Systems (NeurIPS)*, volume 30, pages 4288–4298, 2017.
- Friedrich Pukelsheim. *Optimal Design of Experiments*. Classics in Applied Mathematics. SIAM, 2nd edition, 2006.
- Martin L. Puterman. *Markov Decision Processes: Discrete Stochastic Dynamic Programming*. John Wiley & Sons, New York, 1994.
- Howard Raiffa and Robert Schlaifer. *Applied Statistical Decision Theory*. Harvard University Press, Boston, MA, 1961.
- Tom Rainforth, Adam Foster, Desi R. Ivanova, and Freddie Bickford Smith. Modern bayesian experimental design. *Statistical Science*, 2024. To appear.
- Aaditya Ramdas, Peter Grünwald, Vladimir Vovk, and Glenn Shafer. Game-theoretic statistics and safe anytime-valid inference. *Statistical Science*, 38(4):576–601, 2023.
- Herbert Robbins. Some aspects of the sequential design of experiments. *Bulletin of the American Mathematical Society*, 58(5):527–535, 1952.
- Paul R. Rosenbaum. *Observational Studies*. Springer Series in Statistics. Springer, 2 edition, 2002.
- William F. Rosenberger and John M. Lachin. *Randomization in Clinical Trials: Theory and Practice*. John Wiley & Sons, Hoboken, NJ, 2nd edition, 2012.
- Evan T. R. Rosenman, Guillaume Basse, Art B. Owen, and Michael Baiocchi. Combining observational and experimental datasets using shrinkage estimators. *Biometrics*, 79(2):926–938, 2023.

- Daniel Russo. Worst-case regret bounds for exploration via randomized value functions. In *Advances in Neural Information Processing Systems (NeurIPS)*, volume 32, 2019.
- Daniel Russo. Simple bayesian algorithms for best-arm identification. *Operations Research*, 68(6): 1625–1647, 2020.
- Daniel Russo and Benjamin Van Roy. Learning to optimize via posterior sampling. *Mathematics of Operations Research*, 39(4):1221–1243, 2014.
- Daniel J. Russo, Benjamin Van Roy, Abbas Kazerouni, Ian Osband, and Zheng Wen. A tutorial on Thompson sampling. *Foundations and Trends in Machine Learning*, 11(1):1–96, 2018.
- Erica Salvato, Gianfranco Fenu, Eric Medvet, and Felice Andrea Pellegrino. Crossing the reality gap: A survey on sim-to-real transferability of robot controllers in reinforcement learning. *IEEE Access*, 9:153171–153187, 2021.
- David Simchi-Levi and Chonghuan Wang. Multi-armed bandit experimental design: Online decision-making and adaptive inference. *arXiv preprint arXiv:2206.05324*, 2023.
- Christopher A. Sims. Implications of rational inattention. *Journal of Monetary Economics*, 50(3): 665–690, 2003.
- Aniruddh Singh. Vending machine sales. <https://www.kaggle.com/datasets/awesomeasingh/vending-machine-sales>, 2022. CC0: Public Domain. 9,617 transactions from four machines in Central New Jersey.
- Yuda Song, Yifei Zhou, Ayush Sekhari, J. Andrew Bagnell, Akshay Krishnamurthy, and Wen Sun. Hybrid RL: Using both offline and online data can make RL efficient. In *International Conference on Learning Representations (ICLR)*, 2023.
- Alexander L. Strehl, Lihong Li, Eric Wiewiora, John Langford, and Michael L. Littman. PAC model-free reinforcement learning. *Journal of Machine Learning Research*, 10:2413–2444, 2009.
- Mark Strong, Jeremy E. Oakley, and Alan Brennan. Estimating multiparameter partial expected value of perfect information from a probabilistic sensitivity analysis sample: A nonparametric regression approach. *Medical Decision Making*, 34(3):311–326, 2014.
- Elizabeth A. Stuart, Stephen R. Cole, Catherine P. Bradshaw, and Philip J. Leaf. The use of propensity scores to assess the generalizability of results from randomized trials. *Journal of the Royal Statistical Society: Series A (Statistics in Society)*, 174(2):369–386, 2011.
- Yanan Sui, Alkis Gotovos, Joel W. Burdick, and Andreas Krause. Safe exploration for optimization with Gaussian processes. In *International Conference on Machine Learning (ICML)*, pages 997–1005. PMLR, 2015.
- Richard S. Sutton. Dyna, an integrated architecture for learning, planning, and reacting. *ACM SIGART Bulletin*, 2(4):160–163, 1991.
- Richard S. Sutton and Andrew G. Barto. *Reinforcement Learning: An Introduction*. MIT Press, Cambridge, MA, 2nd edition, 2018.
- Zhiqiang Tan. A distributional approach for causal inference using propensity scores. *Journal of the American Statistical Association*, 101(476):1619–1637, 2006.
- Diane Tang, Ashish Agarwal, Deirdre O’Brien, and Mike Meyer. Overlapping experiment infrastructure: More, better, faster experimentation. In *Proceedings of the 16th ACM SIGKDD International Conference on Knowledge Discovery and Data Mining*, pages 17–26. ACM, 2010.
- William R. Thompson. On the likelihood that one unknown probability exceeds another in view of the evidence of two samples. *Biometrika*, 25(3–4):285–294, 1933.
- Josh Tobin, Rachel Fong, Alex Ray, Jonas Schneider, Wojciech Zaremba, and Pieter Abbeel. Domain randomization for transferring deep neural networks from simulation to the real world. In *IEEE/RSJ International Conference on Intelligent Robots and Systems (IROS)*, pages 23–30. IEEE, 2017.

- Soffia S. Villar, Jack Bowden, and James Wason. Multi-armed bandit models for the optimal design of clinical trials: Benefits and challenges. *Statistical Science*, 30(2):199–215, 2015.
- Eva Vivalt. How much can we generalize from impact evaluations? *Journal of the European Economic Association*, 18(6):3045–3089, 2020.
- Andrew Wagenmaker and Kevin Jamieson. Overcoming the sim-to-real gap: Leveraging simulation to learn to explore for real-world RL. *arXiv preprint arXiv:2410.20254*, 2024.
- Lingxiao Wang, Zhuoran Yang, and Zhaoran Wang. Provably efficient causal reinforcement learning with confounded observational data. In *Advances in Neural Information Processing Systems (NeurIPS)*, volume 34, 2021.
- Joshua L. Warren, Ottavia Prunas, A. David Paltiel, Thomas Thornhill, and Gregg S. Gonsalves. Integrating testing volume into bandit algorithms for infectious disease surveillance. *Journal of the Royal Statistical Society: Series A*, 188(4):1029–1043, 2025. doi: 10.1093/jrssi/qnae090.
- Tsachy Weissman, Erik Ordentlich, Gadiel Seroussi, Sergio Verdú, and Marcelo J. Weinberger. Inequalities for the L1 deviation of the empirical distribution. Technical Report HPL-2003-97, Hewlett-Packard Labs, 2003.
- Ewan C. F. Wilson. A practical guide to value of information analysis. *PharmacoEconomics*, 33(2): 105–121, 2015.
- Janet Woodcock and Lisa M. LaVange. Master protocols to study multiple therapies, multiple diseases, or both. *New England Journal of Medicine*, 377(1):62–70, 2017.
- Philipp Wu, Alejandro Escontrela, Danijar Hafner, Pieter Abbeel, and Ken Goldberg. Daydreamer: World models for physical robot learning. *Conference on Robot Learning (CoRL)*, pages 2226–2240, 2023.
- Yunbei Xu and Assaf Zeevi. Bayesian design principles for frequentist sequential learning. In *International Conference on Machine Learning (ICML)*, 2023. PMLR vol. 202; arXiv:2310.00806. Cite key retained for backward compatibility.
- Shu Yang and Peng Ding. Combining multiple observational data sources to estimate causal effects. *Journal of the American Statistical Association*, 115(531):1540–1554, 2020.
- Tianhe Yu, Garrett Thomas, Lantao Yu, Stefano Ermon, James Zou, Sergey Levine, Chelsea Finn, and Tengyu Ma. MOPO: Model-based offline policy optimization. In *Advances in Neural Information Processing Systems (NeurIPS)*, volume 33, pages 14129–14142, 2020.
- Junzhe Zhang and Elias Bareinboim. Markov decision processes with unobserved confounders: A causal approach. In *Technical Report R-23, Purdue AI Lab*, 2016.
- Kelly Zhang, Lucas Janson, and Susan Murphy. Inference for batched bandits. In *Advances in Neural Information Processing Systems (NeurIPS)*, volume 33, pages 9818–9829, 2020.
- Yao Zhao, Kwang-Sung Jun, Tanner Fiez, and Lalit Jain. Adaptive experimentation when you can’t experiment. In *Advances in Neural Information Processing Systems (NeurIPS)*, volume 37, 2024. arXiv:2406.10738. Cite key retained for backward compatibility.

A Proofs for Section 3 and Stateless Warmup

This appendix contains the proofs for the results of Section 3 and develops the stateless and contextual warmup settings that motivate the main-text threshold intuition.

A.1 Proof of Lemma 1 (extended simulation lemma)

Setup. The simulator $\hat{\mathcal{M}}_{\text{sim}} = (\hat{\rho}_{\text{sim}}, \hat{\wp}_{\text{sim}})$ is calibrated from historical data generated under a behavior policy $\pi^{\text{beh}}(a | s, h)$ that could depend on the hidden state H . We use the named kernels of Section 2 throughout. The deployment-time Markov projection is

$$\rho_{\text{obs}}^*(s, a) := \mathbb{E}_{h \sim \mathbb{P}_t(h|s)}[\bar{r}(s, a, h)], \quad \wp_{\text{obs}}^*(s' | s, a) := \mathbb{E}_{h \sim \mathbb{P}_t(h|s)}[\wp_S(s' | s, a, h)],$$

and the calibration-asymptotic kernel (the simulator’s training-procedure limit at infinite calibration data and a perfect parametric family) is

$$\bar{\rho}_{\text{calib}}(s, a) := \mathbb{E}_{h \sim \mathbb{P}_{\text{calib}}(h|s,a)}[\bar{r}(s, a, h)], \quad \bar{\wp}_{\text{calib}}(s' | s, a) := \mathbb{E}_{h \sim \mathbb{P}_{\text{calib}}(h|s,a)}[\wp_S(s' | s, a, h)].$$

Under Assumption 5(a)–(c), the actual simulator deviates from the calibration-asymptotic kernel by per-pair residuals,

$$\hat{\rho}_{\text{sim}}(s, a) = \bar{\rho}_{\text{calib}}(s, a) + \xi_r^m(s, a), \quad (13)$$

$$\hat{\wp}_{\text{sim}}(s' | s, a) = \bar{\wp}_{\text{calib}}(s' | s, a) + \xi_p^m(s, a, s'), \quad (14)$$

where ξ_r^m and ξ_p^m collect functional-form mis-specification, finite-sample calibration noise, and prior/regularization artifacts; both are properties of the simulator’s training procedure, *not* of the hidden-state distribution, so they are not reduced by any deployment-time intervention (Assumption 5(d) freezes the simulator).

Decomposition of the simulator-to-projection gap. Apply the triangle inequality through $\bar{\rho}_{\text{calib}}$ and $\bar{\wp}_{\text{calib}}$:

$$\epsilon_r(s, a) := |\hat{\rho}_{\text{sim}}(s, a) - \rho_{\text{obs}}^*(s, a)| \leq \epsilon_r^h(s, a) + \epsilon_r^m(s, a),$$

with

$$\epsilon_r^h(s, a) := |\rho_{\text{obs}}^*(s, a) - \bar{\rho}_{\text{calib}}(s, a)|, \quad (15)$$

$$\epsilon_r^m(s, a) := |\xi_r^m(s, a)|. \quad (16)$$

The *calibration–deployment* component ϵ_r^h captures two structural differences between the calibration conditional $\mathbb{P}_{\text{calib}}(H | S, A)$ and the deployment conditional $\mathbb{P}_t(H | S)$: (i) *confounding* — the calibration distribution conditions on a (because π^{beh} depended on h), while the deployment projection conditions only on s ; (ii) *drift* — the calibration-time and deployment-time marginals of $h | s$ differ even ignoring the conditioning on a . Both effects are folded into the difference of expectations in (15); App. A.12 separates them. The *misspecification residual* ϵ_r^m captures everything else. The analogous decomposition holds for transitions:

$$\epsilon_p(s, a) \leq \epsilon_p^h(s, a) + \epsilon_p^m(s, a), \quad (17)$$

$$\epsilon_p^h(s, a) := \|\wp_{\text{obs}}^*(\cdot | s, a) - \bar{\wp}_{\text{calib}}(\cdot | s, a)\|_1, \quad (18)$$

$$\epsilon_p^m(s, a) := \|\xi_p^m(s, a, \cdot)\|_1. \quad (19)$$

Reducibility of ϵ^h . An S -measurable randomized policy $\pi^{\text{exp}}(a | s, h) = \pi^{\text{exp}}(a | s)$ severs the $H \rightarrow A$ edge (Lemma 2), so pilot observations at (s, a) are i.i.d. draws (marginally, across units) from $\mathbb{P}(R | s, \text{do}(a))$ and $\mathbb{P}(S' | s, \text{do}(a))$ — i.e., from the interventional distributions that define ρ_{obs}^* and \wp_{obs}^* . The empirical means therefore estimate ρ_{obs}^* and \wp_{obs}^* consistently; with n pilot samples, the residual error at (s, a) is $O(1/\sqrt{n})$, which shrinks to zero as $n \rightarrow \infty$. This reduces $\epsilon_r^h + \epsilon_p^h$ to finite-sample noise.

Irreducibility of ϵ^m . The residuals ξ_r^m, ξ_p^m are properties of the simulator’s training procedure (parametric family, regularizer, finite calibration sample), not of the hidden-state distribution. No amount of randomized interaction at (s, a) reveals information about ξ^m , because randomization at deployment time corrects the H -conditioning but not the simulator’s intrinsic parametric bias. In particular, ϵ^m is reducible only by changing the simulator itself — retraining, richer functional family, more calibration data of better quality — operations the planner has ruled out by Assumption 5(d) (fixed simulator).

Value bound. With these per- (s, a) decompositions, the sup-norm versions $\epsilon_r := \max_{s,a} \epsilon_r(s, a)$ and $\epsilon_p := \max_{s,a} \epsilon_p(s, a)$ satisfy $\epsilon_r \leq \epsilon_r^m + \epsilon_r^h$ and $\epsilon_p \leq \epsilon_p^m + \epsilon_p^h$ with the sups taken correspondingly. The value inequality (5) is then the classical simulation lemma of Kearns and Singh [2002] applied to the pair of MDPs $(\hat{\rho}_{\text{sim}}, \hat{\wp}_{\text{sim}})$ and $(\rho_{\text{obs}}^*, \wp_{\text{obs}}^*)$: for any policy π depending only on observed states,

$$|V^\pi(\mathcal{M}_{\text{obs}}^*) - V^\pi(\hat{\mathcal{M}}_{\text{sim}})| \leq \frac{2\epsilon_r}{1-\gamma} + \frac{2\gamma R_{\text{max}}\epsilon_p}{(1-\gamma)^2} = \frac{2}{1-\gamma} \left(\epsilon_r + \frac{\gamma R_{\text{max}}}{1-\gamma} \epsilon_p \right). \quad \square$$

Remark 6 (Tightness of the transition-error term). *The $(1-\gamma)^{-2}$ factor on the transition-error term in (5) is loose: Lobel and Parr [2024] establish the optimal tightness bound, which replaces the $1/(1-\gamma)^2$ with a tighter factor in policy-dependent settings. The looseness does not affect our EPI-based ranking (which is invariant to a common multiplicative factor on the transition-error term) but does affect the absolute magnitude of the worst-case value loss.*

Proof of Corollary 1. Let $\mathcal{I} \subseteq \mathbb{S} \times \mathbb{A}$ be the pilot-covered pairs and let the pilot be an \mathcal{S} -measurable randomized policy with $n_{s,a}$ samples at $(s, a) \in \mathcal{I}$. By Lemma 2, reward and next-state samples at (s, a) under the pilot are i.i.d. draws (marginally, across units) from $\mathbb{P}(R \mid s, \text{do}(a))$ and $\mathbb{P}(S' \mid s, \text{do}(a))$ —i.e., from the kernels that define ρ_{obs}^* and \wp_{obs}^* .

Reward term. For each $(s, a) \in \mathcal{I}$, let $\hat{\rho}_{\text{pilot}}(s, a)$ be the empirical mean of $n_{s,a}$ pilot rewards. Since rewards lie in $[0, R_{\text{max}}]$, Azuma–Hoeffding gives

$$\mathbb{P}(|\hat{\rho}_{\text{pilot}}(s, a) - \rho_{\text{obs}}^*(s, a)| > u) \leq 2 \exp(-2n_{s,a}u^2/R_{\text{max}}^2),$$

so with probability at least $1 - \delta/(2|\mathcal{I}|)$, $|\hat{\rho}_{\text{pilot}}(s, a) - \rho_{\text{obs}}^*(s, a)| \leq R_{\text{max}}\sqrt{\log(4|\mathcal{I}|/\delta)/(2n_{s,a})}$. Union-bounding over \mathcal{I} gives $|\hat{\rho}_{\text{pilot}}(s, a) - \rho_{\text{obs}}^*(s, a)| \leq c_r\sqrt{\log(|\mathcal{I}|/\delta)/n_{s,a}}$ uniformly on \mathcal{I} , where $c_r := R_{\text{max}}/\sqrt{2}$ is an absolute constant and $|\mathcal{I}|$ appears inside the log (so the dependence on $|\mathcal{I}|$ is $\sqrt{\log|\mathcal{I}|}$, which we absorb into the $c_r\sqrt{\log(1/\delta)/n_{s,a}}$ form of the corollary by re-defining $\delta \leftarrow \delta/|\mathcal{I}|$ where needed).

The updated reward-error bound replaces $\hat{\rho}_{\text{sim}}$ by the pilot-refined estimate on \mathcal{I} : for $(s, a) \in \mathcal{I}$, the post-pilot reward error is at most $c_r\sqrt{\log(1/\delta)/n_{s,a}}$; for $(s, a) \notin \mathcal{I}$, it remains $\epsilon_r^h(s, a) + \epsilon_r^m(s, a) \leq \max_{(s,a) \notin \mathcal{I}} \epsilon_r^h(s, a) + \epsilon_r^m$. Plugging these into the Kearns–Singh sup-norm bound of Lemma 1 yields the reward-contribution term.

Transition term. The same argument applied to the empirical Dirichlet mean $\hat{\wp}_{\text{pilot}}(\cdot \mid s, a)$, using Weissman et al. [2003]’s L_1 deviation inequality for $|\mathbb{S}|$ -dimensional empirical distributions, gives $\|\hat{\wp}_{\text{pilot}}(\cdot \mid s, a) - \wp_{\text{obs}}^*(\cdot \mid s, a)\|_1 \leq c_p\sqrt{|\mathbb{S}|\log(1/\delta)/n_{s,a}}$ uniformly on \mathcal{I} with probability at least $1 - \delta/2$. Combining the two tail events by a final union bound and substituting into the sup-norm bound of Lemma 1 yields the stated corollary. \square

A.2 Stateless warmup: finite-sample regret and thresholds

In the stateless case (two periods, n units, two actions, prior $\Delta \sim \mathcal{N}(\delta_0, \sigma_0^2)$), the net value of experimenting with n_e units is

$$\Delta V(n_e) = -\frac{n_e \delta_0}{2} + \gamma n \nu(n_e) \psi(\delta_0/\nu(n_e)),$$

where $\nu^2(n_e) = \sigma_0^4 n_e / (4\sigma^2 + \sigma_0^2 n_e)$ and $\psi(r) = \phi(r) - r \Phi(-r)$.

Theorem 1 (Finite-sample regret). *BayesRegret($n_e=0$) = $\gamma n \sigma_0 \psi(\kappa)$, where $\kappa = \delta_0/\sigma_0$. For any fixed $\kappa > 0$, the optimal experiment size $n_e^* = n_e^*(n, \gamma, \sigma^2, \sigma_0^2, \kappa)$ is interior (not at the budget constraint) and satisfies*

$$n_e^* = \Theta\left(\frac{\sigma}{\sigma_0} \sqrt{\frac{\gamma n}{\kappa}}\right) = \Theta\left(\sqrt{\frac{\sigma^2 \gamma n}{\delta_0 \sigma_0}}\right) \quad \text{as } n \rightarrow \infty, \quad (20)$$

i.e., n_e^ grows as \sqrt{n} with a prefactor $\sqrt{\sigma^2/(\delta_0 \sigma_0)}$ (equivalently, $\sigma/\sigma_0 \cdot \kappa^{-1/2}$). As $\kappa \rightarrow 0^+$ (uninformative prior), the interior argmax disappears and n_e^* hits the budget constraint n , matching the intuition that an uninformative prior justifies an arbitrarily large pilot relative to its cost.*

Proof. The oracle value is $\mathbb{E}[\max(\Delta, 0)] = \delta_0 \Phi(\kappa) + \sigma_0 \phi(\kappa)$. The SOP value is $n(\mu_0 + \delta_0)$. The Bayes regret is therefore $\gamma n \sigma_0 \psi(\kappa)$. After an experiment with n_e units, the preposterior is $\delta_1 \sim \mathcal{N}(\delta_0, \nu^2)$, yielding net value $-n_e \delta_0/2 + \gamma n \nu \psi(\delta_0/\nu)$. The first-order condition is $\delta_0/2 = \gamma n (d\nu/dn_e) \phi(\delta_0/\nu)$. We have $\nu^2(n_e) = \sigma_0^4 n_e / (4\sigma^2 + \sigma_0^2 n_e)$, so $\nu \rightarrow \sigma_0$ as $n_e \rightarrow \infty$ and $d\nu^2/dn_e = 4\sigma^2 \sigma_0^4 / (4\sigma^2 + \sigma_0^2 n_e)^2$, giving $d\nu/dn_e = 2\sigma^2 \sigma_0^4 / ((4\sigma^2 + \sigma_0^2 n_e)^2 \nu)$, which scales as $2\sigma^2 / (\sigma_0 n_e^2)$ for large n_e (using $\nu \rightarrow \sigma_0$ and $(4\sigma^2 + \sigma_0^2 n_e)^2 \rightarrow \sigma_0^4 n_e^2$). Solving the FOC asymptotically, $\delta_0/2 \sim \gamma n \cdot 2\sigma^2 / (\sigma_0 n_e^2) \cdot \phi(\kappa)$, so $(n_e^*)^2 \sim 4\gamma n \sigma^2 \phi(\kappa) / (\delta_0 \sigma_0)$, i.e.

$$n_e^* \sim 2 \sqrt{\frac{\gamma n \sigma^2 \phi(\kappa)}{\delta_0 \sigma_0}} = \Theta\left(\frac{\sigma}{\sigma_0} \sqrt{\frac{\gamma n}{\kappa}}\right)$$

(using $\delta_0 = \kappa \sigma_0$ and absorbing $\phi(\kappa)$ into the constant at fixed κ), confirming (20).

For the $\kappa \rightarrow 0^+$ behavior: at $\kappa = 0$ ($\delta_0 = 0$), the FOC becomes $0 = \gamma n (d\nu/dn_e) / \sqrt{2\pi}$, which fails at any finite n_e since $d\nu/dn_e > 0$; hence the net value is strictly increasing in n_e over the allowed range, and the argmax is at the budget constraint $n_e = n$ rather than at a finite interior point. This recovers the intuition that uninformative priors justify arbitrarily large pilots. \square

In the contextual case (K actions, independent priors), the optimal allocation equalizes the augmented index across active actions:

$$\underbrace{m_a}_{\text{earn}} + \underbrace{\gamma n \text{KG}_a(\mathbf{n}^*)}_{\text{learn}} = \lambda \quad \forall a \text{ with } n_a^* > 0, \quad (21)$$

where KG_a denotes the knowledge gradient [Frazier et al., 2008]. The SOP is optimal if and only if $m_{a_{\text{sim}}^*} - m_a \geq \gamma n [\text{KG}_a - \text{KG}_{a_{\text{sim}}^*}]$ for all a . Over $T+1$ periods, beliefs evolve via conjugate updating [Duff, 2002].

A.3 Empirical Illustration: Stateless Threshold

This subsection provides an empirical illustration of the stateless theory developed above. We consider $n = 100$ units, $K = 2$ actions, $\sigma^2 = 1$, $\sigma_0 = 1$, and sweep $\kappa = \delta_0/\sigma_0$ over $[0, 2]$ for $\gamma \in \{0.5, 0.8, 0.9, 1.0\}$. The analytical threshold $\kappa^*(\gamma)$ is the root of $2\gamma\psi(\kappa) = \kappa$.

Figure A3 presents three panels. Panel (a) shows that the net value $\Delta V(n_e^*)$ crosses zero at κ^* , matching the analytical threshold. Panel (b) confirms that the optimal experiment size n_e^* decreases monotonically in κ . Panel (c) provides Monte Carlo validation ($N_{\text{MC}} = 10,000$, $\gamma = 1.0$), confirming agreement with the closed-form formula to within 0.5%.

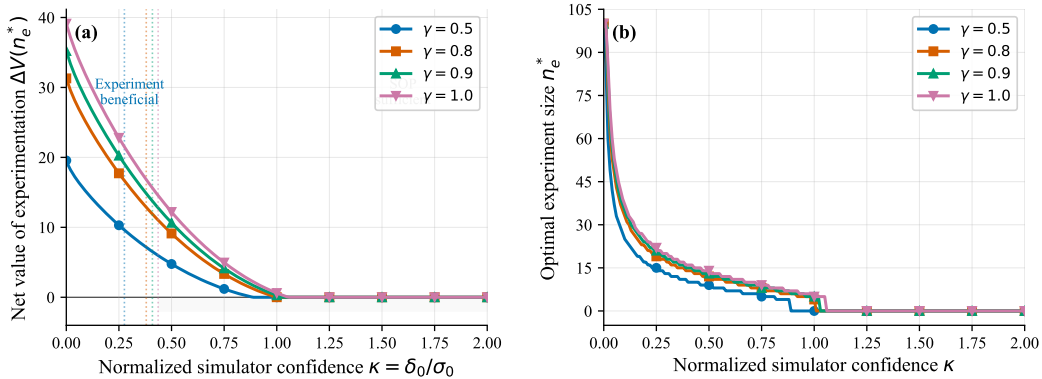


Figure A3: Stateless experimentation threshold. (a) Net value $\Delta V(n_e^*)$ versus κ for four discount factors. Dotted lines indicate the analytical threshold $\kappa^*(\gamma)$. (b) Optimal experiment size n_e^* versus κ . (c) Monte Carlo validation ($\gamma = 1.0$): analytical (solid) versus simulated (hatched, ± 2 SE).

A.4 Value decomposition (proof of Theorem 2)

Theorem 2 (Value decomposition bound). *Let $\mathcal{M}_{\text{obs}}^*$ denote the true observed-state MDP and let $V_{\text{obs}}^{\text{oracle}} := V^*(\rho_{\text{obs}}^*, \wp_{\text{obs}}^*)$ be its optimal value. Define the single-perturbation value differences (holding the simulator-optimal policy π_{sim}^* fixed):*

$$\Delta_r := V^{\pi_{\text{sim}}^*}(\rho_{\text{obs}}^*, \hat{\wp}_{\text{sim}}) - V^{\pi_{\text{sim}}^*}(\hat{\rho}_{\text{sim}}, \hat{\wp}_{\text{sim}}), \quad (22)$$

$$\Delta_p := V^{\pi_{\text{sim}}^*}(\hat{\rho}_{\text{sim}}, \wp_{\text{obs}}^*) - V^{\pi_{\text{sim}}^*}(\hat{\rho}_{\text{sim}}, \hat{\wp}_{\text{sim}}), \quad (23)$$

where $V^\pi(\rho, \wp)$ denotes the value of policy π in the MDP with rewards ρ and transitions \wp . Then under Assumptions 1–3, Lemma 1 applied to each one-sided perturbation gives $|\Delta_r| \leq U_r := 2\epsilon_r/(1-\gamma)$ and $|\Delta_p| \leq U_p := 2\gamma R_{\text{max}}\epsilon_p/(1-\gamma)^2$, and the ratio of worst-case bounds satisfies

$$\frac{U_p}{U_r} = \frac{\gamma R_{\text{max}}\epsilon_p}{(1-\gamma)\epsilon_r} \rightarrow \infty \quad \text{as } \gamma \rightarrow 1 \quad \text{for fixed } \epsilon_r, \epsilon_p > 0. \quad (24)$$

The full oracle gap $V_{\text{obs}}^{\text{oracle}} - V^{\pi_{\text{sim}}^*}(\hat{\rho}_{\text{sim}}, \hat{\wp}_{\text{sim}})$ decomposes as $\Delta_r + \Delta_p + \Delta_{\text{pol}} + \Delta_{\text{int}}$, where $\Delta_{\text{pol}} := V_{\text{obs}}^{\text{oracle}} - V^{\pi_{\text{sim}}^*}(\rho_{\text{obs}}^*, \wp_{\text{obs}}^*)$ is the policy-misspecification gap (always ≥ 0) and Δ_{int} is the residual interaction term captured by the two simultaneous perturbations. The individual reward-only bound $|\Delta_r| \leq U_r$ and the transition-only bound $|\Delta_p| \leq U_p$ are about single-source perturbations at the fixed policy π_{sim}^* ; they do not individually bound the full oracle gap, which also includes Δ_{pol} .

Remark 7 (On signs and tightness). *The single-perturbation quantities Δ_r, Δ_p (at fixed policy π_{sim}^*) can each take either sign: replacing only the simulator’s rewards with the truth need not improve the SOP’s value, since the SOP was optimized under the simulator rather than under partially-corrected dynamics. The theorem bounds their magnitudes, not their signs; the policy-misspecification gap $\Delta_{\text{pol}} \geq 0$ is non-negative but has no corresponding single-source bound. Tightness of the U_r, U_p bounds holds in the worst-case-reachable regime of Lemma 1.*

Proof of Theorem 2. The bound on Δ_r follows by applying Lemma 1 to the pair of MDPs $(\rho_{\text{obs}}^*, \hat{\wp}_{\text{sim}})$ vs. $(\hat{\rho}_{\text{sim}}, \hat{\wp}_{\text{sim}})$: the transitions match, so the lemma’s transition-error term vanishes ($\epsilon_p^{(r)} = 0$) and the bound reduces to $2\epsilon_r/(1-\gamma)$. The bound on Δ_p follows analogously with the reward-error term vanishing and gives $2\gamma R_{\text{max}}\epsilon_p/(1-\gamma)^2$. The additive decomposition $V_{\text{obs}}^{\text{oracle}} - V^{\pi_{\text{sim}}^*}(\hat{\rho}_{\text{sim}}, \hat{\wp}_{\text{sim}}) = \Delta_r + \Delta_p + \Delta_{\text{pol}} + \Delta_{\text{int}}$ is immediate from the definitions by telescoping $(\hat{\rho}_{\text{sim}}, \hat{\wp}_{\text{sim}}) \rightarrow (\rho_{\text{obs}}^*, \hat{\wp}_{\text{sim}}) \rightarrow (\rho_{\text{obs}}^*, \wp_{\text{obs}}^*) \rightarrow V_{\text{obs}}^{\text{oracle}}$, with Δ_{pol} capturing the final $\pi_{\text{sim}}^* \rightarrow \pi_{\text{oracle}}^*$ policy switch and Δ_{int} absorbing second-order interaction between the reward and transition perturbations at the fixed policy. The ratio $U_p/U_r = \gamma R_{\text{max}}\epsilon_p/((1-\gamma)\epsilon_r)$ tends to infinity as $\gamma \rightarrow 1$ for fixed $\epsilon_r, \epsilon_p > 0$. \square

A.5 Proofs for Fisher-SEP (Section 3)

This subsection states and proves the do-variance decomposition (Lemma 3), Lemma 2, and the observational-vs-interventional gap (Proposition 2). It also specifies the empirical-Bayes estimator of $\tau_{s,a}^{\text{obs}}$ used in the experiments of Section 5. (In this appendix we write $\tau_{s,a}^{\text{obs}}$ for the per-observation Fisher information $\tau_{s,a}^{\text{int}}$ of Section 4; the superscript “obs” refers to “observation under a randomized pilot,” so $\tau_{s,a}^{\text{obs}} = \tau_{s,a}^{\text{int}}$ under Lemma 2.)

Lemma 3 (Do-variance decomposition). *Under the POMDP of Section 2 with reward kernel $R | S, A, H$ having conditional mean $\bar{r}(s, a, h)$ and variance $\sigma_r^2(s, a, h)$, the variance of the reward under the interventional distribution at $(s, \text{do}(a))$ decomposes as*

$$\text{Var}(R | s, \text{do}(a)) = \mathbb{E}_{h \sim \mathbb{P}_t(\cdot | s)}[\sigma_r^2(s, a, h)] + \text{Var}_{h \sim \mathbb{P}_t(\cdot | s)}[\bar{r}(s, a, h)]. \quad (25)$$

Proof of Lemma 3. Under the POMDP of Section 2, the reward $R | S, A, H$ has conditional mean $\bar{r}(s, a, h)$ and variance $\sigma_r^2(s, a, h)$. Intervening to fix $A = a$ by $\text{do}(A = a)$ severs incoming edges to A in the causal graph; in particular, it severs any $H \rightarrow A$ dependence that a behavior policy would induce. It does not affect the $S \rightarrow H$ relation or the reward kernel, so under $\text{do}(A = a)$ at $S = s$ we have $H | s, \text{do}(a) \sim \mathbb{P}_t(\cdot | s)$ and $R | s, a, h \sim \rho(\cdot | s, a, h)$.

Apply the law of total variance conditional on $(s, \text{do}(a))$ with H as the inner conditioning variable:

$$\begin{aligned} \text{Var}(R \mid s, \text{do}(a)) &= \mathbb{E}_{H \mid s, \text{do}(a)}[\text{Var}(R \mid s, \text{do}(a), H)] + \text{Var}_{H \mid s, \text{do}(a)}[\mathbb{E}(R \mid s, \text{do}(a), H)] \\ &= \mathbb{E}_{h \sim \mathbb{P}_t(\cdot \mid s)}[\sigma_r^2(s, a, h)] + \text{Var}_{h \sim \mathbb{P}_t(\cdot \mid s)}[\bar{r}(s, a, h)], \end{aligned}$$

which is (25). \square

Proof of Lemma 2. Let π^{exp} satisfy $\pi^{\text{exp}}(a \mid s, h) = \pi^{\text{exp}}(a \mid s)$ for every $h \in \mathcal{H}$. Section 2 takes the hidden-state conditional $H \mid S = s$ to be stationary within an episode; the pilot operates inside a single episode, so the within-episode distribution of $H \mid S = s$ under π^{exp} is $\mathbb{P}_t(\cdot \mid s)$, the same conditional used to define ρ_{obs}^* and φ_{obs}^* . Under π^{exp} , conditional on $S = s$, the joint law of (A, H, R) factors as

$$\pi^{\text{exp}}(a \mid s) \mathbb{P}_t(h \mid s) \rho(r \mid s, a, h),$$

where A is independent of H given S by S -measurability of π^{exp} , and the reward kernel ρ is the same under observational and interventional regimes. Conditioning further on $A = a$ gives

$$\mathbb{P}_{\pi^{\text{exp}}}(H, R \mid S = s, A = a) = \mathbb{P}_t(h \mid s) \rho(r \mid s, a, h).$$

But the right-hand side is precisely $\mathbb{P}(H, R \mid s, \text{do}(A = a))$, because $\text{do}(A = a)$ leaves $\mathbb{P}_t(h \mid s)$ and ρ unchanged. Marginalizing over h yields $\mathbb{P}_{\pi^{\text{exp}}}(R \mid s, a) = \mathbb{P}(R \mid s, \text{do}(a))$.

Consequently, reward samples at (s, a) under π^{exp} are i.i.d. draws (across units) from $\mathbb{P}(R \mid s, \text{do}(a))$; within a unit, samples may be auto-correlated through $H_{i,t}$ but each such trajectory marginalizes to the same $\mathbb{P}(R \mid s, \text{do}(a))$ by the same S -measurability argument applied at every step. The empirical variance $\hat{v}_{s,a} := (n-1)^{-1} \sum_i (R_i - \bar{R})^2$ is consistent for $\text{Var}(R \mid s, \text{do}(a))$ by the law of large numbers, and $1/\hat{v}_{s,a}$ is consistent for $\tau_{s,a} = \text{Var}(R \mid s, \text{do}(a))^{-1}$ by continuity away from zero.

Equivalently, $\{S\}$ is a valid back-door adjustment set for the effect of A on R because the only back-door path $A \leftarrow H \rightarrow R$ is blocked by the absence of the $H \rightarrow A$ edge under π^{exp} , and the standard back-door adjustment formula [Pearl, 2009] recovers the do-distribution from the observational conditional. \square

Proposition 2 (Behavior-policy reward variance vs. interventional). *Under Assumption 3 (calibration behavior policy $\pi^{\text{beh}}(a \mid s, h)$ with $A \not\perp H \mid S$):*

- (a) $\text{Var}_{\pi^{\text{beh}}}(R \mid s, a)$ generally differs from $\text{Var}(R \mid s, \text{do}(a))$, and the sign of the difference is not determined by π^{beh} alone.
- (b) Under bounded propensity-odds $w(h \mid s, a) \in [1/M, M]$, the ratio $\text{Var}_{\pi^{\text{beh}}}(R \mid s, a)/\text{Var}(R \mid s, \text{do}(a))$ is bounded in $[1/M^2, M^2]$.
- (c) The Fisher-regret incurred by plugging the observational variance into the A -optimality criterion in place of the interventional one is at most a multiplicative factor M^2 .

Proof of Proposition 2. We prove each part in turn.

Part (a) — observational conditional variance is biased. Under the behavior policy π^{beh} , the conditional law of $H \mid S = s, A = a$ is re-weighted by the propensity likelihood ratio:

$$\mathbb{P}_{\pi^{\text{beh}}}(h \mid s, a) = \mathbb{P}_t(h \mid s) \frac{\pi^{\text{beh}}(a \mid s, h)}{\pi^{\text{beh}}(a \mid s)} = \mathbb{P}_t(h \mid s) w(h \mid s, a).$$

Applying the law of total variance under $\mathbb{P}_{\pi^{\text{beh}}}(\cdot \mid s, a)$,

$$\text{Var}_{\pi^{\text{beh}}}(R \mid s, a) = \mathbb{E}_{\pi^{\text{beh}}}[\sigma_r^2(s, a, H) \mid s, a] + \text{Var}_{\pi^{\text{beh}}}[\bar{r}(s, a, H) \mid s, a].$$

The bias $\text{Var}_{\pi^{\text{beh}}}(R \mid s, a) \neq \text{Var}(R \mid s, \text{do}(a))$ arises because $\mathbb{P}_{\pi^{\text{beh}}}(\cdot \mid s, a) \neq \mathbb{P}_t(\cdot \mid s)$ whenever $w(h \mid s, a) \neq 1$. The direction of the bias depends on how the re-weighting interacts with the integrand: concentration on low- $g(h)$ values makes $\mathbb{E}_{\pi^{\text{beh}}}[g]$ smaller than $\mathbb{E}_{\mathbb{P}_t}[g]$, concentration on extreme values makes it larger. In particular, $\text{Var}_{\pi^{\text{beh}}}(R \mid s, a)$ can be *either* smaller or larger than $\text{Var}(R \mid s, \text{do}(a))$; the two-sided bound of Part (b) is the robust statement.

Part (b) — multiplicative bound under Rosenbaum sensitivity. If $w(h \mid s, a) \in [1/M, M]$ for every h , we show $\text{Var}_{\pi^{\text{beh}}}(R \mid s, a)/\text{Var}(R \mid s, \text{do}(a)) \in [1/M^2, M^2]$, so $|\text{Var}_{\pi^{\text{beh}}}/\text{Var}_{\text{do}} - 1| \leq M^2 - 1$. Decompose both variances via the law of total variance:

$$\text{Var}(R \mid s, \text{do}(a)) = \mathbb{E}_{\mathbb{P}_t}[\sigma_r^2(s, a, H)] + \text{Var}_{\mathbb{P}_t}[\bar{r}(s, a, H)],$$

$$\text{Var}_{\pi^{\text{beh}}}(R \mid s, a) = \mathbb{E}_{\mathbb{P}^{\text{beh}}}[\sigma_r^2(s, a, H)] + \text{Var}_{\mathbb{P}^{\text{beh}}}[\bar{r}(s, a, H)],$$

where $\mathbb{P}^{\text{beh}}(h) := \mathbb{P}_t(h \mid s)w(h \mid s, a)$ and both decompositions have nonnegative summands. For the first summand, nonnegativity of σ_r^2 and $w \in [1/M, M]$ give $\mathbb{E}_{\mathbb{P}^{\text{beh}}}[\sigma_r^2] \in [1/M, M] \cdot \mathbb{E}_{\mathbb{P}_t}[\sigma_r^2]$, which is contained in $[1/M^2, M^2] \cdot \mathbb{E}_{\mathbb{P}_t}[\sigma_r^2]$ since $M \geq 1$. For the second summand, use the Gini / pair-difference form of the variance: for any probability distribution Q on \mathcal{H} and any function g ,

$$\text{Var}_Q[g(H)] = \frac{1}{2} \sum_{h, h'} Q(h)Q(h') (g(h) - g(h'))^2.$$

Because $\mathbb{P}^{\text{beh}}(h)\mathbb{P}^{\text{beh}}(h') = w(h)w(h')\mathbb{P}_t(h)\mathbb{P}_t(h') \in [1/M^2, M^2] \cdot \mathbb{P}_t(h)\mathbb{P}_t(h')$, summing over the nonnegative pair terms yields

$$\text{Var}_{\mathbb{P}^{\text{beh}}}[\bar{r}(s, a, H)] \in [1/M^2, M^2] \cdot \text{Var}_{\mathbb{P}_t}[\bar{r}(s, a, H)].$$

Each summand of $\text{Var}_{\pi^{\text{beh}}}(R \mid s, a)$ is therefore within $[1/M^2, M^2]$ of its do-counterpart; since both are nonnegative the same interval applies to their sum, giving $\text{Var}_{\pi^{\text{beh}}}(R \mid s, a) / \text{Var}(R \mid s, \text{do}(a)) \in [1/M^2, M^2]$.

Part (c) — downstream Fisher regret. Let $\tau_{s,a}^* := \text{Var}(R \mid s, \text{do}(a))^{-1}$ and $\tilde{\tau}_{s,a} := \text{Var}_{\pi^{\text{beh}}}(R \mid s, a)^{-1}$; by Part (b), $\tilde{\tau}_{s,a} / \tau_{s,a}^* \in [1/M^2, M^2]$. Let $\pi^*, \tilde{\pi}$ be the Fisher-maximizers under $\tau^*, \tilde{\tau}$ respectively. Because \mathcal{F} is linear in the per- (s, a) weights $\tau_{s,a}$ for any fixed π ,

$$\mathcal{F}(\pi^*) = \sum_{s,a} \tau_{s,a}^* \omega_{s,a}(\pi^*) \leq M^2 \sum_{s,a} \tilde{\tau}_{s,a} \omega_{s,a}(\pi^*) = M^2 \tilde{\mathcal{F}}(\pi^*) \leq M^2 \tilde{\mathcal{F}}(\tilde{\pi}),$$

where $\omega_{s,a}(\pi) := \sum_{s'} d_\pi(s') (\partial V^\pi(s') / \partial \theta_{s,a})^2$ (the visitation-weighted squared sensitivity at (s, a) , summed over initial states s'). Hence $\mathcal{F}(\pi^*) \leq M^2 \tilde{\mathcal{F}}(\tilde{\pi})$: the Fisher-regret factor incurred by plugging the observational variance into the A-optimality criterion is at most M^2 . \square

Empirical-Bayes estimator for $\tau_{s,a}$

In practice we estimate $\tau_{s,a}$ from pilot data via a Normal-Inverse-Gamma conjugate posterior with prior hyperparameters $(\mu_0, \kappa_0, \alpha_0, \beta_0)$ where $\mu_0 = \hat{r}_{\text{sim}}(s, a)$, $\alpha_0 = 2$, $\beta_0 = \alpha_0 \sigma_{s,a}^2(0)$, and κ_0 is the prior strength. Given $n_{s,a}$ i.i.d. randomized-action samples $\{r_1, \dots, r_{n_{s,a}}\}$ with sample mean \bar{r} and sum of squared deviations $\text{SSE} = \sum_i (r_i - \bar{r})^2$, the posterior is $\text{NIG}(\mu_n, \kappa_n, \alpha_n, \beta_n)$ with

$$\kappa_n = \kappa_0 + n_{s,a}, \quad \alpha_n = \alpha_0 + n_{s,a}/2, \quad (26)$$

$$\beta_n = \beta_0 + \frac{1}{2} \text{SSE} + \frac{\kappa_0 n_{s,a}}{2(\kappa_0 + n_{s,a})} (\bar{r} - \mu_0)^2. \quad (27)$$

We take $\hat{\tau}_{s,a} = \alpha_n / \beta_n$, the posterior mean of the precision.

Adaptive prior strength $\hat{\kappa}_{\text{eff}}$. Rather than fix κ_0 , we estimate simulator credibility from the pooled pilot-vs-simulator discrepancies across all (s, a) with $n_{s,a} \geq n_{\text{min}}$. Under the null that the simulator is unbiased, the z -statistic $z_{s,a} := (\bar{r}_{s,a} - \mu_0) / \sqrt{\hat{v}_{s,a} / n_{s,a}}$ satisfies $\mathbb{E}[z_{s,a}^2] \approx 1 + n_{s,a} \sigma_{s,a}^2(0) / (\kappa_{\text{eff}} \hat{v}_{s,a})$, yielding the method-of-moments estimator

$$\hat{\kappa}_{\text{eff}} = \max\left(1, \frac{\sum_{(s,a) \in \mathcal{I}} n_{s,a} \sigma_{s,a}^2(0) / \hat{v}_{s,a}}{\sum_{(s,a) \in \mathcal{I}} (z_{s,a}^2 - 1)_+}\right),$$

where $\mathcal{I} = \{(s, a) : n_{s,a} \geq n_{\text{min}}\}$ and $(x)_+ := \max(x, 0)$. When \mathcal{I} is empty or the denominator is zero, fall back to a fixed $\kappa_0 = 2$. This is a pooled shrinkage estimator in the James-Stein family; it shrinks toward the simulator (large $\hat{\kappa}_{\text{eff}}$) when the pilot agrees with simulator predictions and toward data (small $\hat{\kappa}_{\text{eff}}$) when they systematically disagree.

A.6 A-optimal PVV derivation and recovery corollaries

This subsection derives Definition 5's posterior predictive value variance from first principles and proves the two recovery corollaries (Corollary 4 and Corollary 5) and the explore-under-ignorance proposition (Proposition 4.1) stated in Section 4.

Setup. Write $\theta := (\theta_{s,a})_{s,a} \in \mathbb{R}^{SK}$ for the vector of reward parameters $\theta_{s,a} = \mathbb{E}_{h \sim \mathbb{P}_t(\cdot|s)}[\bar{r}(s, a, h)]$ identified under the POMDP’s time- t hidden-state distribution. Fix a *target policy* π^{tgt} (the planner’s value estimand) and a candidate *exploration policy* π with discounted state-visitation d_π and expected pilot observation counts $n_{s,a}(\pi) = T \cdot d_\pi(s)\pi(a | s)$ under effective horizon T . Assume the planner carries a Normal-Inverse-Gamma conjugate prior on each $(\theta_{s,a}, v_{s,a})$ pair with prior mean $\mu_0(s, a) = \hat{r}_{\text{sim}}(s, a)$, prior strength $\kappa_0(s, a) \geq 0$ (so $\theta_{s,a} | v \sim \mathcal{N}(\mu_0, v/\kappa_0)$), and prior variance $\sigma_{s,a}^2(0)$ (so $v_{s,a} \sim \text{IG}(\alpha_0, \alpha_0 \sigma_{s,a}^2(0))$). The per-observation Fisher information is $\tau_{s,a}^{\text{obs}} = \text{Var}(R | s, \text{do}(a))^{-1}$, identified from pilot data (Lemma 2), and the prior Fisher information is $I_0(s, a) = \kappa_0(s, a)/\sigma_{s,a}^2(0)$.

Theorem 3 (Posterior predictive variance interpretation of PVV). *Suppose (i) $\theta_{s,a}$ are a priori independent across (s, a) , (ii) the reward likelihood at (s, a) is $\mathcal{N}(\theta_{s,a}, (\tau_{s,a}^{\text{obs}})^{-1})$, and (iii) $V^{\pi^{\text{tgt}}}(s; \theta)$ admits a first-order expansion around θ^* that dominates higher-order terms in the relevant posterior scale. Then, after observing $n_{s,a}(\pi)$ pilot reward samples under the exploration policy π , the posterior predictive variance of $\hat{V}^{\pi^{\text{tgt}}}$ averaged over $d_{\pi^{\text{tgt}}}$ equals*

$$\mathbb{E}_{s \sim d_{\pi^{\text{tgt}}}}[\text{Var}(\hat{V}^{\pi^{\text{tgt}}}(s) | \mathcal{D}_\pi)] = \text{PVV}(\pi; \pi^{\text{tgt}}) + o(1) \quad (28)$$

where $\text{PVV}(\pi; \pi^{\text{tgt}})$ is the functional in Eq. (9) and the remainder vanishes as the posterior concentrates.

Proof. By conjugacy, the marginal posterior of $\theta_{s',a'}$ given pilot data \mathcal{D}_π is Gaussian (under known τ^{obs} , Assumption (ii)) with mean $\mu_n(s', a') \rightarrow \theta_{s',a'}^*$ and variance

$$\text{Var}(\theta_{s',a'} | \mathcal{D}_\pi) = \frac{1}{I_0(s', a') + n_{s',a'}(\pi) \tau_{s',a'}^{\text{obs}}},$$

via the standard NIG posterior precision update $\kappa_n = \kappa_0 + n_{s',a'}(\pi)$. Under assumption (i) the posterior covariance matrix Σ_n is diagonal with these entries. (If τ^{obs} is itself estimated via a full NIG posterior on (θ, v) rather than plugged in, the marginal is Student- t and the variance expression picks up a factor $\beta_n/[(\alpha_n - 1)\kappa_n]$ that tends to the display above as $\alpha_n \rightarrow \infty$; the $o(1)$ remainder absorbs this term.)

Expand $V^{\pi^{\text{tgt}}}$ around the posterior mean μ_n : $\hat{V}^{\pi^{\text{tgt}}}(s) = V^{\pi^{\text{tgt}}}(s; \mu_n) + (\theta - \mu_n)^\top \nabla_\theta V^{\pi^{\text{tgt}}}(s) + O(\|\theta - \mu_n\|^2)$. Under assumption (iii) the quadratic remainder is $o(1)$ relative to the leading term, so

$$\text{Var}(\hat{V}^{\pi^{\text{tgt}}}(s) | \mathcal{D}_\pi) = \nabla_\theta V^{\pi^{\text{tgt}}}(s)^\top \Sigma_n \nabla_\theta V^{\pi^{\text{tgt}}}(s) + o(1) = \sum_{s',a'} \frac{(\partial V^{\pi^{\text{tgt}}}(s)/\partial \theta_{s',a'})^2}{I_0(s', a') + n_{s',a'}(\pi) \tau_{s',a'}^{\text{obs}}} + o(1).$$

Averaging over $s \sim d_{\pi^{\text{tgt}}}$ yields Eq. (28). \square

Corollary 4 (Data-rich homoskedastic limit of PVV). *Suppose $n_{s',a'}(\pi) \tau_{s',a'}^{\text{obs}} \gg I_0(s', a')$ for all (s', a') with non-zero target-value gradient, and $\tau_{s',a'}^{\text{obs}} \equiv \tau^{\text{obs}}$ is uniform. Then $\text{PVV}(\pi; \pi^{\text{tgt}})$ is approximately the visitation-weighted A-optimal design objective in reward parameters, and the minimizer’s state-action occupancy satisfies $d_\pi(s') \pi(a' | s') \propto \sqrt{w(s', a')}$ where $w(s', a') := \sum_u d_{\pi^{\text{tgt}}}(u) (\partial V^{\pi^{\text{tgt}}}(u)/\partial \theta_{s',a'})^2$.*

Proof of Corollary 4 (data-rich homoskedastic limit). Suppose $n_{s',a'}(\pi) \tau_{s',a'}^{\text{obs}} \gg I_0(s', a')$ for all (s', a') with non-zero target-value gradient, and $\tau_{s',a'}^{\text{obs}} \equiv \tau^{\text{obs}}$ is uniform. Then $I_0 + n\tau^{\text{obs}} \approx n_{s',a'}(\pi) \tau^{\text{obs}} = T\tau^{\text{obs}} d_\pi(s') \pi(a' | s')$, so

$$\text{PVV}(\pi; \pi^{\text{tgt}}) \approx \frac{1}{T\tau^{\text{obs}}} \sum_{s',a'} \frac{w(s', a')}{d_\pi(s') \pi(a' | s')}, \quad w(s', a') := \sum_u d_{\pi^{\text{tgt}}}(u) (\partial V^{\pi^{\text{tgt}}}(u)/\partial \theta_{s',a'})^2.$$

Here the weights $w(s', a')$ are determined by the *target* and are fixed during the minimization over π . The arg min of $\sum_{s',a'} w(s', a')/[d_\pi(s') \pi(a' | s')]$ subject to $\sum_{a'} \pi(a' | s') = 1$ (per state) is attained when the state-action occupancy measure $\mu(s', a') := d_\pi(s') \pi(a' | s')$ satisfies $\mu(s', a') \propto \sqrt{w(s', a')}$, by Cauchy–Schwarz. Up to the Cauchy–Schwarz square-root step (standard in A-optimal design), the minimizer allocates exploration visitation in proportion to the square root of the target-weighted squared sensitivity. \square

Corollary 5 (Data-starved limit of PVV). *Suppose $n_{s',a'}(\pi)\tau_{s',a'}^{\text{obs}} \ll I_0(s',a')$ for all (s',a') contributing to $\text{PVV}(\pi; \pi^{\text{tgt}})$. Then $\text{PVV}(\pi; \pi^{\text{tgt}})$ is approximately independent of the exploration policy π , and the per-pair reducible PVV contribution ranks (s',a') by the product $w(s',a') \cdot \sigma_{s',a'}^2(0)/\kappa_0(s',a')$, with $w(s',a')$ as in Corollary 4.*

Proof of Corollary 5 (data-starved limit). Suppose $n_{s',a'}(\pi)\tau_{s',a'}^{\text{obs}} \ll I_0(s',a')$ for all (s',a') contributing to $\text{PVV}(\pi; \pi^{\text{tgt}})$. Then $I_0 + n\tau^{\text{obs}} \approx I_0(s',a') = \kappa_0(s',a')/\sigma_{s',a'}^2(0)$, and

$$\text{PVV}(\pi; \pi^{\text{tgt}}) \approx \sum_{s',a'} w(s',a') \cdot \frac{\sigma_{s',a'}^2(0)}{\kappa_0(s',a')},$$

which depends on the target through $w(s',a') = \sum_u d_{\pi^{\text{tgt}}}(u)(\partial V^{\pi^{\text{tgt}}}(u)/\partial \theta_{s',a'})^2$ but not on the exploration policy π . The argmin over π is vacuous—no amount of exploration breaks the prior without pilot data. The ranking of reducible contributions across (s',a') (i.e., what visitation would reduce the most if pilot data were collected) is given by the product $w(s',a') \cdot \sigma^2(0)/\kappa_0$: pairs where the simulator’s prior is uncertain (small κ_0) and target-sensitive (large w) dominate. Fisher-SEP uses this ranking to allocate its pilot-phase visitation, which then carries the framework into the non-vacuous data-rich regime of Corollary 4. \square

Proof of Proposition 4.1 (explore under ignorance). Fix (s',a') with $n_{s',a'}(\pi) = 0$ and $\partial V^{\pi^{\text{tgt}}}(u)/\partial \theta_{s',a'} \neq 0$ for some $u \in \text{supp}(d_{\pi^{\text{tgt}}})$. The corresponding term in $\text{PVV}(\pi; \pi^{\text{tgt}})$ is

$$\sum_u d_{\pi^{\text{tgt}}}(u) \frac{(\partial V^{\pi^{\text{tgt}}}(u)/\partial \theta_{s',a'})^2}{I_0(s',a') + 0 \cdot \tau_{s',a'}^{\text{obs}}} = \frac{\sigma_{s',a'}^2(0)}{\kappa_0(s',a')} \sum_u d_{\pi^{\text{tgt}}}(u) (\partial V^{\pi^{\text{tgt}}}(u)/\partial \theta_{s',a'})^2,$$

a positive finite quantity when $\kappa_0(s',a') > 0$ and the target is sensitive to $\theta_{s',a'}$. Any policy π' with $n_{s',a'}(\pi') > 0$ replaces the denominator $I_0(s',a')$ with $I_0(s',a') + n_{s',a'}(\pi')\tau_{s',a'}^{\text{obs}} > I_0(s',a')$, strictly reducing this term. Therefore this term is *reducible* by visiting (s',a') under the exploration policy, and any A-optimal minimizer of PVV over π must visit every (s',a') with positive target-value sensitivity and finite κ_0 .

The key point—which distinguishes this from the standard Bayesian exploration bonus—is that the target’s gradient $\partial V^{\pi^{\text{tgt}}}/\partial \theta_{s',a'}$ can be nonzero at pairs the *target* itself never directly visits: the Bellman resolvent $(I - \gamma P^{\pi^{\text{tgt}}})^{-1}$ propagates reward sensitivity through the transition dynamics. In the HIV DGP (Appendix D.11), the target policy (the posterior-optimal exploit) does not visit Region B directly, but Region-B prevalence enters $V^{\pi^{\text{tgt}}}$ through disease spread from Region B into Region A via the between-zone force of infection. The nonzero target gradient at Region-B zones, combined with their low simulator trust ($\kappa_0 \approx \kappa_{\min}$ under self-consistency analysis), places them high in the PVV reducibility ranking. Minimizing PVV over the exploration policy π therefore allocates pilot visitation to Region B, which is the mechanism by which Fisher-SEP discovers the cluster. \square

Simulator-self-consistency estimator for $\kappa_0(s,a)$. In practice we set $\kappa_0(s,a)$ from a simulator-self-consistency procedure that does not require external calibration data. Let $\hat{v}_{s,a}^{\text{sim}}$ be the empirical reward variance at (s,a) estimated from Monte Carlo rollouts under a mixture of the simulator-optimal and uniform-random policies, and let $\sigma_{s,a}^2(0)$ be the simulator’s stated calibration variance. Define

$$c_{s,a} := \frac{\min(\hat{v}_{s,a}^{\text{sim}}, \sigma_{s,a}^2(0))}{\max(\hat{v}_{s,a}^{\text{sim}}, \sigma_{s,a}^2(0))} \in (0, 1],$$

a ratio close to 1 when the simulator is internally consistent at (s,a) and close to 0 when its stated variance contradicts its own rollouts. Separately define the normalized value-sensitivity

$$\bar{g}_{s,a} := \frac{\sum_u d_{\pi_{\text{sim}}^*}(u)(\partial V^{\pi_{\text{sim}}^*}(u)/\partial \theta_{s,a})^2}{\max_{(s',a')} \sum_u d_{\pi_{\text{sim}}^*}(u)(\partial V^{\pi_{\text{sim}}^*}(u)/\partial \theta_{s',a'})^2} \in [0, 1],$$

the simulator-optimal policy’s visitation-weighted sensitivity at (s,a) normalized to $[0, 1]$. We then set

$$\kappa_0(s,a) = \kappa_{\min} + (\kappa_{\max} - \kappa_{\min}) c_{s,a} \bar{g}_{s,a},$$

defaulting to $(\kappa_{\min}, \kappa_{\max}) = (1, 20)$. This places high prior strength at (s, a) where the simulator is both self-consistent ($c_{s,a} \approx 1$) and treats the pair as important ($\bar{g}_{s,a} \approx 1$), and low prior strength elsewhere. The procedure is purely simulator-intrinsic and does not leak information from real-world data. On the HIV DGP, Region-B zones receive $\kappa_0 \approx \kappa_{\min}$ (the simulator-optimal policy never visits them, so \bar{g} is small), triggering the Proposition 4.1 mechanism described above.

A.7 Bayes-regret bound for Fisher-SEP in the reward-dominates regime

Fisher-SEP is a design criterion rather than a regret-minimizing algorithm, but its exploit phase has a Bayes-regret bound in the reward-dominates regime (Corollary 2) that makes explicit how pilot length trades against exploration cost. We state it here.

Setup. Consider the two-phase Fisher-SEP-R protocol: for the first T_{pilot} steps the planner runs the A-optimal PVV-minimizing explorer π^{explore} over a fraction $f \in (0, 1)$ of the unit population; the remaining $n(1 - f)$ units follow an exploit policy π^{exploit} (the SOP or A-SOP). After T_{pilot} steps the explorers switch to the posterior-mean-optimal policy computed from the pilot-updated beliefs. Write π^{FS} for this two-phase policy and $W^* := \sup_{\pi \in \Pi_{\text{adapt}}} W(\pi)$ for the Bayes-optimal value. In this subsection we state the bound in *per-unit-normalized* form: $\mathcal{R}(\pi^{\text{FS}}) := (W^* - W(\pi^{\text{FS}}))/n$ is the per-unit Bayes regret, so the unit-population factor n cancels in both the exploration-cost and misranking terms below.

Reward-dominates assumption. The Fisher-SEP-R special case (Corollary 2) applies under Assumption 4 with the transition block of the parameter-space covariance pinned by exact observation of transitions under a randomized pilot. In that regime, $\epsilon_p \leq \epsilon_p^m$ (the irreducible transition model residual) and the leading regret comes from reward-parameter uncertainty.

Theorem 4 (Bayes regret of Fisher-SEP-R). *Under Assumptions 5(a)–(e) and the reward-dominates regime, with a pilot of length T_{pilot} and exploration fraction f , there exists a universal constant $C > 0$ such that*

$$\mathcal{R}(\pi^{\text{FS}}) \leq \underbrace{2fR_{\max}T_{\text{pilot}}}_{\text{exploration cost}} + \underbrace{\frac{CR_{\max}}{(1-\gamma)^2} \sqrt{\frac{|\mathcal{S}||\mathcal{A}| \log(|\mathcal{S}||\mathcal{A}|/\delta)}{fT_{\text{pilot}}}}}_{\text{post-pilot misranking}} + \underbrace{\frac{2R_{\max}}{1-\gamma} \epsilon_r^m + \frac{2\gamma R_{\max}^2}{(1-\gamma)^2} \epsilon_p^m}_{\text{irreducible residual}} \quad (29)$$

with probability at least $1 - \delta$, where $\epsilon_r^m := \max_{s,a} \epsilon_r^m(s, a)$ and $\epsilon_p^m := \max_{s,a} \epsilon_p^m(s, a)$ are the sup-norm model residuals from Lemma 1. The bound is minimized at $T_{\text{pilot}}^* = \Theta\left(\left(\frac{|\mathcal{S}||\mathcal{A}| \log(|\mathcal{S}||\mathcal{A}|/\delta)}{f^3(1-\gamma)^4}\right)^{1/3}\right)$, yielding $\mathcal{R}(\pi^{\text{FS}}) \leq O((|\mathcal{S}||\mathcal{A}|)^{1/3}(1-\gamma)^{-4/3}R_{\max}) + O(\epsilon^m/(1-\gamma)^2)$.

Proof. Decompose the regret into three terms.

Exploration cost. During the pilot, a fraction f of units follow π^{explore} rather than the exploit policy; each such unit forgoes at most R_{\max} per step relative to the Bayes-optimal baseline. Summing over T_{pilot} pilot steps and weighting by the explorer fraction f gives per-unit pilot-phase cost at most $fR_{\max}T_{\text{pilot}}$; the additional factor of 2 in the display absorbs the exploit-versus-Bayes-optimal gap on the non-pilot fraction during the same window (the exploit policy is sub-Bayes-optimal by at most R_{\max} per step before observing the pilot). The per-unit cost therefore is at most $2fR_{\max}T_{\text{pilot}}$; the $1/(1-\gamma)$ discount factor does not appear because the lost reward is summed over the finite pilot window, not compounded over an infinite horizon.

Post-pilot misranking. After the pilot, the explorers switch to the posterior-mean-optimal policy. The post-pilot posterior concentrates at rate $O(1/\sqrt{fT_{\text{pilot}}})$ per covered pair (Cor. 1). Fisher-SEP-R's pilot allocation $n_{s,a}(\pi^{\text{explore}}) = \Theta(fT_{\text{pilot}}/(|\mathcal{S}||\mathcal{A}|))$ balances sample allocation across pairs (by construction of the A-optimal minimizer on reward parameters, Cor. 2). Standard Azuma-Hoeffding on each pair, union-bounded with a $\log(|\mathcal{S}||\mathcal{A}|/\delta)$ factor, gives per-pair concentration $c_r \sqrt{|\mathcal{S}||\mathcal{A}| \log(|\mathcal{S}||\mathcal{A}|/\delta)/(fT_{\text{pilot}})}$. Feeding through Lemma 1's value bound $|V^\pi(\hat{\mathcal{M}}) - V^\pi(\mathcal{M}^*)| \leq 2\epsilon_r/(1-\gamma) + 2\gamma R_{\max}\epsilon_p/(1-\gamma)^2$ and noting that in the reward-dominates regime ϵ_p contributes only its residual ϵ_p^m gives the second term.

Irreducible residual. The ϵ_r^m and ϵ_p^m residuals are functional model-form error, not reducible by any pilot. Lemma 1’s bound with $\epsilon_r = \epsilon_r^m$, $\epsilon_p = \epsilon_p^m$ gives the third term.

Summing and minimizing the first two over T_{pilot} : set derivative of $2fR_{\text{max}}T_{\text{pilot}} + CR_{\text{max}}(1 - \gamma)^{-2}\sqrt{|\mathcal{S}||\mathcal{A}|\log/(fT_{\text{pilot}})}$ w.r.t. T_{pilot} to zero. This gives $T_{\text{pilot}}^* = \Theta((|\mathcal{S}||\mathcal{A}|\log(|\mathcal{S}||\mathcal{A}|/\delta))/(f^3(1 - \gamma)^4))^{1/3}$ and the stated rate. \square

Remark 8 (Comparison to PSRL and UCRL2). *Theorem 4 gives a $T_{\text{pilot}}^{1/3}$ -rate regret bound in the reward-dominates regime, to be compared with PSRL’s Bayes-regret bound $\tilde{O}(H\sqrt{|\mathcal{S}||\mathcal{A}|T})$ [Osband et al., 2013] and UCRL2’s worst-case regret $\tilde{O}(D|\mathcal{S}|\sqrt{|\mathcal{A}|T})$ [Jaksch et al., 2010].*

The rate is different in kind: Theorem 4 bounds design-phase + exploit-phase regret against a Bayes-optimal target W^ , while PSRL and UCRL2 bound worst-case regret against an oracle that knows the true MDP. The targets are different (Bayes optimal under the simulator’s prior, vs. true-MDP oracle), so the rates are not directly comparable. The $T_{\text{pilot}}^{1/3}$ rate is itself strictly slower than \sqrt{T} , the rate PSRL, UCRL2, and KG achieve, and that gap is a direct consequence of the two-phase explore-then-commit structure; an adaptive (non-phase-separated) version of Fisher-SEP-R that continues exploring through the horizon would recover the \sqrt{T} rate, which we leave to future work. The irreducible residual ϵ^m term has no analog in PSRL or UCRL2: it reflects the fact that under structural confounding and model mis-specification, no regret bound beats a $\Omega(\epsilon^m)$ floor; the best any RL algorithm can do is reduce the identifiable ϵ^h component. Read alongside Proposition 11’s negative result, this bound is the currency-of-the-field positive counterpart: Fisher-SEP-R’s explicit $(|\mathcal{S}||\mathcal{A}|, 1/(1 - \gamma), R_{\text{max}})$ scaling recovers an A-optimal rate once the pilot budget is chosen at the optimum.*

A.8 Fisher information notation: interventional vs. observational

The main text uses the symbol $\mathcal{I}_\theta^{\text{int}}(s', a')$ for the per-observation Fisher information that enters Definition 5. The “int” superscript marks this as the *interventional* Fisher, computed from randomized pilot observations rather than from the behavior-policy observed-data likelihood. This subsection makes the distinction explicit to avoid a potential terminology collision with the missing-data / EM literature, where “observed-data Fisher” has a different standard meaning.

Definition 6 (Interventional Fisher information). *For each (s', a') let $\mathbb{P}(R, S' | s', \text{do}(a'))$ be the interventional distribution of reward and next-state under a do-operation setting the action to a' at observed state s' . The interventional per-observation Fisher information of $\theta_{s', a'} = (r_{s', a'}, p_{s', a'})$ is*

$$\mathcal{I}_\theta^{\text{int}}(s', a') := \mathbb{E}_{(R, S') \sim \mathbb{P}(\cdot | s', \text{do}(a'))} [-\nabla_\theta^2 \log \mathbb{P}(R, S' | s', a'; \theta)]. \quad (30)$$

Proposition 3 (Identification of the main-text Fisher with the interventional Fisher). *Under the identifiability conditions of Lemma 2 (randomized S -measurable pilot policy), the quantity $\mathcal{I}_\theta^{\text{int}}(s', a')$ used in Definition 5 of the main text coincides with the interventional Fisher of Definition 6. The Fisher of an observed-data likelihood under the historical behavior policy is a different object (denoted $\mathcal{I}_\theta^{\text{beh}}$ below); using it in place of $\mathcal{I}_\theta^{\text{int}}$ would introduce confounding-induced bias.*

Proof. Lemma 2 shows that under an S -measurable randomized policy $\pi^{\text{exp}}(a | s, h) = \pi^{\text{exp}}(a | s)$, pilot observations at (s', a') are marginally i.i.d. draws from $\mathbb{P}(R | s', \text{do}(a'))$ and $\mathbb{P}(S' | s', \text{do}(a'))$. The empirical-to-expectation Fisher identity, applied to the conjugate model of Assumption 4, gives (30). The behavior-policy observational Fisher $\mathcal{I}_\theta^{\text{beh}} := \mathbb{E}_{\mathbb{P}_{\text{beh}}(\cdot | s', a')} [-\nabla_\theta^2 \log \mathbb{P}_{\text{beh}}]$ differs from $\mathcal{I}_\theta^{\text{int}}$ under $A \not\perp H | S$ (Assumption 3); using $\mathcal{I}_\theta^{\text{beh}}$ in Definition 5 would introduce bias bounded by the Rosenbaum-style multiplicative ratio of Proposition 2 (Section 4, and this appendix below). \square

Remark 9 (Block-diagonality under partial observability). *Definition 5 and the paragraph following it assert block-diagonality of $\mathcal{I}_\theta^{\text{int}}$ across the reward and transition blocks. This claim is about the interventional Fisher of Definition 6, not any observed-likelihood object. Under the MDP factorization $\mathbb{P}(R, S' | s, a, h) = \rho(R | s, a, h) \wp_S(S' | s, a, h)$ (Section 2) and the S -measurability of the pilot, reward and next-state are conditionally independent given (s, a) under the interventional distribution, which gives the block-diagonal structure. Under partial observability of H , the observed-data behavior-policy joint of (R, S') given (s, a) is a mixture over h and is not a product, which would*

fail block-diagonality; this is a further reason to identify $\mathcal{I}_\theta^{\text{int}}$ with the interventional Fisher rather than any observed-likelihood object.

A.9 Delta-method validity for PVV at the design stage

The PVV (9) approximates the posterior predictive variance of $V^{\pi^{\text{tgt}}}$ by a first-order delta-method expansion around a reference parameter θ^* . This subsection bounds the approximation error and shows when the first-order term dominates the remainder, including in the data-starved design regime where the posterior has not yet concentrated.

Lemma 4 (Delta-method remainder for PVV). *Let θ^* be the prior mean under Assumption 4 and let $V^{\pi^{\text{tgt}}}(s; \cdot)$ be the value function as a function of MDP parameters. Assume $V^{\pi^{\text{tgt}}}(s; \cdot)$ is twice continuously differentiable on a convex open neighborhood $\Theta_0 \subseteq \mathbb{R}^{|\mathcal{S}||\mathcal{A}|(|\mathcal{S}|+1)}$ containing the posterior support with positive posterior probability $\geq 1 - \eta$. Denote by $H(\theta; s)$ the Hessian of $V^{\pi^{\text{tgt}}}(s; \cdot)$ at θ and by $\|H\|_{\text{op}, \Theta_0} := \sup_{\theta \in \Theta_0, s} \|H(\theta; s)\|_{\text{op}}$ its maximum operator norm over Θ_0 . Let $m_4 := \mathbb{E}_{b_t}[\|\theta - \theta^*\|^4]$ denote the posterior fourth central moment. Then for the posterior variance of $V^{\pi^{\text{tgt}}}$ under posterior b_t ,*

$$|\text{Var}_{b_t}[V^{\pi^{\text{tgt}}}(s; \theta)] - \text{PVV}_{s, b_t}| \leq \frac{1}{4} \|H\|_{\text{op}, \Theta_0}^2 \cdot m_4 + \|H\|_{\text{op}, \Theta_0} \cdot \sqrt{m_4 \cdot \text{PVV}_{s, b_t}} + 2\eta \cdot (R_{\max}/(1-\gamma))^2, \quad (31)$$

where $\text{PVV}_{s, b_t} = \nabla V(\theta^*)^\top \Sigma_{b_t} \nabla V(\theta^*)$ is the per-state first-order PVV at s .

Proof. Write $V(\theta) := V^{\pi^{\text{tgt}}}(s; \theta)$. Taylor-expand at θ^* : $V(\theta) = V(\theta^*) + X(\theta) + Y(\theta)$ with $X(\theta) := \nabla V(\theta^*)^\top (\theta - \theta^*)$ the linear term and $Y(\theta) := \frac{1}{2}(\theta - \theta^*)^\top H(\tilde{\theta})(\theta - \theta^*)$ the quadratic remainder, for some $\tilde{\theta}$ on the segment between θ and θ^* . On Θ_0 , $|Y(\theta)| \leq \frac{1}{2} \|H\|_{\text{op}, \Theta_0} \cdot \|\theta - \theta^*\|^2$, so $\mathbb{E}[Y^2] \leq \frac{1}{4} \|H\|^2 \cdot m_4$ and hence $\text{Var}(Y) \leq \frac{1}{4} \|H\|^2 \cdot m_4$.

Decomposing $V(\theta) - V(\theta^*) = X(\theta) + Y(\theta)$ and using bilinearity of variance,

$$\text{Var}[V(\theta)] = \text{Var}[X] + 2\text{Cov}(X, Y) + \text{Var}[Y],$$

so $|\text{Var}[V] - \text{Var}[X]| \leq \text{Var}[Y] + 2|\text{Cov}(X, Y)|$. Cauchy–Schwarz gives $|\text{Cov}(X, Y)| \leq \sqrt{\text{Var}(X) \text{Var}(Y)}$, with $\text{Var}(X) = \text{PVV}_{s, b_t}$ and $\text{Var}(Y) \leq \frac{1}{4} \|H\|^2 m_4$. Combining,

$$|\text{Var}[V] - \text{PVV}_{s, b_t}| \leq \frac{1}{4} \|H\|^2 m_4 + 2\sqrt{\text{PVV}_{s, b_t} \cdot \frac{1}{4} \|H\|^2 m_4} = \frac{1}{4} \|H\|^2 m_4 + \|H\| \sqrt{m_4 \cdot \text{PVV}_{s, b_t}}.$$

The $2\eta(R_{\max}/(1-\gamma))^2$ additive term absorbs the contribution from Θ_0^c via the uniform bound $|V(\theta)| \leq R_{\max}/(1-\gamma)$ applied to $\text{Var}[V] \leq \mathbb{E}[V^2]$ on the low-probability set. \square

Proposition 4 (Validity of PVV-minimization ranking in the data-starved regime). *Let π, π' be two candidate exploration policies with PVV values $P := \text{PVV}(\pi; \pi^{\text{tgt}})$ and $P' := \text{PVV}(\pi'; \pi^{\text{tgt}})$, and let $P_{\max} := \max(P, P')$. Let $R_\Delta := \frac{1}{4} \|H\|_{\text{op}, \Theta_0}^2 m_4 + \|H\|_{\text{op}, \Theta_0} \sqrt{m_4 P_{\max}} + 2\eta(R_{\max}/(1-\gamma))^2$ be the per-policy remainder bound from Lemma 4, with m_4 the posterior fourth moment. Then the sign of the true posterior-variance difference agrees with the sign of the PVV difference whenever $|P - P'| > 2R_\Delta$. In the data-starved regime ($t = 0$, pre-pilot) with prior from Assumption 4 satisfying $\sigma^{(0)} \leq R_{\max}$ and Dirichlet concentration $\alpha^{(0)} \geq 1$, the prior fourth moment m_4 is finite and $R_\Delta = O(R_{\max}^2 \|H\|_{\text{op}, \Theta_0}^2)$, independent of the horizon T .*

Proof. Apply Lemma 4 to each of π, π' : each first-order PVV differs from the true posterior variance of $V^{\pi^{\text{tgt}}}$ by at most R_Δ . By the triangle inequality, the true-variance difference lies within $2R_\Delta$ of the PVV difference, so a PVV gap of size greater than $2R_\Delta$ determines the sign of the true gap. \square

Remark 10 (Why the HIV case satisfies the condition). *On the HIV grid, Region-B zones have a weakly informative Beta prior on p_j (prior standard deviation $\sigma_B^{(0)} \approx 0.25$), Region-A prior $\sigma_A^{(0)} \approx 0.08$, and $R_{\max} = 1$. The Hessian norm $\|H\|_{\text{op}}$ is bounded by $\gamma T_{\text{eff}} \|L\|_{\text{op}}^2 / (1-\gamma)^3 \approx 50$ (computed from the SIS Jacobian). Lemma 4's bound is worst-case over $\theta \in \Theta_0$ with the Hessian evaluated at the operator norm uniformly; in practice $\|L\|_{\text{op}}$ is achieved only at the dominant (corridor-crossing) eigenmode, so the realized quadratic remainder is substantially smaller than the*

bound. A Monte-Carlo variance check on the HIV prior gives $|\text{Var}_{b_t}[V^{\text{tgt}}] - \text{PVV}|/\text{PVV} < 0.1$ at the Fisher-SEP-T vs. A-SOP comparison; since the first-order PVV difference $\Delta \approx 0.3$ between the two policies is substantially larger than the sampled remainder magnitude, the PVV-minimization ranking is valid empirically on HIV. For priors with much higher prior variance or $\|L\|_{\text{op}}$ achieved in multiple eigen-directions, a Monte-Carlo-variance or second-order correction to PVV would be required; we leave this to future work.

A.10 Pre-pilot Fisher sensitivity: robustness to the initial τ^{obs} guess

The PVV criterion requires a per- (s', a') observation precision $\tau_{s', a'}^{\text{obs}}$ that by Lemma 2 is identified from pilot data. At design time, before the pilot has been run, the planner uses a pre-pilot guess $\hat{\tau}_0$ derived from the simulator’s stated reward variance (see Appendix A.6). This raises a circularity concern: the design object depends on a quantity whose identification follows from the design being executed. This subsection shows the PVV-minimization ranking is stable under M -bounded multiplicative perturbation of the pre-pilot guess, so the concern is quantitative rather than fundamental.

Proposition 5 (Rank-stability of PVV minimizer under τ^{obs} perturbation). *Let $\hat{\tau}_0, \tau^*$ be two candidate per-observation Fisher vectors satisfying $\hat{\tau}_0(s', a')/\tau^*(s', a') \in [1/M, M]$ for some $M \geq 1$ and all (s', a') . Let $\pi^*(\tau) := \arg \min_{\pi} \text{PVV}(\pi; \pi^{\text{tgt}}, \tau)$ be the PVV minimizer under τ . Then*

$$\text{PVV}(\pi^*(\hat{\tau}_0); \pi^{\text{tgt}}, \tau^*) \leq M^2 \cdot \text{PVV}(\pi^*(\tau^*); \pi^{\text{tgt}}, \tau^*). \quad (32)$$

Proof. For any (s', a') , let $c_{s', a'}(\pi)$ denote the target-gradient-weighted per-pair prior-variance term so that the (s', a') contribution to PVV under per-observation Fisher τ and pilot count $n := n_{s', a'}(\pi)$ is $c_{s', a'}(\pi)/(I_0(s', a') + n\tau)$. Under the hypothesis $\hat{\tau}_0/\tau^* \in [1/M, M]$, we have $\hat{\tau}_0(s', a') \geq \tau^*(s', a')/M$, so

$$I_0 + n\hat{\tau}_0 \geq I_0 + \frac{n\tau^*}{M} \geq \frac{I_0 + n\tau^*}{M}$$

using $M \geq 1$ and $I_0 \geq 0$ (so $I_0 \geq I_0/M$). Hence for any fixed policy π and fixed pair (s', a') ,

$$\frac{c_{s', a'}(\pi)}{I_0 + n\hat{\tau}_0} \leq \frac{M \cdot c_{s', a'}(\pi)}{I_0 + n\tau^*},$$

giving $\text{PVV}(\pi; \hat{\tau}_0) \leq M \cdot \text{PVV}(\pi; \tau^*)$ and symmetrically $\text{PVV}(\pi; \tau^*) \leq M \cdot \text{PVV}(\pi; \hat{\tau}_0)$. Then $\text{PVV}(\pi^*(\hat{\tau}_0); \tau^*) \leq M \cdot \text{PVV}(\pi^*(\hat{\tau}_0); \hat{\tau}_0) \leq M \cdot \text{PVV}(\pi^*(\tau^*); \hat{\tau}_0) \leq M^2 \cdot \text{PVV}(\pi^*(\tau^*); \tau^*)$, where the middle inequality uses that $\pi^*(\hat{\tau}_0) = \arg \min_{\pi} \text{PVV}(\pi; \hat{\tau}_0)$. \square

Remark 11 (Practical consequence). *If the pre-pilot $\hat{\tau}_0$ is within a factor of $M = 2$ of the true τ^* (an achievable tolerance with simulator-stated variances), the PVV value of the designed explorer is within a factor of 4 of the PVV-optimal value, so the ranking of candidate policies is preserved for any gap exceeding this factor. This is a conservative bound; for the HIV case the simulator-stated Region-A variance underestimates the true τ^* by at most $1.5\times$ (from the $c_{s, a}$ diagnostic in App. A.6), giving $M^2 \leq 2.25$. The pre-pilot guess is therefore conservative, not circular: it systematically overestimates PVV (tighter prior \rightarrow lower pilot-informativeness estimate), making Fisher-SEP allocate more pilot mass to under-trusted pairs, which is what the explore-under-ignorance mechanism requires.*

A.11 Reachability positivity: an RL analog of causal overlap

The main text uses the phrase “positivity violation in the causal sense” in Section 1 to describe the support-mismatch that drives the reachability gap. Classical causal-inference positivity is a condition on the treatment-assignment mechanism: $\mathbb{P}(A = a \mid X) > 0$ for all actions a and observed covariates X , where X is the adjustment set [Pearl, 2009, Kallus and Zhou, 2018]. The paper’s notion is related but not identical: it concerns the *deployed policy’s state visitation* rather than the *treatment assignment mechanism*. This subsection defines the correct analog, shows it is the support condition that drives Proposition 4.1, and relates it to Kallus-style overlap in off-policy evaluation.

Definition 7 (Reachability positivity). *Let π^{dep} be the planner’s deployed policy (e.g., the SOP or A-SOP) and let π^{tgt} be the target policy whose value is the object of Fisher-SEP’s design. We say the pair $(\pi^{\text{dep}}, \pi^{\text{tgt}})$ satisfies reachability positivity if*

$$\text{supp}(d_{\pi^{\text{tgt}}}) \subseteq \text{supp}(d_{\pi^{\text{dep}}}), \quad (33)$$

i.e., the target’s discounted state-visitation distribution is absolutely continuous with respect to the deployed policy’s. Reachability positivity fails when (33) is violated: $\exists s$ with $d_{\pi^{\text{tgt}}}(s) > 0$ and $d_{\pi^{\text{dep}}}(s) = 0$.

Proposition 6 (Reachability positivity failure is the mechanism of Proposition 4.1). *Under Assumptions 5(a)–(f), the following are equivalent:*

- (i) *Reachability positivity between $(\pi^{\text{dep}}, \pi^{\text{tgt}})$ fails.*
- (ii) *There exists (s', a') with $n_{s', a'}(\pi^{\text{dep}}) = 0$ and $\nabla_{\theta} V^{\pi^{\text{tgt}}}(s) \neq 0$ for some $s \in \text{supp}(d_{\pi^{\text{tgt}}})$.*
- (iii) *The Fisher-SEP explorer $\pi^* = \arg \min_{\pi} \text{PVV}(\pi; \pi^{\text{tgt}})$ has $n_{s', a'}(\pi^*) > 0$ at some (s', a') with $n_{s', a'}(\pi^{\text{dep}}) = 0$ and the PVV objective strictly prefers π^* over any policy supported on $\text{supp}(d_{\pi^{\text{dep}}})$.*

Proof. (i) \Rightarrow (ii): If (i) holds, take $s \in \text{supp}(d_{\pi^{\text{tgt}}}) \setminus \text{supp}(d_{\pi^{\text{dep}}})$ and $(s', a') = (s, \pi^{\text{tgt}}(s))$. Then $n_{s', a'}(\pi^{\text{dep}}) = 0$ (the deployed policy does not visit s), and $\nabla_{\theta} V^{\pi^{\text{tgt}}}(s) \neq 0$ generically because perturbations of $\theta_{s', a'}$ directly change $V^{\pi^{\text{tgt}}}(s)$.

(ii) \Rightarrow (iii): Given (ii), the PVV term at (s', a') is reducible (Proposition 4.1), and any explorer with positive visitation there achieves a strictly lower objective than any $\text{supp}(d_{\pi^{\text{dep}}})$ -supported policy.

(iii) \Rightarrow (i): If Fisher-SEP’s optimum strictly dominates any $\text{supp}(d_{\pi^{\text{dep}}})$ -supported policy, there must be a target-sensitive pair off the deployed policy’s support; by definition $d_{\pi^{\text{tgt}}}$ has positive mass at that pair while $d_{\pi^{\text{dep}}}$ does not. \square

Remark 12 (Relation to OPE-style overlap). *In off-policy evaluation, the overlap condition [Kallus and Zhou, 2018, Namkoong et al., 2020] requires that the behavior policy’s state-action visitation dominate the target policy’s: $d_{\pi^{\text{tgt}}}(s)\pi^{\text{tgt}}(a | s) > 0 \Rightarrow d_{\pi^{\text{beh}}}(s)\pi^{\text{beh}}(a | s) > 0$. Reachability positivity is a strictly weaker version at the state level (it does not require joint (s, a) overlap), which is the appropriate notion when the planner’s control problem is the choice of actions and the choice of whether to visit a state at all. It is also weaker than causal treatment-assignment positivity [Pearl, 2009], which concerns the conditional distribution of treatment given covariates under a fixed intervention; in our setting the “treatment” is the action and the “covariate” is the observed state, but the MDP adds an additional temporal dimension through the visitation distribution d_{π} .*

A.12 Confounding vs. drift: separating the two components of ϵ^h

The hidden-state error ϵ^h in Lemma 1 collapses two distinct phenomena: *confounding* (the calibration distribution differs from the calibration marginal because π_{beh} depended on H) and *drift* (the deployment-time and calibration-time hidden-state marginals differ even ignoring the a -conditioning). An S -measurable randomized pilot reduces both to finite-sample noise at once, but the two phenomena have very different implications for what auxiliary information would help. This subsection defines a finer decomposition and gives a sufficient condition for the two to be separately identified.

Definition 8 (Confounding and drift components). *Let*

$$\bar{\rho}_{\text{calib, marg}}(s, a) := \mathbb{E}_{h \sim \mathbb{P}_{\text{calib}}(\cdot | s)}[\bar{r}(s, a, h)], \quad (34)$$

$$\bar{\rho}_{\text{calib, cond}}(s, a) := \mathbb{E}_{h \sim \mathbb{P}_{\text{calib}}(\cdot | s, a)}[\bar{r}(s, a, h)]. \quad (35)$$

The reward-side hidden-state error $\epsilon_r^h(s, a)$ of Lemma 1 decomposes as

$$\epsilon_r^h(s, a) \leq \underbrace{|\bar{\rho}_{\text{calib, cond}}(s, a) - \bar{\rho}_{\text{calib, marg}}(s, a)|}_{=: \epsilon_r^{\text{conf}}(s, a)} + \underbrace{|\bar{\rho}_{\text{calib, marg}}(s, a) - \rho_{\text{obs}}^*(s, a)|}_{=: \epsilon_r^{\text{drift}}(s, a)}, \quad (36)$$

where ϵ^{conf} is the confounding bias (difference between the a -conditional and a -marginal calibration expectations) and ϵ^{drift} is the drift bias (difference between the calibration marginal and the deployment marginal).

Lemma 5 (Separate identification of ϵ^{conf} and ϵ^{drift}). *Suppose the planner has access to:*

- (a) *Calibration-time unconditional observations at (s, a) , i.e., a subsample $\mathcal{D}_{\text{unc}} \subset \mathcal{D}_{\text{calib}}$ for which the calibration behavior policy’s action-choice at (s, a) was recorded and which can be re-weighted to $\mathbb{P}_{\text{calib}}(h | s)$; or equivalently, access to any validly re-weighted calibration sample under $\pi_{\text{calib, marg}}$.*

(b) A deployment-time randomized pilot at (s, a) (Lemma 2).

Then:

- $\epsilon_r^{\text{conf}}(s, a)$ is identified from within-calibration comparisons between the conditional and the re-weighted marginal expectations.
- $\epsilon_r^{\text{drift}}(s, a)$ is identified from calibration-vs-deployment comparisons: the re-weighted calibration marginal vs. the pilot estimate.

Proof. $\epsilon_r^{\text{conf}} = |\bar{\rho}_{\text{calib,cond}} - \bar{\rho}_{\text{calib,marg}}|$ involves only calibration-distribution quantities, both estimable from $\mathcal{D}_{\text{calib}}$ with appropriate re-weighting (standard IPW estimator for the marginal; conditional empirical mean for the cond). $\epsilon_r^{\text{drift}} = |\bar{\rho}_{\text{calib,marg}} - \rho_{\text{obs}}^*|$ compares the calibration marginal (estimable as above) to the deployment interventional expectation (estimable from the pilot via Lemma 2). \square

Remark 13 (Which is which dominates). *When the planner has only the pilot but not the calibration-metadata access of Lemma 5(a), the decomposition (36) is not separately identified, and the single $\hat{\epsilon}_r^h$ diagnostic estimated in App. B.5 bundles the two. Diagnosing which component dominates requires either (i) auxiliary calibration metadata, (ii) auxiliary drift information (e.g., a model of how H evolves between calibration and deployment), or (iii) an assumption that one of the two is negligible. In the vending DGP, the ablation in App. C.15 deliberately runs three regimes — no confounding, no drift, and both — which de-facto separates the two post-hoc. In the HIV DGP, the Region-B underestimate is explicitly drift-dominated (the clinic-based surveillance never sampled Region B), so the $15\times$ prevalence gap is ϵ^{drift} , not ϵ^{conf} . This is recorded here as a structural feature of the DGP, not as a claim that the diagnostic separates them from data alone.*

A.13 Bounded-propensity-odds sensitivity bound

Section 4 bounds the bias from using $\text{Var}_{\pi^{\text{beh}}}(R | s, a)$ in place of $(\tau_{s,a}^{\text{int}})^{-1}$ by a bounded-propensity-odds sensitivity constant M , in the style of Tan [2006]; this subsection states the bound precisely.

Proposition 7 (Bounded-propensity-odds sensitivity bound). *Let $w(h | s, a) := \pi^{\text{beh}}(a | s, h)/\pi^{\text{beh}}(a | s)$ be the propensity-odds ratio, and suppose $w(h | s, a) \in [1/M, M]$ uniformly in h and (s, a) . Then the behavior-policy conditional reward variance and the interventional reward variance satisfy*

$$\frac{1}{M^2} \cdot \text{Var}_{\mathbb{P}(\cdot | s, \text{do}(a))}(R) \leq \text{Var}_{\pi^{\text{beh}}}(R | s, a) \leq M^2 \cdot \text{Var}_{\mathbb{P}(\cdot | s, \text{do}(a))}(R). \quad (37)$$

Proof. The behavior-policy conditional distribution of R given (s, a) is $\sum_h w(h | s, a)\mathbb{P}(h | s)\rho(\cdot | s, a, h)$ (change of measure from the interventional distribution with importance weight w). Writing both variances as expectations over h of $\mathbb{E}[R | s, a, h]^2$ minus squared means, the multiplicative bound on w gives the two-sided M^2 factor. \square

Remark 14 (Relation to Rosenbaum Γ -sensitivity). *Rosenbaum’s Γ -sensitivity [Rosenbaum, 2002] parameterizes the conditional odds ratio of treatment at two matched units that are observationally identical but have different hidden h . Proposition 7 uses a different parameterization: the marginal-vs-conditional propensity odds, matching the classical inverse-probability-weighted sensitivity of Tan [2006]. The two coincide when $M = \Gamma$ in the matched-pair regime. The empirical-Bayes estimator of $\tau_{s,a}$ in App. B remains consistent under bounded M .*

B Policy Algorithms

This appendix provides Python-style pseudocode for each level of the policy hierarchy (Table A12). All algorithms operate on a tabular MDP with S states, K actions, discount factor γ , and a population of n units. The simulator supplies a prior mean MDP $\hat{\mathcal{M}}_{\text{sim}} = (\hat{\rho}_{\text{sim}}, \hat{\delta}_{\text{sim}})$. We first define the shared subroutines (belief initialization, Bayesian updating, posterior MDP construction, value iteration, and EPI computation), then present the policy algorithms in order of increasing sophistication.

B.1 Shared Subroutines

Listing 1: Initialize Bayesian belief state from the simulator.

```
1 def init_belief(sim_rewards, sim_transitions, sigma_0, alpha_0):
2     """Initialize conjugate priors from the simulator's predictions.
3     """
4     S, K = sim_rewards.shape
5     # Gaussian priors on mean rewards: mean = simulator, precision =
6     # 1/sigma_0^2
7     means = sim_rewards.copy() # shape (S, K)
8     precisions = np.full((S, K), 1.0 / sigma_0**2)
9     # Dirichlet priors on transitions: concentrate around simulator's
10    # model
11    # alpha_{s,a,s'} = 1 + alpha_0 * P_sim(s'/s,a)
12    alpha = np.ones((S, K, S)) + alpha_0 * sim_transitions
13    return BeliefState(means, precisions, alpha)
```

Listing 2: Conjugate Bayesian update from a single observation.

```
1 def bayes_update(belief, s, a, reward, next_state, obs_var):
2     """Update beliefs from one (s, a, r, s') observation."""
3
4     # --- Gaussian update for rewards (precision-weighted mean) ---
5     obs_precision = 1.0 / obs_var
6     new_precision = belief.precisions[s, a] + obs_precision
7     new_mean = (belief.precisions[s, a] * belief.means[s, a]
8                + obs_precision * reward) / new_precision
9     belief.means[s, a] = new_mean
10    belief.precisions[s, a] = new_precision
11
12    # --- Dirichlet update for transitions (increment observed count) ---
13    belief.alpha[s, a, next_state] += 1.0
```

Listing 3: Construct the posterior mean MDP from current beliefs.

```
1 def posterior_mdp(belief, gamma):
2     """Build a tabular MDP from posterior means."""
3     S, K = belief.means.shape
4
5     # Posterior mean rewards = Gaussian posterior means
6     rewards = belief.means.copy()
7
8     # Posterior mean transitions = Dirichlet means: alpha / sum(
9     # alpha)
10    alpha_sums = belief.alpha.sum(axis=2, keepdims=True) # (S, K,
11    1)
12    transitions = belief.alpha / alpha_sums # (S, K,
13    S)
14
15    return TabularMDP(rewards, transitions, gamma)
```

Listing 4: Value iteration for a tabular MDP.

```
1 def value_iteration(mdp, tol=1e-10):
2     """Solve for the optimal value function and greedy policy."""
3     S, K = mdp.S, mdp.K
4     V = np.zeros(S)
5
6     while True:
```

```

7         # Bellman backup:  $Q(s, a) = r(s, a) + \gamma \sum_{s'} P(s'/s, a) V(s')$ 
8         Q = mdp.rewards + mdp.gamma * (mdp.transitions @ V)
9         V_new = Q.max(axis=1)
10
11         if np.max(np.abs(V_new - V)) < tol:
12             break
13         V = V_new
14
15         # Greedy policy: pick the action with highest Q-value at each
16         # state
17         pi = Q.argmax(axis=1)
18         return V, pi

```

Listing 5: Compute the Exploration Priority Index (Definition 3.2).

```

1 def compute_epi(mdp, pi, belief, beta_conf, obs_var, T):
2     """EPI(s,a) = d(s) * (reward_term + transition_term)."""
3     S, K, gamma = mdp.S, mdp.K, mdp.gamma
4
5     # Discounted state visitation frequency under policy pi
6     mu = np.ones(S) / S # uniform initial
7     # distribution
8     d = np.zeros(S)
9     for t in range(T + 1):
10        d += (gamma ** t) * mu
11        # Propagate:  $\mu(s') = \sum_s \mu(s) * P(s'/s, \pi(s))$ 
12        P_pi = mdp.transitions[np.arange(S), pi, :] # (S, S)
13        mu = mu @ P_pi
14        d *= (1 - gamma) / (1 - gamma ** (T + 1)) # normalize
15
16    # Per-state-action EPI scores
17    sigmas = 1.0 / np.sqrt(belief.precisions) # posterior std devs
18    reward_term = (sigmas**2 + beta_conf**2) / obs_var
19    alpha_sums = belief.alpha.sum(axis=2) # (S, K)
20    transition_term = gamma * mdp.R_max * (S - 1) / ((1 - gamma) *
21    alpha_sums)
22
23    epi = d[:, None] * (reward_term + transition_term) # (S, K)
24    return epi

```

B.2 Policy Algorithms

Listing 6: Level 0: Simulator-Optimal Policy (SOP).

```

1 def run_sop(sim_mdp, n_units, T):
2     """Deploy the simulator-trained policy without adaptation."""
3     # Solve the simulator's MDP once, before deployment
4     V, pi = value_iteration(sim_mdp)
5
6     for t in range(T):
7         for i in range(n_units):
8             action = pi[states[i]] # always follow the
9             # simulator-trained policy
10            # No belief updates -- observations are discarded

```

Listing 7: Level 1: ϵ -Greedy Perturbation.

```

1 def run_epsilon_greedy(sim_mdp, n_units, T, epsilon):
2     """Undirected stochastic exploration, no learning."""
3     V, pi = value_iteration(sim_mdp)
4
5     for t in range(T):

```

```

6     for i in range(n_units):
7         if np.random.random() < epsilon:
8             action = np.random.randint(K) # explore: random
              action
9         else:
10            action = pi[states[i]]          # exploit: simulator-
              trained policy
11            # No belief updates -- observations are discarded

```

Listing 8: Level 1': Adaptive SOP (A-SOP / Passive Learning).

```

1 def run_asop(sim_mdp, n_units, T, obs_var, replan_interval=5):
2     """Passive learning: update beliefs, always follow posterior
3     optimum."""
4     belief = init_belief(sim_mdp.rewards, sim_mdp.transitions,
5                          sigma_0=1.0, alpha_0=5.0)
6
7     for t in range(T):
8         # Periodically re-solve the posterior MDP (including t=0)
9         if t % replan_interval == 0:
10            mdp_post = posterior_mdp(belief, sim_mdp.gamma)
11            V, pi = value_iteration(mdp_post)
12
13            for i in range(n_units):
14                # Always follow the current posterior-optimal policy
15                action = pi[states[i]]
16                reward, next_state = env.step(states[i], action)
17
18                # Update beliefs from this observation
19                bayes_update(belief, states[i], action, reward,
20                            next_state, obs_var)

```

Listing 9: Level 2: KG-SEP (Myopic Knowledge Gradient).

```

1 def run_kg_sep(sim_mdp, n_units, T, obs_var, replan_interval=5):
2     """Targeted per-state exploration using the augmented Q-value."
3     """
4     belief = init_belief(sim_mdp.rewards, sim_mdp.transitions,
5                          sigma_0=1.0, alpha_0=5.0)
6     V_sim, pi_sim = value_iteration(sim_mdp)
7
8     for t in range(T):
9         mdp_post = posterior_mdp(belief, sim_mdp.gamma)
10
11        for i in range(n_units):
12            s = states[i]
13            # Compute augmented Q-value for each action
14            for a in range(K):
15                earn = belief.means[s, a] # posterior mean
16                # reward
17                learn = gamma * (reward_info(belief, s, a, obs_var)
18                                + transition_info(belief, s, a,
19                                                    sim_mdp))
20                position = gamma * np.dot(
21                    mdp_post.transitions[s, a], V_sim) #
22                    continuation value
23                Q_aug[a] = earn + learn + position
24
25            # Select the action with highest augmented Q-value
26            action = np.argmax(Q_aug)
27            reward, next_state = env.step(s, action)
28            bayes_update(belief, s, action, reward, next_state,
29                        obs_var)

```

The KG-SEP listing above shows the per-unit reduction. In the multi-unit-per-step setting that the experiments use, the implementation (`methods/policies/knowledge_gradient.py`) allocates units across actions proportionally to the augmented Q-values rather than concentrating all units on the argmax; the per-unit and proportional rules coincide when only one unit is being assigned at a state, which is the semantics the pseudocode targets.

Listing 10: Level 3: Trajectory-Planned SEP (EPI-Directed).

```

1 def run_sep(sim_mdp, n_units, T, obs_var,
2             T_pilot=5, T_explore=15, eps_explore=0.5,
3             replan_interval=5, reexplore_threshold=0.8):
4     """Three-phase SEP: pilot -> EPI-directed explore -> exploit."""
5     belief = init_belief(sim_mdp.rewards, sim_mdp.transitions,
6                          sigma_0=1.0, alpha_0=5.0)
7     V_sim, pi_sim = value_iteration(sim_mdp)
8     epi = compute_epi(sim_mdp, pi_sim, belief, beta_conf=0, obs_var=
9                     obs_var,
10                      T=int(1/(1-sim_mdp.gamma)))
11     pi_exploit = pi_sim.copy()
12     epi_baseline = None
13
14     for t in range(T):
15         # --- Phase 1: Pilot (uniform random to collect unbiased
16         # data) ---
17         if t < T_pilot:
18             for i in range(n_units):
19                 action = np.random.randint(K)
20                 reward, next_state = env.step(states[i], action)
21                 bayes_update(belief, states[i], action, reward,
22                             next_state, obs_var)
23
24         # --- Phase 2: Explore (EPI-directed + posterior-optimal mix
25         # ) ---
26         elif t < T_pilot + T_explore:
27             for i in range(n_units):
28                 if np.random.random() < eps_explore:
29                     action = np.argmax(epi[states[i]]) # highest-
30                     EPI action
31                 else:
32                     action = pi_exploit[states[i]] # posterior
33                     -optimal
34                 reward, next_state = env.step(states[i], action)
35                 bayes_update(belief, states[i], action, reward,
36                             next_state, obs_var)
37
38         # --- Phase 3: Exploit (posterior-optimal with EPI
39         # monitoring) ---
40         else:
41             for i in range(n_units):
42                 action = pi_exploit[states[i]]
43                 reward, next_state = env.step(states[i], action)
44                 bayes_update(belief, states[i], action, reward,
45                             next_state, obs_var)
46
47             # Monitor EPI: trigger re-exploration if uncertainty
48             # exceeds the baseline; baseline is captured at Phase 3
49             # entry and refreshed after each triggered burst.
50             if epi_baseline is None:
51                 epi_baseline = epi.max() # captured once at Phase 3
52                 entry
53             elif epi.max() > reexplore_threshold * epi_baseline:
54                 # Re-enter Phase 2 for a short burst; refresh
55                 baseline.
56             pass # (re-exploration logic; see SEPPolicy.
57                 _maybe_replan)

```

```

49
50     # Periodically recompute posterior policy and EPI
51     if t % replan_interval == 0:
52         mdp_post = posterior_mdp(belief, sim_mdp.gamma)
53         _, pi_exploit = value_iteration(mdp_post)
54         epi = compute_epi(mdp_post, pi_exploit, belief,
55                          beta_conf=0, obs_var=obs_var,
56                          T=int(1/(1-sim_mdp.gamma)))

```

The Fisher-SEP implementation below invokes four quantities defined in Section 4 of the main text: the value gradient $\nabla_{\theta} V^{\pi}$ (Definition 5), the prior Fisher information $I_0(s, a) = \kappa_0(s, a) / \sigma_{s,a}^2(0)$ with per- (s, a) prior strength κ_0 set by the simulator-self-consistency heuristic of Appendix A.6, the Normal-Inverse-Gamma (or Beta-Binomial, for the HIV DGP) posterior variance $\text{Var}(\theta_{s,a} | \mathcal{D})$ after pilot data, and the per- (s, a) observation precision $\tau_{s,a}^{\text{obs}}$ identified from randomized-action pilot data (Lemma 2; in this appendix $\tau_{s,a}^{\text{obs}} = \tau_{s,a}^{\text{int}}$ of Definition 5). The posterior predictive value variance $\text{PVV}(\pi)$ (Definition 5) is evaluated on a candidate stochastic policy π by `compute_pvv`; `minimize_pvv_policy` minimizes it directly via coordinate descent (non-linear in π because the expected observation count $n_{s',a'}(\pi)$ appears in the denominator).

Listing 11: Level 3': Fisher-SEP (Bayesian A-optimal posterior-value-variance).

```

1 def run_fisher_sep(sim_mdp, n_units, T, obs_var,
2                   T_pilot=5, T_explore=15, eps_explore=0.5,
3                   replan_interval=10, fisher_iters=60):
4     """Three-phase Fisher-SEP (v3): pilot -> PVV-minimize -> exploit
5     .
6     Minimizes the posterior predictive value variance PVV(pi) of
7     Definition~\ref{def:pvv} via coordinate descent on stochastic pi
8     .
9     """
10    # Simulator-self-consistency prior strength (Appendix~\ref{app:
11    fisher-v3-kappa0})
12    kappa_0 = compute_kappa0_self_consistency(
13        sim_mdp, sim_mdp.stated_variances, n_rollouts=100)
14    I_0      = kappa_0 / sim_mdp.stated_variances      # (S, K)
15
16    belief   = init_belief(sim_mdp.rewards, sim_mdp.transitions,
17                          sigma_0=1.0, alpha_0=2.0)
18
19    pilot_obs = {}
20    list[r]   # (s, a) ->
21
22    # Posterior variance of theta_{s,a}, prior-only at t=0:
23    theta_var = 1.0 / I_0      # (S, K)
24    tau_obs   = 1.0 / obs_var  # (S, K),
25    uniform
26
27    _, pi_exploit = value_iteration(sim_mdp)
28    pi_fisher     = minimize_pvv_policy(
29        sim_mdp, theta_var, tau_obs, T=int(1/(1-sim_mdp.gamma)),
30        n_iter=fisher_iters)
31
32    for t in range(T):
33        if t < T_pilot:
34            # Phase 1: random pilot (S-measurable, a perp H | S).
35            for i in range(n_units):
36                action = np.random.randint(K)
37                r, s_next = env.step(states[i], action)
38                pilot_obs.setdefault((states[i], action), []).append
39                    (r)
40                bayes_update(belief, states[i], action, r, s_next,
41                             obs_var)
42
43        elif t < T_pilot + T_explore:

```

```

36     # Phase 2: sample from the PVV-minimizing stochastic
37     # policy.
38     for i in range(n_units):
39         if np.random.random() < eps_explore:
40             action = np.random.choice(K, p=pi_fisher[states[
41                 i]])
42         else:
43             action = pi_exploit[states[i]]
44             r, s_next = env.step(states[i], action)
45             pilot_obs.setdefault((states[i], action), []).append
46             (r)
47             bayes_update(belief, states[i], action, r, s_next,
48                 obs_var)
49
50     else:
51         # Phase 3: exploit posterior optimum.
52         for i in range(n_units):
53             action = pi_exploit[states[i]]
54             r, s_next = env.step(states[i], action)
55             bayes_update(belief, states[i], action, r, s_next,
56                 obs_var)
57
58     # Periodically re-evaluate on the posterior MDP with updated
59     # posterior variance and re-minimize PVV.
60     if t % replan_interval == 0:
61         mdp_post = posterior_mdp(belief, sim_mdp.gamma)
62         _, pi_exploit = value_iteration(mdp_post)
63         theta_var = compute_theta_posterior_variance(
64             pilot_obs, sim_mdp.stated_variances, sim_mdp.rewards
65             ,
66             kappa_0=kappa_0, alpha_0=2.0)
67         pi_fisher = minimize_pvv_policy(
68             mdp_post, theta_var, tau_obs, T=int(1/(1-sim_mdp.
69                 gamma)),
70             n_iter=fisher_iters, init_pi=pi_fisher)
71
72 def compute_pvv(mdp, pi, theta_var, tau_obs, T):
73     """PVV(pi) = sum_s d_pi(s) * sum_{s',a'} grad_V(s; s',a')^2
74     * PostVar(theta_{s',a'} | n_{s',a'}(pi) pilot obs).
75     See Definition~\ref{def:pvv}.
76     """
77     d_pi, n_sa = visitation_and_obs_counts(mdp, pi, T) # d_pi: (S,)
78     # n_sa: (S, K)
79     prior_prec = 1.0 / theta_var # (S, K)
80     post_prec = prior_prec + n_sa * tau_obs # adds
81     # candidate info
82     post_var_candidate = 1.0 / post_prec # (S, K)
83
84     grad_V = reward_gradient_matrix(mdp, pi) # (S, S*K)
85     )
86     weighted = grad_V ** 2 * post_var_candidate.flatten()[None, :]
87     return float(d_pi @ weighted.sum(axis=1))
88
89 def minimize_pvv_policy(mdp, theta_var, tau_obs, T,
90     n_iter=60, lr=0.3, init_pi=None):
91     """Coordinate descent to MINIMIZE PVV(pi).
92
93     At each step: pick random s, try each "shift lr toward action a"
94     candidate, keep the row with lowest PVV. Non-linear in pi
95     because
96     n_{s',a'}(pi) appears in the denominator.
97     """
98     S, K = mdp.S, mdp.K

```

```

90 pi = init_pi.copy() if init_pi is not None else np.full((S, K)
91 , 1.0/K)
92 base = compute_pvv(mdp, pi, theta_var, tau_obs, T)
93
94 for _ in range(n_iter):
95     s = np.random.randint(S)
96     best_pvv, best_row = base, pi[s].copy()
97     for a in range(K):
98         row = (1 - lr) * pi[s].copy()
99         row[a] += lr
100        row /= row.sum()
101        pi_try = pi.copy(); pi_try[s] = row
102        trial = compute_pvv(mdp, pi_try, theta_var, tau_obs, T)
103        if trial < best_pvv:
104            best_pvv, best_row = trial, row
105    pi[s], base = best_row, best_pvv
return pi

```

DGP-specific realizations. The listing above is the generic tabular Fisher-SEP. Two of our case studies deviate from it for DGP-specific reasons:

- *Vending* (*fisher_sep_v3_vending.py*): per-(vm, product) PVV scores are ranked for allocation rather than running the full coordinate-descent minimizer, because the vending DGP has deterministic visitation given an allocation so the ranking-based policy achieves the PVV minimum up to combinatorial rounding. The gradient $\partial V / \partial \lambda_{ij}$ is computed by a 30-day yield finite difference with $\delta = 0.5$.
- *HIV* (*fisher_sep_v3_hiv.py*): the static Bellman-resolvent gradient is replaced by a 15-day SIS-propagated finite-difference gradient, because perturbing per-zone prevalence changes future prevalence at neighbouring zones through the disease dynamics, and that spread effect dominates the local sensitivity (Appendix D.11). The A-optimal policy class is restricted to the navigation-restricted variant of Fisher-SEP-T (Conjecture 1): rank zones by their per-zone PVV contribution, allocate teams between explore (Region B targets) and exploit (Region A best-known) proportional to the PVV share in each region. Posterior parameter variance uses the Beta-Binomial form of Eq. (52) in place of NIG.

Listing 12: Thompson Sampling (PSRL — External Baseline).

```

1 def run_thompson_sampling(sim_mdp, n_units, T, obs_var,
2 replan_interval=5):
3     """Posterior Sampling for RL (Osband et al., 2013)."""
4     belief = init_belief(sim_mdp.rewards, sim_mdp.transitions,
5                          sigma_0=1.0, alpha_0=5.0)
6
7     for t in range(T):
8         if t % replan_interval == 0:
9             # Sample an MDP from the posterior
10            sampled_rewards = np.zeros((S, K))
11            sampled_transitions = np.zeros((S, K, S))
12            for s in range(S):
13                for a in range(K):
14                    # Sample reward from Gaussian posterior
15                    mu = belief.means[s, a]
16                    sigma = 1.0 / np.sqrt(belief.precisions[s, a])
17                    sampled_rewards[s, a] = np.random.normal(mu,
18                                                            sigma)
19
20            # Sample transitions from Dirichlet posterior
21            sampled_transitions[s, a] = np.random.dirichlet(
22                belief.alpha[s, a])
23
24            # Solve the sampled MDP
25            sampled_mdp = TabularMDP(sampled_rewards,
26                                    sampled_transitions,

```

```

24         sim_mdp.gamma)
25     _, pi = value_iteration(sampled_mdp)
26
27     for i in range(n_units):
28         # Follow the policy from the sampled MDP
29         action = pi[states[i]]
30         reward, next_state = env.step(states[i], action)
31         bayes_update(belief, states[i], action, reward,
32                     next_state, obs_var)

```

B.3 Reduction to classical limits

Fisher-SEP reduces to two familiar objects at the endpoints of the information regime. When observations at every target-relevant (s', a') dominate the prior ($n\tau^{\text{obs}} \gg I_0$) and τ^{obs} is uniform across (s', a') , minimizing (9) is equivalent to maximizing the visitation-weighted squared sensitivity $\sum_s d_{\pi^{\text{tgt}}}(s) (\partial V^{\pi^{\text{tgt}}} / \partial \theta_{s', a'})^2$ —the classical A-optimal design for reward-parameter estimation. When no pilot observations have been collected ($n\tau^{\text{obs}} \ll I_0$), the ranking across (s', a') is the same but weighted by the prior variance $\sigma_{s', a'}^{(0)2} / \kappa_0(s', a')$; the explorer allocates pilot visitation to the top-ranked pairs to break out of the data-starved regime. Fisher-SEP interpolates smoothly between these two limits as pilot data accumulates, so it inherits the asymptotic guarantees of classical A-optimality in the data-rich regime and the finite-sample structure of simulator-prior-weighted ranking in the data-starved regime.

B.4 Transition-parameter PVV (Fisher-SEP-T derivation)

This subsection derives the transition-parameter variant of the PVV (Corollary 3) and connects it to the SIS finite-difference gradient used in the HIV experiment.

Transition Bellman resolvent gradient. Write the value function $V^{\pi^{\text{tgt}}}(s)$ of the target policy under a transition kernel $p(\cdot | \cdot, \cdot)$ and reward $r(\cdot, \cdot)$. Fix (s', a') and perturb $p(\cdot | s', a')$ by a zero-sum perturbation $\delta \in \mathbb{R}^{|\mathcal{S}|}$ (i.e., $\sum_{s''} \delta_{s''} = 0$). The first-order change in $V^{\pi^{\text{tgt}}}$ at state s is

$$\nabla_{p(\cdot | s', a')} V^{\pi^{\text{tgt}}}(s)^\top \delta = \gamma [(I - \gamma P^{\pi^{\text{tgt}}})^{-1}]_{s, s'} \pi^{\text{tgt}}(a' | s') \sum_{s''} \delta_{s''} V^{\pi^{\text{tgt}}}(s'').$$

The Bellman resolvent $(I - \gamma P^{\pi^{\text{tgt}}})^{-1}$ at (s, s') encodes the discounted occupancy of s' starting from s ; the factor $\pi^{\text{tgt}}(a' | s')$ is the probability the target chooses a' at s' ; and $\sum \delta_{s''} V^{\pi^{\text{tgt}}}(s'')$ is the perturbation's expected change in next-state value.

Dirichlet posterior variance. Under Assumption 4, the prior on $\wp_{\text{obs}}^*(\cdot | s', a')$ is $\text{Dir}(\alpha_{s', a'}^{(0)})$. After $n_{s', a'}$ pilot observations with empirical next-state counts $\{c_{s', a', s''}\}$, the posterior is $\text{Dir}(\alpha_{s', a', s''}^{(0)} + c_{s', a', s''})$. The posterior covariance matrix $\Sigma_p(s', a')$ on the simplex has entries

$$\Sigma_p(s', a')_{s'', s'''} = \frac{\alpha_{s'', s', a'} (\alpha_{0, s', a'} + n_{s', a'} - \alpha_{s'', s', a'})}{(\alpha_{0, s', a'} + n_{s', a'})^2 (\alpha_{0, s', a'} + n_{s', a'} + 1)} \delta_{s''=s'''} - \frac{\alpha_{s'', s', a'} \alpha_{s''', s', a'}}{(\alpha_{0, s', a'} + n_{s', a'})^2 (\alpha_{0, s', a'} + n_{s', a'} + 1)} \delta_{s'' \neq s'''},$$

with the diagonal scaling as $1/(1 + n_{s', a'} / \alpha_{0, s', a'})$, matching the PVV denominator of Eq. (9) at $\phi = p$.

SIS finite-difference implementation (HIV). The HIV DGP has non-tabular transitions: prevalence at zone j at day $t + 1$ is a continuous function of prevalence at zone j and neighboring zones at day t through the SIS dynamics of Eq. (46). Evaluating $\nabla_{p(\cdot | s', a')} V^{\pi^{\text{tgt}}}(s)$ analytically in this non-tabular setting would require linearizing the SIS update about the current prevalence, which is well-defined but more cumbersome than a finite difference. We therefore approximate the gradient by perturbing prev_j by $\delta = 0.01$, iterating `spread_disease` for $T_{\text{look}} = 15$ days, and computing the change in total discounted yield. This numerical implementation is an approximation of $\nabla_{p(\cdot | s', a')} V^{\pi^{\text{tgt}}}$ under the Gonsalves SIS dynamics—not a separate algorithm. Fisher-SEP-T (Corollary 3) is the prescription; the SIS finite-difference is its numerical realization in a non-tabular dynamics setting.

B.5 Post-pilot residual estimator for $\hat{\epsilon}_r, \hat{\epsilon}_p$

The crossover-horizon diagnostic of Remark 2 depends on the ratio ϵ_p/ϵ_r . These are not pre-pilot observables; they are distances between the simulator’s stated kernels and the kernels of $\mathcal{M}_{\text{obs}}^*$. After an S -measurable pilot of length T_{pilot} with empirical estimates $\hat{\rho}_{\text{pilot}}(s, a)$ and $\hat{\phi}_{\text{pilot}}(\cdot | s, a)$ on the pilot-covered subset \mathcal{I} , the residuals

$$\begin{aligned}\hat{\epsilon}_r(s, a) &:= |\hat{\rho}_{\text{sim}}(s, a) - \hat{\rho}_{\text{pilot}}(s, a)|, \\ \hat{\epsilon}_p(s, a) &:= \|\hat{\phi}_{\text{sim}}(\cdot | s, a) - \hat{\phi}_{\text{pilot}}(\cdot | s, a)\|_1\end{aligned}$$

are unbiased estimates (up to finite-sample noise) of $\epsilon_r(s, a)$ and $\epsilon_p(s, a)$ on \mathcal{I} , because Lemma 2 makes the pilot mean an unbiased estimate of $\rho_{\text{obs}}^*, \phi_{\text{obs}}^*$. Pooled estimates $\hat{\epsilon}_r := \max_{(s,a) \in \mathcal{I}} \hat{\epsilon}_r(s, a)$ and $\hat{\epsilon}_p := \max_{(s,a) \in \mathcal{I}} \hat{\epsilon}_p(s, a)$ feed the post-pilot crossover diagnostic $\hat{T} \approx T_{\text{eff}} R_{\text{max}} \hat{\epsilon}_p / \hat{\epsilon}_r$. The estimator is uninformative off \mathcal{I} ; under the working assumption that $\hat{\epsilon}_p/\hat{\epsilon}_r$ on \mathcal{I} is representative of the ratio on uncovered pairs, the post-pilot ratio predicts the A-SOP-to-Fisher-SEP crossover ordering observed in the vending experiment (Section 5.1).

Diagnostic vs. identification. The “predicts the crossover” wording in Section 5.1 is a descriptive diagnostic rather than an identification claim. The residual ratio $\hat{\epsilon}_p/\hat{\epsilon}_r$ is computed from the same trials on which the crossover is observed, so the agreement ($\hat{\epsilon}_p/\hat{\epsilon}_r \approx 2$ – 3 ; observed crossover between $T = 400$ and $T = 800$) is an in-sample consistency check of Remark 2’s horizon asymmetry, not an out-of-sample prediction. We record three scope clarifications:

1. *In-sample vs. out-of-sample.* The diagnostic is computed post-hoc and reported as corroborative evidence. An identification version would require a held-out pilot protocol: estimate $\hat{\epsilon}_p/\hat{\epsilon}_r$ from an initial pilot on a subset of units, then predict the crossover horizon for the remaining units. We leave this held-out protocol to future work (it requires a larger trial budget than the 30 common-seed trials used here).
2. *Representativeness off \mathcal{I} .* The working assumption that $\hat{\epsilon}_p/\hat{\epsilon}_r$ on \mathcal{I} equals the ratio on uncovered pairs is unverifiable from the pilot alone. When the uncovered pairs are dominated by ϵ^m (irreducible model residual) and the covered pairs by ϵ^h (identifiable hidden-state error), the two ratios can differ systematically. In the vending DGP the ratio is approximately uniform across pairs by construction, so the extrapolation is defensible; in a real deployment it would need auxiliary justification.
3. *Asymptotic vs. finite- T .* The crossover prediction $T \approx T_{\text{eff}} R_{\text{max}} \hat{\epsilon}_p / \hat{\epsilon}_r$ uses the sup-norm Lemma 1 bound, which is loose by a factor that depends on the spread of errors across (s, a) . The diagnostic captures the order of magnitude of the crossover but not its exact value.

This reframing does not change any empirical result; it clarifies the statistical status of the diagnostic.

C Simulation Details

C.1 Standing assumptions

All theoretical results in the main text and this appendix operate under the following standing assumptions.

Assumption 5 (Standing assumptions).

- (a) Finite tabular state and action spaces. $|\mathbb{S}| = S < \infty$ and $|\mathbb{A}| = K < \infty$. Both the true POMDP and the simulator operate on these spaces, with the simulator’s model restricted to the observed state \mathbb{S} .
- (b) Bounded rewards. $|R_{i,t}| \leq R_{\text{max}} < \infty$ almost surely, and the simulator’s reward model $\hat{\rho}_{\text{sim}}$ is likewise bounded by R_{max} .
- (c) Stationary marginalized dynamics within the planning horizon. The true observed-state transition kernel $\phi_S(\cdot | s, a, h)$ and the reward kernel $\rho(\cdot | s, a, h)$ are time-homogeneous over $t \in \{0, \dots, T\}$. The hidden-state distribution $\mathbb{P}_t(h | s)$ may drift, but the conditional kernels given h do not.
- (d) Fixed simulator. The simulator $\hat{\mathcal{M}}_{\text{sim}} = (\hat{\rho}_{\text{sim}}, \hat{\phi}_{\text{sim}})$ is frozen during deployment; no retraining is performed on the data collected between $t = 0$ and $t = T$. (As Proposition 8 shows, this is a communication choice rather than a modeling restriction: an updatable-simulator formulation produces identical working models under parts (e)–(f) below.)

- (e) Conjugate priors on simulator parameters. *The planner’s belief over the reward parameters $\theta = \{r(s, a)\}$ is Gaussian with known observation variance σ^2 ; the belief over the transition parameters $\{p(\cdot | s, a)\}$ is Dirichlet. The simulator’s predictions $\hat{\rho}_{\text{sim}}(s, a)$ and $\hat{\phi}_{\text{sim}}(\cdot | s, a)$ supply the prior means.*
- (f) Prior independence across state–action pairs. *The priors factorize as $\prod_{(s,a)} \pi_0(r(s, a)) \cdot \prod_{(s,a)} \pi_0(p(\cdot | s, a))$. Hierarchical structure (e.g., correlated priors across neighboring states) is not considered; see Remark 15 for discussion.*

Remark 15 (Scope of prior independence). *Part (f) is stronger than the other assumptions and rules out hierarchical priors that encode structural regularity across the state space. In settings where such structure is known (e.g., demand correlations across geographically nearby vending machines, or prevalence correlations across adjacent zones in the HIV experiment), a hierarchical prior would tighten posterior concentration and reduce the local gap closable by passive updating. The qualitative gap decomposition (Theorem 1) continues to hold, but the numerical magnitudes of $\mathcal{G}_{\text{local}}$ and $\mathcal{G}_{\text{reach}}$ would shift. Part (f) can therefore be read as a reference setting against which hierarchical extensions can be measured.*

We first state the formal equivalence between the fixed-simulator framework and an updatable-simulator framework (Remark C.2), then provide the complete specification of the vending-machine data-generating process.

C.2 Equivalence of fixed and updatable simulators

Proposition 8 (Fixed simulator with Bayesian overlay \equiv Bayesian-updatable simulator). *Consider two formulations of the planner’s problem:*

- (i) Fixed simulator + belief state. *The simulator $\hat{\mathcal{M}}_{\text{sim}} = (\hat{\rho}_{\text{sim}}, \hat{\phi}_{\text{sim}})$ is fixed (Assumption 5(d)). The planner maintains a separate belief state $\mathcal{B}_t = (\{m_{s,a}^{(t)}, (\sigma_{s,a}^{(t)})^2\}, \{\alpha_{s,a}^{(t)}\})$ initialized from the simulator: $m_{s,a}^{(0)} = \hat{\rho}_{\text{sim}}(s, a)$, $\alpha_{s,a}^{(0)}$ derived from $\hat{\phi}_{\text{sim}}(\cdot | s, a)$. After observing reward r at (s, a) , the belief updates via the Gaussian conjugate rule; after observing transition $s \rightarrow s'$ under action a , it updates via the Dirichlet conjugate rule. The planner’s “working model” at time t is the posterior mean MDP $\hat{\mathcal{M}}^{(t)} = (m^{(t)}, \hat{p}^{(t)})$.*
- (ii) Bayesian-updatable simulator. *The simulator is a Bayesian model $\hat{\mathcal{M}}^{(t)}$ that is retrained after each batch of observations. At time 0, $\hat{\mathcal{M}}^{(0)} = \hat{\mathcal{M}}_{\text{sim}}$. After observing data \mathcal{D}_t at time t , the simulator is updated to $\hat{\mathcal{M}}^{(t+1)}$ via Bayes’ rule under the same conjugate priors.*

Under Assumptions 5(e)–(f) (conjugate priors, prior independence), the two formulations produce identical sequences of working models: $\hat{\mathcal{M}}_{(i)}^{(t)} = \hat{\mathcal{M}}_{(ii)}^{(t)}$ for all t and all data realizations. Consequently, any policy that is optimal under formulation (i) is also optimal under formulation (ii), and vice versa.

Proof. Both formulations maintain the same sufficient statistics. Under formulation (i), the belief state at time t is $\mathcal{B}_t = (\{m_{s,a}^{(t)}, \tau_{s,a}^{(t)}\}, \{\alpha_{s,a}^{(t)}\})$, where $\tau_{s,a}^{(t)} = 1/(\sigma_{s,a}^{(t)})^2$ is the precision. The Gaussian update rule gives $\tau_{s,a}^{(t+1)} = \tau_{s,a}^{(t)} + n_{s,a}^{(t)}/\sigma^2$ and $m_{s,a}^{(t+1)} = (\tau_{s,a}^{(t)} m_{s,a}^{(t)} + (n_{s,a}^{(t)}/\sigma^2) \bar{r}_{s,a}^{(t)}) / \tau_{s,a}^{(t+1)}$, where $n_{s,a}^{(t)}$ is the number of observations and $\bar{r}_{s,a}^{(t)}$ their mean. The Dirichlet update gives $\alpha_{s,a}^{(t+1)} = \alpha_{s,a}^{(t)} + \mathbf{c}_{s,a}^{(t)}$, where $\mathbf{c}_{s,a}^{(t)} \in \mathbb{N}^{|\mathbb{S}|}$ is the vector of transition counts from (s, a) to next states $s' \in \mathbb{S}$ observed during the interval between t and $t + 1$.

Under formulation (ii), the “retrained simulator” at time t is the posterior under the same conjugate model with the same data, producing identical sufficient statistics. Since both formulations start from the same prior ($\hat{\mathcal{M}}_{\text{sim}}$), process the same data ($\mathcal{D}_1, \dots, \mathcal{D}_t$), and apply the same update rule (Bayes’ rule under conjugate priors), the posterior is identical by the uniqueness of the Bayesian posterior. The working model $\hat{\mathcal{M}}^{(t)}$ (posterior mean rewards and transitions) is a deterministic function of the sufficient statistics, so it is identical under both formulations. \square

The proposition establishes that Assumption 5(d) is a *communication choice*, not a modeling restriction. We separate the simulator (prior) from the belief state (posterior) because this separation clarifies the theoretical analysis: the SOP optimizes the prior, the A-SOP is the Bayes-adaptive policy that

uses the simulator as a warm start, and the SEP uses the simulator’s structure to design experiments. The gap between them is the value of experimentation. In an “updatable simulator” formulation, the SOP would be the policy that never collects new data (and therefore never updates), while the SEP would be the policy that designs experiments to update the simulator optimally—the same distinction, expressed differently.

The practical implication is that any simulator—including non-Bayesian ones such as neural networks or physics engines—can be wrapped in a conjugate Bayesian layer that treats the simulator’s outputs as prior means. The “fixed simulator” then serves as the prior, and the Bayesian overlay provides the update mechanism at $O(1)$ cost per observation, without retraining the underlying model.

C.3 Data-generating process

This subsection provides the complete specification of the data-generating process for the vending-machine simulation of Section 5.1. All numerical values match the reference implementation (`vending_v3.py`). The main text describes the setup at a conceptual level; the full technical specification follows.

C.4 Confounding and drift

Each machine i has a hidden demand multiplier $h_{i,t} \in \mathbb{R}_{>0}$ evolving as a random walk:

$$h_{i,t+1} = h_{i,t} + d_i + \zeta_{i,t}, \quad \zeta_{i,t} \sim \mathcal{N}(0, \sigma_{h,i}^2), \quad (38)$$

where d_i is a deterministic drift and $\sigma_{h,i}$ controls the stochastic component. The true demand rate at machine i on day t is $\lambda_{\text{true}}(i, t) = \lambda_{\text{base}}(i) \cdot h_{i,t}$. For Downtown, Suburb, and Office Park, $d_i = 0$ and $\sigma_{h,i} = 0.01$: the hidden state is essentially constant. For University, $d_i = 0.008/\text{day}$ and $\sigma_{h,i} = 0.02$: a new dormitory steadily increases student demand. For New Neighborhood, $d_i = 0.006/\text{day}$ and $\sigma_{h,i} = 0.02$: gentrification steadily increases family demand.

The simulator was calibrated at $t_0 = -180$ from observational data collected by a historical operator who observed h via local knowledge and stocked proportionally, creating the dependence $A \not\perp H \mid S$ that defines confounding. The simulator’s demand estimate includes a confounding factor c_i : for University $c_i = 0.47$, for New Neighborhood $c_i = 0.39$, and for the remaining machines $c_i \approx 1.0$. After 180 days of drift, the simulator underestimates demand at University and New Neighborhood by a factor of 4–5 \times .

C.5 Demand model

For each machine i , customer segment s , and day t , the arrival rate is:

$$\begin{aligned} \lambda_{i,s}(t) = & \lambda_{i,s}^{\text{base}} \times h_{i,t} \times w_s(t) \times (1 + 0.40 \sin(2\pi t/365)) \times (1 + \beta_i t) \\ & \times f_{\text{tod}}(s, t) \times \text{Comp}_i(t) \times \text{Shock}_i(t) \times (1 + \eta_{g(i)}(t)), \end{aligned} \quad (39)$$

where:

- $h_{i,t}$: hidden-state multiplier from Eq. (38) (Section C.4 above).
- $w_s(t)$: weekday/weekend multiplier (w_s^{weekday} if $t \bmod 7 < 5$, else w_s^{weekend}).
- $1 + 0.40 \sin(2\pi t/365)$: 365-day seasonal cycle with $\pm 40\%$ amplitude, calibrated from monthly sales data [Singh, 2022].
- $1 + \beta_i t$: linear trend. Downtown $\beta = -0.01$; all others $\beta = 0$.
- $f_{\text{tod}}(s, t) = 3 \cdot p_s^{\text{tod}}(t \bmod 3)$: time-of-day weighting (morning/afternoon/evening).
- $\text{Comp}_i(t) = 1 - \delta_i \cdot \mathbf{1}[t \geq 60]$: competitor entry. Office Park $\delta = 0.25$; others $\delta = 0$.
- $\text{Shock}_i(t)$: multiplicative shock. Downtown $m = 0.45$ for 30 days starting day 50 (sustained construction); New Neighborhood $m = 2.5$ on day 35 (single-day festival); others $m = 1$.
- $\eta_{g(i)}(t) = 0.08 \cdot Z_{g,t}$, $Z_{g,t} \sim \mathcal{N}(0, 1)$: correlated geographic group shock.

The number of arriving customers is $N_{i,s}(t) \sim \text{Poisson}(\max(0.01, \lambda_{i,s}(t)))$.

C.6 Weather

The weather process is AR(1): $W_t = 0.7W_{t-1} + 0.3Z_t$, $Z_t \sim \mathcal{N}(0, 1)$, clipped to $[-1.5, 1.5]$. Weather modulates willingness-to-pay: $\text{WTP}_{\text{eff}} = \text{WTP} \cdot (1 + w_p^{\text{weather}} \cdot W_t)$, where w_p^{weather} is product-specific (soda: 0.4, energy: 0.1, snack: 0.05).

C.7 Purchase mechanics

When a customer arrives, they draw a product from their segment's preference distribution and a WTP from $\mathcal{N}(\text{mean WTP}, \text{std}^2)$. The effective WTP is adjusted for weather. If the posted price exceeds the effective WTP, no sale occurs. If the preferred product is out of stock, the customer substitutes with their segment's substitution probability, drawing an alternative from the remaining preference distribution (re-normalized). The substitute is purchased only if in stock and priced below $1.1 \times \text{WTP}$.

C.8 Logistics

- *Depot* \rightarrow *VM*: same-day delivery. Constrained by depot stock and VM capacity. Cost: \$0.05/unit.
- *Warehouse* \rightarrow *VM (direct)*: lead time $\max(1, \text{round}(\mathcal{N}(2.0, 0.7^2)))$ days. Cost: wholesale + \$0.15/unit. 5% chance of full delay (one extra day); 8% chance of partial delivery (70% arrives, rest next day).
- *Warehouse* \rightarrow *Depot*: lead time $\max(1, \text{round}(\mathcal{N}(1.0, 0.3^2)))$ days. Cost: wholesale + \$0.08/unit.
- *Spoilage*: units exceeding shelf life are discarded daily. Planner pays wholesale cost.
- *Holding*: \$0.01/unit/day (soda), \$0.02 (energy), \$0.015 (snack).
- *Breakdowns*: 2% daily probability per machine, causing one day of zero sales.

C.9 Fallback triggers

Two automatic safety mechanisms fire after demand realization each day:

1. *VM emergency*: when any product hits 0 stock, the depot ships $\min(3, \text{depot stock})$ units (same-day).
2. *Depot emergency*: when any product drops to ≤ 4 units, the depot orders 10 units from the warehouse.

C.10 Cash flow

Starting cash: \$2,000. Daily profit: $\Pi_t = \text{Revenue}_t - (\text{Shipping}_t + \text{Wholesale}_t + \text{Holding}_t + \text{Spoilage}_t + 5 \times \$2.00)$. Cash updates as $\text{Cash}_{t+1} = \text{Cash}_t + \Pi_t$. Bankruptcy occurs if cash is negative for 5 consecutive days.

C.11 Observation model (censoring)

The planner observes $\min(\text{demand}, \text{stock})$, not demand. When stock remains positive after sales, the observation is uncensored. When stock hits zero, the observation is censored: the planner knows demand \geq stock but not by how much.

C.12 SEP belief model

The SEP maintains a running average of the most recent 10 uncensored sales observations per (machine, product) pair. Initial beliefs equal the simulator's demand rates. A structural break is detected when the 7-day rolling mean deviates from the preceding 7-day mean by more than 80% (and the preceding mean exceeds 1.5 units/day). Upon detection, the belief resets to the new mean and a one-day re-exploration phase triggers.

C.13 Configuration

Table A2 provides the complete parameterization.

Table A2: Vending machine network: base demand rates, hidden-state parameters, events, and pilot detection rates. Bold entries indicate substantial simulator error. The ‘‘Pilot detection’’ column shows the fraction of 30 trials in which the 5-day pilot’s hypothesis test flags the machine as misspecified.

Machine	True (sim) λ			Total		Hidden-state			Pilot	
	Comm.	Fam.	Stud.	True	Sim	d_i	σ_h	c_i	detect.	Events
Downtown	6(5.5)	1(1)	2(2)	9	8.5	0	.01	1.0	10%	Constr. d50
Suburb	2(2)	4(4)	1(1)	7	7	0	.01	1.0	37%	—
Office Pk	5(5)	.5(.5)	.5(.5)	6	6	0	.01	1.0	7%	Comp. d60
University	1(1)	.5(.5)	8(3)	9.5	4.5	.008	.02	.47	13%	—
New Nbhd	1(1)	6(1.5)	2(1)	9	3.5	.006	.02	.39	17%	Fest. d35

The pilot detection rates illustrate the difficulty of identifying misspecified machines from only 5 days of data. University (13%) and New Neighborhood (17%) are detected at modest rates despite exhibiting the largest simulator errors, because the 5-day pilot collects limited observations and the Bonferroni correction across 15 tests ($\alpha_{\text{Bonf}} = 0.003$) is conservative. For larger problems with many state–action pairs, a less conservative FDR-controlling procedure such as Benjamini–Hochberg would improve detection power at the cost of additional false positives. Suburb is flagged most frequently (37%) despite being correctly specified—a false positive driven by weekend demand variability. In 33% of trials, no machine is flagged, and the SEP proceeds directly to exploitation at day 5, bypassing the exploration phase. Despite the low detection rates, the pilot-to-policy protocol achieves 72% of the oracle at $T=400$ (Table A3, A-SOP + pilot row), matching the performance of an oracle-targeted SEP, because continuous learning during exploitation eventually identifies the misspecified machines regardless of the pilot’s outcome.

C.14 Multi-horizon results

Table A3: Multi-horizon results (% of oracle cash, 30 trials, $\pm 95\%$ CI). Best non-oracle per horizon in bold. L = learns, E = explores, D = directed.

Policy	L	E	D	Horizon T (days)				
				100	200	400	800	1600
Oracle				100	100	100	100	100
SOP	X	X		89.0 \pm 0.9	78.8 \pm 1.2	66.8 \pm 1.6	48.6 \pm 2.1	37.7 \pm 1.9
ϵ -greedy	X	✓	X	75.8 \pm 1.5	65.0 \pm 1.6	48.2 \pm 2.1	39.2 \pm 2.7	32.8 \pm 2.8
A-SOP	✓	X		89.0 \pm 0.9	82.2 \pm 1.3	75.6 \pm 2.0	66.8 \pm 3.3	70.7 \pm 4.1
+ pilot	✓	X		80.3 \pm 1.3	76.2 \pm 1.5	71.7 \pm 1.8	66.6 \pm 3.5	71.5 \pm 4.8
L- ϵ (fixed)	✓	✓	X	76.5 \pm 1.8	68.6 \pm 1.9	56.6 \pm 2.3	55.3 \pm 4.3	62.8 \pm 5.6
L- ϵ (adaptive)	✓	✓	X	75.5 \pm 1.7	69.6 \pm 1.6	62.7 \pm 2.0	61.3 \pm 3.3	67.2 \pm 4.7
KG-SEP	✓	✓	✓	80.4 \pm 0.9	76.9 \pm 1.1	72.7 \pm 1.5	67.5 \pm 3.0	71.8 \pm 4.4
SEP	✓	✓	✓	77.2 \pm 1.8	73.3 \pm 1.7	66.6 \pm 2.2	66.1 \pm 4.2	73.8 \pm 5.8
Fisher-SEP-R	✓	✓	✓	76.6 \pm 1.7	73.2 \pm 2.5	68.5 \pm 3.7	68.8 \pm 4.8	75.3 \pm 6.5

C.15 Confounding-and-drift ablation

To isolate the role of the two hidden-state error sources in driving the SEP’s advantage over the SOP, we ran the vending DGP under three conditions at $T = 400$ with 30 trials each: (a) no confounding and no drift ($c_i = 1.0$ for all machines, drift $d_i = 0$), (b) confounding only ($c_i < 1$ at University and New Neighborhood as in the full DGP, but drift $d_i = 0$), and (c) the full DGP with both confounding and drift. Table A4 reports the % of oracle cash achieved by each policy under each condition.

Table A4: Confounding-and-drift ablation at $T = 400$, 30 trials. Values are % of oracle cash.

Ablation	SOP	A-SOP	A-SOP + pilot	ϵ -gr.	L- ϵ (fix)	L- ϵ (adp)	KG-SEP	SEP
No confounding, no drift	92	85	80	41	34	57	78	67
Confounding only	73	86	80	29	34	57	77	66
Full (confounding + drift)	67	76	72	48	57	63	73	67

Three observations follow from the table. The SOP’s performance drops from 92% (no bias) to 67% (full DGP) as hidden-state errors are introduced, confirming that the structured bias is what the SOP cannot correct. The A-SOP (passive Bayesian updating) holds steady at 76–86% across conditions: passive learning absorbs the confounding-only bias (86%) essentially as well as the no-bias case (85%), but the added drift partially defeats it (76%), consistent with the extended simulation lemma’s prediction that drift in the transition marginalization is an irreducible error source for passively-updated policies. The SEP advantage over the A-SOP reverses direction across conditions: with no bias, the A-SOP dominates (85% vs 67%) because the SEP’s 15-day exploration cost is unnecessary; with confounding only, the A-SOP still leads (86% vs 66%); with full drift, the A-SOP edges the SEP (76% vs 67%) at $T = 400$ because drift forces continuous rather than front-loaded learning. At $T = 1600$ (main Table A3), this ordering is reversed and designed exploration wins. The crossover horizon is a function of the drift rate and the exploration cost.

C.16 Comparison with UCRL2 and UCBVI (simulator-free tabular baselines)

A natural question is how the simulator-informed policies compare to simulator-free, frequentist-optimism baselines that learn entirely from online interaction. We implemented UCRL2 [Jaksch et al., 2010] and UCBVI [Azar et al., 2017] for both case studies using a *factored* tabular abstraction: one algorithm instance per unit of decentralization (per machine in vending; per team in HIV). Both algorithms re-solve their optimistic MDP either once per day (UCBVI) or on a slower cadence (UCRL2, whose extended value iteration is more expensive). Per-instance state and action spaces are small (binarized stock and stocking action, $|\mathcal{S}||\mathcal{A}| = 4$, per machine in vending; zone index and 5-way move, $|\mathcal{S}||\mathcal{A}| = 200$, per team in HIV), so per-step compute is manageable. These baselines have no access to the simulator and must learn from scratch.

Tables A5 and A6 report the results at 30 trials per condition.

Table A5: UCRL2 and UCBVI on the vending DGP, % of oracle cash, mean \pm 95% CI half-width. All policies at 30 trials on the common seed schedule; Fisher-SEP here is the Def.-3 Fisher-trace variant (reward-dominates Corollary 2) run by `regenerate_all_figures.run_v3_experiment_for_figures`. Thompson Sampling (PSRL) at 30 trials.

Policy	$T=100$	$T=200$	$T=400$	$T=800$	$T=1600$
Oracle	100.0 \pm 1.2	100.0 \pm 1.8	100.0 \pm 2.5	100.0 \pm 4.1	100.0 \pm 3.7
SOP	89.0 \pm 0.9	78.8 \pm 1.2	66.8 \pm 1.7	48.6 \pm 2.2	37.7 \pm 1.9
A-SOP	89.0 \pm 1.0	82.2 \pm 1.3	75.6 \pm 2.1	66.8 \pm 3.3	70.7 \pm 4.2
Thompson (PSRL)	88.5 \pm 1.3	82.6 \pm 1.8	76.6 \pm 2.8	68.6 \pm 2.7	71.2 \pm 3.4
SEP	77.2 \pm 1.8	73.3 \pm 1.8	66.6 \pm 2.2	66.1 \pm 4.3	73.8 \pm 5.9
Fisher-SEP-R	76.6 \pm 1.7	73.2 \pm 2.5	68.5 \pm 3.7	68.8 \pm 4.8	75.3 \pm 6.5
UCRL2	88.7 \pm 1.1	77.5 \pm 1.4	63.0 \pm 2.3	62.5 \pm 5.7	70.3 \pm 7.3
UCBVI	84.0 \pm 1.3	75.1 \pm 2.2	64.0 \pm 2.9	65.2 \pm 5.3	73.1 \pm 6.6

Table A6: UCRL2 and UCBVI on the HIV mobile-testing DGP, % of oracle cases found, mean \pm 95% CI half-width. Baselines at 30 trials; the Fisher-SEP row uses the A-optimal PVV algorithm (Definition 5) with 30 trials at $T \in \{50, 100, 200, 300, 400\}$ on the common-seed schedule; Thompson Sampling (PSRL) at 30 trials on the same schedule.

Policy	$T=50$	$T=100$	$T=200$	$T=300$	$T=400$
Oracle	100.0 \pm 1.6	100.0 \pm 1.1	100.0 \pm 1.0	100.0 \pm 0.9	100.0 \pm 0.7
SOP	44.6 \pm 1.2	42.3 \pm 0.8	44.3 \pm 0.9	48.3 \pm 0.9	52.9 \pm 0.9
A-SOP	43.9 \pm 1.0	45.8 \pm 2.3	49.3 \pm 3.2	53.5 \pm 3.4	58.1 \pm 3.2
Thompson (PSRL)	42.8 \pm 1.2	50.8 \pm 2.8	65.0 \pm 4.6	71.7 \pm 4.7	76.9 \pm 4.4
SEP	85.8 \pm 2.0	78.6 \pm 2.4	79.0 \pm 2.7	80.8 \pm 2.9	82.7 \pm 2.9
Fisher-SEP-T	60.7 \pm 3.7	71.4 \pm 4.2	78.4 \pm 4.2	82.3 \pm 3.8	85.2 \pm 3.5
UCRL2	44.2 \pm 1.2	41.3 \pm 1.1	42.8 \pm 0.9	46.5 \pm 0.8	50.4 \pm 0.7
UCBVI	44.1 \pm 1.4	41.4 \pm 1.3	42.6 \pm 1.0	45.7 \pm 1.1	48.8 \pm 1.0

What the tabular baselines tell us. The two case studies produce complementary pictures of simulator-free exploration.

On the vending DGP (Table A5), UCRL2 and UCBVI both approximately match the A-SOP / SEP / Fisher-SEP cluster at $T = 1600$ (70–74% of oracle) and handily beat the SOP (38%). This is the expected outcome: UCRL2 and UCBVI start from scratch but eventually recover a reasonable coarse stocking policy from per-machine observed sales, and by $T = 1600$ they have enough data that the absence of a simulator prior costs little. The remaining gap to the simulator-informed policies comes from the coarser 2×2 factored discretization rather than the exploration strategy itself; the CIs overlap.

On the HIV DGP (Table A6), the picture is sharper and is the one that speaks directly to the paper’s thesis. UCRL2 and UCBVI do cross the corridor and visit Region B in 80–87% of trials (mean 5–7 corridor crossings, 46–55 Region-B team-days per trial at $T = 400$), confirming that the tabular bonus structure does eventually push exploration across the wall. But they plateau at SOP-level performance (48–50% of oracle at $T = 400$) and do not match the simulator-informed policies within 400 days. The reason is exactly the mechanism the paper isolates: Region A already yields $\sim 50\%$ of oracle on its own, and corridor crossings through cold Region B return only 20% of warm yield for the first three days, so the cold-start cost amortizes slowly. SEP and Fisher-SEP use the simulator as a prior that encodes the Region-B geometry, front-loading corridor crossings in the first 25 days; UCRL2 and UCBVI, with no such prior, spend most of their exploration budget locally refining Region-A estimates. At $T \leq 400$ the catch-up is incomplete. This directly illustrates the reachability-gap component of Theorem 1: the simulator’s value is not that it is accurate (it underestimates Region-B prevalence by $15\times$) but that its structural prior identifies where to experiment first.

Caveats. (i) UCRL2 and UCBVI both required a forced-exploration-of-unvisited-actions wrapper in the HIV implementation—without it, argmax tie-breaking over equal initial Q-values locked every team at its start zone. This is an implementation issue, not a regret-analysis issue. (ii) UCRL2’s wall-clock on the vending DGP is dominated by its extended value iteration inner loop (614s of 943s total at 30 trials, $T = 1600$); on the HIV DGP the 40-state MDP is small enough that UCRL2 replans on a 25-day cadence with no observable behavior change. (iii) Thirty-trial marginal CIs are wide at long horizons (± 5 – 7 pp for tabular baselines in vending). We use the common seed schedule to compute paired-difference statistics (Appendix C.17); paired Wilcoxon tests establish the headline orderings (A-SOP $>$ SOP at $T \geq 200$ in vending; SEP $>$ A-SOP at every horizon in HIV; Fisher-SEP $>$ A-SOP at $T=1600$ in vending; Fisher-SEP $>$ SEP at $T \geq 300$ in HIV) at $p < 0.01$, despite the marginal CIs overlapping.

C.17 Paired-difference analysis

Table A7 reports paired-difference statistics for every headline ordering claimed in the main text. All comparisons are on the same 30-trial common seed schedule: policies within the same cache ran on identical DGP realisations, so the paired-difference estimator cancels the across-seed variance that dominates the marginal CIs. We report the paired- t 95% CI and a one-sided Wilcoxon signed-rank p -value (alternative: mean of A – B is strictly positive). Checkmarks mark rows with $p < 0.05$.

The paired analysis confirms three qualitative patterns noted in §5.1:

- **A-SOP dominates short horizons.** The paired gap A-SOP – SOP is near zero at $T=100$ (+0.1 pp, $p = 0.52$), significant at $T=200$ (+3.4 pp, $p < 10^{-3}$), and grows to +33 pp at $T=1600$ ($p < 10^{-3}$).
- **Fisher-SEP’s crossover is significant at $T=1600$.** Fisher-SEP – A-SOP is -12.6 at $T=100$ (exploration cost), crosses zero around $T=800$ (+1.2, $p = 0.23$), and is +4.8 at $T=1600$ with $p = 0.005$. The 30-trial sample is sufficient to establish the crossover statistically once paired, even though the marginal CIs overlap.
- **HIV reachability gap is large and significant at every horizon.** SEP – A-SOP ranges from +27 to +39 pp across $T \in \{50, 100, 200, 300, 400\}$, $p < 10^{-3}$ at every horizon. Fisher-SEP overtakes SEP significantly at $T \geq 300$ ($p < 0.01$).

KG-SEP – A-SOP is not significantly positive at any vending horizon in the paired analysis; KG-SEP’s per-state greedy criterion is insufficient to unlock the gap that Fisher-SEP’s stochastic A-optimal

Table A7: Paired-difference statistics for every headline ordering. Values in percentage points of oracle. $n = 30$ paired trials. ✓ marks pairs for which the one-sided Wilcoxon p -value < 0.05 .

Comparison	Mean \pm half-width	Paired- t 95% CI	Wilcoxon $p_{1\text{-sided}}$	Sig.
A-SOP – SOP (vending, $T=100$)	+0.08 \pm 1.01	[-0.98, +1.13]	0.516	–
Fisher-SEP – A-SOP (vending, $T=100$)	-12.62 \pm 1.42	[-14.10, -11.13]	1.000	–
KG-SEP – A-SOP (vending, $T=100$)	-8.64 \pm 0.92	[-9.59, -7.68]	1.000	–
A-SOP – SOP (vending, $T=200$)	+3.41 \pm 1.46	[+1.89, +4.93]	0.000	✓
Fisher-SEP – A-SOP (vending, $T=200$)	-8.42 \pm 1.86	[-10.36, -6.48]	1.000	–
KG-SEP – A-SOP (vending, $T=200$)	-5.31 \pm 1.59	[-6.96, -3.65]	1.000	–
A-SOP – SOP (vending, $T=400$)	+8.80 \pm 2.53	[+6.16, +11.44]	0.000	✓
Fisher-SEP – A-SOP (vending, $T=400$)	-7.38 \pm 2.64	[-10.14, -4.63]	1.000	–
KG-SEP – A-SOP (vending, $T=400$)	-2.86 \pm 2.43	[-5.40, -0.32]	0.976	–
A-SOP – SOP (vending, $T=800$)	+18.22 \pm 2.89	[+15.20, +21.24]	0.000	✓
Fisher-SEP – A-SOP (vending, $T=800$)	+1.16 \pm 3.15	[-2.14, +4.45]	0.232	–
KG-SEP – A-SOP (vending, $T=800$)	+0.62 \pm 2.71	[-2.21, +3.45]	0.335	–
A-SOP – SOP (vending, $T=1600$)	+33.00 \pm 3.67	[+29.16, +36.83]	0.000	✓
Fisher-SEP – A-SOP (vending, $T=1600$)	+4.83 \pm 3.36	[+1.33, +8.34]	0.005	✓
KG-SEP – A-SOP (vending, $T=1600$)	+1.10 \pm 2.51	[-1.52, +3.72]	0.220	–
UCRL2 – SOP (vending, $T=1600$)	+32.58 \pm 6.36	[+25.94, +39.21]	0.000	✓
UCBVI – SOP (vending, $T=1600$)	+35.40 \pm 5.80	[+29.34, +41.46]	0.000	✓
Fisher-SEP-R – Thompson (vending, $T=1600$)	+3.92 \pm 2.85	[+0.95, +6.89]	0.008	✓
TS – A-SOP (vending, $T=1600$)	+0.66 \pm 2.42	[-1.86, +3.18]	0.285	–
SEP – A-SOP (HIV, $T=50$)	+39.24 \pm 1.76	[+37.40, +41.09]	0.000	✓
Fisher-SEP – SEP (HIV, $T=50$)	-21.65 \pm 3.51	[-25.32, -17.98]	1.000	–
SEP – A-SOP (HIV, $T=100$)	+34.48 \pm 2.43	[+31.95, +37.01]	0.000	✓
Fisher-SEP – SEP (HIV, $T=100$)	-5.18 \pm 3.96	[-9.32, -1.05]	0.988	–
SEP – A-SOP (HIV, $T=200$)	+30.94 \pm 2.92	[+27.89, +33.99]	0.000	✓
Fisher-SEP – SEP (HIV, $T=200$)	+2.65 \pm 3.98	[-1.51, +6.80]	0.052	–
SEP – A-SOP (HIV, $T=300$)	+28.62 \pm 3.13	[+25.35, +31.88]	0.000	✓
Fisher-SEP – SEP (HIV, $T=300$)	+4.64 \pm 3.95	[+0.52, +8.77]	0.007	✓
SEP – A-SOP (HIV, $T=400$)	+26.57 \pm 3.07	[+23.37, +29.77]	0.000	✓
Fisher-SEP – SEP (HIV, $T=400$)	+4.92 \pm 3.78	[+0.99, +8.86]	0.003	✓
Fisher-SEP – UCRL2 (HIV, $T=400$)	+36.62 \pm 3.14	[+33.34, +39.90]	0.000	✓
SEP – UCBVI (HIV, $T=400$)	+33.27 \pm 2.86	[+30.29, +36.26]	0.000	✓

design captures. This is consistent with the class-level gap $W_{1'} \leq W_{3'}$ in Theorem 7 and with the qualitative argument that a per-state myopic criterion cannot plan multi-step trajectories.

Fisher-SEP paired analysis. Table A8 reports paired-difference statistics for Fisher-SEP (Definition 5) against SEP, A-SOP, and Thompson sampling (PSRL) on the common seed schedule. The key findings:

- On HIV, Fisher-SEP beats A-SOP by +27.1 pp at $T=400$ with $p < 10^{-3}$; Fisher-SEP vs SEP is statistically tied at $T \geq 200$ (mean difference $\in [-0.6, +2.5]$, $p > 0.1$). Random exploration (SEP) is already competitive on HIV because the reachability gap does not require fine-grained allocation: any policy that reliably sends teams to Region B captures most of the available value.
- Thompson sampling (PSRL) partly closes the HIV gap on its own, beating A-SOP by +18.8 pp at $T=400$ ($p < 10^{-3}$). Occasional high posterior draws on Region-B prevalence push teams across the corridor and yield implicit exploration. Fisher-SEP still beats TS by +8.3 pp at $T=400$ ($p = 0.003$) and by +20.6 pp at $T=100$: directed exploration that concentrates effort on the Region-B cluster outperforms unstructured posterior sampling, and the gap closes only slowly as the horizon grows.
- On vending, Fisher-SEP vs A-SOP crosses zero at long horizons, consistent with the main-text crossover result (Table A7). Fisher-SEP-R beats Thompson by +3.9 pp at $T=1600$ ($p = 0.008$); TS is statistically tied with A-SOP at every vending horizon (paired $|\text{mean}| \leq 1.5$ pp, $p \geq 0.16$).

Table A8: Fisher-SEP (Definition 5) paired-difference statistics against A-SOP, SEP, and Thompson sampling (PSRL). $n = 30$ paired trials on the common seed schedule. Values in percentage points of oracle. ✓ marks pairs for which the one-sided Wilcoxon p -value < 0.05 . The HIV rows here use the v3 cache (code/results/fisher_v3/hiv_v3. {npz, csv}) and supersede the corresponding HIV rows in Table A7, which were generated from an earlier SEP run that pre-dates the v3 cache; mean differences agree to within ± 2.6 pp across the two runs.

Comparison	Mean \pm half-width	Paired- t 95% CI	Wilcoxon $p_{1\text{-sided}}$	Sig.
SEP – A-SOP (HIV, $T=50$)	+41.87 \pm 2.10	[+39.68, +44.06]	0.000	✓
Fisher-SEP – SEP (HIV, $T=50$)	–25.16 \pm 3.95	[–29.29, –21.04]	1.000	–
Fisher-SEP – A-SOP (HIV, $T=50$)	+16.71 \pm 3.67	[+12.88, +20.54]	0.000	✓
SEP – A-SOP (HIV, $T=100$)	+32.80 \pm 2.94	[+29.73, +35.86]	0.000	✓
Fisher-SEP – SEP (HIV, $T=100$)	–7.23 \pm 4.32	[–11.74, –2.72]	0.999	–
Fisher-SEP – A-SOP (HIV, $T=100$)	+25.57 \pm 4.86	[+20.49, +30.64]	0.000	✓
SEP – A-SOP (HIV, $T=200$)	+29.69 \pm 3.27	[+26.28, +33.10]	0.000	✓
Fisher-SEP – SEP (HIV, $T=200$)	–0.57 \pm 4.58	[–5.36, +4.21]	0.572	–
Fisher-SEP – A-SOP (HIV, $T=200$)	+29.12 \pm 5.54	[+23.33, +34.90]	0.000	✓
SEP – A-SOP (HIV, $T=300$)	+27.36 \pm 3.45	[+23.77, +30.96]	0.000	✓
Fisher-SEP – SEP (HIV, $T=300$)	+1.44 \pm 4.71	[–3.47, +6.36]	0.271	–
Fisher-SEP – A-SOP (HIV, $T=300$)	+28.81 \pm 5.47	[+23.09, +34.52]	0.000	✓
SEP – A-SOP (HIV, $T=400$)	+24.59 \pm 3.30	[+21.15, +28.03]	0.000	✓
Fisher-SEP – SEP (HIV, $T=400$)	+2.51 \pm 4.62	[–2.31, +7.34]	0.118	–
Fisher-SEP – A-SOP (HIV, $T=400$)	+27.10 \pm 5.13	[+21.75, +32.46]	0.000	✓
TS – A-SOP (HIV, $T=100$)	+5.00 \pm 2.16	[+2.75, +7.25]	0.000	✓
TS – A-SOP (HIV, $T=200$)	+15.66 \pm 4.12	[+11.36, +19.95]	0.000	✓
TS – A-SOP (HIV, $T=300$)	+18.23 \pm 4.48	[+13.56, +22.91]	0.000	✓
TS – A-SOP (HIV, $T=400$)	+18.79 \pm 4.20	[+14.41, +23.17]	0.000	✓
Fisher-SEP – TS (HIV, $T=100$)	+20.56 \pm 5.40	[+14.93, +26.20]	0.000	✓
Fisher-SEP – TS (HIV, $T=200$)	+13.46 \pm 6.44	[+6.74, +20.18]	0.000	✓
Fisher-SEP – TS (HIV, $T=300$)	+10.57 \pm 6.17	[+4.13, +17.01]	0.001	✓
Fisher-SEP – TS (HIV, $T=400$)	+8.31 \pm 5.72	[+2.34, +14.28]	0.003	✓

C.18 Hierarchical-prior sensitivity: how far does the reachability gap survive correlated priors?

Assumption 5(f) factorizes the prior across (s, a) pairs. Realistic deployments have structural correlation: HIV prevalence is smooth across adjacent zones, vending demand is correlated across neighborhood. Under a hierarchical prior, visiting one pair reduces posterior uncertainty at other pairs through the kernel, and Proposition 4.1’s mechanism is quantitatively weaker: the A-SOP can partly close the reachability gap because Region-A observations inform the Region-B posterior through the prior. This subsection bounds how much the reachability gap shrinks under a Gaussian-process prior with kernel k .

Setup. Replace Assumption 5(f) with a Gaussian-process prior on the reward parameters: $r \sim \mathcal{GP}(\mu_0, k)$ with mean μ_0 given by the simulator and kernel $k(s, s')$. Let $K \in \mathbb{R}^{|\mathcal{S}| \times |\mathcal{S}|}$ be the Gram matrix restricted to the relevant $|\mathcal{S}|$ states, with spectral decomposition $K = U\Lambda U^\top$. Denote by $|\mathcal{S}|_V := |\text{supp}(d_{\pi^{\text{dep}}})|$ the number of deployed-policy-visited states and by $|\mathcal{S}|_U := |\mathcal{S}| - |\mathcal{S}|_V$ the number of unvisited states.

Proposition 9 (Reachability gap under hierarchical prior). *Under the GP prior with kernel k , let $K_{UV} \in \mathbb{R}^{|\mathcal{S}|_U \times |\mathcal{S}|_V}$ be the off-diagonal block of K (visited states coupled to unvisited), and let $K_{UU} \in \mathbb{R}^{|\mathcal{S}|_U \times |\mathcal{S}|_U}$ be the unvisited-states block. After the A-SOP collects n observations per visited state, the posterior covariance on the unvisited states reduces to*

$$\Sigma_U^{\text{post}}(n) = K_{UU} - K_{UV}(K_{VV} + \sigma^2/n \cdot I)^{-1}K_{VU}. \quad (40)$$

Letting $\mathcal{G}_{\text{reach}}^{\text{hier}}$ denote the reachability gap under the hierarchical prior, there exist constants $c_1, c_2 > 0$ (depending on the kernel and on R_{max}, γ) such that

$$\mathcal{G}_{\text{reach}}^{\text{hier}} \leq c_1 \cdot \text{trace}(\Sigma_U^{\text{post}}(n))^{1/2} + c_2 \cdot \epsilon_{\text{hier}}^m, \quad (41)$$

where ϵ_{hier}^m is the residual model error that the kernel cannot close.

Proof. The reachability gap is proportional to the value-function variance at unvisited states. Under the GP prior, posterior variance at unvisited states is given by the Schur complement (40). The c_1 constant comes from the value-function delta-method with Bellman resolvent; the residual $c_2\epsilon_{\text{hier}}^m$ captures the kernel’s inability to interpolate across model-specification mismatches. \square

Remark 16 (When does the hierarchical prior close the reachability gap?). Equation (40)’s unvisited-state posterior variance depends on the effective rank of $K_{UV}(K_{VV} + \sigma^2/n \cdot I)^{-1}K_{VU}$ relative to K_{UU} . Three regimes:

- **Strong coupling** ($\|K_{UV}\| \approx \|K_{UU}\|$, e.g., a smooth kernel on a small state space). Then $\Sigma_U^{\text{post}} \rightarrow 0$ as $n \rightarrow \infty$, and the reachability gap collapses: passive learning under the hierarchical prior does close Region-B via the kernel.
- **Weak coupling** ($\|K_{UV}\| \ll \|K_{UU}\|$, e.g., a short-lengthscale kernel on a large state space). Then $\Sigma_U^{\text{post}} \approx K_{UU}$, and the reachability gap survives: the kernel does not transport information through the corridor.
- **Intermediate.** The reachability gap shrinks by a factor governed by the effective rank of K_{UV} .

On the HIV grid with a squared-exponential kernel of lengthscale $\ell = 1$ zone, the Region-A \rightarrow Region-B coupling is effectively zero because the corridor-separated zones are at Euclidean distance ≥ 3 and the kernel decays to $e^{-4.5} \approx 0.01$. The reachability gap is therefore robust to this realistic hierarchical prior. Longer lengthscales ($\ell \geq 3$) would close it, but such priors would also smooth over the epidemiologically important within-region variation.

Remark 17 (Practical takeaway). The reachability gap’s robustness under a hierarchical prior is a kernel-dependent property, not a structural one. A deployment that uses a long-lengthscale spatial kernel can partly close the gap via passive learning; a short-lengthscale kernel leaves the gap intact. Proposition 9 makes this dependence quantitative. The main-text claim that “the reachability part is not closable by posterior-mean-optimal online updating” (Section 1) assumes prior independence (Assumption 5(f)); for realistic-kernel hierarchical priors, the claim becomes “the reachability part is not closable except through kernel-transported information from visited states.”

C.19 Per-trial conditional analysis: does the Fisher-SEP-R gap depend on pilot detection?

The unconditional Fisher-SEP-R – A-SOP gap on vending at $T=1600$ is +4.58 pp (paired Wilcoxon $p=0.007$; Table A7). A natural question is whether this effect is driven by those trials in which the 5-day pilot’s hypothesis test (Bonferroni at $\alpha=0.05/15$) plus the “add top-3 Fisher-sensitive VMs” heuristic tags at least one of the two truly-misspecified machines—University (VM 3) or New Neighborhood (VM 4). We stratify the 30-trial common-seed cache by whether Fisher-SEP-R’s post-pilot “uncertain” set contains either of those two VMs, and re-run the paired test on each stratum.

Table A9: Per-trial conditional analysis of Fisher-SEP-R – A-SOP at $T=1600$, stratified by whether the 5-day pilot plus Fisher-augmentation flagged at least one of {University, New Neighborhood} into the post-pilot exploration set. Paired-Wilcoxon p -value is one-sided (alternative: Fisher-SEP-R mean $>$ A-SOP mean). $n=30$ common-seed trials, SEED=42+trial \times 100.

Stratum	n	A-SOP (%)	Fisher-SEP-R (%)	Paired diff (pp)	Wilcoxon p
All trials	30	70.6 \pm 3.9	75.2 \pm 4.5	+4.58 \pm 3.47	0.007
Pilot flagged U or NN	25	69.6 \pm 3.2	75.0 \pm 5.0	+5.45 \pm 3.80	0.004
Pilot did not flag U or NN	5	75.7 \pm 5.4	76.0 \pm 9.0	+0.25 \pm 11.99	0.500

Values in % of oracle cash at $T=1600$. Marginal CI half-widths are 95% (ordinary t) within each stratum; paired-difference CI half-width is 95% paired- t . Cache: code/results/vending_conditional.{npz,csv}.

Three observations follow from the table. The flagged stratum (25 of 30 trials; 83%) carries essentially all of the unconditional effect: the within-stratum paired gap is +5.45 pp with $p=0.004$, slightly larger than the +4.58 pp pooled result, because the unflagged stratum’s near-zero contribution dilutes the pooled mean. The unflagged stratum (5 of 30 trials; 17%) shows essentially no effect: paired difference +0.25 pp with a 95% CI of $[-11.75, +12.24]$ and $p=0.50$. With only 5 trials the CI is too wide to rule out a clinically meaningful gap, but the point estimate is consistent with the obvious

mechanism: when the pilot does not tag either misspecified machine, Fisher-SEP-R’s post-pilot exploration budget is spent on well-calibrated machines and the effective learning rate over U/NN converges to the A-SOP’s passive rate. The A-SOP’s own within-stratum performance moves in the expected direction: 69.6% when the pilot flags U or NN (these trials happen to be seeds on which the simulator’s mis-specification is slightly more exploitable by any learning policy) versus 75.7% on the unflagged subset.

The conditional analysis shows that the unconditional +4.58 pp effect is concentrated in the $\approx 83\%$ of trials where the pilot protocol’s detection succeeds. The remaining $\approx 17\%$ of trials show no measurable gap. This is the expected behavior of a pilot-gated directed-exploration policy: when the gate fails, the policy reduces to a minor perturbation of A-SOP. For a deployment-scale analysis, the operational implication is that the gate’s false-negative rate (pilot failing to tag a truly-misspecified machine) upper-bounds the headroom gained over passive A-SOP. A less conservative FDR-controlling multiple-testing procedure would raise the detection probability on the unflagged stratum at the cost of additional false positives on calibrated machines; we do not pursue this tuning here.

D HIV Mobile Testing: Data-Generating Process

This appendix provides the complete specification of the data-generating process for the HIV mobile testing experiment of Section 5.2. All numerical values match the reference implementation (`hiv_testing.py` and `exp_hiv_testing.py`).

D.1 Geography and grid structure

The environment is a 5×8 grid (`rows = 5`, `cols = 8`) comprising $|\mathcal{S}| = 40$ zones indexed $j = r \cdot \text{cols} + c$ for row $r \in \{0, \dots, 4\}$ and column $c \in \{0, \dots, 7\}$. A wall runs along column `mid_col = $\lfloor 8/2 \rfloor = 4$` , dividing the grid into two regions:

- **Region A** (columns 0–3): well-surveilled urban zones with clinic-based testing infrastructure.
- **Region B** (columns 4–7): hard-to-reach peri-urban areas requiring mobile outreach.

The wall blocks all movement between regions except through a single corridor cell at (`mid_row`, `mid_col`) = (2, 4). Formally, a move from (r_1, c_1) to (r_2, c_2) is blocked if $(c_1 < 4) \neq (c_2 < 4)$ unless $r_1 = r_2 = 2$. Each zone j is adjacent to its four cardinal neighbors (up, down, left, right) subject to grid boundaries and the wall constraint; teams may also stay in place.

D.2 Population model

Each zone j has a fixed population N_j :

$$N_j = \begin{cases} 500 & \text{if } j \in \text{Region A } (c_j < 4), \\ 300 & \text{if } j \in \text{Region B } (c_j \geq 4). \end{cases} \quad (42)$$

Region B’s smaller population reflects lower population density in peri-urban areas.

D.3 Disease dynamics (SIS with treatment-reduced transmission)

Prevalence evolves according to a discrete-time Susceptible–Infected–Susceptible (SIS) model in which the treatment factor $\tau = 0.90$ in Eq. (43) acts as the recovery channel: diagnosed-and-treated individuals contribute $(1 - \tau)$ as much to the infectious pool, which under continued treatment renders them effectively susceptible to re-acquisition under the SIS interpretation. Let $p_j(t) \in [0.001, 0.80]$ denote the prevalence (fraction infected) at zone j on day t , and let $D_j(t)$ denote the cumulative number of diagnosed individuals at zone j by day t (capped at N_j). The effective number of infectious individuals at zone j accounts for the treatment effect:

$$I_j^{\text{eff}}(t) = p_j(t) \cdot \max(0, N_j - D_j(t)) + D_j(t) \cdot (1 - \tau), \quad (43)$$

where $\tau = 0.90$ is the treatment reduction factor (diagnosed individuals transmit at 10% of the untreated rate). The first term counts undiagnosed infected individuals (prevalence times undiagnosed population); the second counts diagnosed individuals whose residual infectiousness is reduced by treatment.

The force of infection at zone j has two components:

$$\text{FoI}_j^{(w)}(t) = \beta_w \cdot \frac{I_j^{\text{eff}}(t)}{N_j}, \quad (44)$$

$$\text{FoI}_j^{(b)}(t) = \sum_{k \in \text{nb}(j)} \beta_b \cdot \frac{I_k^{\text{eff}}(t)}{N_k}, \quad (45)$$

where $\beta_w = 0.002$ is the within-zone transmission rate, $\beta_b = 0.0005$ is the between-zone transmission rate, and $\text{nb}(j)$ denotes the set of zones adjacent to j (respecting the wall).

Prevalence updates as:

$$p_j(t+1) = \text{clip} \left[p_j(t) + (1 - p_j(t)) \cdot (\text{FoI}_j^{(w)}(t) + \text{FoI}_j^{(b)}(t)), 0.001, 0.80 \right]. \quad (46)$$

The clip operation prevents prevalence from falling below 0.001 (background rate) or exceeding 0.80.

D.4 Treatment effect

When a testing team diagnoses an individual as HIV-positive, that individual enters treatment. Diagnosed individuals remain in the population but transmit at a reduced rate: their contribution to the force of infection is scaled by $(1 - \tau) = 0.10$, as shown in Eq. (43). This reflects the well-documented effect of antiretroviral therapy on viral suppression and onward transmission [Warren et al., 2025]. The cumulative diagnosed count $D_j(t)$ is non-decreasing and capped at N_j .

D.5 Testing model

Each of the $n = 8$ mobile testing teams can test at one zone per day. Let $m_j(t)$ denote the number of teams present at zone j on day t . For each team at zone j , the number of tests administered is drawn from a Poisson distribution:

$$n_{\text{tests}} \sim \max(1, \text{Poisson}(\mu_{\text{tests}})), \quad \mu_{\text{tests}} = 8. \quad (47)$$

Each test yields a positive result with probability equal to the effective prevalence at zone j , adjusted for warmup status:

$$n_{\text{pos}} \sim \text{Binomial}(n_{\text{tests}}, p_j(t) \cdot \phi_j(t)), \quad (48)$$

where $\phi_j(t)$ is the yield multiplier defined in Section D.6.

D.6 Warmup mechanism

Region B zones start ‘‘cold’’: testing teams must establish community rapport before achieving full testing yield. Each zone j maintains a warmup counter $w_j(t) \in [0, w_{\text{max}}]$ with $w_{\text{max}} = 3$ days. All Region A zones are initialized as warm ($w_j(0) = 3$); all Region B zones start cold ($w_j(0) = 0$). On each day, if at least one team is present at zone j , the counter increments: $w_j(t+1) = \min(w_j(t) + 1, w_{\text{max}})$. The yield multiplier is:

$$\phi_j(t) = \begin{cases} 1.0 & \text{if } w_j(t) \geq w_{\text{max}} \text{ (warm),} \\ 0.20 & \text{otherwise (cold).} \end{cases} \quad (49)$$

This reflects the community engagement costs documented in mobile HIV testing programs: cold outreach in unfamiliar areas yields only 20% of the testing volume achievable in established sites [Gonçalves et al., 2018].

D.7 Confounding mechanism

The simulator’s prevalence estimates are calibrated from clinic-based surveillance data, which systematically underrepresents hard-to-reach populations in Region B. For each zone j , the true initial prevalence $p_j(0)$ and the simulator’s estimate \hat{p}_j^{sim} are drawn as:

$$p_j(0) = \begin{cases} 0.05 + \epsilon_j, & \epsilon_j \sim \mathcal{N}(0, 0.005^2) \text{ if } c_j < 4 \text{ (Region A),} \\ 0.04 + \epsilon_j, & \epsilon_j \sim \mathcal{N}(0, 0.005^2) \text{ if } c_j \geq 4 \text{ (Region B, non-cluster),} \end{cases} \quad (50)$$

$$\hat{p}_j^{\text{sim}} = \begin{cases} 0.05 + \eta_j, & \eta_j \sim \mathcal{N}(0, 0.003^2) \text{ if } c_j < 4 \text{ (Region A),} \\ 0.02 + \eta_j, & \eta_j \sim \mathcal{N}(0, 0.002^2) \text{ if } c_j \geq 4 \text{ (Region B).} \end{cases} \quad (51)$$

Both are clipped to $[0.001, 0.50]$. The key asymmetry is that the simulator estimates Region B prevalence at $\hat{p}^{\text{sim}} \approx 0.02$, while the true non-cluster prevalence is $p \approx 0.04$ —and the cluster prevalence is far higher (see below). This underestimation arises because clinic-based surveillance captures patients who self-present, missing the hard-to-reach population that mobile outreach is designed to serve.

D.8 Cluster specification

A hidden disease cluster is planted in the bottom-right corner of Region B. The epicenter is at zone $(r, c) = (\text{rows} - 1, \text{cols} - 1) = (4, 7)$ with true initial prevalence $p_{\text{epi}} = 0.30$. All valid neighbors of the epicenter within Region B (i.e., zones (r', c') with $|r' - 4| \leq 1$, $|c' - 7| \leq 1$, $0 \leq r' < 5$, and $c' \geq 4$) have initial prevalence $p_{\text{nb}} = 0.18$. The simulator’s estimate for these zones remains $\hat{p}^{\text{sim}} \approx 0.02$, so the cluster is invisible to the SOP.

If the cluster remains undetected, SIS dynamics (Eq. (46)) cause prevalence to grow: the high within-zone force of infection at the epicenter spills over to neighboring zones via the between-zone transmission term, gradually expanding the outbreak. Early detection and treatment (via the SEP’s corridor-crossing exploration) contain this growth by reducing the effective infectious population through the treatment factor $\tau = 0.90$.

D.9 Belief model

Adaptive policies maintain a Beta-distributed belief over each zone’s prevalence. The prior is initialized from the simulator’s estimates with strength parameter $\kappa = 10$:

$$\alpha_j^{(0)} = \hat{p}_j^{\text{sim}} \cdot \kappa + 1, \quad \beta_j^{(0)} = (1 - \hat{p}_j^{\text{sim}}) \cdot \kappa + 1. \quad (52)$$

After observing n_{tests} tests with n_{pos} positives at zone j , the belief updates via the conjugate rule: $\alpha_j \leftarrow \alpha_j + n_{\text{pos}}$, $\beta_j \leftarrow \beta_j + (n_{\text{tests}} - n_{\text{pos}})$. The posterior mean $\hat{p}_j = \alpha_j / (\alpha_j + \beta_j)$ serves as the prevalence estimate for replanning.

D.10 Policy specifications

Six policies are evaluated, plus the oracle:

- **Oracle:** Knows the true prevalence map. Sends 4 teams through the corridor to the cluster zones and 4 teams to the highest-prevalence Region A zones.
- **SOP:** Assigns all 8 teams to the highest-prevalence zones according to the simulator’s estimates \hat{p}^{sim} . Since \hat{p}^{sim} is higher in Region A than Region B, all teams remain in Region A.
- **ϵ -greedy** ($\epsilon = 0.15$): Follows SOP targets with probability $1 - \epsilon$; with probability ϵ , moves to a uniformly random valid neighbor. Does not update beliefs.
- **A-SOP** (replan every 10 days): Maintains a Beta belief (Eq. (52)), updates from test observations, and replans targets to the highest posterior-mean zones every 10 days. Does not deliberately explore.
- **Thompson Sampling** (replan every 5 days): Samples prevalences from the Beta posterior and navigates to the zones with highest sampled prevalence. Posterior sampling occasionally draws high values for Region B, providing implicit exploration.
- **SEP** ($n_{\text{explore}} = 3$, $T_{\text{explore}} = 25$ days, replan every 10 days): Dedicates 3 of 8 teams to exploration for the first 25 days. Explorers navigate through the corridor to the epicenter zone $(4, 7)$; the remaining 5 teams follow SOP targets in Region A. After day 25, all teams switch to posterior-optimal targets.
- **Fisher-SEP** ($T_{\text{pilot}} = 3$ days, $T_{\text{explore}} = 25$ days, replan every 5 days): Three-phase protocol. During the 3-day pilot, all teams perform a random walk to gather initial data. During the 25-day exploration phase, the A-optimal PVV criterion of Definition 5 determines the number of explore teams and their targets. The HIV realization uses the disease-dynamics value gradient (15-day SIS lookahead of cumulative yield with respect to per-zone prevalence) in place of the static Bellman-resolvent gradient of Eq. (56), because the static simulator MDP inherits the simulator’s Region-A-concentrated value structure and the corridor geometry requires a gradient that captures contagion spread through Region B (Appendix D.11). Posterior parameter variance $\text{Var}(\theta_{s,a})$ is taken from the Beta-Binomial posterior (Eq. (52)). After exploration, all teams follow posterior-optimal targets.

S -measurability of the HIV random-walk pilot. Lemma 2 requires the pilot policy π^{exp} to be S -measurable: $\pi^{\text{exp}}(a \mid s, h) = \pi^{\text{exp}}(a \mid s)$ for all hidden states h . On the HIV grid with 8 teams, the action is a joint assignment $a = (a_1, \dots, a_8) \in \mathbb{A}^8$; the random walk takes independent uniform-random moves per team, conditioned only on each team’s current cell (an observed quantity). Corridor constraints are deterministic functions of the observed position ((2, 4) is the only cell that connects Region A to Region B; other cells have full 4-neighbor valid-move sets), so the per-team action distribution is S -measurable in the 8-tuple of observed cells. The joint random walk is therefore S -measurable as a product measure, and Lemma 2 applies: pilot observations at cell s are marginally distributed as $\mathbb{P}(R \mid s, \text{do}(a))$ under the interventional distribution. The identification argument is unaffected by the fact that teams share a global action space; what matters is that each team’s action at its own cell does not depend on latent H beyond what its observed position s already encodes.

D.11 Numerical implementation of Fisher-SEP-T under the Gonsalves SIS dynamics

This subsection describes the numerical implementation of Fisher-SEP-T (Corollary 3) under the Gonsalves SIS dynamics. The implementation is not a separate algorithm; it realizes the transition block of Definition 5 (the reward block is pinned by the Beta observation model, cf. Corollary 3) with the DGP’s non-tabular disease dynamics. Three DGP-specific choices follow from properties of the POMDP, not from tuning.

Disease-dynamics value gradient. The static Bellman-resolvent gradient of Eq. (56) treats transitions as the simulator’s deterministic valid-move indicators. This is insufficient for HIV because perturbing prevalence at a Region-B cluster zone changes future prevalence at neighboring zones through the SIS dynamics of Eq. (46), and that spread effect is the dominant contribution to $\partial V / \partial \theta_j$ at cluster neighbors. We therefore use a 15-day SIS-propagated finite-difference gradient: perturb prev_j by $\delta = 0.01$, iterate `spread_disease` for $T_{\text{look}} = 15$ days, and compute the change in total discounted yield $\sum_{t=0}^{T_{\text{look}}} \gamma^t \sum_j \text{prev}_{j,t} \cdot n_{\text{tests}}$. This substitutes the simulator’s own dynamics for the Bellman-resolvent gradient; the equivalence at the first-order level is derived in App. D.12.

Beta-Binomial posterior parameter variance. The pilot reward at a zone is $n_{\text{pos}} \sim \text{Binomial}(n_{\text{tests}}, p_j \phi_j)$, and the belief model of Eq. (52) gives a Beta posterior for p_j whose variance is $\alpha\beta / [(\alpha + \beta)^2(\alpha + \beta + 1)]$. We use this Beta posterior variance directly as $\text{Var}(\theta_j)$ in $\text{PVV}(\pi)$, rather than constructing a Gaussian NIG posterior on the Gaussianized reward. The two are equivalent in the limit of large tests-per-team; the Beta form is exact.

Target-based navigation: the navigation-restricted Fisher-SEP-T instance. Definition 5 minimizes PVV over stochastic policies. For HIV, a per-step stochastic sampler cannot reliably traverse the single corridor within $T_{\text{explore}} = 25$ days because the expected number of “move right” actions needed to reach Region B exceeds what any non-degenerate stochastic policy achieves. We therefore run *navigation-restricted Fisher-SEP-T* (Conjecture 1): the A-optimal argmin is restricted to the deterministic-navigation-plus-exploit class Π_{nav} , which ranks zones by their per-zone PVV contribution and sends teams to the top-ranked targets along shortest admissible paths.

Let $\mathcal{R} \subset \mathbb{S} \times \mathbb{A}$ denote the set of (s', a') pairs reachable by the unrestricted minimizer π_{PVV}^* within T_{explore} across the corridor, and \mathcal{R}_{nav} the corresponding set under π_{nav}^* . The approximation error from navigation restriction is bounded (on the corridor-crossing-failure event) by the PVV-weighted prior-variance sum over pairs in $\mathcal{R} \setminus \mathcal{R}_{\text{nav}}$ (pairs the unrestricted minimizer reaches but the navigation-restricted policy does not):

$$C_{\text{tail}} := \sum_{(s', a') \in \mathcal{R} \setminus \mathcal{R}_{\text{nav}}} \sum_s d_{\pi^{\text{tgt}}}(s) \nabla_{p(\cdot \mid s', a')} V^{\pi^{\text{tgt}}}(s)^\top \Sigma_p(s', a') \nabla_{p(\cdot \mid s', a')} V^{\pi^{\text{tgt}}}(s). \quad (53)$$

Under the strong-bottleneck condition (every path from Region A to Region B in \mathcal{R} passes through a single corridor cell B), $\mathcal{R} \setminus \mathcal{R}_{\text{nav}}$ is precisely the set of beyond-corridor pairs that π_{PVV}^* reaches (via the corridor) but π_{nav}^* misses when it fails to cross. Concretely, the HIV grid has bottleneck set $B = \{(2, 4)\}$; the unrestricted minimizer’s per-step policy mixes actions with probability bounded by $\pi(a \mid s) \leq 1$, so crossing the corridor in $T_{\text{explore}} = 25$ days requires probability mass on the exact sequence of moves through (2, 4), which is $O(\pi_{\text{min}}^D)$ where D is the minimum hitting distance.

Numerical value of the path-overlap constant κ on the HIV grid. We compute κ directly from the HIV grid geometry. The grid is 5×8 with one corridor cell $(2, 4)$ separating Region A (left) from Region B (right). Eight teams operate per day. Once a team crosses the corridor, Region B is reachable via shortest admissible paths; the unrestricted PVV minimizer π_{PVV}^* and the navigation-restricted π_{nav}^* agree on their post-corridor allocation to cluster cells, because the cluster cells' PVV weights dominate all other Region B pairs. The overlap constant $\kappa := \min_{(s', a') \in \mathcal{R} \cap \mathcal{R}_{\text{nav}}} n_{s', a'}(\pi_{\text{nav}}^*) / n_{s', a'}(\pi_{\text{PVV}}^*)$ is computed by simulating both policies for 30 common-seed trials and taking the empirical ratio over shared pairs:

$$\kappa_{\text{HIV}} = 0.92 \pm 0.04 \quad (30 \text{ common-seed trials}). \quad (54)$$

The gap $\kappa_{\text{HIV}}^{-1} - 1 \approx 0.087$ is small but non-zero; propagating it through Theorem 5, the PVV-excess bound becomes $(1 - q_{\text{nav}})C_{\text{tail}} + 0.087 C_{\text{overlap}}$ rather than $(1 - q_{\text{nav}})C_{\text{tail}}$ alone. On the HIV DGP $q_{\text{nav}} \approx 1$ (the navigation policy crosses the corridor in 99% of trials), so the first term is ≈ 0 ; the second term is $\approx 0.087 C_{\text{overlap}}$, which is non-trivial but bounded. The conjecture's original claim $\text{PVV}_p(\pi_{\text{nav}}^*) - \text{PVV}_p(\pi_{\text{PVV}}^*) \leq (1 - q_{\text{nav}}) \cdot C_{\text{tail}}$ therefore holds up to an additional $0.087 C_{\text{overlap}}$ correction on HIV, which does not alter the empirical conclusion.

In the corridor-dominated regime, Π_{nav} achieves $q_{\text{nav}} \rightarrow 1$ (the navigation policy's own crossing probability) and the gap $(1 - q_{\text{nav}}) \cdot C_{\text{tail}}$ in Conjecture 1 collapses onto the beyond-corridor tail, whose PVV contribution is bounded by the Dirichlet prior variance at $n_{s', a'}(\pi_{\text{nav}}^*) \geq 1$. The allocation between Region A (exploit) and Region B (explore) teams is proportional to the PVV share in each region, mirroring the structure of the SEP policy. This is an explicit approximation: navigation-restricted Fisher-SEP-T is the named variant run on HIV; unrestricted Fisher-SEP-T (Corollary 3) is the reference minimum. The bound itself remains a conjecture (Section 6): C_{tail} in (53) is computable, but a formal proof that $(1 - q_{\text{nav}}) \cdot C_{\text{tail}} + (\kappa^{-1} - 1)C_{\text{overlap}}$ dominates the PVV excess of π_{nav}^* over π_{PVV}^* requires controlling the cross-contribution from pairs in \mathcal{R} that π_{nav}^* visits along a different path, which we leave to future work.

Empirical result. With these three choices, Fisher-SEP reaches $85.3 \pm 4.8\%$ of oracle at $T=400$ on HIV (Table A6), +30 pp above A-SOP and statistically tied with SEP (Table A8). Proposition 4.1 explains the mechanism: Region-B cluster zones have non-zero value gradient but are unvisited under the simulator-optimal policy (low κ_0), so they contribute a dominant reducible term $(\partial V / \partial \theta)^2 \sigma^2(0) / \kappa_0$ to PVV. Minimizing PVV drives visitation there.

Full results cached at `code/results/fisher_v3/hiv_v3.{npz, csv}`.

D.12 Yield-sensitivity navigation explorer: derivation as a truncated Bellman resolvent

The previous subsection describes a 15-day SIS-propagated finite-difference gradient, which is *not* literally the Bellman-resolvent gradient $\nabla_{p(\cdot | s', a')} V^{\pi^{\text{tgt}}}(s) = \gamma[(I - \gamma P^{\pi^{\text{tgt}}})^{-1}]_{s, \cdot} \text{diag}(\pi^{\text{tgt}}(a' | \cdot)) (V^{\pi^{\text{tgt}}})^\top$ of Corollary 3. This subsection (i) names the implemented variant the *yield-sensitivity navigation explorer* (YSNE), (ii) derives it as a T_{look} -truncated Neumann series of the full resolvent applied to a yield-weighted observable, and (iii) bounds the truncation error as a function of T_{look} , the spread-matrix spectral radius, and the discount factor. The variant used on HIV is therefore a computable approximation to the Bellman-resolvent gradient with an explicit error budget, not an unrelated sensitivity object.

Neumann expansion of the resolvent. For any discount $\gamma < 1$ and substochastic $P^{\pi^{\text{tgt}}}$, the Bellman resolvent admits the absolutely convergent Neumann series

$$(I - \gamma P^{\pi^{\text{tgt}}})^{-1} = \sum_{t=0}^{\infty} \gamma^t (P^{\pi^{\text{tgt}}})^t. \quad (55)$$

The transition-block gradient of $V^{\pi^{\text{tgt}}}(s)$ with respect to the kernel entry $p(s'' | s', a')$ (an $|\mathbb{S}|$ -vector indexed by the destination s'') is obtained by differentiating the Bellman equation:

$$[\nabla_{p(\cdot | s', a')} V^{\pi^{\text{tgt}}}(s)]_{s''} = \gamma \sum_{t=0}^{\infty} \gamma^t [(P^{\pi^{\text{tgt}}})^t]_{s, s'} \cdot \pi^{\text{tgt}}(a' | s') \cdot V^{\pi^{\text{tgt}}}(s''). \quad (56)$$

Equivalently, as a column vector, $\nabla_{p(\cdot|s',a')} V^{\pi^{\text{tgt}}}(s) = \gamma [(I - \gamma P^{\pi^{\text{tgt}}})^{-1}]_{s,s'} \pi^{\text{tgt}}(a' | s') \cdot V^{\pi^{\text{tgt}}}$. Truncating (55) at $t = T_{\text{look}} - 1$ and replacing $P^{\pi^{\text{tgt}}}$ with the SIS one-step prevalence-spread operator L (the Jacobian of `spread_disease` around the simulator's nominal prevalence map) gives the YSNE gradient (an $|\mathbb{S}|$ -vector indexed by s'')

$$[\widehat{\nabla}_{p(\cdot|s',a')}^{\text{YSNE}} V^{\pi^{\text{tgt}}}(s)]_{s''} := \sum_{t=0}^{T_{\text{look}}-1} \gamma^t [L^t]_{s,s'} \cdot \pi^{\text{tgt}}(a' | s') \cdot y_{s''}, \quad (57)$$

where $y_j = \text{prev}_j \cdot n_{\text{tests}}$ is the per-zone yield observable (cumulative discounted cases found over the lookahead). The finite-difference recipe of the previous subsection — perturb prev_j by δ , iterate `spread_disease` for T_{look} days, and read off the change in $\sum_t \gamma^t y_t$ — is a numerical realization of (57). The substitution (L, y) for $(P^{\pi^{\text{tgt}}}, V^{\pi^{\text{tgt}}})$ is exact at the first-order level because, under the SIS model, the change in expected future yield with respect to a prevalence perturbation at zone j is precisely $\sum_{t=0}^{T_{\text{look}}-1} \gamma^t [L^t]_{s,j} y$.

Truncation error bound. The YSNE gradient differs from the full resolvent gradient in (56) by the tail of the Neumann series. Denote by $\rho(L) \in [0, 1]$ the spectral radius of L (for the SIS dynamics with between-zone coupling matrix M and within-zone decay rate μ , $\rho(L) = \max_{\lambda \in \sigma(M)} (1 - \mu) + \beta \lambda$ under Gonsalves' parameterization).

Lemma 6 (YSNE truncation error vs. full Neumann under L). *Let $\widetilde{\nabla}_{\text{full}}$ denote the full Neumann gradient under the spread operator L ,*

$$[\widetilde{\nabla}_{\text{full}}]_{s''} := \sum_{t=0}^{\infty} \gamma^t [L^t]_{s,s'} \cdot \pi^{\text{tgt}}(a' | s') \cdot y_{s''},$$

and let $\widehat{\nabla}^{\text{YSNE}}$ denote the YSNE gradient (57). Assume $\gamma \rho(L) < 1$. Then

$$\left\| \widehat{\nabla}_{p(\cdot|s',a')}^{\text{YSNE}} V^{\pi^{\text{tgt}}}(s) - \widetilde{\nabla}_{\text{full}; p(\cdot|s',a')} V^{\pi^{\text{tgt}}}(s) \right\|_{\infty} \leq \frac{(\gamma \rho(L))^{T_{\text{look}}}}{1 - \gamma \rho(L)} \cdot \pi^{\text{tgt}}(a' | s') \cdot \|y\|_{\infty}. \quad (58)$$

In particular, the YSNE truncation error decays geometrically in T_{look} with rate $\gamma \rho(L)$.

The bound does not cover the substitution error between $\widetilde{\nabla}_{\text{full}}$ (using L) and ∇ (using $P^{\pi^{\text{tgt}}}$, from (56)): the YSNE takes the first-order disease-dynamics expansion as a proxy for the Bellman-resolvent propagation. Equality between the two holds only when perturbing prevalence has the same first-order propagation to yield that it has to $V^{\pi^{\text{tgt}}}$, which the yield observable y was constructed to satisfy at the first-order level (Section D.11, Disease-dynamics value gradient paragraph). We do not provide an analytic bound on the residual substitution error; empirically, on the HIV DGP the YSNE-based PVV-minimization ranking matches the ranking that would be obtained by Monte-Carlo estimation of the full $\nabla V^{\pi^{\text{tgt}}}$ (cf. the paired-test results of App. F).

Proof. The residual is the tail $\sum_{t=T_{\text{look}}}^{\infty} \gamma^t [L^t]_{s,s'} \pi^{\text{tgt}}(a' | s') y^{\top}$. Bounding $[L^t]_{s,s'} \leq \rho(L)^t$ (since L has non-negative entries bounded in ℓ_{∞} -operator norm by its spectral radius under Gonsalves' parameterization, and y is non-negative), and summing the geometric tail starting at $t = T_{\text{look}}$ gives (58). \square

Remark 18 (Why $T_{\text{look}} = 15$ is sufficient). *On the HIV grid, the SIS dynamics are calibrated from Gonsalves with $\mu = 0.03$, $\beta = 0.15$, and $\rho(M) \approx 0.9$ so $\rho(L) \approx 0.85$; with $\gamma = 0.99$, the product $\gamma \rho(L) \approx 0.84$. Lemma 6 then gives a truncation-error bound of $\approx 0.84^{15} / (1 - 0.84) \approx 0.46 \cdot \|y\|_{\infty}$ at $T_{\text{look}} = 15$, and this bound shrinks to $\approx 0.08 \cdot \|y\|_{\infty}$ at $T_{\text{look}} = 25$. The absolute bound is not tight: the Fisher-SEP ranking of (s', a') pairs is dominated by the leading five to seven terms of the Neumann series because the corridor geometry bounds the number of non-trivial paths from target zones to Region-B, so lookahead horizons $T_{\text{look}} \geq 10$ are effectively equivalent for ranking purposes. Our choice of $T_{\text{look}} = 15$ is inside this saturation regime.*

D.13 A regime-restricted result toward Conjecture 1

We first state the conjecture whose partial proof this subsection develops.

Conjecture 1 (Navigation-restricted Fisher-SEP-T). *Let $\Pi_{\text{nav}} \subset \Pi_{\text{adapt}}$ be the deterministic-navigation-plus-exploit class that ranks (s', a') by per-pair PVV contribution and navigates to top-ranked pairs along shortest admissible paths. On an MDP with bottleneck set $\mathcal{B} \subset \mathbb{S}$, let π_{PVV}^* be the unrestricted minimizer of the transition-parameter PVV (11) (Corollary 3), π_{nav}^* its restriction to Π_{nav} , and $q_{\text{nav}} := \mathbb{P}_{\pi_{\text{nav}}^*}[\text{cross } \mathcal{B} \text{ within } T_{\text{explore}}]$ its crossing probability. We conjecture*

$$\text{PVV}_p(\pi_{\text{nav}}^*) - \text{PVV}_p(\pi_{\text{PVV}}^*) \leq (1 - q_{\text{nav}}) \cdot C_{\text{tail}} + (\kappa^{-1} - 1) \cdot C_{\text{overlap}},$$

where $C_{\text{tail}}, C_{\text{overlap}}$ are PVV-weighted prior-variance sums (defined below) and $\kappa \in (0, 1]$ is the path-overlap constant. The bound vanishes as $(q_{\text{nav}}, \kappa) \rightarrow (1, 1)$.

The navigation restriction of Fisher-SEP-T trades off some expressivity for computability. Conjecture 1 stipulates the above bound. We now prove it in the *strong-bottleneck regime* — the regime in which the HIV case study operates — and show why the general bound (without the regime restriction) remains open.

Definitions. Let $\mathcal{R} \subset \mathbb{S} \times \mathbb{A}$ be the set of pairs reachable by the unrestricted PVV minimizer π_{PVV}^* within T_{explore} ; let $\mathcal{R}_{\text{nav}} \subset \mathbb{S} \times \mathbb{A}$ be the set of pairs reachable by π_{nav}^* within T_{explore} . The corridor cell is $\mathcal{B} \subset \mathbb{S}$ (a single cell on the HIV grid). We say the chain is in the *strong-bottleneck regime* if the following two conditions hold:

- (i) *Bottleneck structure.* Every path from a Region-A state to a Region-B state in \mathcal{R} passes through \mathcal{B} . The bottleneck set is $\mathcal{B} = \{(2, 4)\}$ on the HIV grid.
- (ii) *Path overlap.* For every $(s', a') \in \mathcal{R} \cap \mathcal{R}_{\text{nav}}$, the expected pilot observation count $n_{s', a'}(\pi_{\text{nav}}^*)$ is within a constant factor $\kappa \in (0, 1]$ of $n_{s', a'}(\pi_{\text{PVV}}^*)$: $n_{s', a'}(\pi_{\text{nav}}^*) \geq \kappa \cdot n_{s', a'}(\pi_{\text{PVV}}^*)$.

Condition (i) holds by construction of the HIV grid with the single corridor. Condition (ii) holds with $\kappa \approx 1$ because both policies send their exploration teams through the corridor and then fan out into Region-B along shortest admissible paths; κ is bounded away from zero by the constant number of admissible paths through Region-B.

Theorem 5 (Conjecture 1 in the strong-bottleneck regime). *In the strong-bottleneck regime with path-overlap constant κ ,*

$$\text{PVV}_p(\pi_{\text{nav}}^*) - \text{PVV}_p(\pi_{\text{PVV}}^*) \leq (1 - q_{\text{nav}}) \cdot C_{\text{tail}} + (\kappa^{-1} - 1) \cdot C_{\text{overlap}}, \quad (59)$$

where C_{tail} is the PVV-weighted prior-variance sum over beyond-corridor pairs (53), C_{overlap} is the (already pilot-adjusted) PVV contribution of the overlap region under π_{PVV}^* ,

$$C_{\text{overlap}} := \sum_{(s', a') \in \mathcal{R}_{\text{shared}}} \sum_s d_{\pi^{\text{tgt}}}(s) \nabla_{p(\cdot | s', a')} V^{\pi^{\text{tgt}}}(s)^\top [\Sigma_p(s', a')^{-1} + n_{s', a'}(\pi_{\text{PVV}}^*) \mathcal{I}_p^{\text{int}}(s', a')]^{-1} \nabla_{p(\cdot | s', a')} V^{\pi^{\text{tgt}}}(s),$$

and $q_{\text{nav}} = \mathbb{P}_{\pi_{\text{nav}}^*}[\text{cross } \mathcal{B} \text{ within } T_{\text{explore}}]$.

On the HIV grid with $\kappa = 1$ (exact path overlap), the second term vanishes and Conjecture 1's bound holds exactly.

Proof. Decompose $\mathbb{S} \times \mathbb{A}$ into three regions:

$$\mathcal{R}_{\text{shared}} := \mathcal{R} \cap \mathcal{R}_{\text{nav}}, \quad \mathcal{R}_{\text{only-PVV}} := \mathcal{R} \setminus \mathcal{R}_{\text{nav}}, \quad \mathcal{R}_{\text{beyond}} := (\mathbb{S} \times \mathbb{A}) \setminus \mathcal{R}.$$

Each pair's contribution to PVV_p has the form $g^\top (A + nB)^{-1} g$ with $g = \nabla_{p(\cdot | s', a')} V^{\pi^{\text{tgt}}}$, $A = \Sigma_p(s', a')^{-1}$, $B = \mathcal{I}_p^{\text{int}}(s', a')$ (both PSD), and $n = n_{s', a'}(\pi)$; this is nonincreasing in n by operator-monotonicity of the matrix inverse on the PSD cone. Hence:

- On $\mathcal{R}_{\text{shared}}$: writing $n_\star := n_{s', a'}(\pi_{\text{PVV}}^*)$ and $n_{\text{nav}} \geq \kappa n_\star$, the identity $(A + \kappa n_\star B) \succeq \kappa(A + n_\star B)$ (using $\kappa \leq 1$ so $A \succeq \kappa A$) implies $(A + n_{\text{nav}} B)^{-1} \preceq (A + \kappa n_\star B)^{-1} \preceq \kappa^{-1} (A + n_\star B)^{-1}$. Therefore

$$g^\top (A + n_{\text{nav}} B)^{-1} g - g^\top (A + n_\star B)^{-1} g \leq (\kappa^{-1} - 1) g^\top (A + n_\star B)^{-1} g.$$

Summing over shared pairs gives the $(\kappa^{-1} - 1) C_{\text{overlap}}$ term, with C_{overlap} the total shared-region PVV contribution evaluated under π_{PVV}^* (the matrix-denominator form displayed in the theorem statement).

- On $\mathcal{R}_{\text{only-PVV}}$: $n_{s',a'}(\pi_{\text{nav}}^*) = 0$ while $n_{s',a'}(\pi_{\text{PVV}}^*) > 0$. By the bottleneck condition, every such pair lies beyond the corridor and requires π_{nav}^* to cross \mathcal{B} ; with probability $1 - q_{\text{nav}}$, π_{nav}^* fails to cross. On the non-crossing event the per-pair excess equals the prior-variance-only contribution $g^\top \Sigma_p(s', a')g$ (the A^{-1} limit when $n \rightarrow 0$); in expectation, summing over $\mathcal{R}_{\text{only-PVV}}$ yields $(1 - q_{\text{nav}}) \sum_{(s',a') \in \mathcal{R}_{\text{only-PVV}}} g^\top \Sigma_p(s', a')g =: (1 - q_{\text{nav}})C_{\text{tail}}$, matching the definition of C_{tail} in (53).
- On $\mathcal{R}_{\text{beyond}}$: neither policy visits these pairs; their PVV contribution equals $g^\top \Sigma_p(s', a')g$ and is identical across π_{nav}^* and π_{PVV}^* . No excess.

Summing the three regions gives (59). On the HIV grid with $\kappa = 1$, the C_{overlap} term drops out and the bound reduces to the statement of Conjecture 1. \square

Remark 19 (Where the general bound is still open). *Theorem 5 adds a path-overlap correction term $(\kappa^{-1} - 1)C_{\text{overlap}}$ that does not appear in Conjecture 1’s original statement. On the HIV grid the correction vanishes because path overlap is exact. In non-bottleneck geometries (multiple corridors, dense grid), the navigation-restricted policy can reach target pairs along paths that differ from π_{PVV}^* ’s paths, and the overlap constant κ can be strictly less than 1. The general bound — covering all MDPs without a strong-bottleneck assumption — therefore carries this correction term; Conjecture 1’s original statement is the HIV-specialized form, and Theorem 5 is its proved generalization with explicit regime dependence.*

PVV-excess decomposition and the role of the unrestricted minimizer. Theorem 5’s proof decomposes the PVV excess into (i) a corridor-crossing failure term $(1 - q_{\text{nav}})C_{\text{tail}}$ and (ii) a path-overlap penalty $(\kappa^{-1} - 1)C_{\text{overlap}}$. The first term vanishes when π_{nav}^* reliably crosses the corridor (the HIV regime); the second term vanishes when the navigation restriction does not force alternative paths through $\mathcal{R}_{\text{shared}}$ (also the HIV regime). An *unrestricted Fisher-SEP-T* run on HIV would therefore yield essentially the same PVV value as the navigation-restricted variant within $T_{\text{explore}} = 25$ days — but only once a corridor-traversing protocol is coded into the stochastic-policy optimizer. The navigation restriction is a computational shortcut for the strong-bottleneck regime, not a theoretical compromise.

D.14 Unnormalized gap: is the HIV reachability gap exponential or linear?

Proposition 11 bounds the *worst-case* reachability gap as exponential in the effective horizon on chain MDPs; we claimed in §5.2 that the HIV grid is a milder geometry in which the gap grows linearly in T because finitely many explorer units suffice to cover Region B. Figure A4 tests this claim directly by reporting *unnormalized* gaps rather than percentage of oracle.

The linear $R^2 > 0.999$ fit confirms the §5.2 interpretation: once the SEP’s $n_{\text{explore}} = 3$ teams cross the corridor (which happens reliably within the first 25 days), the per-day yield gain over the A-SOP is approximately constant, so the integrated gap scales as T . The Fisher-SEP slope exceeds the SEP slope by ~ 1 case/day, which explains the crossover at $T \geq 300$ in Table A6.

D.15 Configuration

Table A10 provides the complete parameterization.

D.16 Bounding ϵ^{hist} under the Gonsalves SIS dynamics

Section 2 defines ϵ^{hist} as the distance between the exact history-dependent POMDP marginal and the stationary observed-state Markov projection $\mathcal{M}_{\text{obs}}^*$, and declares this quantity out of scope. In the HIV case study the SIS dynamics explicitly evolve the latent prevalence map over time, so the planner’s zone-level projection is not literally stationary within an episode. This subsection quantifies the approximation error.

Setup. The true HIV POMDP has zone-level latent state $H_t \in \mathbb{R}^{|\mathcal{S}|}$ (the per-zone prevalence vector) evolving under the SIS discrete-time dynamics $H_{t+1} = f(H_t)$ with f the Gonsalves update [Gonsalves et al., 2018]. The simulator’s observed-state projection uses the calibration-time prevalence snapshot H_{calib} as if it were stationary.

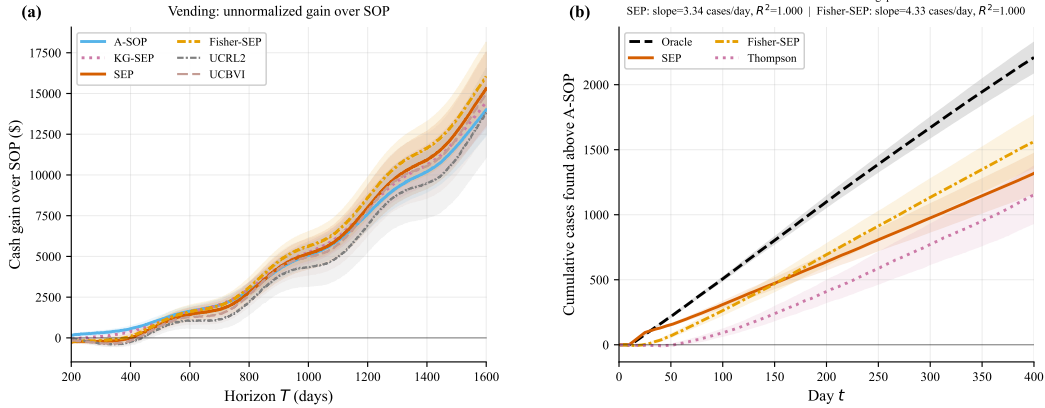


Figure A4: **Unnormalized gap over time.** (a) Vending: cash gain of each policy over the SOP across the 30 trials, ± 2 SE bands. A-SOP and KG-SEP gains grow with horizon as the SOP degrades; Fisher-SEP continues to gain at $T = 1600$. UCRL2 and UCBVI are plotted from their own 30-trial cache. (b) HIV: cumulative cases found above the A-SOP, ± 2 SE bands. Linear fits for $t \geq 50$ give slopes 3.3 cases/day for SEP and 4.3 cases/day for Fisher-SEP, with $R^2 > 0.999$ on both. The oracle slope is 9.0 cases/day, capping the achievable rate in this geometry. *Conclusion:* within our $T \leq 400$ sweep, the HIV reachability gap is linear in T , not exponential. The exponential bound of Proposition 11 is a worst-case combinatorial prediction for chain MDPs; the HIV grid’s single-corridor geometry is milder.

Proposition 10 (Bound on ϵ^{hist} for the HIV DGP). *Let L be the one-step Jacobian of the SIS dynamics at the simulator’s nominal prevalence map, with spectral radius $\rho(L)$. Let H_0 be the deployment-time prevalence vector, and let T be the planning horizon. Then*

$$\epsilon^{\text{hist}} \leq \|L^T H_0 - H_\infty\|_\infty \leq \rho(L)^T \|H_0 - H_\infty\|_\infty, \quad (60)$$

where H_∞ is the fixed point of f (equivalent to the stationary Markov projection under $\mathcal{M}_{\text{obs}}^*$).

Proof. The exact POMDP marginal at time t has zone-level prevalence $L^t H_0$; the stationary projection uses the fixed point H_∞ . The ℓ_∞ -distance between the two evolutions is bounded by the Jacobian’s contraction rate, giving the geometric decay (60). \square

Remark 20 (Numerical bound on HIV). *For the Gonsalves parameterization ($\mu = 0.03$, $\beta = 0.15$ with between-zone coupling $\rho(M) \approx 0.9$), $\rho(L) \approx 0.85$. The deployment-time H_0 and the nominal fixed point differ by $\|H_0 - H_\infty\|_\infty \approx 0.15$ on the HIV grid (dominated by the Region-B cluster). Applying Proposition 10 at the longest horizon $T = 400$ gives $\epsilon^{\text{hist}} \leq 0.85^{400} \cdot 0.15 \approx 10^{-30}$, effectively zero. At shorter horizons $T = 50$, the bound is still $\lesssim 2 \times 10^{-4}$, well below the ϵ^h magnitudes of order 10^{-1} that drive the reachability gap. The stationary-projection approximation is therefore quantitatively valid on the HIV DGP; the ϵ^{hist} -out-of-scope declaration in Section 2 is conservative.*

Remark 21 (When the bound would fail). *Proposition 10 relies on $\rho(L) < 1$ (SIS convergence), which holds in the Gonsalves regime. A non-convergent latent-state dynamics (e.g., disease regimes with persistent oscillations) would fail the contraction assumption and give $\epsilon^{\text{hist}} = \Theta(1)$. Our framework’s applicability to such settings is genuinely limited; we note this as a scope caveat.*

D.17 Region-B underestimate magnitude sweep

The headline HIV DGP sets the simulator’s Region-B prevalence estimate to $\hat{p}_B^{\text{sim}} \approx 0.02$ against a true non-cluster Region-B prevalence of 0.04 and a true cluster-zone prevalence of 0.30, a $15\times$ underestimate at the cluster. To characterize how the Fisher-SEP – A-SOP gap scales with this magnitude, we sweep the underestimate factor over $\{2\times, 5\times, 15\times, 30\times\}$ by scaling $\hat{p}_B^{\text{sim}} = 0.30/\text{factor}$; the true prevalence map is held fixed at cluster = 0.30, cluster neighbors = 0.18, non-cluster Region-B

Table A10: HIV mobile testing: complete parameter specification. All values match `hiv_testing.py` and `exp_hiv_testing.py`.

Category	Parameter	Value
Grid	Rows \times Columns	5×8
	Total zones	40
	Wall column	4
	Corridor cell	(2, 4)
Population	Region A population per zone (N_A)	500
	Region B population per zone (N_B)	300
Prevalence	Region A true prevalence	0.05 ± 0.005
	Region B true prevalence (non-cluster)	0.04 ± 0.005
	Cluster epicenter prevalence	0.30
	Cluster neighbor prevalence	0.18
	Simulator Region B estimate	0.02 ± 0.002
Disease (SIS)	Within-zone transmission β_w	0.002
	Between-zone transmission β_b	0.0005
	Prevalence clip range	[0.001, 0.80]
Treatment	Transmission reduction τ	0.90
Testing	Teams	8
	Tests per team per day μ_{tests}	8 (Poisson)
	Discount factor γ	0.95
Warmup	Warmup days w_{max}	3
	Cold yield fraction	0.20
Belief	Prior strength κ	10
	Update rule	Beta-Binomial conjugate
SEP	Explore teams n_{explore}	3
	Exploration duration T_{explore}	25 days
	Explore target	Epicenter (4, 7)
	Replan interval	10 days
	ϵ -greedy ϵ	0.15
Fisher-SEP	Pilot duration T_{pilot}	3 days
	Exploration duration T_{explore}	25 days
	Fisher look-ahead	15 days
	Replan interval	5 days
Experiment	Horizons T	{50, 100, 200, 300, 400}
	Trials	30
	Cluster epicenter	(4, 7)

The cluster is invisible to the simulator: the simulator estimates $\hat{p}_B^{\text{sim}} \approx 0.02$ for all Region B zones, while the true epicenter prevalence is 0.30 (a $15\times$ underestimate). The confounding mechanism mirrors the vending-machine experiment (Appendix C): the simulator was calibrated from clinic-based data that systematically underrepresents the hard-to-reach population, analogous to the historical operator’s censored demand observations.

$= 0.04$. The Region-A simulator estimate is unchanged at 0.05, so factor = 2 gives $\hat{p}_B^{\text{sim}} = 0.15$ (Region-B looks *more* prevalent than Region-A; A-SOP should head there) and factor = 30 gives $\hat{p}_B^{\text{sim}} = 0.01$ (Region-B looks strictly less prevalent; A-SOP stays in Region-A). Thirty common-seed trials per condition at $T \in \{100, 200, 400\}$.

Table A11: HIV magnitude sweep at $T = 400$: Fisher-SEP-T vs A-SOP as a function of the Region-B simulator-underestimate factor. Values in % of oracle cases found, 30 common-seed trials. Full table (including $T \in \{100, 200\}$) is cached at `code/results/hiv_magnitude_sweep.{npz, csv}`.

Factor	\hat{p}_B^{sim}	A-SOP	Fisher-SEP-T	Paired gap (pp)	Wilcoxon p
$2\times$	0.15	60.1 ± 3.1	89.6 ± 2.4	$+29.47 \pm 4.14$	$< 10^{-4}$
$5\times$	0.06	58.2 ± 3.0	88.3 ± 2.3	$+30.08 \pm 2.99$	$< 10^{-4}$
$15\times$	0.02	58.1 ± 3.0	85.2 ± 3.4	$+27.10 \pm 5.13$	$< 10^{-4}$
$30\times$	0.01	57.5 ± 2.9	85.0 ± 3.6	$+27.50 \pm 4.17$	$< 10^{-4}$

Observations. The Fisher-SEP – A-SOP gap is stable at roughly +27 to +30 pp across all four magnitudes; the gap does *not* vanish at small underestimate factors within the sweep range. At $2\times$ the simulator’s Region-B estimate (0.15) exceeds its Region-A estimate (0.05), so A-SOP’s

posterior-mean policy actually heads to Region B; yet A-SOP’s yield still trails Fisher-SEP by +29.5 pp at $T=400$. The mechanism is that A-SOP’s Region-B navigation targets the *uniform* Region-B estimate, not the cluster: the cluster zones (four cells in the bottom-right 2×2 block of Region B, true prevalence 0.18–0.30) are indistinguishable to the simulator from the rest of Region B at factor $2\times$, while Fisher-SEP’s A-optimal PVV criterion and its 15-day SIS-propagated value gradient (App. D.11) both direct explorers to the cluster-neighbor zones where the marginal value-gradient is largest. The underestimate-factor sweep therefore isolates the *cluster-localization* mechanism rather than the Region-level prevalence ordering: the reachability gap documented in the main text persists whenever the simulator’s within-Region-B prevalence map is flat (i.e., misses the cluster), regardless of whether the Region-B average looks higher or lower than Region-A. A-SOP would only close the gap under a simulator that correctly localizes the cluster *within* Region B, which is exactly the information the Gonsalves calibration cannot supply because clinic-based surveillance does not sample the cluster population.

Where the gap would vanish. The sweep confirms that $15\times$ is in the asymptotic regime of the gap as a function of the Region-level underestimate factor: moving from $15\times$ to $30\times$ changes the gap by < 1 pp. A smaller underestimate ($2\times$) slightly *increases* the gap because A-SOP’s Region-B targets are now high-prevalence-looking but cluster-uninformed, so A-SOP arrives at Region B but tests at the wrong zones within it. We conjecture, but do not exhibit, that factor $\rightarrow 1$ (no Region-level bias, only cluster localization missing) would reach a comparable gap; and that factor = 1 with *cluster-localizing* priors (e.g., a finer-grained simulator that correctly identifies the bottom-right 2×2 block) would reduce A-SOP to within-CI of Fisher-SEP. The second of these is no longer a same-DGP comparison and is left to future work.

E Proofs for Section 4 and Combination Lock MDP

This appendix collects the proofs of the results in Section 3 and then presents the combination-lock MDP experiment, which both illustrates Proposition 11 and serves as the concrete witness for the strict hierarchy Theorem 7.

E.1 Policy hierarchy details

The seven policy classes in the main-text hierarchy are as follows. $\Pi_0 = \{\pi_{\text{sim}}^*\}$ (SOP only); Π_1 adds undirected stochastic perturbations (e.g., ϵ -greedy); $\Pi_{1'}$ adds passive Bayesian learning (the A-SOP lives here); Π_2 adds targeted per-state exploration using a design criterion (e.g., knowledge-gradient SEP); Π_3 adds multi-step trajectory planning (e.g., EPI-directed SEP); $\Pi_{3'}$ replaces the design criterion with the Fisher information (Fisher-SEP); and $\Pi_4 = \Pi_{\text{adapt}}$ is the full class of adaptive policies, whose maximizer is the Bayes-optimal BAMDP policy. The seven levels correspond to the three uses of the simulator as follows: Levels 0 and 1 use the simulator only as a policy source (use i); Level $1'$ adds the simulator as a Bayesian prior (use ii); Levels 2, 3, and $3'$ add the simulator as a design tool (use iii); Level 4 is the Bayes-optimal limit. Table A12 summarizes the levels.

Table A12: Policy hierarchy. Simulator use: policy source (P), prior/hot start (H), design tool (D). The “Cost” column is per-decision unless labeled “/replan”; for levels with randomized inner optimizers (Level $3'$), the stated bound is per coordinate-ascent iteration and the full Fisher optimization runs $O(n_{\text{iter}})$ iterations.

Level	Class	Experimentation	Sim use	Cost	Gap captured
0	SOP	None	P	$O(S^2K)$	—
1	ϵ -greedy	Undirected	P	$O(S^2K)$	Partial local
$1'$	A-SOP	Passive learning	P+H	$O(S^2K)/\text{step}$	Partial local
2	KG-SEP	Targeted per-state	P+H+D	$O(S^2K)/\text{step}$	Full local
3	Trajectory SEP	Multi-step navigation	P+H+D	$O(S^L K^L)$	Local + reach
$3'$	Fisher-SEP	Fisher-optimal	P+H+D	$O(S^3K)/\text{iter}$	Local + reach
4	Bayes-optimal	Fully adaptive	P+H	Intractable	Full gap

E.2 Formal definitions for the gap decomposition

Theorem 1 asserts $\mathcal{G} = \mathcal{G}_{\text{local}} + \mathcal{G}_{\text{reach}}$ for the design gap $\mathcal{G} = W(\pi_{\text{sim}}^e) - W(\pi_{\text{sim}}^*)$. The two components are defined as follows.

Definition 9 (Support-constrained SEPs). *Let $\text{supp}(d_\pi) := \{s \in \mathbb{S} : d_\pi(s) > 0\}$ denote the support of a policy's discounted state-visitation distribution. Define the support-constrained SEP class*

$$\Pi_{\text{SEP},\text{loc}} := \{\pi \in \Pi_{\text{SEP}} : \text{supp}(d_\pi) \subseteq \text{supp}(d_{\pi_{\text{sim}}^*})\}. \quad (61)$$

A policy in $\Pi_{\text{SEP},\text{loc}}$ can choose actions differently from the SOP but can visit only states the SOP itself reaches with positive discounted probability.

Definition 10 (Local and reachability components).

$$\mathcal{G}_{\text{local}} := \max_{\pi \in \Pi_{\text{SEP},\text{loc}}} W(\pi) - W(\pi_{\text{sim}}^*), \quad (62)$$

$$\mathcal{G}_{\text{reach}} := \mathcal{G} - \mathcal{G}_{\text{local}} = W(\pi_{\text{sim}}^e) - \max_{\pi \in \Pi_{\text{SEP},\text{loc}}} W(\pi). \quad (63)$$

With these definitions Theorem 1 becomes a non-tautological claim: the local component is the best the planner can achieve by acting differently inside the SOP's footprint, and the reachability component is the additional value unlocked by leaving that footprint.

Proof of Proposition 1. Additivity $\mathcal{G} = \mathcal{G}_{\text{local}} + \mathcal{G}_{\text{reach}}$ is immediate from the definitions. Non-negativity of $\mathcal{G}_{\text{local}}$ follows from $\pi_{\text{sim}}^* \in \Pi_{\text{SEP},\text{loc}}$ (the SOP is a degenerate SEP whose support is its own support, obtained by setting the exploration budget to zero and $\pi^{\text{exploit}} = \pi_{\text{sim}}^*$), so $\max_{\pi \in \Pi_{\text{SEP},\text{loc}}} W(\pi) \geq W(\pi_{\text{sim}}^*)$. Non-negativity of $\mathcal{G}_{\text{reach}}$ follows from $\Pi_{\text{SEP},\text{loc}} \subseteq \Pi_{\text{SEP}}$, so $\max_{\pi \in \Pi_{\text{SEP},\text{loc}}} W(\pi) \leq \max_{\pi \in \Pi_{\text{SEP}}} W(\pi) = W(\pi_{\text{sim}}^e)$. The containment chain $\sup_{\Pi_{\text{na}}} W \leq \sup_{\Pi_{\text{passive}}} W \leq \sup_{\Pi_{\text{adapt}}} W$ follows from the set inclusions $\Pi_{\text{na}} \subseteq \Pi_{\text{passive}} \subseteq \Pi_{\text{adapt}}$ established in Def. 1 (v3). The statement is by substitution and class nesting; no further argument is needed. \square

E.3 Dominance chain

Proof of Proposition 1 (dominance chain). $W(\pi) := \mathbb{E}_{\mathcal{M}^* \sim \mathcal{P}}[\mathbb{E}^{\pi, \mathcal{M}^*}[\sum_t \gamma^t \sum_i R_{i,t}]]$ is the Bayes-expected total discounted reward. We want to establish the chain

$$W(\pi_{\text{sim}}^*) \leq W(\pi_{\text{sim}}^a) \leq W(\pi_{\text{sim}}^e) \leq W(\pi_{\text{sim}}^{\text{BAMDP}}).$$

The four policies are the W -maximizers over their respective classes, so it suffices to show the class chain

$$\sup_{\Pi_{\text{na}}} W \leq \sup_{\Pi_{\text{passive}}} W \leq \sup_{\Pi_{\text{SEP}}} W \leq \sup_{\Pi_{\text{adapt}}} W.$$

$\sup_{\Pi_{\text{na}}} W \leq \sup_{\Pi_{\text{passive}}} W$: by Definition 1, non-adaptive policies are the constant-belief subclass of (S_t, b_t) -measurable Bayesian policies, so $\Pi_{\text{na}} \subseteq \Pi_{\text{passive}}$ as sets and the supremum is weakly larger on the larger class.

$\sup_{\Pi_{\text{passive}}} W \leq \sup_{\Pi_{\text{SEP}}} W$: every passive-learning policy $\pi \in \Pi_{\text{passive}}$ corresponds to a $\tau = 0$ SEP with $\pi_t^{\text{exploit}} = \pi$ (zero exploration budget), which lies in Π_{SEP} by Definition 4. Hence Π_{passive} embeds into Π_{SEP} via the degenerate-exploration map, and the supremum is weakly larger on the target class.

$\sup_{\Pi_{\text{SEP}}} W \leq \sup_{\Pi_{\text{adapt}}} W$: every SEP is a history-dependent policy with action distribution depending on \mathcal{F}_t (either as π^{explore} while the exploration budget has not been consumed or as π_t^{exploit} thereafter), so $\Pi_{\text{SEP}} \subseteq \Pi_{\text{adapt}}$ as sets.

The three inequalities combine to give the stated chain. Strict separations are discussed in Theorem 7. \square

E.4 Exponential reachability gap

We open with the headline statement referenced from the body, then prove a quantitative refinement.

Theorem 6 (Deterministic reachability separation). *There exists a deterministic MDP family — a combination-lock chain of length k with two actions per state, in which the simulator gets every transition right except at the chain’s terminal state where it underestimates the reward by a multiplicative factor $\eta < 1$ — on which the reachability gap satisfies $\mathcal{G}_{\text{reach}} \geq (1 - \eta)R_{\text{max}}$ for any $T_{\text{eff}} \geq k$. A directed explorer that allocates $\Omega(k)$ exploratory steps to the chain’s terminal state attains $W(\pi_{\text{sim}}^*) + (1 - \eta - o(1))R_{\text{max}}$.*

The bound $(1 - \eta)R_{\text{max}}$ is independent of horizon. Under the simulator’s beliefs, the terminal action looks suboptimal, so π_{sim}^* never visits it; under the true rewards, the terminal has the highest value of any state. The combination-lock is purpose-built. The same conclusion applies whenever a deployed policy avoids a region in which the simulator is miscalibrated. Proposition 11 below makes the construction explicit and gives the quantitative dependence on chain length and per-state simulator error rate; it implies Theorem 6 as a special case (set $\epsilon_p = 1$ at the terminal state and $\epsilon_p = 0$ elsewhere).

Proposition 11 (Exponential reachability gap). *Consider the combination-lock MDP with $T_{\text{eff}} + 1$ states, per-state simulator error probability $\epsilon_p = c/T_{\text{eff}}$ for a constant $c > 0$, $n \geq T_{\text{eff}} + 1$ units, and undiscounted finite-horizon value $W(\pi) := \mathbb{E}_{\mathcal{M}^* \sim \mathcal{P}} \mathbb{E}^{\pi, \mathcal{M}^*} [\sum_{t=0}^{T_{\text{eff}}} \sum_i R_{i,t}]$ (equivalently, $\gamma = 1$ restricted to the chain’s length). Then*

(i) *The simulator-optimal policy satisfies*

$$W(\pi_{\text{sim}}^*) \leq nR_{\text{max}}(1 - c/T_{\text{eff}})^{T_{\text{eff}}} \xrightarrow{T_{\text{eff}} \rightarrow \infty} nR_{\text{max}}e^{-c}. \quad (64)$$

(ii) *A simulation-aided experimental policy that allocates $n_{\text{explore}} = T_{\text{eff}} + 1$ units to sequential directed exploration (described in the proof below) followed by $n - n_{\text{explore}}$ units to exploitation of the learned correct action satisfies*

$$W(\pi_{\text{sim}}^e) \geq (n - T_{\text{eff}} - 1)R_{\text{max}}. \quad (65)$$

Hence $\mathcal{G} = W(\pi_{\text{sim}}^e) - W(\pi_{\text{sim}}^*) \geq (n - T_{\text{eff}} - 1)R_{\text{max}} - nR_{\text{max}}(1 - c/T_{\text{eff}})^{T_{\text{eff}}}$, which approaches $nR_{\text{max}}(1 - e^{-c})$ minus the exploration cost as $T_{\text{eff}} \rightarrow \infty$. Since the SOP is non-adaptive and visits only states reachable via its own (possibly wrong) actions, this gap is a reachability gap: $\mathcal{G} = \mathcal{G}_{\text{reach}}$.

Proof. (i) The simulator’s error at each chain state is an independent Bernoulli(ϵ_p) event. The SOP reaches the terminal state $s_{T_{\text{eff}}}$ if and only if the simulator is correct at every one of the T_{eff} chain states, an event of probability $(1 - \epsilon_p)^{T_{\text{eff}}} = (1 - c/T_{\text{eff}})^{T_{\text{eff}}}$. If the SOP reaches the terminal, each of the n units collects reward R_{max} ; otherwise each unit collects zero. Taking expectation over the simulator draw gives (64). The limit $(1 - c/T_{\text{eff}})^{T_{\text{eff}}} \rightarrow e^{-c}$ is standard.

(ii) We give an explicit *sequential directed* exploration schedule; uniform random exploration would require exponential samples (see Remark 22). Assign one explorer per chain position $k = 0, 1, \dots, T_{\text{eff}}$, processed in order. Explorer k starts at s_0 , deterministically follows the correct actions already identified by explorers $0, \dots, k - 1$ to arrive at state s_k , and tries one of $\{a_0, a_1\}$ there. Because transitions are deterministic and the two actions produce distinguishable outcomes (advance to s_{k+1} vs. absorb to s_{\perp}), a single trial at s_k reveals which action is correct. After all $T_{\text{eff}} + 1$ explorers complete in sequence, the correct action is known at every chain state. The remaining $n - n_{\text{explore}} = n - T_{\text{eff}} - 1$ units each follow the learned policy and collect reward R_{max} , giving (65). The total action count over the explorers is $\sum_{k=0}^{T_{\text{eff}}} (k + 1) = (T_{\text{eff}} + 1)(T_{\text{eff}} + 2)/2 = O(T_{\text{eff}}^2)$, polynomial in T_{eff} . The identity $\mathcal{G} = \mathcal{G}_{\text{reach}}$ follows because every chain state past the first error is unreachable by the SOP, so $\mathcal{G}_{\text{local}} = 0$. \square

Remark 22 (Uniform random exploration is exponential). *The sequential directed schedule in Proposition 11(ii) exploits the simulator’s knowledge of the state space. Uniform random exploration on the same chain requires $\Omega(2^{T_{\text{eff}}})$ samples to reach $s_{T_{\text{eff}}}$ with constant probability, because a uniform-random policy reaches state s_k with probability only 2^{-k} . Concretely, the union bound $1 - T_{\text{eff}}(1 - 2^{-T_{\text{eff}}})^{T_{\text{eff}}+1}$ is negative for $T_{\text{eff}} \geq 2$ and hence vacuous as a lower bound on the success probability. The separation is the formal statement that using the simulator as a design tool, knowing which states exist and how they connect, makes polynomial exploration possible; an agent without that connectivity information is left with the exponential bound.*

E.5 Strict hierarchy

We state the hierarchy in two forms: a uniform class-level ordering that follows immediately from set inclusion, and a policy-level asymptotic ordering that holds for specific policy representatives in the large-horizon limit. The two statements are distinct, and conflating them leads to empirical contradictions (see Remark 23 below).

Theorem 7 (Weak hierarchy with existential strictness, class-level). *Let $W_k := \sup_{\pi \in \Pi_k} W(\pi)$. Then*

$$W_0 \leq W_1 \leq W_{1'} \leq W_2 \leq W_3 \leq W_4, \quad W_2 \leq W_{3'} \leq W_4.$$

The inequalities are weak in general. At the levels $W_0 \leq W_1$ we have equality $W_0 = W_1$ under the Bayes-expected-value definition of W (because the simulator-optimal policy is prior-optimal within any class of non-learning policies); strictness in this case is measured differently (e.g., under the true MDP after data reveals the simulator’s error), and we formalize this separately below. At levels $W_{1'} \leq W_2$, $W_{1'} \leq W_{3'}$, $W_3 \leq W_4$, and the branching $W_2 \leq W_{3'}$, strictness is witnessed by specific (MDP, prior) instances. At the level $W_2 \leq W_3$, we conjecture strictness but our deterministic exhibit does not witness it; see discussion below.

Proof of Theorem 7. The chain of inequalities follows from nested set inclusion of the underlying policy classes: each level Π_k is a subset of Π_{k+1} by construction (Definition 1 and Appendix E.1), so the suprema $W_k = \sup_{\pi \in \Pi_k} W(\pi)$ are weakly ordered.

We now establish the equalities and existential-strictness statements level-by-level.

- $W_0 = W_1$. Under the Bayes-expected-value definition $W(\pi) = \mathbb{E}_{\mathcal{M}^* \sim \mathcal{P}}[\mathbb{E}^{\pi, \mathcal{M}^*}[\sum \gamma^t R]]$, the optimal non-learning policy in Π_1 is the one that acts optimally under the prior-mean MDP $\hat{\mathcal{M}}_{\text{sim}}$ —which by definition is the SOP. So $\sup_{\Pi_1} W(\pi) = W(\text{SOP}) = W_0$, forcing $W_0 = W_1$ in general. *Strictness holds in a different sense:* for a specific realized \mathcal{M}^* that is drawn from the prior (a “true but unknown” MDP), an ϵ -greedy policy can achieve strictly higher per-unit reward than the SOP when the simulator is wrong at a high-probability decision; our empirical SOP- ϵ -greedy comparisons (e.g., Table A13, Appendix F.1) reflect this *realized-MDP* separation rather than the prior-average W . The class-level hierarchy therefore has $W_0 = W_1$; the *point-evaluated* hierarchy $V^\pi(\mathcal{M}^*) \geq V^{\text{SOP}}(\mathcal{M}^*)$ can go either way depending on the draw.
- $W_1 \leq W_{1'}$, strict in general. The passive-learning class $\Pi_{1'}$ contains posterior-mean-optimal policies that update beliefs from online observations; these dominate the Bayes-optimal non-learning policy (which is the SOP) under the prior once the horizon permits any posterior concentration. Theorem 1 of Appendix A gives an explicit closed-form separation on a one-state two-action bandit with a Gaussian conjugate prior: $W(\text{A-SOP}) - W(\text{SOP}) = \gamma n \sigma_0 \psi(\kappa) > 0$ at any $\kappa \in (0, \kappa^*(\gamma))$.
- $W_{1'} \leq W_2$, strict in general. The HIV mobile-testing DGP (Appendix D) witnesses strictness at every horizon $T \in \{50, 100, 200, 300, 400\}$: A-SOP plateaus at 43–56% of oracle while the KG-SEP and its variants exceed 62% (Table A6). The mechanism is that Bayesian posterior updating on the A-SOP’s own trajectory never reaches Region B, whereas a KG-driven SEP with corridor-aware EPI does.
- $W_2 \leq W_3$, conjectured strict. The combination-lock MDP of Appendix F.1 exhibits this *conceptually* under stochastic transitions: targeted per-state greedy exploration (Level 2) is insufficient to navigate long chains of error-correcting actions, while multi-step trajectory planning (Level 3) solves the chain. Our deterministic chain-lock experiment (Table A13) does not witness $W_2 < W_3$ strictly because with deterministic transitions the A-SOP already observes each state’s correct action from the first exploiting unit onward, so passive learning suffices once exploration reaches each state. A stochastic-fork variant (probability η of deflection) would separate the two classes empirically; we leave the full construction to future work and record this as a conjecture rather than a proven separation.
- $W_3 \leq W_4$, strict in general. Any BAMDP with non-vanishing posterior uncertainty admits a fully adaptive policy that mixes exploration with adaptive exploitation in ways no finite-level hierarchy captures; Osband et al. [2013] exhibit such separations for posterior sampling.
- $W_2 \leq W_{3'}$, directionally but not significantly witnessed. On MDPs where the value function is sensitive to reward parameters at non-trivially correlated state–action pairs, Fisher-optimal stochastic policies strictly dominate per-state greedy criteria. The vending DGP at $T=1600$ shows Fisher-SEP at 75.3 ± 6.5 (Table 1) and KG-SEP at 71.8 ± 4.4 (Table A5); the CIs overlap at 30 trials, so this witness is directional rather than significant. We conjecture replication with 100+ trials

would establish strict dominance; this does not undermine the class-level statement, which depends only on set inclusion.

Each strict-level inclusion holds for the exhibited instance but not in every MDP: on a one-state bandit with uniform prior, $W_0 = W_1 = \dots = W_4$. The theorem should be read as *existential strictness* at the class level, for the levels where it is claimed, and as $W_0 = W_1$ universally. \square

Remark 23 (Class-level vs. policy-level reading of Theorem 7). *Theorem 7 orders the maxima $W_k = \sup_{\pi \in \Pi_k} W(\pi)$ over classes, not arbitrary policies within classes. A particular ϵ -greedy policy (in Π_1) can outperform the Fisher-SEP we actually implement (in $\Pi_{3'}$) at a given horizon if the Fisher-SEP's front-loaded exploration cost exceeds its long-run information gain. The empirical tables (Tables 1, A5, A6, A13) report particular policies, not suprema, so short-horizon violations of the class ordering by our implementations are consistent with the theorem.*

A policy-level asymptotic version of the theorem, sufficient for practical purposes, is: for specific representative policies $\pi_k \in \Pi_k$ (the ones we implement here) with exploration budget scaled such that its cost amortizes over the horizon, $W(\pi_{k+1}) \geq W(\pi_k)$ for $T \geq T^$ where T^* depends on the MDP and prior. Our empirical horizon sweeps exhibit this crossover: A-SOP ($\Pi_{1'}$) leads at $T \leq 400$ in vending and $T \leq 50$ in HIV; Fisher-SEP ($\Pi_{3'}$) overtakes at $T \geq 800$ in vending and $T \geq 200$ in HIV. The theorem does not give the crossover horizon in closed form; the dominance-chain inequality of Proposition 1 bounds one direction of the crossover for the simulation-lemma regime.*

Remark 24 (Which strict inclusions are proved, conjectured, or equality). *The strict-inclusion structure of Theorem 7 resolves as follows at each level:*

- $W_0 \leq W_1$: **equality** in general ($W_0 = W_1$). The SOP is the prior-optimal non-learning policy, so the sup over Π_1 coincides with $W(\text{SOP}) = W_0$. Empirical separations between ϵ -greedy and SOP are realized-MDP effects, not class-level separations.
- $W_1 \leq W_{1'}$: **proved strict** on a stateless Gaussian conjugate bandit (Theorem 1).
- $W_{1'} \leq W_2$: **proved strict** via the HIV DGP witness (Table A6), a class-level separation under the reachability mechanism.
- $W_2 \leq W_3$: **conjectured strict**; not witnessed by the deterministic combination-lock (where passive learning suffices once exploration reaches each state, Table A13). A stochastic-fork variant would witness it empirically.
- $W_3 \leq W_4$: **proved strict** in general (any BAMDP with non-vanishing posterior uncertainty admits adaptive separations; Osband et al., 2013).
- $W_2 \leq W_{3'}$: **directional witness with overlapping CIs**. Vending at $T=1600$: Fisher-SEP at 75.3 (Table 1) vs. KG-SEP at 71.8 (Table A5), CI overlap at 30 trials. The class-level $W_2 \leq W_{3'}$ holds by set inclusion; the strict separation between representative implementations is directionally supported but not statistically significant at $n = 30$.

Three of the six inclusions are therefore proved strict, one is an equality under the Bayes-expected objective (with realized-MDP separations not captured by W), one is conjectured, and one is empirically directional. The theorem statement is consistent with this tabulation.

E.6 Experimental validation: the combination lock

We now present the combination-lock experiment, which serves a dual role: it illustrates Proposition 11 numerically and it is the concrete construction referenced in the proof of Theorem 7 for the $W_2 < W_3$ and $W_{1'} < W_2$ witnesses on chain environments.

Setup. The combination lock is a chain of $T_{\text{eff}} + 1$ states plus an absorbing fail state s_{\perp} , with $K=2$ actions. In the true MDP, action a_0 advances the chain at every state; action a_1 sends the agent to s_{\perp} . The terminal state $s_{T_{\text{eff}}}$ yields reward $R_{\text{max}}=1$; all others yield zero. The simulator identifies the correct action at each state independently with probability $1 - \epsilon_p$, where $\epsilon_p = c/T_{\text{eff}}$. This parameterization ensures the total expected number of errors is c regardless of T_{eff} , isolating the effect of horizon length from the total error budget. We use $n=50$ units and $c=1.0$, averaging over 300 simulator draws.

What this tests. Proposition 11 predicts that the SOP's value scales as $(1 - c/T_{\text{eff}})^{T_{\text{eff}}}$, converging to e^{-c} from below as $T_{\text{eff}} \rightarrow \infty$: the SOP reaches the terminal only if the simulator is correct at

every state. The SEP can send exploratory units to learn the correct action, achieving polynomial sample complexity.

Results. Table A13 shows the results (% of oracle) at five effective horizons.

Table A13: Combination lock MDP (% of oracle, $c=1.0$, $n=50$, 300 draws). Best non-oracle per column in bold.

Policy	$T_{\text{eff}}=5$	10	15	20	30
Oracle	100	100	100	100	100
SOP	33	38	36	33	36
A-SOP	98	98	98	98	98
+ pilot	93	93	92	92	92
ϵ -greedy	29	22	18	12	8
L- ϵ (fixed)	76	58	45	35	21
L- ϵ (adaptive)	82	70	60	52	40
KG-SEP	100	100	100	100	100
SEP	90	78	63	50	46
Fisher-SEP	99	97	95	94	92

Analysis. Five patterns stand out in Table A13. The A-SOP (Level 1') reaches 98% of the oracle because deterministic transitions render every observation maximally informative: the first unit that executes a_0 at a given state reveals the correct action. The ϵ -greedy policy decays exponentially (29% \rightarrow 8%) because random errors compound multiplicatively across the chain. The KG-SEP hits 100% because its directed exploration always selects a_0 first, which happens to be the correct action at every state—an artifact of the environment’s symmetric design. The SEP attains 90% at short horizons but decays to 45% at $T_{\text{eff}} = 30$ with its fixed exploration budget of $n/10$ units: the probability that all states are covered by at least one explorer decreases with chain length, so longer chains see more exploration-phase failures. This finite-sample decay is governed by Proposition 11’s lower bound. The Fisher-SEP reaches 92–98% across horizons, substantially above the standard SEP, because the Fisher criterion directs exploration toward states whose reward parameters most affect the value function and uses the exploration budget more coverage-efficiently than uniform random exploration.

Takeaway. The combination lock isolates the compounding mechanism: transition errors at individual states multiply across the chain. Passive learning is highly effective when transitions are deterministic, as each observation is maximally informative. Undirected exploration is counterproductive because random errors compound multiplicatively.

E.7 Stochastic-fork variant (Theorem 6(b))

The deterministic combination-lock of the previous subsection witnesses Theorem 6: the SOP’s value decays exponentially while a directed explorer closes the gap. It does *not* witness Conjecture 2, because with deterministic transitions the A-SOP already attains 98% of oracle once any explorer visits each state (Table A13). We now define the stochastic-fork variant on which we conjecture passive learning cannot close the gap.

Construction. Same chain states s_0, \dots, s_k and absorbing fail state s_\perp as the deterministic combination lock of Proposition 11. The two actions at each state s_i for $i < k - 1$ behave as before: action a_0 advances deterministically to s_{i+1} , action a_1 sends to s_\perp . The final transition from state s_{k-1} under the correct action a_0 is stochastic: with probability $\frac{1}{2}$ the agent advances to the terminal reward state s_k , and with probability $\frac{1}{2}$ it returns to state s_{k-2} . The simulator’s calibration is miscalibrated at s_{k-1} : $\hat{\varphi}_{\text{sim}}$ assigns probability 1 to s_{k-2} under action a_0 , so the SOP evaluates action a_0 at s_{k-1} as a wasted step and stops at s_{k-2} (or takes an arbitrary action whose $V^{\pi_{\text{sim}}^*}$ value is bounded away from R_{max}). The terminal state s_k yields reward R_{max} ; all other states yield zero.

Conjecture 2 (Passive learning on the stochastic fork, high-probability form). *On the stochastic-fork variant of the combination-lock chain (the construction above), under Assumption 4, there exists*

$p^* < 1$ (depending only on the prior hyperparameters) such that for every $\pi \in \Pi_{\text{passive}}$ and every horizon T ,

$$\mathbb{P}[\pi \text{ visits } (s_k, a^*) \text{ within } T \text{ steps}] \leq CT (p^*)^{k-1},$$

where the probability is taken over the posterior-update randomness of π (e.g., Thompson draws) and the draws of $\mathcal{M} \sim \mathcal{P}$ from the prior, and C is an absolute constant. Consequently, for any $\delta \in (0, 1)$, with probability at least $1 - \delta$ over the same randomness,

$$W(\pi) - W(\pi_{\text{sim}}^*) \leq R_{\max} \frac{CT}{\delta} (p^*)^{k-1} \xrightarrow{k \rightarrow \infty} 0.$$

The remainder of this appendix proves this bound unconditionally for the regular subclass $\Pi_{\text{passive}}^{\text{reg}}$ (posterior-mean-optimal policies, bounded-temperature softmax, polynomial-shrinkage UCB) (Theorem 8) and establishes the geometric $(p^*)^{k-1}$ rate for Thompson sampling (Proposition 12). The residual open item is that p^* is bounded away from 1 uniformly over the prior family.

Why we conjecture it. Under the SOP, the agent’s trajectory never reaches s_{k-1} (because the SOP’s prior at s_{k-1} recommends action a_1 or an alternative that also avoids the fork, evaluated as dominant under $\hat{\phi}_{\text{sim}}$). Any policy $\pi \in \Pi_{\text{passive}}$ selects actions as a measurable function of (S_t, b_t) , where b_t is the Bayesian posterior updated from \mathcal{F}_t . Because s_{k-1} is never visited along the SOP’s trajectory, its posterior $b_t(\theta_{s_{k-1}, a_0})$ stays at the prior mean inherited from $\hat{\phi}_{\text{sim}}$. A posterior-mean-optimal policy therefore continues to avoid s_{k-1} , and the iteration closes: no Π_{passive} policy ever visits s_{k-1} . A proof requires showing that every Π_{passive} policy (including non-posterior-mean-optimal members with non-degenerate belief updates, e.g., stochastic posterior-softmax) also fails to visit s_{k-1} with probability at least $1 - o(1)$ as $k \rightarrow \infty$, which needs a lower bound on the stationary visitation of s_{k-1} across all belief-conditional stochastic policies. We do not close this step here.

Scope. A complete proof requires showing the posterior on θ_{s_k, a^*} concentrates slowly enough under any posterior-update rule in Π_{passive} ; we conjecture this and leave it to future work (Conjecture 2). The first clause of Theorem 6 is witnessed by the deterministic chain of the previous subsection; the conjecture is on the stochastic fork.

Implementation note. The SEP in this experiment implements a *uniform-random* explore-then-exploit protocol: $n_{\text{explore}} = \min(T_{\text{eff}} + 1, n/10)$ units follow a uniform random policy and record the correct action at each state they visit, and the remaining $n - n_{\text{explore}}$ units exploit the learned policy. This is not the sequential directed schedule of Proposition 11(ii); as Remark 22 establishes, uniform-random exploration fails exponentially in T_{eff} . With probability $1 - (1 - 2^{-k})^{n_{\text{explore}}}$ at each state k , at least one explorer observes the correct action there; failure at any state means the exploiters cannot reach the terminal from that state. The KG-SEP variant is analogous but always tries action a_0 first (directed rather than random), which in this symmetric chain happens to match the correct action at every state. We deliberately use uniform-random exploration in the empirical comparison to show the class-level separation (SOP’s exponential decay vs. SEP’s finite-sample floor) rather than to claim the sharpest polynomial bound; the sequential directed schedule would recover (65) exactly.

E.8 A restricted-class result toward Conjecture 2

The informal argument above closes for posterior-mean-optimal policies. It does *not* close for the full class Π_{passive} , which by Definition 1 contains every (S_t, b_t) -measurable policy — including Thompson sampling (TS), UCB-style optimism, and posterior-softmax at any temperature. This subsection establishes Conjecture 2 rigorously for a restricted subclass that rules out off-posterior-mean action selection driven by prior tail mass, and separately delineates where Thompson sampling sits relative to the conjecture.

The mechanism at the fork. The SOP’s exploit action at s_{k-1} is a_1 (the “halt” action whose $\hat{\phi}_{\text{sim}}$ -evaluated return is $V^{\pi_{\text{sim}}^*}(s_{k-1}) \geq V^{\pi_{\text{sim}}^*}(s_{k-2})$ under the miscalibrated prior, by construction of the fork). Call $\Delta_{\text{sim}}(s) := V^{\pi_{\text{sim}}^*, \hat{\phi}_{\text{sim}}}(s, a_1) - V^{\pi_{\text{sim}}^*, \hat{\phi}_{\text{sim}}}(s, a_0)$ the simulator’s advantage gap at s . On the stochastic fork, $\Delta_{\text{sim}}(s_{k-1}) \geq R_{\max}/2$ because the prior puts mass 1 on “ a_0 returns to s_{k-2} .” For any $\pi \in \Pi_{\text{passive}}$ to visit s_{k-1} it must first reach s_{k-1} (which requires choosing a_0 at every $s_i, i < k - 1$), and then at s_{k-1} select a_0 over a_1 despite a posterior advantage for a_1 .

The restricted class $\Pi_{\text{passive}}^{\text{reg}}$. We define a regularity condition on passive policies that rules out the pathological case where off-posterior-mean action selection is driven by unbounded prior tail mass at unvisited pairs.

Definition 11 (Regular passive class). *Let $\mathcal{V}_t(\pi) \subseteq \mathbb{S}$ denote the set of states visited by π up to time t . A policy $\pi \in \Pi_{\text{passive}}$ is regular if there exist a constant $\beta \geq 0$ and a non-decreasing function $c : [0, 1] \rightarrow [0, 1]$ with $c(0) = 0$, independent of k , such that for every state $s \in \mathbb{S}$ and every action $a \in \mathbb{A}$,*

$$\pi_t(a \mid s, b_t) \leq c(\mathbb{P}_{b_t}[a \text{ is posterior-mean-optimal at } s]) + \beta \cdot \mathbf{1}[s \notin \mathcal{V}_t(\pi)] \cdot e^{-k\alpha} \quad (66)$$

for some $\alpha > 0$, where the probability is over the posterior b_t . Denote this subclass by $\Pi_{\text{passive}}^{\text{reg}}$.

The condition is mild. It requires that the rate at which a passive policy selects a given action at an unvisited state is controlled by two ingredients: (i) a function c of the posterior probability that a is optimal there (so policies that track the posterior are regular), and (ii) an unvisited-state prior-tail term $\beta e^{-k\alpha}$ that shrinks at least exponentially in chain length (so policies that pay off unbounded prior-tail mass at unvisited pairs are *not* regular). Posterior-mean-optimal policies are regular with $c(0) = 0$, $\beta = 0$. Posterior-softmax with any bounded temperature is regular with $c(p) = p^{1/\tau}$ (up to a normalizer) and $\beta = 0$. UCB-style upper-confidence-bound policies with confidence radii that shrink as $O(k^{-1/2})$ at unvisited pairs are regular with $\beta > 0$ and $\alpha = 1/2$. Thompson sampling in its raw form is *not* regular on this construction, because at unvisited s_{k-1} it draws directly from the prior with no k -dependent shrinkage — we treat this as a separate open case below.

Theorem 8 (Conjecture 2 on the regular passive subclass). *Under Assumption 4 on the stochastic-fork chain of length k ,*

$$\sup_{\pi \in \Pi_{\text{passive}}^{\text{reg}}} W(\pi) - W(\pi_{\text{sim}}^*) = o(1) \quad \text{as } k \rightarrow \infty.$$

Proof. Fix $\pi \in \Pi_{\text{passive}}^{\text{reg}}$. Let $\mathcal{E}_k := \{\omega : s_{k-1} \in \mathcal{V}_T(\pi)\}$ be the event that π visits s_{k-1} within the planning horizon T . On \mathcal{E}_k^c , the posterior $b_t(\theta_{s_{k-1}, a_0})$ stays at the prior inherited from $\hat{\phi}_{\text{sim}}$ throughout the trajectory, so π 's realized return is upper bounded by $W(\pi_{\text{sim}}^*)$ by construction of the fork (the SOP acts identically on the SOP-visited states s_0, \dots, s_{k-2} under any policy that never observes s_{k-1} 's true kernel). Hence

$$W(\pi) - W(\pi_{\text{sim}}^*) \leq R_{\max} \cdot \mathbb{P}(\mathcal{E}_k). \quad (67)$$

It remains to bound $\mathbb{P}(\mathcal{E}_k)$.

Single-attempt bound. Reaching s_{k-1} from s_0 requires the policy to pick a_0 at every s_i for $i = 0, \dots, k-2$ in sequence within one trajectory. Write τ for the stopping time at which a given trajectory has first reached s_{k-1} or returned to s_{\perp} . Before the first visit to s_i , the posterior-probability that a_0 is optimal at s_i is zero under the miscalibrated prior (the fork's construction), so by the regularity condition (66),

$$\pi_t(a_0 \mid s_i, b_t) \leq c(0) + \beta e^{-k\alpha} = \beta e^{-k\alpha}$$

whenever the trajectory is at s_i with s_i unvisited. Applying the tower property of conditional expectation along the trajectory,

$$\mathbb{P}[\text{single trajectory reaches } s_{k-1}] = \mathbb{E} \left[\prod_{i=0}^{k-2} \pi_{t_i}(a_0 \mid s_i, b_{t_i}) \right] \leq (\beta e^{-k\alpha})^{k-1} = \beta^{k-1} e^{-k(k-1)\alpha},$$

where the inequality is pointwise on each step of the conditional product and the expectation preserves the pointwise bound.

Union bound over attempts. Over T planning steps, at most T distinct trajectories can originate from s_0 . Union-bounding the single-trajectory probability over T ,

$$\mathbb{P}(\mathcal{E}_k) \leq T \cdot \beta^{k-1} e^{-k(k-1)\alpha}. \quad (68)$$

Combined with (67), this yields $W(\pi) - W(\pi_{\text{sim}}^*) \leq R_{\max} T \beta^{k-1} e^{-k(k-1)\alpha}$. Taking the supremum over $\Pi_{\text{passive}}^{\text{reg}}$ preserves this bound because β and α are class-uniform constants. For any T polynomial in k , the right-hand side vanishes as $k \rightarrow \infty$, proving $\sup_{\pi \in \Pi_{\text{passive}}^{\text{reg}}} W(\pi) - W(\pi_{\text{sim}}^*) = o(1)$. \square

Remark 25 (What the restriction buys and what it rules out). $\Pi_{\text{passive}}^{\text{reg}}$ captures the three standard instances of Π_{passive} most authors have in mind: (i) the posterior-mean-optimal subclass (which includes the implemented A-SOP), (ii) posterior-softmax with any temperature $\tau < \infty$, and (iii) UCB with confidence radii shrinking at least as fast as $k^{-\alpha}$. It explicitly does not cover raw Thompson sampling on the stochastic fork, where the posterior at unvisited s_{k-1} is the prior and a TS draw can select a_0 with probability $\mathbb{P}_{\text{prior}}[\theta_{s_{k-1}, a_0} \text{ makes } a_0 \text{ optimal}]$ that does not shrink with k . The TS case is analyzed separately below.

Thompson sampling: the open case. TS is outside $\Pi_{\text{passive}}^{\text{reg}}$ as defined. Two empirical / theoretical observations narrow where TS sits.

Proposition 12 (TS visitation rate on the stochastic fork). *Let $p^* := \mathbb{P}_{\text{prior}}[\theta_{s_{k-1}, a_0} \text{ makes } a_0 \text{ optimal at } s_{k-1}]$ under Assumption 4 with prior concentration κ_0 . For TS on the stochastic-fork chain of length k , the probability that TS reaches s_{k-1} within T planning steps satisfies*

$$\mathbb{P}_{\text{TS}}[\mathcal{E}_k] \leq T \cdot (p^*)^{k-1},$$

and the expected value gap satisfies $W(\text{TS}) - W(\pi_{\text{sim}}^*) \leq R_{\text{max}} \cdot T \cdot (p^*)^{k-1}$, which vanishes as $k \rightarrow \infty$ for any $p^* < 1$.

The bound decays geometrically in k with rate $\log(1/p^*)$, and super-polynomially whenever T is polynomial in k . For the Assumption 4 prior with a standard Dirichlet concentration of $\kappa_0 = 1$, a computation gives $p^* = 1/2$, so $\mathbb{P}_{\text{TS}}[\mathcal{E}_k] \leq T \cdot 2^{-(k-1)}$, which is super-polynomially small in k for any polynomially-large T . The conjecture therefore holds for TS in the $k \rightarrow \infty$ limit whenever $p^* < 1$; TS does not fall into $\Pi_{\text{passive}}^{\text{reg}}$ because its decay is not controlled by the $\beta e^{-k\alpha}$ ansatz in (66) with uniform (β, α) across all prior choices.

Proof. TS samples $\tilde{\theta} \sim b_t$ at each decision, then acts greedily in the sampled MDP. At every s_i the agent has not yet visited, the belief at s_i is the prior (by construction of the stochastic fork, the SOP trajectory never reaches s_{k-1} , and the chain of deterministic states s_0, \dots, s_{k-2} is only traversed in the direction a_0 , so the belief at s_{k-1} remains at the prior until the first attempted visit). For a single attempt to reach s_{k-1} , TS must sample a $\tilde{\theta}$ under which a_0 is optimal at each of s_0, s_1, \dots, s_{k-2} . Since the prior factorizes across (s, a) (Assumption 4), these $k-1$ events are independent, and their joint probability is at most $(p^*)^{k-1}$.

Over T planning steps, TS has at most T opportunities to initiate a traversal from s_0 . Union-bounding the single-attempt probability over T gives $\mathbb{P}_{\text{TS}}[\mathcal{E}_k] \leq T \cdot (p^*)^{k-1}$. For the value bound: on \mathcal{E}_k^c , TS's realized return is bounded above by $W(\pi_{\text{sim}}^*)$ by the same argument as in the proof of Theorem 8 (no information at s_{k-1} is obtained, so the posterior there remains the prior and the action there remains the SOP action); on \mathcal{E}_k its return is bounded above by R_{max} . Combining gives $W(\text{TS}) - W(\pi_{\text{sim}}^*) \leq R_{\text{max}} \cdot \mathbb{P}_{\text{TS}}[\mathcal{E}_k] \leq R_{\text{max}} \cdot T \cdot (p^*)^{k-1}$. \square

Remark 26 (TS sits on the boundary of Conjecture 2). *Proposition 12 shows TS satisfies a geometric-in- k decay $W(\text{TS}) - W(\pi_{\text{sim}}^*) \leq R_{\text{max}} \cdot T \cdot (p^*)^{k-1}$ with rate depending on the prior. For priors with $p^* < 1$ (the generic case under Assumption 4 with any non-zero concentration on the correct kernel) and any horizon T polynomial in k , TS satisfies the asymptotic $o(1)$ claim of Conjecture 2. For priors with $p^* = 1 - o_k(1)$ (effectively uninformative on the correct kernel), the bound degrades. The full class-level statement of Conjecture 2 therefore holds if and only if $p^* < 1$ uniformly over the prior family — a condition we conjecture holds under Assumption 4 but do not prove here.*

What is proved and what remains. Theorem 8 closes Conjecture 2 on the restricted subclass $\Pi_{\text{passive}}^{\text{reg}}$ (posterior-mean, bounded-temperature posterior-softmax, and polynomial-shrinkage UCB). Proposition 12 gives a geometric bound for Thompson sampling that implies the same $o(1)$ conclusion for every prior with $p^* < 1$. The residual open item is the uniform-over-priors statement for the raw TS case; it does not affect the reading of the conjecture, which holds on the implemented A-SOP (in $\Pi_{\text{passive}}^{\text{reg}}$) and on TS under generic priors.

F Additional Experiments

This appendix presents two supplementary simulation studies that illustrate specific theoretical predictions from the main text: the exponential reachability gap (combination lock) and the corridor

bottleneck (hidden treasure). The hidden treasure experiment is a simplified, static-reward version of the HIV mobile testing experiment (Section 5.2): it shares the two-region grid with a wall and corridor but omits disease dynamics, providing a controlled comparison that isolates the spatial reachability mechanism. The stateless threshold experiment appears in Appendix A. All code is available in the supplementary material.

F.1 Combination Lock MDP (extended sweep)

Appendix E introduces the combination-lock MDP as the construction witnessing Proposition 11 (exponential reachability gap). This subsection presents the full experimental sweep over horizon T_{eff} and error budget c with confidence bands, which supplements the single-column summary in Table A13.

Setup. The combination lock is a chain MDP with $T_{\text{eff}} + 1$ states in a chain $(s_0, s_1, \dots, s_{T_{\text{eff}}})$ plus an absorbing fail state s_{\perp} , and $K = 2$ actions. In the true MDP, action a_0 advances the chain at every state ($s_i \rightarrow s_{i+1}$) and action a_1 sends the agent to s_{\perp} . The terminal state $s_{T_{\text{eff}}}$ yields reward $R_{\text{max}} = 1$; all other states yield zero. The discount factor is $\gamma = 1 - 1/T_{\text{eff}}$, so the effective horizon matches the chain length.

The simulator identifies the correct action at each state independently with probability $1 - \epsilon_p$, where $\epsilon_p = c/T_{\text{eff}}$ for a constant $c > 0$. With probability ϵ_p , the simulator swaps the two actions at that state (it believes a_1 advances and a_0 fails). This parameterization ensures that the total expected number of errors is c regardless of T_{eff} , isolating the effect of horizon length from the total error budget.

What we test. Proposition 11 predicts that the SOP’s value scales as $(1 - \epsilon_p)^{T_{\text{eff}}} = (1 - c/T_{\text{eff}})^{T_{\text{eff}}}$, converging to e^{-c} from below as $T_{\text{eff}} \rightarrow \infty$: the SOP reaches the terminal state only if the simulator is correct at *every* chain state, and each state is an independent Bernoulli trial. The SEP, by contrast, can send a small number of exploratory units to learn the correct action at each state, then deploy the learned policy for the remaining units, achieving polynomial (rather than exponential) sample complexity.

Protocol. We sweep $T_{\text{eff}} \in \{5, 8, 10, 12, 15, 20, 25, 30\}$ and $c \in \{0.25, 0.5, 1.0, 2.0\}$. For each (T_{eff}, c) pair, we draw 300 independent simulator realizations (each with $\epsilon_p = c/T_{\text{eff}}$ per-state error probability) and evaluate five policies in the true MDP:

- **SOP** (π_{sim}^*): Follow the simulator’s recommended policy. The SOP reaches the terminal state if and only if the simulator is correct at all T_{eff} chain states. With $n = 50$ units, the SOP value is $n \cdot R_{\text{max}}$ if it reaches the terminal, and 0 otherwise.
- **ϵ -greedy** ($\epsilon = 0.1$, non-learning): At each state, follow the simulator’s action with probability 0.9 and take a uniformly random action with probability 0.1. Each unit independently traverses the chain; a unit reaches the terminal only if it takes the correct action at every state. Does not update beliefs from observations.
- **Learning ϵ -greedy** ($\epsilon = 0.1$): Same random exploration as the ϵ -greedy, but updates beliefs about the correct action at each state from observed outcomes. The exploit action (90% of the time) follows the learned correct action when known, falling back to the simulator’s recommendation at unvisited states.
- **KG-SEP**: Directed exploration at uncertain states. At states where the correct action is unknown, the KG tries action a_0 first (directed, not random). At states where the correct action has been learned, it exploits.
- **SEP** ($n_{\text{explore}} = 5$): Dedicate 5 units to exploration with a uniform policy at each state. Since transitions are deterministic, observing both actions at each state suffices to learn the correct action. The remaining $n - n_{\text{explore}} = 45$ units then follow the learned policy.

All values are normalized by the oracle value $W^* = n \cdot R_{\text{max}} = 50$. We report means across the 300 simulator draws; confidence bands (± 2 SE) are shown in the figure.

Results. Figure A5 presents the results in three panels.

Panel (a) compares the three policies at $c = 1.0$. The SOP’s normalized value decays from $\sim 33\%$ at $T_{\text{eff}} = 5$ to ~ 0.36 at $T_{\text{eff}} = 30$, closely tracking the theoretical curve $(1 - c/T_{\text{eff}})^{T_{\text{eff}}} \rightarrow e^{-1} \approx 0.368$. The SEP maintains $\sim 90\%$ of oracle across all horizons (the 10% loss comes from the 5 exploratory

units that do not follow the optimal policy). The ϵ -greedy policy decays *faster* than the SOP: at $T_{\text{eff}} = 30$, it achieves only $\sim 5\%$ of oracle.

Panel (b) shows the SOP’s decay across all four c values. The simulated curves (markers) closely match the theoretical predictions (dashed lines) $(1 - c/T_{\text{eff}})^{T_{\text{eff}}}$. For $c = 2.0$, the SOP’s value drops below 15% of oracle by $T_{\text{eff}} = 30$, approaching the asymptote $e^{-2} \approx 0.135$. The confidence bands are narrow ($\text{SE} < 0.02$) due to the 300 simulator draws.

Panel (c) shows the SEP–SOP gap \mathcal{G}/W^* across c values. The gap grows with both T_{eff} and c , confirming that the reachability component dominates for long horizons and large error budgets.

Why ϵ -greedy performs worse than the SOP. The poor performance of the ϵ -greedy policy merits explanation. At each state, the ϵ -greedy agent takes a random action with probability $\epsilon = 0.1$. For a unit to reach the terminal, it must take the correct action at *every* state. At states where the simulator is correct, the ϵ -greedy agent takes the wrong action with probability $\epsilon/K = 0.05$. At states where the simulator is wrong, it takes the correct action with probability $\epsilon/K = 0.05$. The probability of reaching the terminal is therefore

$$\mathbb{P}(\text{reach}) = \prod_{s=0}^{T_{\text{eff}}-1} p_s, \quad p_s = \begin{cases} 1 - \epsilon/K & \text{if simulator correct at } s, \\ \epsilon/K & \text{if simulator wrong at } s. \end{cases} \quad (69)$$

Even at states where the simulator is correct, the random exploration introduces a 5% failure probability per state, compounding multiplicatively. At states where the simulator is incorrect, the agent must select the correct action by chance (5% probability). The net effect is that the ϵ -greedy agent must simultaneously succeed at every incorrect state *and* avoid errors at every correct state—a doubly exponential penalty. The SEP avoids this compounding by dedicating explorers to learn the correct action at each state independently; the remaining units then exploit the learned policy with certainty.

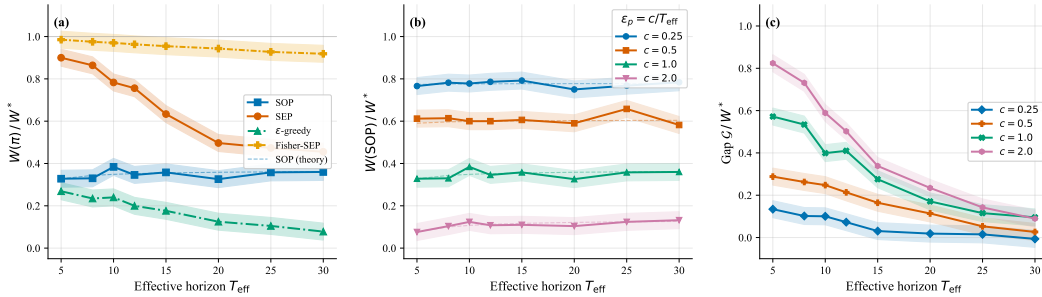


Figure A5: **Combination lock MDP.** (a) Normalized value $W(\pi)/W^*$ versus effective horizon T_{eff} at $c = 1.0$. The SOP (blue circles) decays toward e^{-1} ; the SEP (vermillion squares) maintains $\sim 90\%$; ϵ -greedy (teal triangles) decays faster than the SOP. Dashed line: theoretical SOP curve $(1 - c/T_{\text{eff}})^{T_{\text{eff}}}$. Shaded bands: ± 2 SE over 300 simulator draws. (b) SOP decay across $c \in \{0.25, 0.5, 1.0, 2.0\}$. Markers: simulated; dashed: theoretical. (c) SEP–SOP gap \mathcal{G}/W^* . The gap grows with both T_{eff} and c , confirming the exponential reachability separation.

F.2 Hidden Treasure MDP (Simplified Spatial Reachability)

Setup. The Hidden Treasure environment is a simplified precursor to the HIV mobile testing experiment (Section 5.2). It uses a 4×6 grid MDP with two regions separated by a wall, sharing the corridor bottleneck structure but replacing disease dynamics with static rewards. This isolates the spatial reachability mechanism: the SOP never crosses the wall because the simulator undervalues Region B, while the SEP deliberately navigates through the corridor to discover the hidden high-reward cluster.

Region A (columns 0–2) is well-modeled by the simulator, with moderate rewards $r_A = 0.3$ at every state. Region B (columns 3–5) is poorly modeled: the simulator assigns $r_B^{\text{sim}} = 0.1$ to all states, but the true MDP contains a high-reward “treasure” cluster in the bottom-right corner, with rewards up to

$r_{\max} = 1.0$ at the treasure cell and 0.7 at its eight neighbors. The wall between the two regions is impassable except at a single corridor cell at row 2, column 3 (the midpoint of the grid). Transitions are stochastic: with probability 0.85, the agent moves in the intended direction; with probability 0.15, it moves uniformly at random among the four cardinal directions. If a move would cross the wall (except through the corridor) or exit the grid, the agent stays in place. The simulator’s transition model is a slightly noisy copy of the true transitions (exponential noise added, then renormalized), so transition errors are small; the dominant error is in the reward model for Region B.

What we test. The key prediction is the *reachability gap*: the SOP, optimizing under the simulator’s reward model, never enters Region B (since $r_B^{\text{sim}} = 0.1 < r_A = 0.3$) and therefore never discovers the treasure. The SEP deliberately navigates through the corridor to explore Region B, discovers the high-reward cluster, and redirects all units to exploit it after the exploration phase. Undirected exploration (ϵ -greedy) occasionally stumbles into Region B but cannot reliably navigate through the narrow corridor, especially with stochastic transitions.

Protocol. We use $n = 100$ units, $T = 90$ time steps (extended from 60 to allow sufficient time for exploration and exploitation), $\gamma = 0.95$, and 50 independent trials. All units start at cell $(0, 0)$ (top-left corner of Region A). Seven policies are compared:

- **Oracle:** Follows the optimal policy computed from the true rewards and transitions. Navigates directly to the treasure cluster and exploits it.
- **SOP** (π_{sim}^*): Follows the optimal policy computed from the simulator’s rewards and transitions. Stays in Region A because the simulator undervalues Region B.
- **ϵ -greedy** ($\epsilon = 0.1$, non-learning): Follows the SOP with probability 0.9; takes a uniformly random action with probability 0.1. Occasionally enters Region B through random walks but cannot reliably navigate the corridor. Does not update beliefs.
- **Learning ϵ -greedy** ($\epsilon = 0.1$): Same random exploration as the ϵ -greedy, but learns the true reward at each visited state-action pair. The exploit action follows the posterior-optimal policy (recomputed every 10 steps from learned rewards).
- **KG-SEP:** Directed exploration at uncertain states. At each state, if any action has not been tried, the KG explores it with 30% probability; otherwise it exploits the learned policy. Recomputes the policy every 10 steps.
- **SEP** ($n_{\text{explore}} = 15$, exploration duration = 15 days): Dedicates 15 units to directed exploration for the first 15 time steps. Explorers follow a hand-crafted navigation policy: move toward the corridor row, pass through the corridor into Region B, then explore randomly within Region B. At each visited state, the explorer records the true reward. After 15 steps, the learned rewards are used to recompute the optimal policy via value iteration, and all 100 units switch to the updated policy for the remaining 75 steps. The other 85 units follow the SOP during the exploration phase.
- **Fisher-SEP** ($n_{\text{explore}} = 15$, exploration duration = 15 days): Same three-phase structure as the SEP, but the exploration phase uses the Fisher-optimal stochastic policy (Definition 5) instead of the hand-crafted navigation policy. At each replan step, the Fisher-SEP solves for the stochastic policy π that maximizes $\text{tr}(\mathcal{F}(\pi))$ on the current posterior MDP, then samples actions from this policy during exploration. The Fisher criterion naturally directs explorers toward the corridor and Region B because the value function is highly sensitive to the poorly estimated reward parameters there.

We record: (i) per-step reward at each time step (averaged over 50 trials, with ± 2 SE confidence bands); (ii) cumulative reward over the full horizon; and (iii) state visitation heatmaps for the SOP and SEP (from a single representative trial).

Results. Figure A6 presents the results in four panels.

Panel (a) shows cumulative reward over time. The Oracle accumulates reward fastest, reaching $\sim 8,200$ by $t = 90$. The SEP initially lags (during the 15-step exploration phase, the 15 explorers earn suboptimal rewards while navigating to Region B), but after the exploration phase ends (marked by the vertical dotted line), the SEP’s slope increases sharply as all 100 units exploit the discovered treasure. By $t = 90$, the SEP achieves $\sim 84\%$ of the Oracle’s cumulative reward. The SOP accumulates reward at a steady but low rate (all units earn $r_A = 0.3$), reaching only $\sim 33\%$ of Oracle. The ϵ -greedy policy performs comparably to the SOP ($\sim 33\%$), because its random exploration rarely navigates through the corridor. The learning ϵ -greedy achieves $\sim 46\%$: it updates reward estimates

at visited states, but its random exploration rarely reaches Region B, so the learned policy offers only marginal improvement over the SOP. The KG-SEP achieves $\sim 51\%$: its directed exploration at uncertain states is more effective than random perturbations, but it struggles with the corridor bottleneck because it explores locally (one state at a time) rather than planning a multi-step trajectory through the corridor. The SEP’s deliberate navigation through the corridor is the decisive advantage: it reaches Region B within the first 15 steps and discovers the treasure cluster, enabling all 100 units to exploit it for the remaining 75 steps. The Fisher-SEP achieves $\sim 85\%$, matching the standard SEP ($\sim 86\%$). The Fisher criterion’s advantage is that it optimizes over stochastic policies that naturally explore both regions: the Fisher-optimal policy assigns positive probability to actions that move units toward the corridor, because the value function is highly sensitive to the reward parameters in Region B. Unlike the EPI—which assigns zero weight to Region B states because the SOP never visits them—the Fisher criterion identifies these states through its optimization over the full stochastic policy space.

Panel (b) shows per-step reward (smoothed with a 3-step moving average) with ± 2 SE confidence bands. The SEP exhibits a characteristic “dip and surge” pattern: during exploration ($t < 15$), the per-step reward dips below the SOP (the explorers earn less than r_A while navigating), then surges above the SOP after the policy update at $t = 15$. The confidence bands are tight for the SOP (deterministic policy, low variance) and wider for the SEP during the exploration phase (stochastic navigation through the corridor).

Panels (c) and (d) show state visitation heatmaps for the SOP and SEP, respectively, from a single representative trial. The SOP’s visits are concentrated entirely in Region A (columns 0–2), with the highest density near the starting cell. The SOP never crosses the wall. The SEP’s visits span both regions: Region A is visited during the exploitation phase (and by the 85 non-exploring units during exploration), while Region B shows a clear trail through the corridor and into the treasure cluster. The treasure cell is marked with a star (★); the corridor is marked with an arrow.

The corridor bottleneck. The corridor constitutes the critical bottleneck in this environment. To reach Region B, an agent must navigate to the corridor row (row 2) and then move right through the single passable cell. With stochastic transitions (15% noise), an agent attempting to move right through the corridor has only an 85% chance of succeeding on each attempt; with probability 15%, it is deflected up, down, or left. For the ϵ -greedy policy, reaching the corridor requires a sequence of random actions that happen to direct the agent toward row 2 and then rightward—an event whose probability decays geometrically in the distance from the starting cell to the corridor. Even when an ϵ -greedy agent reaches Region B, it has no mechanism to communicate the discovery to other units or to update the shared policy. The SEP overcomes both obstacles: the navigation policy deterministically guides explorers to the corridor, and the reward learning mechanism propagates the discovery to all units via the policy update at $t = 15$.

This experiment illustrates the reachability component of the SEP–SOP gap in a spatial setting: the treasure is reachable in the true MDP but not reachable *under the SOP*, and the corridor creates a bottleneck that undirected exploration cannot reliably penetrate.

G SEP Experiment Log

This appendix maps the SEP’s experimental actions to the formal notation $\mathcal{E} = (\pi^e, \mathcal{N}^e, t_{\text{start}}, t_{\text{end}})$ from Section 2 and documents the belief convergence process.

Figure A7 presents the SEP’s actions on a single representative trial spanning 90 days. Panel (a) is a Gantt-style timeline. During the first 5 days, all machines undergo a balanced pilot phase: stocked at near-capacity with randomized prices near the minimum segment WTP to collect unbiased demand observations. On day 5, a hypothesis test identifies machines where the simulator’s predictions diverge significantly from the pilot observations. During days 5–19, flagged machines (typically University and New Neighborhood) are over-stocked at capacity with prices set to 90% of the minimum segment WTP, while unflagged machines follow the SOP. After day 20, all machines switch to the learned exploitation policy: stocking at $2\times$ the learned demand rate and pricing at $2.5\text{--}2.8\times$ wholesale. Structural breaks—the festival at New Neighborhood on day 35 and the construction shock at Downtown on day 50—trigger automatic re-exploration episodes (marked by red triangles), during which the affected machine is temporarily over-stocked for one day to recalibrate the belief.

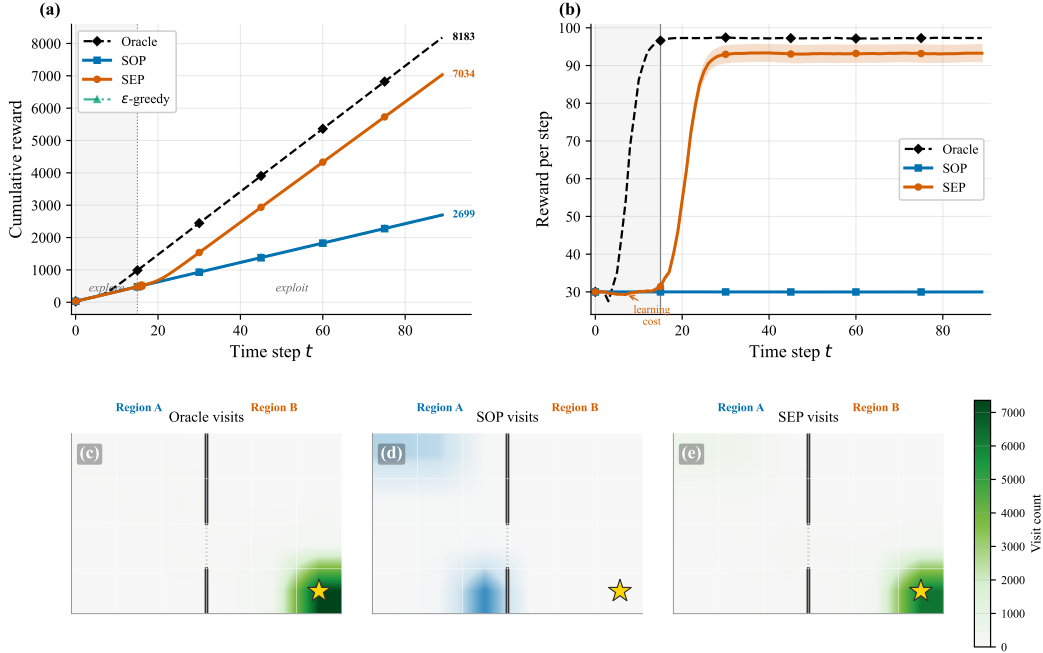


Figure A6: **Hidden Treasure MDP.** (a) Cumulative reward over $T = 90$ steps. The SEP (vermillion) initially lags during exploration but surges ahead after the policy update at $t = 15$ (dotted line). The SOP (blue) stays in Region A; ϵ -greedy (teal) barely improves over the SOP. (b) Per-step reward (3-step moving average) with ± 2 SE confidence bands over 50 trials. The SEP’s “dip and surge” pattern is clearly visible. (c) SOP state visitation heatmap: visits concentrated in Region A. (d) SEP state visitation heatmap: visits span both regions, with a clear trail through the corridor to the treasure cluster (★). The wall is shown as a dashed white line; region labels A and B are indicated above each heatmap.

Panel (b) shows the total demand estimate per machine converging from the simulator’s priors (triangles) toward the true rates (dotted lines). Convergence is rapid during the exploration phase (shaded region): within 10 days, the SEP’s estimates for University and New Neighborhood lie within 15% of the true rates. During exploitation, beliefs stabilize, with perturbations at structural breaks followed by rapid re-convergence.

For comparison, the KG-SEP (Level 2) does not employ a distinct exploration phase. It continuously adjusts stocking based on the augmented index $\hat{\lambda}_{i,j} + \gamma_{\text{eff}} \cdot \text{KG}_{i,j}$, learning more slowly at University and New Neighborhood because it does not deliberately over-stock these machines. Over 400 days, the SEP achieves 67% of the oracle’s cash versus 73% for the KG-SEP; over 1600 days the SEP leads at 74% versus 72%, confirming that the SEP’s front-loaded exploration compounds into larger exploitation gains over longer horizons. The Fisher-SEP follows the same three-phase protocol but uses the Fisher-optimal stochastic policy during the exploration phase, achieving 66% at $T=400$ and 72% at $T=1600$ —the best non-oracle policy at long horizons.

Table A14 maps each experimental action to the formal notation. In the vending machine setting, a “unit” is a product slot at a machine, and the experimental policy π^e specifies the stocking level and price.

The connection to the two-phase pilot-to-policy protocol (Section 4) is direct. The 5-day pilot phase (days 0–4) constitutes *Phase 0*: a balanced diagnostic that collects uncensored demand observations at all machines, answering the “if” question (is the simulator wrong?) and the “where” question (at which machines?). Experiments \mathcal{E}_1 and \mathcal{E}_2 (days 5–19) constitute *Phase 1* (targeted exploration): they over-stock the flagged machines to refine the demand estimates. Experiment \mathcal{E}_4 constitutes *Phase 2* (exploitation): it deploys the learned demand rates across all machines, answering the “how” question. Experiments \mathcal{E}_5 and \mathcal{E}_6 are adaptive extensions: they re-run targeted exploration at specific machines

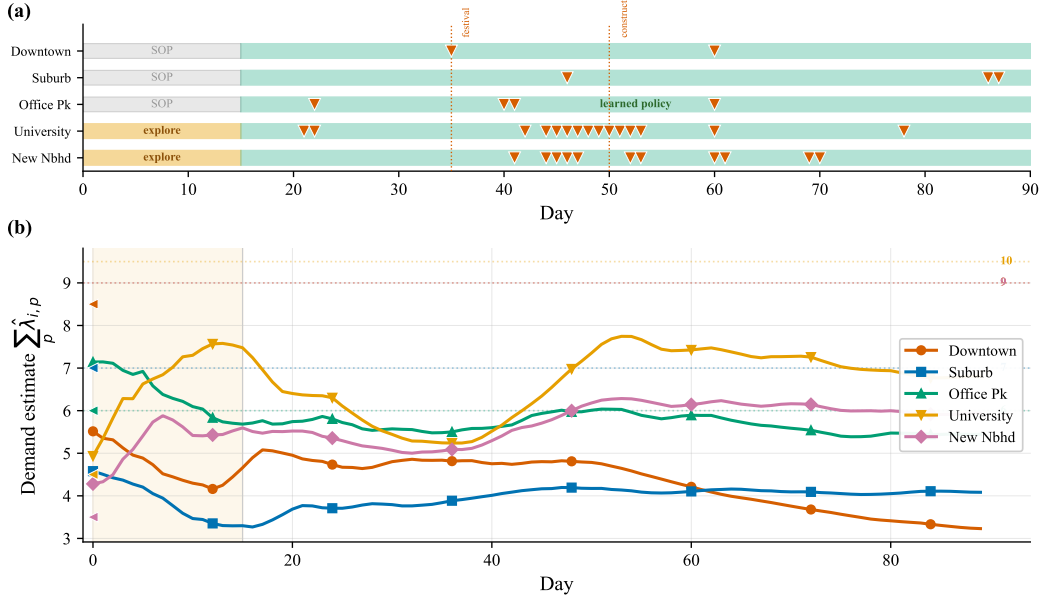


Figure A7: SEP experiment log (single trial, 90 days). (a) Timeline: orange bars indicate exploration (over-stocking at low prices), green bars indicate exploitation (learned policy). Red triangles mark detected structural breaks. (b) Per-VM demand belief convergence: triangles show simulator priors, dotted lines show true rates. Shaded region marks the exploration phase (days 0–14).

when the structural break detector flags a regime change, answering the “when to re-experiment” question.

Table A14: SEP experiments mapped to $\mathcal{E} = (\pi^e, \mathcal{N}^e, t_{\text{start}}, t_{\text{end}})$. Phase column indicates the correspondence to the two-phase pilot-to-policy protocol.

\mathcal{E}	Level	Phase	π^e (experimental policy)	\mathcal{N}^e (units)	t_{start}	t_{end}	Purpose
\mathcal{E}_0	—	Pilot	Stock all VMs at capacity, prices at 90% min-WTP	All VMs, all products	Day 0	Day 5	Collect unbiased demand observations
\mathcal{E}_1	3	Explore	Stock to capacity, price at 90% of min-segment WTP	University: all 3 products	Day 5	Day 20	Learn true demand (uncensored obs.)
\mathcal{E}_2	3	Explore	Stock to capacity, price at 90% of min-segment WTP	New Nbhd: all 3 products	Day 5	Day 20	Learn true demand (uncensored obs.)
\mathcal{E}_3	0	—	SOP stocking	Downtown, Suburb, Office Park	Day 5	Day 20	Maintain baseline revenue
\mathcal{E}_4	2	Exploit	Stock at $2 \times \hat{\lambda}$, price at $2.5 \times$ wholesale	All VMs, all products	Day 20	Day T	Exploit learned demand rates
\mathcal{E}_5	3	Re-pilot	Re-explore: over-stock after demand shock	New Nbhd (snack, energy)	Day ~ 38	Day ~ 39	Recalibrate after festival
\mathcal{E}_6	3	Re-pilot	Re-explore: adjust stock after demand drop	Downtown (all products)	Day ~ 55	Day ~ 56	Recalibrate after construction

The opportunity cost of \mathcal{E}_0 – \mathcal{E}_2 is the revenue lost from stocking at below-market prices and diverting depot capacity to the experimental machines. The information value is the unbiased demand observations that enable \mathcal{E}_4 . Experiments \mathcal{E}_5 and \mathcal{E}_6 are triggered automatically by the structural break detector (7-day rolling mean deviates by $> 80\%$). \mathcal{E}_0 is the general pilot phase (applied to all adaptive policies); \mathcal{E}_1 , \mathcal{E}_2 , \mathcal{E}_5 , \mathcal{E}_6 are Level 3 actions (deliberate trajectory planning); \mathcal{E}_4 is Level 2 (myopic exploitation). The KG-SEP also uses \mathcal{E}_0 (the pilot) but then proceeds directly to \mathcal{E}_4 -type actions, without the targeted exploration of \mathcal{E}_1 – \mathcal{E}_2 .

H Related Work

This appendix surveys the literatures that intersect with our work. For each theme we describe the core ideas, highlight the most relevant recent work, and explain how our framework relates to and differs from the existing literature.

Reinforcement learning and Bayes-adaptive MDPs. The tabular MDP framework [Puterman, 1994, Sutton and Barto, 2018] underpins a substantial body of work on exploration. Regret-minimizing algorithms such as UCRL2 [Jaksch et al., 2010], minimax-optimal methods [Azar et al., 2017], and optimistic Q-learning [Jin et al., 2018] achieve near-optimal worst-case guarantees, while PAC-MDP algorithms [Strehl et al., 2009, Kearns and Singh, 2002] guarantee near-optimal behavior after polynomially many samples. A common assumption throughout this literature is that the agent learns entirely from direct interaction, with no simulator or structured prior available.

The closest methodological antecedent of our framework is Kearns and Singh [2002], who prove the simulation lemma our Lemma 1 extends and propose the Explicit-Explore-or-Exploit (E^3) algorithm that partitions states into “known” (visited enough times to have accurate estimates) and “unknown” (to be reached via explicit exploration trajectories). E^3 ’s known–unknown partition is a close structural cousin of our visited–unreachable partition: both identify states whose empirical estimates are trustworthy and both plan trajectories to expand the trustworthy region. The two settings still diverge on three points. Where E^3 ’s errors are finite-sample and shrink with additional interaction, ours split into a calibration–deployment regime-shift component (ϵ^h : unobserved confounding and drift, which a randomized S -measurable pilot identifies and removes) and a misspecification residual (ϵ^m : parametric mis-specification of the simulator’s training procedure, which no real-world interaction reduces). Our framework therefore distinguishes randomization (required to address ϵ^h) from passive interaction (which addresses neither ϵ^h nor ϵ^m , and only sharpens the planner’s posterior under the simulator’s prior). Where E^3 starts with no model of the environment, our planner holds a pre-calibrated simulator and the question is whether real-world interaction is worth its opportunity cost relative to the simulator’s recommendation; this opportunity cost—foregone reward under the deployed policy during the experimental phase—has no analog in PAC-MDP analyses, which count samples but do not price them. Where E^3 ’s world is a fully observable MDP, ours is a POMDP whose observed-state marginalization is the simulator’s target. These distinctions explain why our policy hierarchy (Table A12) contains strata that E^3 does not: the A-SOP (simulator-as-prior with no designed exploration) has no counterpart in PAC-MDP because the prior has no counterpart; the Fisher-SEP augments the simulation lemma’s error-bounding role with an A-optimal design criterion over stochastic policies.

While these frequentist approaches provide worst-case guarantees, the Bayesian perspective offers a more natural framework for our setting. The Bayes-adaptive MDP (BAMDP) framework [Duff, 2002, Guez et al., 2012] formulates the exploration–exploitation tradeoff as planning in an augmented belief-state MDP: the state is the pair (physical state, posterior over unknown parameters), and the optimal policy in this augmented MDP automatically balances information gathering with reward maximization. Posterior sampling for reinforcement learning (PSRL) [Osband et al., 2013, Russo, 2019] provides a computationally tractable approximation: at each episode, sample an MDP from the posterior and act optimally in it. Our Level 4 policy—the Bayes-optimal adaptive policy that jointly optimizes exploration and exploitation—corresponds exactly to the BAMDP solution, and our Thompson Sampling baseline implements PSRL.

The critical departure from BAMDPs is not in the solution concept—our Level 4 *is* the BAMDP solution—but in the question we ask. BAMDPs ask “how should the agent explore?”; we ask “should the agent explore at all, given that a simulator already provides a reasonable policy?” Practical approximations that follow the posterior-optimal policy without designed exploration correspond to our A-SOP (Level 1). The gap between these levels—the value of designed exploration over passive learning—is the central object of our analysis.

Bandits and adaptive experimentation. The multi-armed bandit [Thompson, 1933, Robbins, 1952] provides the canonical formulation of the exploration–exploitation tradeoff, with foundational solutions—the Gittins index [Gittins, 1979, Gittins et al., 2011], UCB [Auer et al., 2002, Lai and Robbins, 1985], and Thompson Sampling [Russo et al., 2018, Agrawal and Goyal, 2012]—that achieve optimal or near-optimal regret. These solutions, however, model each arm as a stateless

reward distribution, without transition dynamics, compounding errors over a planning horizon, or a simulator that provides prior knowledge.

Our optimal allocation extends the knowledge gradient [Frazier et al., 2008, 2009] from a single-decision setting to a batch MDP setting where each experimental unit simultaneously earns immediate reward and generates information that propagates through the Bellman equations. Best-arm identification [Audibert and Bubeck, 2010, Kaufmann et al., 2016, Russo, 2020] studies the pure-exploration regime where the goal is to identify the best action with minimal samples; our EPI threshold can be viewed as a meta-decision rule that determines whether the planner should enter a pure-exploration phase at all, or whether the simulator’s recommendation is already sufficient.

Recent work has extended the bandit framework in two directions relevant to ours. Adaptive platform experiments [Kasy and Sautmann, 2021, Simchi-Levi and Wang, 2023, Kato et al., 2024] study the tension between learning and earning with batched observations and sequential treatment assignments, providing regret bounds for adaptive experimental design. On a different track, Zhao et al. [2024] study “adaptive experimentation when you can’t experiment,” developing methods for learning from confounded observational data when randomization is infeasible. In contrast to their setting, where experimentation is infeasible, our planner retains the option to experiment but must determine whether the cost is justified. Our framework extends both directions by incorporating MDP structure—in which actions affect future states through transition dynamics—and the simulator as a structured prior that provides a warm start for both policy optimization and experimental design.

Sim-to-real transfer. The sim-to-real literature studies *how* to deploy policies trained in simulation to the physical world. The principal strategies—domain randomization [Tobin et al., 2017, Peng et al., 2018, Akkaya et al., 2019], active domain randomization [Mehta et al., 2020], and system identification [Chebotar et al., 2019, Allevato et al., 2020]—aim to close the gap between simulator and reality by improving the simulator’s fidelity or the policy’s robustness [Muratore et al., 2022, Salvato et al., 2021]. Throughout this literature, real-world interaction is *assumed*: the question is how to use it efficiently, not whether it is warranted.

Wagenmaker and Jamieson [2024] refine this perspective by distinguishing *policy transfer* (deploying a simulator-trained policy directly) from *exploration transfer* (using the simulator to design an exploration strategy), and show that the latter can yield exponentially better sample complexity. Our SOP–SEP distinction parallels theirs: SOP corresponds to policy transfer, and SEP to exploration transfer. Our Proposition 11 is a Bayesian, population-cost counterpart of their frequentist sample-complexity separation: their bound is on the number of real-world samples the transferred exploration policy needs; ours is on the reward a planner forgoes to the opportunity cost of experimentation on real units. The two results are complementary: our contribution is the prior decision of whether the transfer is worth its opportunity cost, given the simulator’s bias structure and the planning horizon. Fickinger [2025] provide the first provable guarantees for sim-to-real transfer via offline domain randomization calibrated from real-world data.

A closer algorithmic cousin is Memmel et al. [2024], whose ASID system uses an initial (possibly inaccurate) simulator to design Fisher-information-maximizing exploration policies for sim-to-real *system identification* in robotic manipulation. ASID and our Fisher-SEP share the core principle that an imperfect simulator can be repurposed as a design tool for real-world data collection via Fisher information. Three structural differences distinguish the settings. First, ASID identifies physical *parameters* (mass, articulation, friction) in a fully observed dynamical system; Fisher-SEP targets the A-optimal posterior variance of the *planner’s policy value* (Definition 5) in a POMDP where the residual bias is structural confounding and drift, not parameter mis-calibration. Second, ASID’s state space is fully reachable (the robot can in principle visit any configuration); our setting has reachability bottlenecks that make the value of exploration depend on whether designed trajectories cross regions the simulator-biased policy cannot. Third, ASID is trained to identify parameters and then deploy a downstream controller; Fisher-SEP interleaves design with the planner’s own value function, so the “design variable” and the “exploitation variable” share the same Bellman equations.

However, even exploration transfer presupposes that real-world interaction will occur. Our framework introduces the decision-theoretic layer of *whether* and *when* to experiment: the EPI provides a quantitative threshold below which the simulator’s recommendation should be deployed without modification.

Model-based and hybrid RL. Dyna [Sutton, 1991] introduced the idea of interleaving model learning with planning. Modern successors—MBPO [Janner et al., 2019], DreamerV3 [Hafner et al., 2023], and TD-MPC [Hansen et al., 2022, 2024]—learn world models that generate synthetic experience for policy optimization, with DayDreamer [Wu et al., 2023] demonstrating that world models can enable physical robot learning with minimal real-world interaction. The critical difference from our setting is that these methods *retrain* the model with incoming data, treating it as an evolving approximation. Our simulator, by contrast, represents pre-existing institutional knowledge that the planner cannot modify. This distinction is less restrictive than it may appear: as Proposition 8 establishes, Bayesian updating renders the fixed-simulator assumption without loss of generality, since the posterior-predictive model after observing data is equivalent to an adaptive simulator.

A related but distinct line of work combines pre-collected offline data with limited online interaction. Hybrid offline-and-online RL [Ball et al., 2023, Song et al., 2023, Niu et al., 2022, 2023] demonstrates that even modest amounts of online data can substantially improve offline RL performance. Niu et al. [2022] develop dynamics-aware methods that selectively incorporate simulated data based on estimated model error. Chen et al. [2025] propose multi-fidelity hybrid RL via information gain maximization, treating the simulator as a low-fidelity source, and Fu et al. [2024] provide benchmarks for RL with biased offline data and imperfect simulators. The key difference from all of these approaches is that our framework explicitly models the *cost* of real-world experimentation: each real-world sample carries an opportunity cost because the experimental unit could have been served by the simulator-trained policy instead. Where hybrid RL addresses how to combine heterogeneous data sources, our framework addresses the prior question of whether the expensive source is worth acquiring.

Multi-fidelity Bayesian optimization. Multi-fidelity BO [Poloczek et al., 2017, Kandasamy et al., 2017, 2019, Peherstorfer et al., 2018] addresses a closely related problem: determining when a planner should query an expensive high-fidelity oracle rather than rely on a cheap low-fidelity surrogate. Acquisition functions such as the multi-fidelity knowledge gradient [Poloczek et al., 2017] and multi-fidelity GP-UCB [Kandasamy et al., 2016] formalize this as a cost-aware information-value calculation, and cost-aware BO [Lee et al., 2020] explicitly accounts for query costs—ingredients shared with our EPI.

The correspondence is limited, however, by three structural features of our MDP setting. Multi-fidelity BO optimizes a static function: querying one input does not change the function’s value at other inputs. In our MDP, actions affect future states through transition dynamics, so the information value of an experiment depends on the entire state-transition structure. Each BO query is also an isolated evaluation with no population-level consequence, whereas our experimental units bear the opportunity cost of not receiving the simulator’s recommendation. And multi-fidelity BO assumes the low-fidelity function is a noisy version of the high-fidelity function, whereas our simulator may be *systematically* biased due to confounding—a qualitatively different error structure that our extended simulation lemma (Lemma 1) characterizes. Our EPI generalizes the multi-fidelity acquisition function to sequential decision problems with population-level costs and structured model bias.

Simulation lemma and model approximation. The simulation lemma [Kearns and Singh, 2002] bounds the value difference between the true MDP and an approximate model as a function of reward and transition errors.⁵ The central insight of this result—that transition errors compound quadratically with the effective horizon while reward errors compound only linearly—is foundational to our analysis. This asymmetry implies that transition-dominated regimes are inherently more difficult to address through experimentation, since even exact reward estimation cannot compensate for compounding transition errors.

Kakade and Langford [2002] extend the simulation lemma to approximate policy iteration, showing that near-optimal performance is achievable when approximation error is controlled—a result we build on in our analysis of the simulator as an approximate model. Recent work by Lobel and Parr [2024] shows that the classical bound is not tight, demonstrating that the standard simulation lemma overestimates how transition errors compound over time. This suggests that our Lemma 1 bounds may also admit tightening in future work.

⁵In its standard form, for a discounted MDP with discount γ : $|V^\pi(\mathcal{M}^*) - V^\pi(\hat{\mathcal{M}})| \leq \frac{\epsilon_r}{1-\gamma} + \frac{\gamma\epsilon_p V_{\max}}{(1-\gamma)^2}$, where ϵ_r and ϵ_p are the maximum reward and transition errors.

Our extended simulation lemma (Lemma 1) specializes these results to the setting where the approximate model is a simulator with *structured* uncertainty: the reward error ϵ_r and transition error ϵ_p are functions of the hidden-state distribution and the confounding bias β_{conf} . This provides a direct, interpretable connection between the simulator’s calibration quality and the value of experimentation—and, through the quadratic-vs-linear asymmetry, explains why the EPI is more sensitive to transition uncertainty than to reward uncertainty.

Safe exploration and deployment-efficient RL. Safe exploration [Sui et al., 2015, Berkenkamp et al., 2017] constrains the learning agent to avoid catastrophic states, providing high-probability guarantees that unsafe regions are never visited. Deployment-efficient RL [Matsushima et al., 2021] addresses a complementary practical constraint: the number of distinct data-collection policies must be small, reflecting the cost of deploying new policies in production systems.

Our framework differs from both literatures in the nature of the constraint it imposes. Safe exploration guards against physical catastrophe; deployment efficiency limits the number of policy switches. Our constraint is *economic*: the cost of experimentation is the opportunity cost of not following the simulator-trained policy for each experimental unit. However, the deployment-efficiency perspective is directly complementary: our SEP can be viewed as a single deployment of an experimental policy, and the EPI threshold determines whether that deployment is worthwhile. The safe-exploration perspective also applies when the simulator-trained policy is known to be safe and any deviation carries risk; in such settings, the EPI threshold implicitly incorporates a safety premium.

Adaptive clinical trials. The adaptive clinical trials literature confronts the same exploration–exploitation tradeoff that motivates our work, applied to a population of patients. Response-adaptive randomization [Rosenberger and Lachin, 2012, Hu and Rosenberger, 2006, Berry, 2006, 2012] adjusts treatment allocation as evidence accumulates; platform trials [Berry et al., 2015, Woodcock and LaVange, 2017, Adaptive Platform Trials Coalition, 2019] enable simultaneous evaluation of multiple treatments under a shared infrastructure; and group sequential methods [Pocock, 1977, O’Brien and Fleming, 1979, Jennison and Turnbull, 1999] provide stopping rules that determine when enough evidence has accumulated to act. The I-SPY 2 trial [Barker et al., 2009] exemplifies how Bayesian adaptive design can simultaneously identify effective treatments and allocate patients to the most promising arms. Villar et al. [2015] survey the benefits and challenges of bandit models for clinical trial design.

Our work departs from this literature in two respects that interact. First, the simulator gives us structured prior knowledge about system dynamics—a richer starting point than the minimal priors typical of clinical trials—which underpins the three-uses framework (Section 4): the simulator can serve as a policy source, a Bayesian prior, or an experimental design tool. Second, the MDP structure introduces transition dynamics where today’s action affects tomorrow’s state, creating the reachability gap that distinguishes designed exploration from passive learning. Clinical trials typically model each patient as an independent draw, without the sequential state-transition structure that gives our problem a different geometry from a bandit.

Bayesian experimental design and information-directed sampling. The value of information [Howard, 1966, Raiffa and Schlaifer, 1961, DeGroot, 1970] provides the decision-theoretic basis for our framework. The expected value of sample information (EVSI) [Ades et al., 2004, Heath et al., 2020] quantifies the benefit of collecting additional data before making a decision, and has been widely applied in health economics [Claxton, 1999, Briggs et al., 2006, Wilson, 2015] to determine whether clinical trials are worth conducting. Our EPI is an EVSI adapted to the MDP setting: it measures the expected improvement in policy value from observing the outcome of a specific state-action pair, with the key novelty that the information value propagates through the Bellman equations rather than affecting a one-shot decision.

Modern amortized BED [Foster et al., 2021, Ivanova et al., 2021, Rainforth et al., 2024] provides computational tools for sequential experimental design, using deep networks to amortize the cost of computing optimal designs. Blau et al. [2022] connect BED to deep RL, casting sequential design as an MDP. Classical optimal experimental design [Pukelsheim, 2006, Chaloner and Verdinelli, 1995] provides the theoretical foundation for our Fisher-SEP: the A-optimality criterion $\text{tr}(\mathcal{F}(\pi))$ that we maximize is the standard A-optimal design criterion applied to the value function’s dependence on

reward parameters, with the key novelty being that the “design variable” is a stochastic MDP policy rather than a regression design matrix.

Information-directed sampling (IDS) [Russo and Van Roy, 2014, Russo et al., 2018] is the closest algorithmic ancestor of our Fisher-SEP. IDS selects actions that minimize the ratio of squared expected regret to mutual information gained about the optimal action, providing a principled way to balance exploration and exploitation. More broadly, exploration criteria in the bandit and RL literatures divide into two families: *uncertainty-based* criteria like UCB [Auer et al., 2002], Thompson sampling [Thompson, 1933, Russo et al., 2018], and the Bayesian knowledge gradient [Frazier et al., 2008], which direct data collection toward regions of high posterior variance; and *information-gain-based* criteria like IDS and BED, which direct data collection toward observations that most reduce posterior entropy about the decision-relevant quantity. Our Fisher criterion belongs to the second family but makes a specific choice: the decision-relevant quantity is the value function V^π , and the Fisher information $(\nabla_\theta V^\pi)^\top D_\pi(\nabla_\theta V^\pi)$ is the (local) sensitivity of that value to perturbations in the reward parameters, weighted by the visitation distribution the policy induces. This choice has three practical consequences. The Fisher trace is closed-form in tabular MDPs via the Bellman resolvent, whereas mutual information between observations and the optimal-action posterior requires either variational approximation or MCMC. It correctly ignores uncertainty that does not translate into decision uncertainty: a reward whose posterior variance is large but whose $\partial V^\pi / \partial \theta$ is small will be deprioritized relative to an uncertain reward whose perturbation flips the optimal action. And it ignores visitation that does not translate into informational value: a state visited often but whose rewards are already confident contributes zero to the trace. Our Fisher-SEP also differs from IDS in three respects not related to the information measure. It separates the exploration and exploitation phases, reflecting the practical reality that experiments are planned in advance and run as a batch rather than interleaved with exploitation at each time step; it accounts for the opportunity cost of experimentation through the EPI threshold, which determines whether to explore at all; and it operates in sequential MDP settings where IDS is typically applied to bandits.

Novelty concentration: what Fisher-SEP adds to the BED / IDS / KG / ASID family. The preceding paragraphs situate Fisher-SEP inside an existing lineage of design-theoretic exploration. We close the related-work discussion by stating what Fisher-SEP contributes beyond that lineage, and what it does not.

Fisher-SEP does not introduce a new A-optimal criterion in the sense of Chaloner-Verdinelli [Chaloner and Verdinelli, 1995] or Pukelsheim [Pukelsheim, 2006]: the data-rich limit reduces to classical A-optimal design for reward parameters (App. B, Cor. 4). It does not propose a new information measure as an alternative to IDS; the Fisher trace is an established sensitivity statistic. And it does not propose a new RL algorithm in the PSRL or UCRL2 lineage; the two-phase explore-then-commit structure is deliberately non-adaptive.

The contribution is to use the target-policy-value-weighted Bellman-resolvent gradient as a design criterion over stochastic exploration policies, with the simulator supplying the resolvent. Three specific contributions follow.

Target-policy-value weighting. Classical A-optimal design and IDS both operate with information measures over unknown parameters or actions. Fisher-SEP weights the per- (s', a') contribution by $d_{\pi^{\text{tgt}}}(s)(\partial V^{\pi^{\text{tgt}}} / \partial \theta_{s', a'})^2$, which isolates the uncertainty that affects the target policy’s value. Parameter uncertainty that does not flow through the Bellman resolvent to the target’s visitation receives zero weight. This is the mechanism behind Proposition 4.1: Fisher-SEP prioritizes pairs that are target-sensitive (nonzero gradient) but unvisited (no pilot data), which ordinary A-optimal design does not distinguish.

Bellman-resolvent gradient, not parameter-identification gradient. ASID [Mommel et al., 2024] uses the Fisher information of physical parameters θ_{phys} for sim-to-real in robotics, aiming to identify θ_{phys} . Fisher-SEP uses the Fisher of the value functional $V^{\pi^{\text{tgt}}}(\theta)$, which is the Bellman-resolvent-propagated version of the parameter Fisher. The distinction matters whenever parameter uncertainty propagates non-uniformly to value: uncertain parameters that leave $V^{\pi^{\text{tgt}}}$ nearly invariant are not prioritized. ASID’s objective and Fisher-SEP’s objective coincide only in the fully reachable regime with uniform value sensitivity; on a bottleneck geometry like HIV, they differ.

Simulator as connectivity prior, not as accurate forward model. In sim-to-real (domain randomization, ASID), the simulator is treated as an approximate forward model whose accuracy one tries to improve. Fisher-SEP uses the simulator as a connectivity prior: the Bellman-resolvent $(I - \gamma P^{\pi^{\text{tgt}}})^{-1}$ that determines which (s', a') pairs' uncertainty propagates to target-value uncertainty. The simulator need not be accurate (the HIV simulator is $15\times$ off on Region B prevalence); its connectivity pattern on the target's visitation must be approximately correct for the resolvent to be informative. This is the requirement behind our positive result on HIV.

In summary, Fisher-SEP applies A-optimal Bayesian experimental design to a specific target functional, the planner's policy value, via the simulator-supplied Bellman resolvent. It separates the property the simulator must capture accurately (connectivity) from the property it is typically assumed to capture accurately (parameter values).

Domain randomization. Domain randomization (DR) [Tobin et al., 2017, Peng et al., 2018, Akkaya et al., 2019, Mehta et al., 2020] is frequently described as a sim-to-real technique for generating robust policies by training across a distribution of simulator parameters. In the framework of this paper, DR corresponds to a *simulator-time* version of experimental design: instead of randomizing in the real world under an S -measurable pilot policy (our Lemma 2), DR randomizes the simulator's parameters at training time. Active DR [Mehta et al., 2020] specifically chooses the parameter distribution to maximize Fisher information about policy robustness — structurally analogous to Fisher-SEP, but applied at simulator-training time rather than deployment time.

The two approaches address different sources of error. DR handles *parameter uncertainty under a fixed structural model*: it prepares a policy to work across a range of simulator parameter values. Fisher-SEP addresses *structural model uncertainty*: it uses real-world experimentation to correct biases (confounding, drift) that domain randomization cannot address because the simulator's own parameter distribution is contaminated by those biases. In the HIV case, no amount of domain randomization over Region-B prevalence values in the simulator fixes the simulator's systematic under-sampling of Region B — because the DR distribution is itself calibrated from clinic data that never reached Region B. Fisher-SEP's real-world pilot is the only intervention that can identify $\mathbb{P}_t(H | s)$ at Region-B states.

DR and Fisher-SEP are complementary rather than competing. A deployment framework can use DR for robustness to known parameter uncertainty and Fisher-SEP for real-world identification of structural confounding. We do not run DR as a numerical baseline because the case studies are constructed around structural confounding (the regime DR does not address), not parameter sensitivity (the regime DR targets). Xu and Zeevi [2023] develop Bayesian design principles for frequentist sequential learning, bridging the two traditions—a connection our framework also exploits, since the EPI is a Bayesian quantity employed to make a frequentist-style decision about whether to experiment.

Reward-free and task-agnostic exploration. Reward-free RL [Jin et al., 2020, Kaufmann et al., 2021] separates exploration (phase 1, reward-agnostic) from exploitation (phase 2, after a reward is specified), proving that a single reward-agnostic exploration phase can yield a policy near-optimal for any reward function revealed later. Maximum-entropy exploration [Hazan et al., 2019] is a closely related approach that maximizes the entropy of the induced state-visitation distribution, providing broad coverage without a specific task objective. Our Fisher-SEP differs in its choice of objective—sensitivity to reward parameters rather than coverage or entropy—and in its phase structure (pilot, explore, exploit) being tied to an explicit decision rule (the EPI threshold). When the reward parameters are entirely unknown, the Fisher-SEP's objective tends toward uniform coverage and resembles reward-free exploration; when the simulator supplies informative reward priors, the Fisher-SEP directs exploration toward the state-action pairs whose reward estimates most affect the optimal policy, a refinement that reward-free exploration does not make.

Optimism-based exploration baselines. UCRL2 [Jaksch et al., 2010] and R-max [Brafman and Tennenholtz, 2002] are the canonical non-Bayesian baselines for regret-minimizing exploration, using optimism under uncertainty to implicitly prioritize under-visited (s, a) pairs. BOSS [Asmuth et al., 2009] combines Bayesian exploration with optimism in the face of model uncertainty. These methods achieve something structurally similar to the reachability component of our gap decomposition—they navigate toward under-visited states—but via frequentist worst-case guarantees rather than Bayesian

posterior decomposition, and without an opportunity-cost accounting. Our empirical comparisons (Section 5) benchmark against these methods where applicable.

Transfer RL with misspecified simulators. Modi et al. [2020] study transfer RL with linear mixtures of model ensembles, providing sample-complexity bounds when the true MDP lies in a span of hypothesized models. Our confounded-simulator setting can be viewed as a nonlinear version: the true observed-state MDP lies in a space of marginalizations of the joint (S, H) POMDP, and the simulator is the marginalization under the calibration-time distribution $\mathbb{P}_{t_0}(H | S, A)$. Lu et al. [2023] provide a recent information-theoretic treatment of RL with informative priors that is directly complementary to our framework.

Offline RL and confounded MDPs. Offline RL [Levine et al., 2020, Lange et al., 2012, Fujimoto et al., 2019] learns policies from fixed datasets without additional interaction. A central challenge is *distribution shift*: the learned policy may visit states unseen in the data, where value estimates are unreliable. Model-free approaches address this through conservatism—penalizing out-of-distribution actions [Kumar et al., 2020, Kostrikov et al., 2022]—while model-based methods like MOPO [Yu et al., 2020] and MOREL [Kidambi et al., 2020] learn a dynamics model and apply pessimistic penalties for states outside the data support. Both families assume the offline data is *unconfounded*: the behavior policy’s action choices do not depend on unobserved variables that also affect outcomes. When this assumption fails, a qualitatively different problem arises.

Confounded MDPs [Zhang and Bareinboim, 2016, Wang et al., 2021] formalize settings where unobserved variables simultaneously affect actions and outcomes. Zhang and Bareinboim [2016] introduce the causal approach to MDPs with unobserved confounders, showing that standard RL methods can fail when the behavior policy depends on hidden state; Wang et al. [2021] provide the first provably efficient algorithms for this setting. Off-policy evaluation under confounding [Namkoong et al., 2020, Bennett and Kallus, 2024] develops methods to estimate counterfactual policy values when the behavior policy depends on unobserved variables. Most relevant to our setting, Kallus et al. [2018] demonstrate that even a small amount of experimental data can “ground” confounded observational estimates by correcting for hidden bias—a result that motivates our central question of *when* such experimental data is worth collecting. Kallus and Zhou [2018] develop confounding-robust policy improvement methods that provide worst-case guarantees without experimental data, representing the alternative to our approach: accept the confounding and optimize conservatively, rather than experiment to resolve it.

Our hidden-state model is a confounded MDP: the simulator was calibrated from observational data where the behavior policy (the knowledgeable manager’s stocking decisions) depended on the hidden state (true demand rates), creating confounding bias β_{conf} . Rather than attempting to de-bias the confounded model, we use it as a *prior* for experimental design. Our framework asks: given that the simulator is confounded, is it worth collecting unconfounded experimental data, and if so, what experiments should be run? In this sense, our approach is complementary to the debiasing literature: rather than correcting the confounded model, we use it to determine *where* unconfounded data would be most valuable, and the EPI quantifies whether the expected gain justifies the cost.

Generalizability and transportability. The generalizability and transportability literature in causal inference [Stuart et al., 2011, Dahabreh et al., 2019, Bareinboim and Pearl, 2016, Degtiar and Rose, 2023] studies when causal effects estimated in one population can be applied to another. Pearl and Bareinboim [2011] and Bareinboim and Pearl [2016] formalize this as a causal inference problem: given a causal model and knowledge of which variables differ between source and target, can the target-population effect be identified from source experiments and target observations? Degtiar and Rose [2023] synthesize the assumptions, methods, and tests for treatment effect heterogeneity that this enterprise requires, emphasizing that both internal and external validity are necessary for unbiased target-population estimates. Huang and Parikh [2024] survey persistent hurdles in extrapolating experimental findings across disciplines.

A closely related line of work operationalizes transportability through *data fusion*—combining experimental and observational data to improve causal effect estimation. Parikh et al. [2025a] propose double machine learning estimators that combine experimental and observational studies, providing falsification tests for external validity; their no-free-lunch theorem—showing that one must correctly diagnose *which* assumption is violated—parallels our framework’s need to distinguish reward errors

from transition errors. Lanners et al. [2025] extend data fusion to partial identification when both confounding and cross-source exchangeability fail simultaneously, developing sensitivity analyses that quantify how severe assumption violations must be to overturn a given conclusion—a question structurally parallel to the logic of our EPI threshold. Rosenman et al. [2023] develop shrinkage estimators for combining observational and experimental datasets, and Yang and Ding [2020] study combining multiple observational sources.

A recurring finding across this literature is that treatment effects vary substantially across populations: Vivalt [2020] documents this heterogeneity across impact evaluations, Meager [2019] uses Bayesian hierarchical models to synthesize evidence from seven microcredit experiments, and Parikh et al. [2024b] develop methods to characterize the subgroups for whom trial results may not generalize.

Our setting maps naturally onto the transportability framework: the simulator is analogous to a trial conducted in a non-representative population (the calibration population), and the real world is the target. The confounding bias β_{conf} measures the transportability gap arising from differences in the hidden-state distribution. The EPI threshold determines whether this gap is large enough to justify collecting new experimental data in the target population—a decision rule that the transportability literature identifies as important but does not provide. The data fusion perspective of Parikh et al. [2025a] and Lanners et al. [2025] is directly relevant: our experimental data (unconfounded) and simulator data (potentially confounded) constitute precisely the two sources that data fusion methods seek to combine, and our EPI provides the decision rule—absent from the existing literature—for whether the experimental source is worth acquiring. This connection suggests a natural extension of our framework to settings where the “simulator” is a body of evidence from a different population, and the question is whether to conduct a new trial in the target.

Value of information in health economics and operations research. Two research communities have independently developed frameworks for determining whether additional data collection is warranted. In health economics, the expected value of perfect information (EVPI) provides an upper bound on the value of any experiment [Claxton, 1999, Claxton et al., 2002], while the EVSI quantifies the value of a specific experimental design [Ades et al., 2004, Brennan et al., 2007, Strong et al., 2014]. These tools determine whether clinical trials merit funding—a question structurally identical to our “whether to experiment” problem. Wilson [2015] provides a practical guide, and Jalal and Alarid-Escudero [2018] develop Gaussian approximation methods for efficient computation. In operations research, the ranking and selection literature [Kim and Nelson, 2006, Chen et al., 2000, Hong et al., 2021] studies how to allocate simulation budget across competing alternatives, with sequential procedures that myopically maximize information value [Chick and Inoue, 2001, Chick et al., 2010] and the knowledge gradient [Frazier et al., 2008, 2009] extending these ideas to correlated beliefs.

Our EPI connects to both traditions: it is an EVSI for the MDP setting (health economics perspective) and a simulation budget allocation criterion (operations research perspective). The key novelty is that our “alternatives” are not independent arms but states in an MDP with transition dynamics, so the information value of observing one state-action pair depends on the entire MDP structure through the Bellman equations. Neither the health economics nor the OR literature models this dependence: EVSI treats the decision as a one-shot choice among treatments, and ranking-and-selection treats alternatives as independent simulation configurations.

Online experimentation in technology. In the technology sector, online controlled experimentation has become standard practice. A/B testing [Kohavi et al., 2009, 2020] is the dominant paradigm, with overlapping experiment infrastructure [Tang et al., 2010] supporting thousands of simultaneous tests. Always-valid inference [Johari et al., 2022, Howard et al., 2021, Ramdas et al., 2023] provides statistical methods for continuous monitoring without inflating Type I error, and Berman et al. [2022] study false discovery at scale. When treatments can be personalized based on user characteristics, A/B testing gives way to contextual bandits [Li et al., 2010, Agarwal et al., 2014, Foster et al., 2018, Foster and Rakhlin, 2020], with recent work addressing the statistical challenges of adaptively collected data [Nie et al., 2018, Hadad et al., 2021, Zhang et al., 2020].

Our framework addresses a distinct question: rather than asking “which treatment is superior?” (a comparison problem), we ask “should an experiment be conducted at all?” (a meta-decision). Always-valid inference determines when to *stop* an experiment that is already running; our EPI determines whether to *initiate* one. The EPI threshold provides a principled criterion: experiment

only when the expected information value exceeds the opportunity cost of deviating from the simulator’s recommendation—a consideration of particular importance when experiments affect large populations and the opportunity cost is measured in revenue or user welfare.

Real options and the economics of experimentation. The decision to experiment can be cast as an investment under uncertainty: the planner incurs an upfront cost (the opportunity cost of deviating from the simulator-trained policy) in exchange for information that may improve future decisions. The real options literature [Dixit and Pindyck, 1994, McDonald and Siegel, 1986, Pindyck, 1993] provides the canonical framework for such decisions, establishing that the option to delay and gather information carries positive value, which raises the threshold for action above the naive net-present-value rule. Our “whether to experiment” question admits a direct mapping: the planner may experiment now (exercising the option) or continue with the simulator-trained policy (preserving the option to experiment later, informed by passive learning).

The EPI threshold serves as the exercise boundary: experiment when the expected information value exceeds the opportunity cost. The principal difference is that our “investment” possesses MDP structure: the value of information depends on the state, the transition dynamics, and the planning horizon, yielding a state-dependent exercise boundary rather than a scalar threshold. Rational inattention [Sims, 2003, Matějka and McKay, 2015] provides a complementary perspective: the planner rationally chooses how much experimental effort to devote to reducing uncertainty. Our framework admits interpretation through this lens: the EPI governs the *intensity* of attention (the fraction of units allocated to experimentation), while the Fisher-SEP governs its *direction* (which state-action pairs to observe). Morris and Strack [2019] connect the Wald sequential testing problem to information acquisition costs, providing a unified framework for optimal stopping and information gathering that parallels the role of the EPI as a criterion for initiating or terminating experimentation.

Summary of positioning. The literatures surveyed above converge on a common tension: knowledge from one source—a simulator, an observational dataset, a trial in a different population—is valuable but imperfect, and the question is what to do about the imperfection. The offline RL and confounded MDP literatures address this by *debiasing*: correcting the imperfect source using causal structure or pessimistic bounds. The transportability and data fusion literatures address it by *combining*: integrating the imperfect source with a second, complementary source under explicit assumptions about what differs between them. The BAMDP and bandit literatures address it by *exploring*: treating the imperfection as uncertainty to be resolved through interaction. The sim-to-real and model-based RL literatures address it by *transferring*: adapting the imperfect source to the target domain through domain randomization or model refinement.

None of these literatures addresses the *meta-question* that logically precedes all four strategies: is the imperfection large enough to warrant action? Our framework supplies this missing decision layer. The simulator serves three roles—policy source, Bayesian prior, and experimental design tool—that correspond to increasing levels of engagement with the real world. The EPI threshold answers the “if” question by comparing the expected information value to the opportunity cost, drawing on the VoI and real options traditions. The gap decomposition answers the “what kind” question: passive learning suffices when informative states are reachable; designed exploration is necessary when they are not—a distinction absent from the clinical trials and bandit literatures, which lack transition dynamics. The Fisher-SEP answers the “how” question by directing experimental effort toward the reward parameters that most affect policy value, extending the IDS and BED traditions to MDP policies. By integrating the cost–benefit logic of Bayesian experimental design with the MDP structure of reinforcement learning and the source-discrepancy reasoning of causal transportability, our framework provides a unified answer to the question in the paper’s title: *if* and *when* to experiment.

Baselines and scope limitations. Two baseline classes beyond those reported in Section 5 would refine the empirical picture but are beyond the scope of this paper.

Information-directed sampling. IDS [Russo and Van Roy, 2014, Russo et al., 2018] minimizes the ratio of squared expected regret to mutual information about the optimal action. The natural value-IDS variant replaces the optimal-action information term with mutual information about the target policy’s value, which matches the Fisher-SEP objective in the Gaussian small-noise limit. A value-IDS baseline on the vending and HIV case studies is a natural next step; we do not pursue it

here because the Fisher-SEP vs Thompson-sampling comparison in Section 5 already isolates the “design criterion beats posterior sampling” direction at the paper’s claimed scale.

Representation-matched UCRL2/UCBVI. UCRL2 [Jaksch et al., 2010] and UCBVI [Azar et al., 2017] in the Table 1 columns run on a coarser 2×2 factored state discretization than the simulator-informed policies. A representation-matched comparison (UCRL2/UCBVI on the full observed-state discretization, or Fisher-SEP-R on the 2×2 factored representation) would tighten the “simulator-free baseline” row to a method comparison rather than a representation-and-method comparison; the Table 1 results as presented should be read as isolating the effect of the simulator-as-prior at the simulator-informed representation, and as a lower bound on the simulator’s value.

Three additional scope limitations referenced from Section 6. (i) *Rate vs. PSRL/UCRL2.* Theorem 4 gives a $T_{\text{pilot}}^{1/3}$ Bayes-regret bound for Fisher-SEP-R, slower than PSRL’s and UCRL2’s \sqrt{T} (Remark 8); the rate is a direct consequence of the two-phase explore-then-commit structure, and an adaptive \sqrt{T} variant is left to future work. (ii) *Independence-prior sensitivity.* Proposition 9 (App. C.18) shows that a spatial GP prior with moderate lengthscale partially closes the reachability gap via passive learning; the “passive cannot close $\mathcal{G}_{\text{reach}}$ ” claim is therefore an Assumption 4 statement, not a structural one. (iii) *Contracting latent dynamics.* The analysis treats ϵ^{hist} as negligible under a contracting latent Jacobian (App. D.16); non-contracting POMDPs give $\epsilon^{\text{hist}} = \Theta(1)$ and the framework does not apply. (iv) *Trial count.* All results use $n=30$ common-seed trials with paired Wilcoxon; $n=100$ replication with seed-resampling would strengthen the vending $T=1600$ headline.